Examining the effects of BRAF, MEK and CDK4/6 inhibition on anti-tumor immunity in *BRAF*^{V600} melanoma

Emily J Lelliott

ORCID identifier 0000-0002-5028-6938

Doctor of Philosophy

July 2020

Faculty of Medicine, Dentistry and Health Sciences

Sir Peter MacCallum Department of Oncology

The University of Melbourne

Submitted in total fulfilment for the degree of Doctor of Philosophy

Abstract

The recent advent of targeted and immune-based therapies has revolutionized the treatment of melanoma, and transformed outcomes for patients with metastatic disease. However, the mechanisms underpinning the clinical efficacy of these approaches are still being elucidated. The majority of patients develop resistance to the current standard-of-care targeted therapy, dual BRAF and MEK inhibition (BRAFi+MEKi), prompting evaluation of a new combination incorporating a CDK4/6 inhibitor. Based on promising preclinical data, combined BRAF, MEK and CDK4/6 inhibition (triple therapy) has recently entered clinical trials for the treatment of *BRAF*^{V600} melanoma. Interestingly, while BRAFi+MEKi therapy was initially developed on the basis of potent tumor-intrinsic effects, it was later discovered to have significant immune-potentiating activity. Recent studies have also identified immune-related impacts of CDK4/6 inhibition, though these are less well defined and appear to be both immune-potentiating and immune-inhibitory. *BRAF*^{V600} melanoma patients are also eligible for immunotherapies, and hence the immunomodulatory activity of these targeted inhibitors makes first-line treatment decisions complex. The aim of this thesis was to examine the immunomodulatory effects of BRAF, MEK and CDK4/6 inhibition, with an ultimate goal of providing critical information to aid in the clinical management of *BRAF*^{V600} melanoma patients.

Examining mechanisms of the immunomodulatory effects of targeted therapies requires preclinical mouse models of melanoma that are both immunogenic, and harbor the oncogenic drivers targeted by the therapies being evaluated. To address this, we developed a novel immunogenic *Braf*^{V600E}*Cdkn2a*$^{-/-}$*Pten*$^{-/-}$ melanoma mouse model, called YOVAL1.1. YOVAL1.1 tumors are transplantable in immunocompetent mice and amenable to standard-of-care melanoma therapies, including BRAFi+MEKi and

immune checkpoint blockade. This, coupled with the *Cdkn2a* status, which infers some sensitivity to CDK4/6 inhibitors, makes this an ideal preclinical model to evaluate the immunomodulatory effects of the triple therapy. Using this model, we demonstrated that triple therapy promotes durable tumor control through tumor-intrinsic mechanisms, while promoting immunogenic cell death and T cell infiltration. However, despite this, tumors treated with triple therapy were unresponsive to immune checkpoint blockade. Flow cytometric and single cell RNA-seq analyses of tumor infiltrating immune populations revealed that triple therapy markedly depleted pro-inflammatory macrophages and cross priming $CD103^{+}$ dendritic cells, the absence of which correlated with poor overall survival and clinical responses to immune checkpoint blockade in melanoma patients. Indeed, immune populations isolated from tumors of mice treated with triple therapy failed to stimulate T cell responses *ex vivo.* Hence, while combined BRAF, MEK and CDK4/6 inhibition demonstrated favorable tumor-intrinsic activity, these data suggest that collateral effects on tumor-infiltrating myeloid populations may impact on anti-tumor immunity.

Several recent studies have reported immune-potentiating effects of CDK4/6 inhibition, and subsequent synergy with immune checkpoint blockade. However, T cells are the primary target of these immunotherapies, and an understanding of the direct effects of CDK4/6 inhibition on this cellular subset was lacking. In this thesis, using integrated epigenomic, transcriptomic and single cell CITE-seq analyses, we identified a novel role for CDK4/6 in regulating T cell fate. Specifically, we demonstrated that CDK4/6 inhibition promoted the phenotypic and functional acquisition of T cell memory. Genome-wide CRISPR/Cas9 screening and phospho-proteomics revealed that memory formation in response to CDK4/6 inhibition was cell intrinsic and required RB. Pre-conditioning human CAR T cells with a CDK4/6 inhibitor enhanced their

persistence and tumor control, and clinical treatment with a CDK4/6 inhibitor promoted expansion of memory T cells in a melanoma patient, priming a response to immune checkpoint blockade.

Collectively these findings highlight the multi-faceted immunomodulatory activity of BRAF, MEK and CDK4/6 inhibition. The addition of a CDK4/6 inhibitor to dual BRAFi+MEKi led to the depletion of intratumoral myeloid subsets that may be critical for supporting a therapeutically beneficial T cell response. In contrast, as an individual therapy, CDK4/6 inhibition promoted effector and memory T cell activity, suggesting that, with optimal scheduling to prevent myeloid depletion, CDK4/6 inhibitors may be used to enhance and prolong BRAFi/MEKi-induced anti-tumor T cell immunity. Defining the mechanisms that underpin the clinical efficacy of these available therapies is a critical step forward in optimising novel combination and scheduling approaches to combat melanoma and improve patient outcomes.

Declaration

This declaration is to certify that:

i) This thesis comprises only my original work towards the PhD except where indicated in the preface section

ii) Due acknowledgement has been made in the text to all other material used

iii) The thesis is fewer than 100,000 words (excluding tables, appendices and references)

Emily Lelliott

Faculty of Medicine, Dentistry and Health Sciences

Sir Peter MacCallum Department of Oncology

The University of Melbourne

Parkville, Australia

July 2020

Preface

I would like to acknowledge those who directly contributed to the work presented in this thesis.

Significant intellectual and/or technical contributions are duly noted by authorships or acknowledgements in the publications presented in Chapters 2, 3 and 4 of this thesis.

Specific author contributions and funding sources are detailed in the publications presented in Chapters 2, 3 and 4 of this thesis.

Publication status and further details are provided in the preface section of Chapters 2, 3 and 4 of this thesis.

All work presented in this thesis was conducted during the prescribed period of the PhD.

Publications

Lelliott EJ, Kong I, Zethoven M, Ramsbottom KM, Martelotto L, Meyran D, Zhu JJ, Costacurta M, Kirby L, Sandow J, Lim L, Dominguez P, Todorovski I, Haynes NM, Beavis PA, Neeson PJ, Hawkins ED, McArthur GA, Parish IA, Johnstone RW, Oliaro J, Sheppard KE, Kearney CJ, Vervoort SJ. Pharmacological inhibition of CDK4/6 augments long-term anti-tumor immunity through the induction of T cell memory. *Cancer Discovery* [under review].

Kearney CJ, Vervoort SJ, Ramsbottom KM, Todorovski I, **Lelliott EJ**, Zethoven M, Pijpers L, Semple T, Mortelotto L, Parish I, Scott N, Oliaro J and Johnstone RW. SUGAR-seq enables simultaneous detection of glycans, epitopes and the transcriptome in single cells. *Science Advances* [under revision].

Lelliott EJ, Mangiola S, Ramsbottom KM, Zethoven M, Lim L, Lau P, Oliver AJ, Martelotto L, Kirby L, Martin C, Patel R, Slater A, Cullinane C, Papenfuss A, Haynes NM, McArthur GA, Oliaro J, Sheppard KE. Combined BRAF, MEK and CDK4/6 inhibition depletes intratumoral immune-potentiating myeloid populations in melanoma. *Cancer Immunol Res* [in press].

Freeman AJ, **Lelliott EJ**, Oliaro J. Inhibition of tumor autophagy: a strategy to improve anti-tumor immunity? *Signal Transduct Target Ther*. 2020 Dec 04;5(1):286.

Smith L, Arabi S, **Lelliott EJ,** McArthur GA, Sheppard KE. Obesity and the impact on cutaneous melanoma: friend or foe? *Cancers (Basel)*. 2020 Jun 15;12(6):E1583.

AbuHammad S, Cullinane C, Martin C, Bacolas Z, Ward T, Chen H, Slater A, Ardley K, Kirby L, Chan KT, Brajanovski N, Smith LK, Rao AD, **Lelliott EJ,** Kleinschmidt M, Vergara IA, Papenfuss AT, Lau P, Ghosh P, Haupt S, Haupt Y, Sanij E, Poortinga G, Pearson RB, Falk H, Curtis DJ, Stupple P, Devlin M,

Street I, Davies MA, McArthur GA, Sheppard KE. Regulation of PRMT5-MDM4 axis is critical in the response to CDK4/6 inhibitors in melanoma. *Proc Natl Acad Sci* U S A. 2019 Sep 3;116(36):17990-18000.

Lelliott EJ, Cullinane C, Martin CA, Walker R, Ramsbottom KM, Souza-Fonseca-Guimaraes F, Abuhammad S, Michie J, Kirby L, Young RJ, Slater A, Lau P, Meeth K, Oliaro J, Haynes N, McArthur GA, Sheppard KE. A novel immunogenic mouse model of melanoma for the preclinical assessment of combination targeted and immune-based therapy. *Sci Rep*. 2019 Feb 4;9(1):1225.

Michie J, Beavis PA, Freeman AJ, Vervoort SJ, Ramsbottom KM, Narasimhan V, **Lelliott EJ**, Lalaoui N, Ramsay RG, Johnstone RW, Silke J, Darcy PK, Voskoboinik I, Kearney CJ, Oliaro J. Antagonism of IAPs enhances CAR T-cell efficacy. *Cancer Immunol Res*. 2019 Feb;7(2):183-192.

Martin CA, Cullinane C, Kirby L, Abuhammad S, **Lelliott EJ**, Waldeck K, Young RJ, Brajanovski N, Cameron DP, Walker R, Sanij E, Poortinga G, Hannan RD, Pearson RB, Hicks RJ, McArthur GA, Sheppard KE. Palbociclib synergizes with BRAF and MEK inhibitors in treatment naive melanoma but not after the development of BRAF inhibitor resistance. *Int J Cancer*. 2018 May 15;142(10):2139-2152.

Acknowledgements

I would like to extend my heartfelt gratitude to all those who have supported me during my PhD. First and foremost, thank you to my supervisors Karen Sheppard, Grant McArthur and Nicole Haynes. Karen and Grant, thank you for giving me the opportunity to work in your lab and to grow as a scientist. I can't thank you enough for treating me with respect and for giving me the autonomy to run with my ideas. Karen, thank you for always having time for me, and for supporting me during good times and bad. Grant, thank you for challenging me and always putting my research in perspective of the bigger picture. Nicole, thank you for everything you have taught me – I learn so much even in the briefest of conversations with you – but more than that thank you for your amazing friendship over these years.

I also want to thank Jane Oliaro for her endless and unwavering support since I infiltrated her lab two years ago – and whose mentorship and guidance has been invaluable to me. Jane, thank you for all your feedback, advice, expertise, for introducing me to your collaborators, for helping move my work forward and for always pushing me to have confidence in myself. Thank you also to Jane's star lab member, Kelly Ramsbottom. Kel, your help the past couple of years has been immeasurable. To both Jane and Kel, you have been my work family and best friends these last two years, thank you for all the coffee and lunch dates, and for letting me hang out with you despite the fact I'm constantly lecturing you not to sit in the sun.

I owe a huge thank you to my PhD mentor, Sarah Ellis. I wouldn't have made it through without our regular coffee catch ups – thank you so much for your mentorship and your friendship.

I would like to acknowledge and thank Carleen Cullinane and the Translational Research Laboratory – Ben Blyth, Rachael Walker, Susan Jackson, Kerry Warren and Jeanette Schreuders – for all their guidance and technical assistance. A special mention to Carleen for her mentorship, and for supporting me to pursue my ideas. Thank you also to Conor Kearney and Stephin Vervoort for your supervision and leadership on one of my projects, and to Ricky Johnstone for supporting the collaboration. To everyone listed in the preface of each chapter, thank you for your assistance with experiments. A special mention goes to Ian Parish for his invaluable expertise and insightful comments, and for being so humble and approachable. A massive thank you to Luciano Martelotto, who has gone above and beyond for me multiple times and is always so patient and calm when I'm running late on stressful days. Thank you also to Shom Goel for all his mentorship and advice.

To all the staff in the core facilities and staff at Peter Mac; Flow Cytometry (Ralph Rossi and Viki Milovac), Bioinformatics (Jason Li) Victorian Centre for Functional Genomics (Kaylene Simpson), Molecular Genomics (Gisela MirArnau) and the Animal Facility, thank you for your support. Thank you also to all the lab managers and support staff, as well as the education team, with special mention to Caroline Owen for all her advice and support throughout my PhD.

A massive thank you to all my other friends/mentors/colleagues at Peter Mac who have made this time more than bearable – Toby Williams, Laura Kirby, Daniela Castiblanco, Simone Neussing, Aparna Rao, Shatha Abuhammad, Florian Wiede, Richard Young, Joe Sia, Lizzy Pijpers, Matteo Costacurta, Balaji Virassamy, Amanda Oliver, Andrew Freeman, Deborah Meyran, Jade Tran, Krystina Minichiello, all of Cluster 10 and others members of the Cancer Immunology Research program. Although I see almost none of you outside the walls of Peter Mac (because I have no social life), our animated

chats in the office, the lab, the animal house or just in the corridors, always brighten my day.

To my good friends outside of Peter Mac, Caroline Haddad, Kate Palmer and Blair Ney, thank you for your unwavering companionship even though I rarely see you - your friendships mean the world to me. A huge thank you to Jane Younger for both your mentorship and friendship – you were by far my most valuable mentor leading up to this PhD journey. I also want to express my long-standing gratitude to my previous boss Simon Havas, for the understanding and support he gave me during my career transition and one of the most difficult periods of my life.

Finally, I want to thank my wonderful family – Mum, Dad, Greg, Timo, Kerry, Annette, Jayne, Katy, Pat, Madoka, Erin, Mizu and all my extended aunts, uncles and cousins. I couldn't ask for a more caring and supportive network and I am truly lucky to have you all. Thank you also to my inanimate dog TJ for being such a predictable and stable companion, and of course my cat Samuel, who is endlessly entertaining and kept me sane while writing my thesis.

I dedicate this thesis to my good friend and life mentor, Ben Strada, whose life was lost to melanoma in 2012 at the age of 40. He was the inspiration for this journey.

Table of Contents

ABSTRACT **3**

DECLARATION **7**

PREFACE **9**

PUBLICATIONS **11**

ACKNOWLEDGEMENTS **13**

TABLE OF CONTENTS **17**

LIST OF FIGURES **21**

CHAPTER 1: LITERATURE REVIEW **23**

1. MELANOMA: CURRENT THERAPIES AND CLINICAL CHALLENGES 23

1.1 Targeted therapies 24

1.1.1 Inhibitors of $BRAF^{V600}$ and MEK *24*

1.1.2 Inhibitors of CDK4/6 as an emerging clinical approach *27*

1.1.3 Combined inhibition of BRAF, MEK and CDK4/6 ..... *28*

1.2 Immune checkpoint inhibitors 30

1.3 Limitations of existing therapies 32

2. CANCER IMMUNITY AND THE TUMOR IMMUNE MICROENVIRONMENT 33

2.1 The Cancer Immunity Cycle 34

2.1.1 Control of early malignancy by the innate immune system *34*

2.1.2 Tumor antigens and initiation of the adaptive immune response *36*

2.1.3 Tumor-specific adaptive immunity *37*

2.1.4 Immunosuppression in the tumor microenvironment *40*

2.2 Using immune checkpoint blockade to enhance anti-tumor T cell immunity 41

2.2.1 CTLA-4 checkpoint blockade *42*

2.2.2 PD-1 checkpoint blockade *44*

2.3 T cell effector, memory and dysfunctional states in anti-tumor immunity 45

3. TARGETED THERAPIES AND THE IMMUNE SYSTEM 48

3.1 Immunomodulation by BRAF and MEK inhibitors 48

3.2 Immunomodulation by CDK4/6 inhibitors 51

3.2.1 Tumor-intrinsic immunomodulatory effects of CDK4/6 inhibition 52

3.2.2 The impact of CDK4/6 inhibition on T cells 54

3.3 Targeted therapy and immune checkpoint blockade combinations 56

3.3.1 Combining MAPK/ERK targeting with immune checkpoint blockade 56

3.3.2 Combining CDK4/6 inhibition with immune checkpoint blockade 58

4. THESIS AIMS AND HYPOTHESES 59

CHAPTER 2: A NOVEL IMMUNOGENIC MOUSE MODEL OF MELANOMA FOR THE PRECLINICAL ASSESSMENT OF COMBINATION TARGETED AND IMMUNE-BASED THERAPY 63

1. PREFACE 63

2. INTRODUCTION 64

3. PUBLICATION IN *SCIENTIFIC REPORTS*, 2019 67

4. SUPPLEMENTARY DATA 78

CHAPTER 3: COMBINED BRAF, MEK AND CDK4/6 INHIBITION DEPLETES INTRATUMORAL IMMUNE-POTENTIATING MYELOID POPULATIONS IN MELANOMA.. 85

1. PREFACE 85

2. INTRODUCTION 86

3. PUBLICATION ACCEPTED IN *CANCER IMMUNOLOGY RESEARCH* 88

4. SUPPLEMENTARY DATA 123

CHAPTER 4: PHARMACOLOGICAL INHIBITION OF CDK4/6 AUGMENTS LONG-TERM ANTI-TUMOR IMMUNITY THROUGH THE INDUCTION OF T CELL MEMORY 135

1. PREFACE 135

2. INTRODUCTION 136

3. PUBLICATION UNDER PEER REVIEW BY *CANCER DISCOVERY* 138

4. SUPPLEMENTARY DATA 189

CHAPTER 5: DISCUSSION 211

1. SUMMARY AND DISCUSSION 211

1.1 The YOVAL1.1 syngeneic melanoma model 212

1.2 Immunomodulatory effects of combined BRAF, MEK and CDK4/6 inhibition 214

1.3 Induction of T cell memory in response to CDK4/6 inhibition 222

2. FUTURE PERSPECTIVES 226

2.1 CDK4/6 inhibitors as adjuvants to ICB 226

2.2 Using CDK4/6 inhibitors to improve CAR T cell therapy 228

2.3 CDK4/6 inhibitors as adjuvants to other therapies 229

2.4 Optimizing scheduling for combined BRAF, MEK and CDK4/6 inhibition 231

3. CONCLUSION 232

CHAPTER 6: REFERENCES 235

List of Figures

Figure 1 – MAPK/ERK and $p16^{INK4A}$/CyclinD-CDK4/6/RB signaling pathways in health and disease .. 26

Figure 2 – Mechanisms of CTLA-4 and PD-1 immune checkpoint blockade …….. 43

Figure 3 – Immunomodulation by oncogenic BRAF and inhibitors of BRAF and MEK in melanoma ... 49

Figure 4 – Immunomodulatory effects of CDK4/6 inhibition ……... 53

Chapter 1: Literature Review

1. Melanoma: current therapies and clinical challenges

Melanoma is the deadliest and most aggressive form of skin cancer, predominately arising from exposure to damaging ultraviolet (UV) radiation from the sun (1-3). Not surprisingly, this disease is most prevalent in countries where UV levels are high and a large proportion of the population are fair-skinned (1). Indeed, Australia and New Zealand have the highest incidence rates of melanoma globally (1) and it is the most common cancer affecting young Australian adults (4). This has led to the coining of melanoma as 'Australia's national cancer' (5).

Given most cases of melanoma first develop on the skin, the disease is often caught early, prior to metastatic spread. In these cases, surgical resection of the primary lesion has a high probability of curing the patient, and for this reason, melanoma has historically demonstrated high survival rates (6, 7). Conversely, prior to the advent of modern therapies, melanoma that metastasized to secondary organs was considered to be one of the deadliest of all cancers. Indeed, up until 2011, patients presenting with advanced metastatic melanoma had a median overall survival of 5.1 months from diagnosis, with a 3-year survival probability of less than 5% (8). Effective therapies were severely lacking and there had been no progress in therapeutic development for decades. In 2011, the development of two new classes of therapeutics revolutionized the landscape of melanoma treatment; targeted therapies and immunotherapies. Although arriving to the clinic around the same time, these therapies were unrelated and mechanistically distinct. However, each demonstrated unprecedented success and hope for the treatment of metastatic melanoma. Today, both targeted therapies and immunotherapies are standard-of-care treatments for patients presenting with metastatic

melanoma. However, despite this, the prognosis for these patients remains poor, reflecting the limitations of these therapies. These therapies, their limitations and emerging developments will be discussed in the following sections.

1.1 Targeted therapies

Targeted therapies, as the name suggests, are designed to precisely target and inhibit tumor-intrinsic aberrant signaling pathways that drive cell survival and proliferation. Melanoma arises from a type of pigment-producing skin cell, called a melanocyte, through the accumulation of genetic mutations that are often a result of DNA damage induced by repeated exposure to UV radiation or other environmental factors (2, 3, 9). When genetic mutations arise in genes encoding proteins critical for the regulation of cell survival or entry into the cell cycle, uncontrolled cell proliferation and malignant transformation can occur (10). Such mutations are referred to as 'oncogenic driver mutations'. These mutations result in constitutive activation of growth signaling pathways that are responsible for both the initiation of tumorigenesis and the maintenance of cancer growth. In a concept known as 'oncogene addiction', malignant cells become reliant on these aberrant signaling pathways (11), and as a result, blocking these pathways with targeted small molecule inhibitors can profoundly disrupt cancer progression through the rapid induction of tumor cell cytostasis or death.

1.1.1 Inhibitors of $BRAF^{V600}$ and MEK

A number of oncogenic driver mutations are found in melanoma, though the most common is a mutation in the gene encoding the protein kinase, BRAF. This mutation occurs at codon 600, resulting in substitution of a valine (V) residue, often with a glutamate (E), which renders the kinase constitutively active (12-14). This $BRAF^{V600}$ mutation occurs in around 40-50% of melanomas (15) and leads to

constitutive activation of the mitogen-activated protein kinase/extracellular signal-regulated kinase 1/2 (MAPK/ERK) signaling pathway (12-14) (**Figure 1**). This pathway is a critical regulator of cell cycle, survival and differentiation, and is typically activated only in the presence of growth factors, which bind receptor tyrosine kinase receptors on the cell surface, activating the GTP binding protein RAS and initiating a tightly controlled cascade of kinase-mediated activation events (RAF→MEK→ERK) (16) (**Figure 1**). However, as in the case of *BRAF*^{V600} melanoma, aberrant activation of MAPK/ERK signaling is seen in a number of cancers due to dysregulation of one of the protein components in the pathway (16, 17). Indeed, in melanoma other oncogenic driver mutations mediate tumorigenesis via activation of MAPK/ERK signaling, including mutations in NRAS, which is the most prevalent form of melanoma after *BRAF*^{V600} (15). Interestingly, driver mutations that mediate activation of this pathway can co-exist in the same tumor but are mutually exclusive at a single cell level (18), indicating that a single MAPK/ERK activation event is sufficient to drive oncogenesis. This thesis will focus predominately on the most prevalent form of melanoma – *BRAF*^{V600} melanoma.

Small molecule inhibitors of mutant BRAF were developed to block protein kinase activity and prevent activation of MAPK/ERK signaling in tumor cells (19) (**Figure 1**). Remarkably, clinical trials of the first BRAF inhibitor, vemurafenib, showed such extraordinary success that trials were stopped prematurely so that patients in alternative arms of the trial could access the treatment (20). Vemurafenib was subsequently approved by the U.S Food and Drug Administration (FDA) for the treatment of *BRAF*^{V600} melanoma in 2011, followed by two more BRAF inhibitors (dabrafenib and encorafenib) in the years following (21, 22). The clinical response to BRAF inhibition was typified by rapid and robust tumor regression in almost all

patients treated, with very minimal toxicities (20). However, those responses were short-lived, as tumors rapidly developed resistance to these drugs (20, 23). Resistance has been shown to occur through various genomic and transcriptional alterations that lead to MAPK/ERK reactivation, as well as activation of alternative pathways involved in growth and survival (reviewed in ref. 23). Nonetheless, BRAF inhibitors improved median progression-free survival (PFS) from 1.6 months (on the standard chemotherapy, dacarbazine) to 5.3 months (20); a momentous survival benefit for a disease in which no progress had been made for decades.

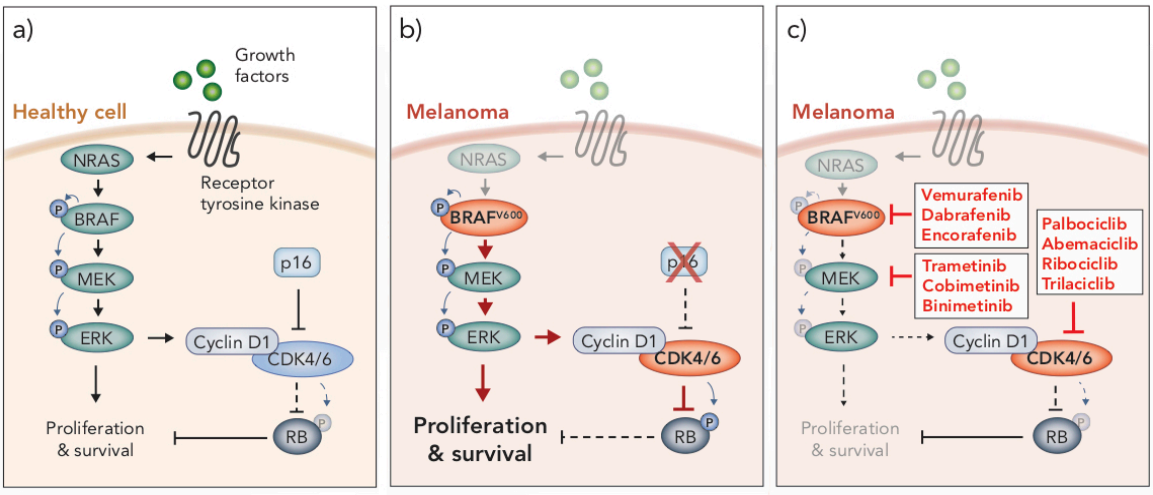

Figure 1 – MAPK/ERK and p16^{INK4A}/CyclinD-CDK4/6/RB signaling pathways in health and disease. a) In healthy cells, growth factors bind receptor tyrosine kinases on the surface of the cell to stimulate proliferation and survival through the MAPK/ERK signaling pathway, which is mediated through a cascade of phosphorylation events (BRAF → MEK → ERK). MAPK/ERK signaling promotes cyclin D1-CDK4/6 complex formation. Inhibition of CDK4/6 by p16 prevents CDK4/6-mediated phosphorylation of RB, thereby allowing RB to carry out its tumor suppressive function. b) BRAF^{V600} mutations and loss of p16 are often seen in melanoma. BRAF^{V600} is constitutively active and promotes aberrant overactivation of MAPK/ERK signaling. In the absence of p16, CDK4/6 phosphorylates and inhibits the tumor suppressor RB. These events lead to uncontrolled cellular proliferation and survival. c) Clinical inhibitors against BRAF^{V600}, MEK and CDK4/6 block MAPK/ERK signaling and CDK4/6-mediated suppression of RB, thereby attenuating cell cycle and survival.

The predominant mechanism of resistance to BRAF inhibitors is reactivation of MAPK/ERK signaling (23, 24). As such, shortly after BRAF inhibitors entered the clinic, trials commenced to examine the efficacy of combining BRAF inhibition with inhibition of its downstream substrate kinase MEK, with the goal of overcoming MAPK/ERK reactivation (25, 26) (**Figure 1**). This combination demonstrated considerable success, improving median PFS by a further 5 months compared to BRAF inhibition alone, and still with minimal toxicities (25, 26). As such, numerous MEK inhibitors have been developed for clinical use (trametinib, cobimetinib, binimetinib) and dual BRAF and MEK inhibition is now considered the standard-of-care treatment for *BRAF*^{V600} melanoma patients. However, similar to BRAF inhibitor monotherapy, the majority of patients treated with dual BRAF and MEK inhibitors inevitably develop resistance less than a year into treatment (25, 26). As such, further clinical trials are ongoing to examine other molecular targets to treat this disease.

1.1.2 Inhibitors of CDK4/6 as an emerging clinical approach

An emerging target in melanoma is the cyclin-dependent kinases 4 and 6 (CDK4/6). These kinases, which are regulated by type D cyclins, phosphorylate and inhibit the tumor suppressor retinoblastoma protein (RB) (27) (**Figure 1**). RB is a central regulator of G1-S cell cycle transition (28, 29). In its hypophosphorylated form, RB binds to and inhibits E2 transcription factors (E2F), preventing transcription of genes associated with cell cycle progression and entry into S phase (28, 30, 31). Hence, CDK4/6 plays a critical role in cell cycle regulation in G1, through mediation of the phosphorylation status and subsequent function of RB (32, 33) (**Figure 1**). Aberrant activity of CDK4/6 leads to hyperphosphorylated RB, E2F-mediated progression through G1 and uncontrolled cell proliferation – a hallmark of cancer (34). Overactivity of CDK4/6 is commonly due to an inactivating mutation or deletion in the *INK4a* gene

(also known as *CDKN2A*), which encodes the CDK4/6 inhibitor, $p16^{INK4a}$ (35) (**Figure 1**). The $p16^{INK4a}$/CyclinD-CDK4/6/RB axis is dysregulated in numerous cancers, including around 90% of melanomas (36, 37). In many cancers, this is due to loss of function of RB itself, however, in melanoma RB is often functional, and instead aberrant activation of this pathway is predominately driven by a loss of $p16^{INK4a}$ and, subsequently, constitutive CDK4/6 activity (38). Interestingly, the functional loss of $p16^{INK4a}$ and RB appear to be mutually exclusive events in this pathway (31, 34, 39), similar to the activating mutations in MAPK/ERK signaling.

Augmented CDK4/6 activity is observed in many cancers in addition to melanoma, making it an attractive therapeutic target for the treatment of a variety of malignancies (28, 31, 40). The CDK4/6 inhibitor, palbociclib, entered its first clinical trial in 2011 for advanced solid tumors or non-Hodgkins lymphoma and was generally well tolerated (41). Importantly, only patients with tumor types in which RB was functional were recruited to these trials, as CDK4/6 inhibitors rely on the de-repression of functional RB to inhibit E2F and cell cycle progression. Following promising clinical outcomes, palbociclib was FDA approved for the treatment of hormone receptor (HR)-positive, human epidermal growth factor receptor 2 (HER2)-negative breast cancer in 2015 (42). Two other CDK4/6 inhibitors (ribociclib, and abemaciclib) have since been FDA approved and, along with a fourth inhibitor (trilaciblib), continue to be evaluated in numerous clinical trials for various other malignancies, including metastatic melanoma (reviewed in ref. 43).

1.1.3 Combined inhibition of BRAF, MEK and CDK4/6

Downstream of MAPK/ERK signaling, activated ERK translocates to the nucleus and activates a suite of transcription factors (e.g. ETS, ELC1, MYC, STAT1/3), mediating a network of transcriptional changes that promote cell growth, survival and

differentiation (44). Importantly, one of the secondary response genes induced by MAPK/ERK signaling is *CCND1*, which encodes the CDK4/6 binding partner Cyclin D1 (45, 46). MAPK/ERK signaling also functions posttranslationally to mediate assembly of the CyclinD-CDK4/6 complex (47). Hence, MAPK/ERK signaling impinges on the $p16^{INK4a}$/CyclinD-CDK4/6/RB axis downstream (**Figure 1**). Accordingly, aberrant activation of the latter is associated with resistance to MAPK/ERK inhibition. Specifically, elevated expression of Cyclin D1 is associated with resistance to BRAF inhibition in $BRAF^{V600E}$ melanoma, particularly when CDK4 is also overexpressed (48), and a loss of *CDKN2A* expression (indicative of elevated CDK4/6 activity) correlates with poor progression free survival in patients treated with dual BRAF and MEK inhibition (49). Together these observations made CDK4/6 an attractive kinase to target in combination with MAPK/ERK inhibitors. Indeed, a number of preclinical studies have shown synergy of CDK4/6 inhibition with BRAF/MEK inhibitors (50-52). In these studies, combined BRAF and CDK4/6 inhibition overcomes resistance to BRAF inhibitor monotherapy *in vitro* and *in vivo* in pre-clinical xenograft models of human melanoma. The triple combination, however, has not been evaluated *in vivo*, though it has similar efficacy to that of dual BRAF and CDK4/6 inhibition and is superior to dual BRAF and MEK inhibition *in vitro* using human melanoma cell lines (50). Dual inhibition of MEK and CDK4/6 has also shown promise in pre-clinical studies evaluating tumors with elevated MAPK/ERK signaling that is mediated through mechanisms other than mutant BRAF, such as mutations in RAS. For example, this combination has shown synergy in preclinical KRAS mutant colorectal cancer models (53), and is efficacious against a subset of NRAS and other melanoma subtypes (54, 55). Indeed, early clinical trials of dual MEK and CDK4/6 inhibition in NRAS mutant melanoma demonstrated encouraging results (NCT01719380). A phase Ib/II clinical

trial examining the safety and efficacy of combination BRAF and CDK4/6 inhibition was terminated early, though the combination was generally well tolerated (NCT01777776). Clinical trials to assess the triple combination of BRAF, MEK and CDK4/6 inhibition recently began at Massachusetts General Hospital in Boston, USA, and are now underway at the Peter MacCallum Cancer Centre in Victoria, Australia.

1.2 Immune checkpoint inhibitors

In 2011, not only was the first targeted therapy approved for the treatment of melanoma, so too was the first field-changing immunotherapy, ipilimumab. In contrast to targeted therapies, which aim to directly inhibit tumor growth by blocking tumor-intrinsic pathways, immunotherapies aim to activate the host immune system to control and eradicate cancer. Ipilimumab is an immune checkpoint antibody developed against a molecule called cytotoxic T-lymphocyte-associated protein 4 (CTLA-4). CTLA-4 is an inhibitory receptor found on the surface on T cells (56), a critical immune subset required for host anti-tumor immunity, which will be discussed further in section 2. In brief, ipilimumab binds to and blocks the inhibitory activity of CTLA-4, de-repressing anti-tumor T cell immunity (57). In clinical trials, ipilimumab significantly improved median overall survival (OS) from 9.1 months to 11.2 months compared to conventional chemotherapy, and most notably promoted durable tumor control, with significantly improved 3 year survival probability (58, 59). This led to FDA approval of ipilimumab for the treatment of metastatic melanoma in 2011.

Prior to the success of ipilimumab in melanoma, the potential of immune-based therapies to treat cancer was under-appreciated. Melanoma was the first malignancy to demonstrate a notable and measurable benefit from immunotherapy (59). This profoundly reshaped our understanding of the role of immunity in cancer and generated

considerable interest in the use of immunotherapies to treat, not only melanoma, but all cancers. In 2014 a second immune checkpoint inhibitor, nivolumab, entered the clinic. Similar to ipilimumab, nivolumab de-represses T cell immunity, but achieves this through targeting another inhibitory receptor on T cells, programmed cell death protein 1 (PD-1) (57), which will be discussed further in section 2.2.2. The discovery that PD-1 was a negative regulator of anti-tumor immunity led to a series of preclinical studies and clinical trials demonstrating that blockade of PD-1 could be used as a cancer therapy for the treatment of melanoma and other cancers (reviewed in 60, 61). In a seminal phase III clinical trial (CheckMate-066), nivolumab significantly improved PFS of melanoma patients compared to chemotherapy, from 2.2 months to 5.1 months (median OS not reached), and similar to ipilimumab, promoted durable tumor control (62). Anti-PD-1 therapies also compared favorably to ipilimumab in regards to both efficacy and tolerability (63, 64). Together these trials prompted FDA approval of two anti-PD-1 monoclonal antibodies, nivolumab and pembrolizumab, as standard-of-care treatments for refractory and unresectable melanoma, and for evaluation in a number of other malignancies (65). More recent trials have shown superior anti-tumor efficacy with the dual combination of CTLA-4 and PD-1 blockade in melanoma, with a striking five-year overall survival of 52% (63, 66, 67). This suggests concurrent administration may be a beneficial therapeutic strategy; though this combination has an increased risk of toxicities (63, 66). Overall, the advent of CTLA-4 and PD-1 immune checkpoint inhibitors dramatically shifted the field of cancer therapeutics, earning the 2018 Nobel Prize in Physiology and Medicine, and prompting the inclusion of immune evasion as a hallmark of cancer.

1.3 Limitations of existing therapies

Despite such remarkable therapeutic advances, prognosis for patients with late stage melanoma remains poor. While targeted therapies improve survival in almost all patients treated, a minority receive long-term benefits due to the eventual emergence of drug resistance (68, 69). Combinatorial targeted therapy strategies are currently being developed with a goal to overcome this. However, tumors are inherently highly adaptable and therefore targeting tumor-intrinsic pathways rarely leads to durable tumor regression. Immunotherapies, on the other hand, work by engaging a host immune response to the cancer, and the immune system is arguably the only anti-cancer tool that is equally as adaptable as the tumor itself. This is reflected in the clinical response to immune checkpoint blockade, where the majority of patients who initially respond to these therapies continue to respond and achieve long-term sustained tumor regression (70). Such durable responses may be attributed to the adaptability of the immune system in efficiently controlling cancer through a variety of mechanisms in a way that tumor-directed drugs often cannot. However, in contrast to targeted therapy, only a minority of patients respond to immune checkpoint blockade (58, 59, 62). The reasons for this remain unclear and will be discussed further in sections 2.2 and 2.3. Additionally, while PD-1 blockade is generally well tolerated, toxicity can be high in select patients and in some cases fatal, and the toxicity profile of CTLA-4 blockade is even higher (71, 72). The risk of adverse events to immune checkpoint inhibitors, along with a significantly high cost of administering these therapies (73), highlights a pressing need to better understand and predict which patients are most likely to respond, so that therapy choice and timing can be personalized.

The short-lived responses to targeted therapy and the low overall response rates to immunotherapies means that many melanoma patients inevitably receive both of

these therapeutic classes some time throughout the duration of their treatment. For example, a patient who progresses on targeted therapy may be switched to an immunotherapy as a second line of treatment. However, while the clinical success of targeted therapies is attributable to tumor-intrinsic inhibitory mechanisms, it is now clear that these therapies also modulate anti-tumor immunity. The immunomodulatory activity of targeted therapies, and the potential of combined targeted therapy and immunotherapy approaches will be discussed in section 3.

2. Cancer immunity and the tumor immune microenvironment

Host immunity plays an essential role in the recognition and eradication of malignant cells in a process referred to as 'immunosurveillance'. Immunosurveillance comprises three fundamental stages; tumor elimination, equilibrium and tumor escape (74). In the first stage, cells that have undergone malignant transformation may be recognized by the host immune system and eradicated, in a process that prevents tumor establishment and progression. In melanoma, it is likely that this early phase of immunosurveillance contributes to the spontaneous regression of primary lesions observed in the clinic (75). During the equilibrium stage, tumor cells, under extreme pressure from the immune system, undergo a process known as 'immunoediting' (76, 77), whereby they acquire genetic and transcriptional alterations to evade immune attack. The third stage, tumor escape, occurs when tumor cells have accumulated sufficient mechanisms to evade host immunity, leading to escape from immune control and subsequent tumor progression. A failure in effective immunosurveillance and eventual tumor immune escape is a major mechanism that drives tumor progression and metastatic disease in melanoma patients (78). The role of the immune system in the

defense against melanoma, and cancer more broadly, will be discussed in the following sections.

2.1 The Cancer Immunity Cycle

2.1.1 Control of early malignancy by the innate immune system

The innate immune system is the first line of defense against host cells that undergo malignant transformation. Innate immunity is orchestrated by a multitude of immune cell types that join forces to rapidly eliminate newly transformed cells. Key to this early immunosurveillance are natural killer (NK) cells; a type of cytotoxic lymphocyte that is able to recognize and destroy malignant cells, including melanoma cells (79-82), and prevent tumor progression. NK cells interact directly with potential target cells through formation of an immunological synapse, where a complex balance of multiple inhibitory and activatory signals triggered by cognate ligands on the tumor cell directs NK cell activity (83). If activated, NK cells kill both directly, through the release of cytotoxic granules (containing perforin and granzymes) into the target to initiate cell death, and indirectly, through the secretion of cytotoxic and inflammatory factors (e.g. TNFα and IFNγ) (84). However, melanoma cells often avoid NK cell attack by modulating NK cell receptor ligand expression (85). Indeed, impaired NK cell function is associated with advanced disease and poor prognosis in melanoma, while NK cell infiltration and activity in tumors is associated with a more positive outcome (86). Furthermore, a high NK cell signature in either the primary tumor or metastatic lesions of melanoma patients is predictive of improved survival (87, 88), underscoring the essential role of NK cells in the control of melanoma.

Macrophages are also a critical component of early tumor immunosurveillance, but have the unique potential to differentiate into subsets that can either attenuate or

promote tumor progression. Macrophages are found as resident cells in many tissues, including skin (89), and are therefore present during early melanoma development, although they can also be recruited during the later stages of tumorigenesis. Tumor-associated macrophages (TAMs) are involved in all stages of melanoma progression, and serve a key role in regulating the network of interactions between melanoma cells and the diverse cell types that comprise the tumor immune microenvironment (90). Under various stimuli, macrophages can polarize into two distinct subtypes; classically activated macrophages (M1), and alternatively activated macrophages (M2). Under the influence of a dysfunctional tumor secretome, macrophages commonly polarize into a pro-tumoral M2-like phenotype, secreting factors that promote tumor growth, angiogenesis and cancer metastasis, and inhibit anti-tumor immunity (91). Accordingly, M2 TAMs are key mediators of early cancer progression, and their presence is most often associated with poor clinical outcomes in melanoma and many other cancer types (92, 93). In contrast however, TAMs that adopt a pro-inflammatory M1-like phenotype play a critical role in potentiating anti-tumor immunity through phagocytosis and production of pro-inflammatory cytokines and chemokines that facilitate the recruitment of other immune subsets (93, 94). As such, the ratio of M1/M2 TAMs is considered a superior biomarker than total TAMs for prognosis in melanoma and other cancers (92, 95, 96). Indeed, a higher ratio of M1/M2 TAMs is strongly associated with less aggressive tumors and better overall survival in the clinic (94, 97), highlighting that the type of TAMs, rather than the abundance of TAMs, dictates their role in anti-tumor immunity.

When these critical innate cells fail to restrain tumor development as a first line of defense, the adaptive immune system, along with other components of the innate immune system, mounts a more specific wave of defense in an attempt to prevent

further tumor development (98). This arm of the immune system involves the intricately coordinated actions of multiple cell types with unique functions, starting with the uptake of tumor antigens by a specialized antigen presenting cell, the dendritic cell.

2.1.2 Tumor antigens and initiation of the adaptive immune response

For effective initiation of adaptive immunity, tumor antigens that uniquely identify a malignantly transformed host cell as foreign, need to be captured and presented to cytotoxic T lymphocytes of the adaptive immune system. Throughout tumorigenesis, tumor cells accumulate mutations that often give rise to neoantigens, which are new antigens not previously encountered by the immune system (99). Such neoantigens confer 'immunogenicity' to the tumor, which is essential for the tumor cells to be recognized as foreign and elicit an adaptive immune response. Melanoma cells harbor the highest mutational burden of all cancer types, acquiring more than one hundred mutations per megabase (100) due to chronic exposure to DNA-damaging UV radiation. This qualifies melanoma as one of the most immunogenic malignancies on the neoantigen spectrum (101). In addition to neoantigens that arise through somatic mutations, other common antigens that confer immunogenicity to melanoma cells include melanoma associated antigens, such as MART-1 and gp100, and cancer-testis antigens, including NY-ESO-1 (reviewed in 102).

During tumor establishment and growth, a lack of adequate nutrients, coupled with harsh hypoxic conditions and innate immune attack, leads to a significant amount of tumor cell death. As a result, tumor antigens are 'shed' into the tumor microenvironment where they are taken up by dendritic cells (DCs) (103). Inside the DC, antigens are processed into peptides, assembled onto major histocompatibility complex (MHC) molecules and presented on the surface of the cell (104, 105). Following antigen uptake at the tumor site, DCs then migrate to the draining lymph

nodes, where they present these tumor peptides to cells of the adaptive immune system and play an essential role in the initiation of an anti-tumor T cell response, which is discussed further in section 2.1.3. DCs exist in diverse and complex subsets, but are broadly defined under two main categories; conventional DCs (cDCs) and plasmacytoid DCs (pDCs) (106). While both subsets are resident in lymphoid tissues, cDCs can also be classified as non-lymphoid, and this variety is most commonly associated with the tumor microenvironment (106, 107). A particular subset of non-lymphoid DC, identified by the expression of CD103, is implicated as the critical subset involved in tumor antigen cross-presentation and T cell activation in melanoma and other cancer types (108). As a result, a CD103+ DC-associated signature is a strong prognostic indicator across a number of tumor types (108). In addition to priming new anti-tumor T cell responses, CD103+ DCs also possess the unique ability to further stimulate previously activated T cells. Hence, CD103+ DCs play a critical role in both the initiation of T cell immunity in lymph nodes, and the maintenance of adaptive T cell immunity at the tumor site.

2.1.3 Tumor-specific adaptive immunity

T cells of the adaptive immune system can be broadly defined by the expression of CD4 or CD8, with CD8+ cytotoxic T lymphocytes (CTLs) considered to be the principle effector cells in anti-tumor immunity. The presence of tumor infiltrating lymphocytes (TILs), which includes CTLs, positively correlates with disease outcome in a number of cancer types (109-112), including melanoma (113). Unlike cytotoxic lymphocytes of the innate immune system, such as NK cells, CTLs are highly specific and only carry out cytotoxic function when they recognize cognate antigen on a target cell via their unique T cell receptor (TCR). Naïve CD8+ T cells exhibit a vast repertoire of unique TCRs specific for a single antigen. During development in the thymus, CD8+

T cells undergo a strict selection process to select for TCRs that do not recognize self-antigens (114), restricting their activity to antigens from foreign pathogens or damaged cells, such as tumor cells that express neoantigens. Naïve CD8+ T cells circulate through the lymphatic system and interact with antigen presenting cells (APCs), primarily DCs, in the lymph node, forming an immunological synapse with the APC where they scan for their specific antigen. Upon antigen recognition, a naïve CD8+ T cell is activated, and undergoes a process known as clonal expansion, where the cell massively proliferates to produce an army of CTLs specific for that particular antigen. Efficient activation and expansion of CD8+ T cells requires three signals; 1) the recognition of foreign or tumor antigens presented on MHC Class I (MHC I) molecules on the surface of the APC (115), 2) co-stimulation from the ligands, CD80 (B7-1) and CD86 (B7-2), also expressed on the surface of the APC, and 3) inflammatory cytokines, such as IL-12 and Type I interferons, that are secreted by the APC (116, 117).

Upon activation, tumor-specific naïve CD8+ T cells undergo significant transcriptional and epigenetic reprogramming to become cytotoxic effector T cells that exit the lymphoid organs and traffic to the site of the tumor; a process that relies on the expression of a suite of adhesion molecules and chemokine receptors (118). For example, L-selectin (also known as CD62L), a lymph node-homing molecule, is expressed at high levels on the surface of naïve CD8+ T cells and is downregulated following T cell activation to allow T cells to exit the lymph node (119). Once out of the lymph node, other adhesion molecules are subsequently upregulated to mediate exit from circulation and into the periphery (120, 121). Activated CTLs also upregulate several chemokine receptors, such as CXCR3 and CCR5, to facilitate chemokine-mediated recruitment to the tumor site, with CXCR3 one of the major chemokine receptors expressed by activated TILs in melanoma (122, 123). Accordingly, as with

many human cancers, the prognosis of melanoma is heavily influenced by the intratumoral production of chemokines that promote the recruitment of effector CTLs (124). Once at the tumor site, CTLs carry out their effector functions similar to NK cells, by forming an immunological synapse with target tumor cells and killing directly via the perforin-granzyme pathway (125), or indirectly through the secretion of cytotoxic molecules, such as TNFα, or inflammatory cytokines, such as IFNγ. IFNγ plays a critical role in enhancing T cell killing by altering tumor-intrinsic pathways that lead to upregulation of MHC I and other immunomodulatory molecules that infer susceptibility to immune attack (126). Indeed, genetic mutations that confer resistance to IFNγ are commonly found in melanoma, leading to impaired anti-tumor immunity by rendering melanoma cells insensitive to T cell killing (127).

Optimal anti-tumor immunity also relies on the activity of a class of CD4+ T lymphocytes known as T helper (Th) cells. Th cells differentiate into a range of subsets, including Th1, Th2 and Th17 cells, and predominately contribute to anti-tumor immunity by supporting cytotoxic CD8+ T cell immunity. Th cells achieve this through various mechanisms, including enhancing CTL activation and function via the production of cytokines such as IL-2 (128), and enhancing the capacity of DCs to promote CTL activity (129). Similar to Th cells, B lymphocytes are another component of the adaptive immune response that can promote the activity of CTLs (reviewed in 130). Notably, intratumoral B cells secrete inflammatory factors and chemokines that recruit T cells to the tumor site, and cross-present tumor antigens to stimulate T cell responses within the tumor microenvironment. Indeed, the presence of B cells in melanoma tumors is a predictive marker for survival and responses to immunotherapy (131-133).

2.1.4 Immunosuppression in the tumor microenvironment

The presence of immunosuppressive immune cell subsets is a major barrier to effective anti-tumor immunity in solid cancers, and melanoma in particular has an extremely immunosuppressive microenvironment (134). As discussed in section 2.1.2, melanoma is highly immunogenic, and is therefore subject to extreme immune pressure during the equilibrium phase of immunosurveillance. As a result, these tumors adopt effective mechanisms of immune evasion in order to avoid elimination by the immune system, including secreting factors that promote the differentiation or recruitment of immunosuppressive immune subsets into the tumor microenvironment (134, 135).

In addition to M2 TAMs, which were discussed in section 2.1.1, two other major immune subsets contribute to immunosuppression within the tumor microenvironment; T regulatory cells (Tregs) and myeloid-derived suppressor cells (MDSC). In a non-pathological setting, Tregs, which are defined by the expression of CD4, CD25 and FOXP3, play a critical role in immune homeostasis by restraining immunity and preventing self-reactive or overactive immune responses (136). Tregs exert their immunosuppressive effects through complex contact-dependent and contact-independent mechanisms that are still being elucidated (137). Accumulation of Tregs in melanoma is frequently observed (138) and the ratio of CD8+ T cells versus Treg in the tumor microenvironment is predictive for survival of patients with melanoma (139). Tregs are recruited to the tumor site in response to tumor production of pro-inflammatory chemokines, including CCL5, CCL22, CCL28, S1P and CXCL12 (140-147), and immunosuppressive cytokines in the tumor microenvironment, such as IL-10 and TGFB, also promote the differentiation of Tregs (148).

MDSCs are an immunosuppressive cellular subset of myeloid lineage, primarily recruited to tumors via tumor cell secretion of the chemoattractants CCL2 and CCL5

(149-151). There are two main types of MDSCs; polymorphonuclear (PMN)-MDSC, which are the predominate subset found in lymphoid tissues, and monocytic (M)-MDSC, the subset most commonly found in tumors (152). Immunosuppression driven by myeloid dysfunction is a hallmark of cancer immunity, and MDSCs within tumors are pathologically activated and potently immunosuppressive (152, 153). They promote tumor progression through metabolic changes that suppress T cell immunity, secretion of chemokines that attract immunosuppressive Tregs (e.g. CCL4 and CCL5), and through the expression of PD-L1, the ligand for the inhibitor receptor PD-1 on T cells (152, 154, 155). MDSCs are also an immature cell type that can rapidly differentiate into immunosuppressive M2 TAMs (152).

The composition of the tumor immune microenvironment therefore heavily influences the magnitude of an anti-tumor immune response, and as such, plays a critical role in the success of immunotherapies such as immune checkpoint blockade.

2.2 Using immune checkpoint blockade to enhance anti-tumor T cell immunity

Immune checkpoints are regulatory mechanisms that are essential to maintain immune homeostasis and fine-tune immune responses during infection. Two examples of T cell immune checkpoint regulators are cytotoxic T-lymphocyte-associated protein 4 (CTLA-4) and programmed cell death protein 1 (PD-1). They exert their biological effect at distinct times during the T cell response to ensure that adaptive immunity effectively protects the body from pathogens, while preserving self-tolerance and preventing autoimmunity. In the setting of tumor pathology however, engagement of immune checkpoints contributes to tumor immune evasion, and hence, blocking the activity of these receptors can improve anti-tumor immune responses. Both CTLA-4 and PD-1/PD-L1 are FDA approved targets for immune checkpoint blockade.

Antibodies that block these molecules have revolutionized cancer treatment, and are an approved standard-of-care therapy for melanoma. The mechanisms underpinning the success of these therapies will be discussed in the following sections.

2.2.1 CTLA-4 checkpoint blockade

CTLA-4 was first discovered in 1987 (156), but its role as an immune checkpoint for regulating T cell activity was not uncovered until 1994 (157, 158). CTLA-4 prevents T cell activation at the priming phase, when naïve T cells interact with antigen presenting cells. As described in section 2.1.3, CD8+ T cell activation requires T cell receptor recognition of cognate antigen presented on MHC I and co-stimulation through binding of CD28 on T cells with its co-stimulatory ligands, B7-1 and B7-2, on the antigen presenting cell. This activation leads to upregulation of CTLA-4, which subsequently outcompetes CD28 for B7 binding due to a higher affinity interaction (159) (**Figure 2**), thereby negatively regulating T cell activation and proliferation (160). In addition to directly antagonizing CD28, CTLA-4 also interferes with T cell-APC conjugate formation through modification of the cytoskeleton (161, 162), and also recruits other inhibitory signaling molecules to the immunological synapse (163). This ultimately dampens the activity of several transcription factors that promote T cell proliferation, effector function and survival, including NFAT, AP-1 and NF-κB (163).

Less than a year after its discovery as an immune checkpoint, a seminal study showed that antibody blockade of CTLA-4 could be used to promote immune-mediated tumor rejection (56). CTLA-4 blockade has since shown efficacy in a number of preclinical tumor models (reviewed in 164). The primary mechanism is thought to be direct de-repression of CD8+ T cell activity by blocking CTLA-4 antagonism of CD28 (**Figure 2**). However, recent studies have demonstrated that CTLA-4 blockade has

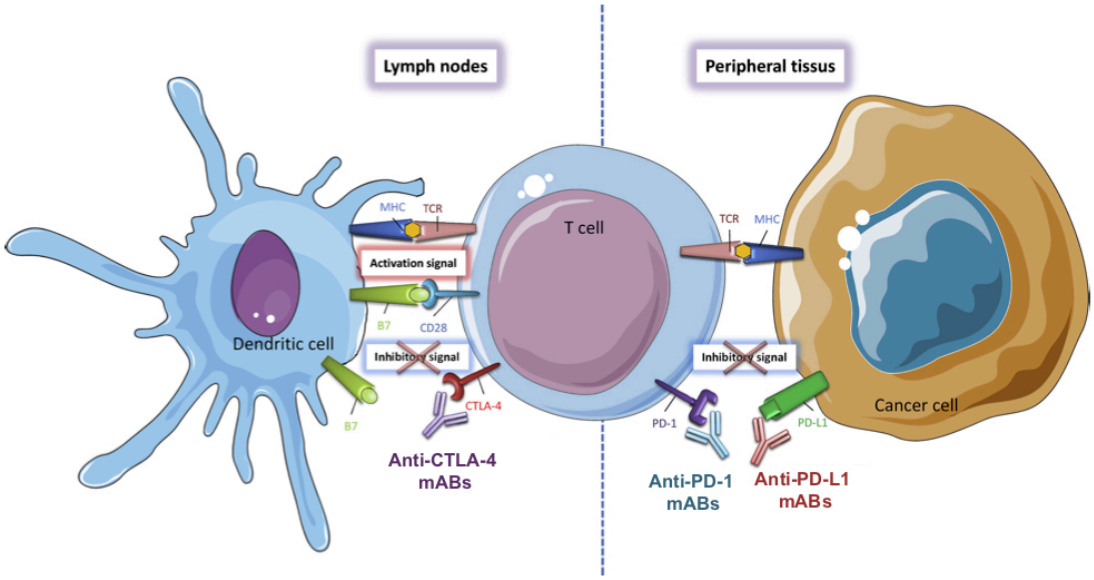

Figure 2 – Mechanisms of CTLA-4 and PD-1 immune checkpoint blockade. T cells interact and form an immunological synapse with dendritic cells in the lymph node and with tumor cells in peripheral tissue. In the lymph node, T cells become activated through TCR-mediate recognition of antigen presented on MHC, and co-stimulation through CD28 ligation to B7. CTLA-4 also binds to B7 and mediates inhibitory signaling, which restrains T cell activation. In the periphery, T cells recognize tumors through TCR binding to antigen presented on MHC. PD-1 expressed by activated T cells binds to PD-L1 expressed on tumor cells and mediates inhibitory signaling, which dampens T cell effector function. Blockade of CTLA-4 or PD-1 using monoclonal antibody therapies de-represses T cell activity through blocking inhibitory signals that, respectively, promote T cell priming in the lymph node or enhance effector function in the periphery. Figure adapted from Desnoyer et al., 2020 (171).

multiple anti-tumor effects, including the reversal of Treg mediated immunosuppression (165). CTLA-4 is constitutively expressed on Tregs and contributes to their regulatory and immunosuppressive action through multiple mechanisms (166, 167). CTLA-4 expression on Tregs is much higher than that of CD8+ T cells, and as a result, CTLA-4 antibodies bind Tregs in high amounts and consequently promote their depletion via NK-mediated antibody-dependent cell-mediated toxicity (168).

While CTLA-4 blockade showed efficacy in numerous tumor models, this was largely dependent on the stage of disease and tumor burden (169). In addition, less

immunogenic cancers, including the B16 melanoma model, demonstrated limited responses (170). However, despite mixed success in preclinical studies, anti-CTLA-4 therapy proved more effective in clinical trials, leading to the FDA approval of the first CTLA-4 blocking antibody, ipilimumab, in 2011 for unresectable late stage melanoma.

2.2.2 PD-1 checkpoint blockade

PD-1 was identified as a negative regulator of T cell activation in 1999 when it was discovered that loss of the mouse PD-1 orthologue, *Pdcd1*, caused severe autoimmunity (172). Unlike CTLA-4, which exerts its regulatory effect predominantly at the priming phase between T cells and APCs, PD-1 functions at the effector phase of the T cell response (173) (**Figure 2**). PD-1 expression is up-regulated on T cells following TCR stimulation, and binds to the B7 homologues, PD-L1 and PD-L2, which are constitutively expressed on antigen presenting cells, but can be induced on non-immune cells by pro-inflammatory cytokines such as IFNγ (174). PD-1 primarily functions by dampening TCR signaling through the tyrosine phosphatase, SHP2, which attenuates T cell activity by dephosphorylating proximal signaling molecules downstream of TCR ligation (175). PD-1 also restrains immune responses through the inhibition of intracellular signaling mediated through CD28 (176), similar to CTLA-4.

Since the advent and ensuing success of anti-PD-1/PD-L1 as a cancer immunotherapy, the mechanisms of action continue to be explored. While originally thought to simply re-invigorate T cells with high expression of PD-1 within the tumor microenvironment, a recent study found that the success of anti-PD-1 therapy relied on the clonal replacement of these cells through the recruitment of new T cells into the tumor microenvironment (177). Indeed, evidence suggests that myeloid-derived T cell chemoattractants are required for anti-PD-1 efficacy (94, 178), further supporting the importance of T cell recruitment for the success of this immunotherapy. Further, T cells

exist across a spectrum of functional and dysfunctional states, and it is proposed that these different states vary in their capacity to respond anti-PD-1 therapy. The various functional states of T cells and their role in anti-tumor immunity and responses to immune checkpoint blockade will be discussed in the next section.

2.3 T cell effector, memory and dysfunctional states in anti-tumor immunity

T cell dysfunction in the tumor microenvironment is a major barrier to effective anti-tumor immunity, and is an area of considerable research interest. Much of our understanding of T cell differentiation and functional states has historically come from examining T cell responses in acute and chronic infectious disease models, and has only recently been applied to tumor immunology. During acute infection, the T cell response is tri-phasic, with an initial expansion phase following antigen encounter, a contraction phase where the infection is cleared and antigen-specific T cells are eliminated by apoptosis, and a memory phase, where a subset of antigen-specific T cells remain in a quiescent state poised to rapidly re-initiate a response upon antigen re-encounter. However, in a chronic infection setting, inflammation and persistent antigen exposure leads to progressive loss of effector function, and a dysfunctional state referred to as T cell ‘exhaustion’ (reviewed in 179). In solid tumors, T cell exposure to chronic inflammation, harsh metabolic conditions and persistent antigen exposure leads to a dysfunctional T cell state analogous to that observed in chronic infections (180, 181).

Exhausted T cells are considered ‘hypofunctional’ effector T cells due to impaired cytotoxic function and a reduced capacity to secrete cytokines, although this definition is still being debated (182). These cells express high levels of inhibitory receptors (such as PD-1 and CTLA-4), which further induce T cell dysfunction (179). For example, the PD-1/PD-L1 axis plays a unique role in controlling prolonged T cell

activation and fate determination in the later stages of an immune response, and ligation of PD-1 induces downstream signaling that contributes to an exhaustion phenotype (179). Melanoma cells, as well as other tumor cells, further exploit this mechanism by upregulating PD-1 ligands to promote T cell dysfunction and generate a tumor microenvironment that facilitates tumor growth and invasion (183).

The transcriptional landscape of T cell exhaustion parallels that seen in other dysfunctional states, such as anergy and tolerance (184). The term 'dysfunction', however, is widely debated, as the cellular programs that induce these states are considered to be physiologically normal feedback mechanisms that are in place to prevent immune over-reactivity (185). In fact, many of the transcription factors that initially drive T cell activity subsequently participate in these feedback loops. An example is the NFAT family of transcription factors, which regulate the expression of key genes associated with T cell activation and effector function, such as *Ifng* and *Il2 (186, 187)*. However, depending on the type and duration of TCR stimulation, and whether or not there is concomitant activation of AP-1 transcription factors, NFAT can also act as a key mediator of T cell exhaustion by promoting the expression of inhibitory receptors, including PD-1 (188). While PD-1 checkpoint blockade was originally thought to re-invigorate exhausted T cells, recent studies suggest that T cell exhaustion does not represent a reversible loss of function, but is rather a stable and distinct state of terminal differentiation (185, 189-191). The advent of modern technologies, including single-cell transcriptomics, has also provided new molecular insights into the heterogenous nature of T cells found in melanoma and other tumor types (131, 192). As a result, it is now appreciated that the intratumoral CD8+ T cell pool comprises a spectrum of phenotypic states, which all vary in their capacity to carry out effector functions and respond to checkpoint blockade therapy.

T cells with stem or memory-like properties, which sit at the opposite end of the spectrum to exhaustion, have recently gained attention as critical subsets required for sustained anti-tumor activity (180, 193, 194). Memory T cells exist in a quiescent state, similar to naïve T cells. However, unlike naïve cells, memory T cells exhibit a unique epigenetic landscape in which effector response genes are 'poised' for transcription (195). As such, these cells are epigenetically programmed to respond rapidly to antigen re-encounter. Bona fide T cell memory implies the absence of antigen, complicating their precise definition in tumor immunology. In tumors, terms like 'progenitor' and 'stem-like' are often used to define T cell subsets with memory-like features, such as enhanced capacity for long-term survival and self-renewal. For example, an intratumoral subpopulation of 'progenitor exhausted' T cells, characterized by co-expression of PD-1 and TCF-1, persist long-term and demonstrate superior capacity for self-renewal and differentiation in response to immune checkpoint blockade (180, 196, 197). Indeed, higher numbers of these 'progenitor exhausted' cells correlate with favorable clinical responses to immune checkpoint blockade in melanoma patients (180). Similarly, less differentiated 'stem like' T cell subsets in the tumor microenvironment can reconstitute a phenotypically diverse T cell compartment while retaining the capacity for self-renewal (198). These memory-like T cells subsets within the tumor microenvironment are implicated as the primary responders to immune checkpoint blockade and are the key mediators of long-term anti-tumor immunity (180, 193, 197-199).

Both T cell dysfunction and stemness are governed by diverse transcriptional and epigenetic regulatory networks (200), and targeting these networks to direct T cell fate and improve responses to immunotherapy will be the next challenge in melanoma research. In the meantime, immune checkpoint blockade continues to be approved for a

growing number of cancer types in addition to melanoma (201). Thousands of clinical trials are underway to test the efficacy of these checkpoint inhibitors either alone, or in combination with other anti-cancer agents. Indeed, the incorporation of immune checkpoint blockade with targeted therapies for the treatment of melanoma is an emerging area of clinical interest, and will be discussed in the following sections.

3. Targeted therapies and the immune system

While the rationale behind targeted therapies is to inhibit intrinsic mechanisms of tumorigenesis, many oncogenic targets, including BRAF, MEK and CDK4/6, are also involved in immune signaling pathways, in both malignant cells and healthy immune cells. Indeed, there is now considerable evidence implicating a role for host immunity in the efficacy of these targeted therapies, which will be the focus of the following sections.

3.1 Immunomodulation by BRAF and MEK inhibitors

Tumors are notorious for evolving mechanisms to avoid immune surveillance, and oncogenic BRAF in melanoma cells can induce changes that facilitate tumor immune escape. For example, activated MAPK/ERK signaling via oncogenic BRAF is associated with tumor cell production of immunosuppressive cytokines (VEGF, IL-6, IL-10) and downregulation of MHC I, which leads to impairment of DC maturation, reduced T cell recognition and recruitment of suppressive MDSCs and Tregs into the tumor microenvironment (202-204) (**Figure 3)**. Conversely, BRAF inhibition is associated with significant immunological changes in the tumor microenvironment that are generally considered favorable for anti-tumor immunity. These changes include increased tumor infiltrating lymphocytes (TILs) (205-207), a higher ratio of cytotoxic T

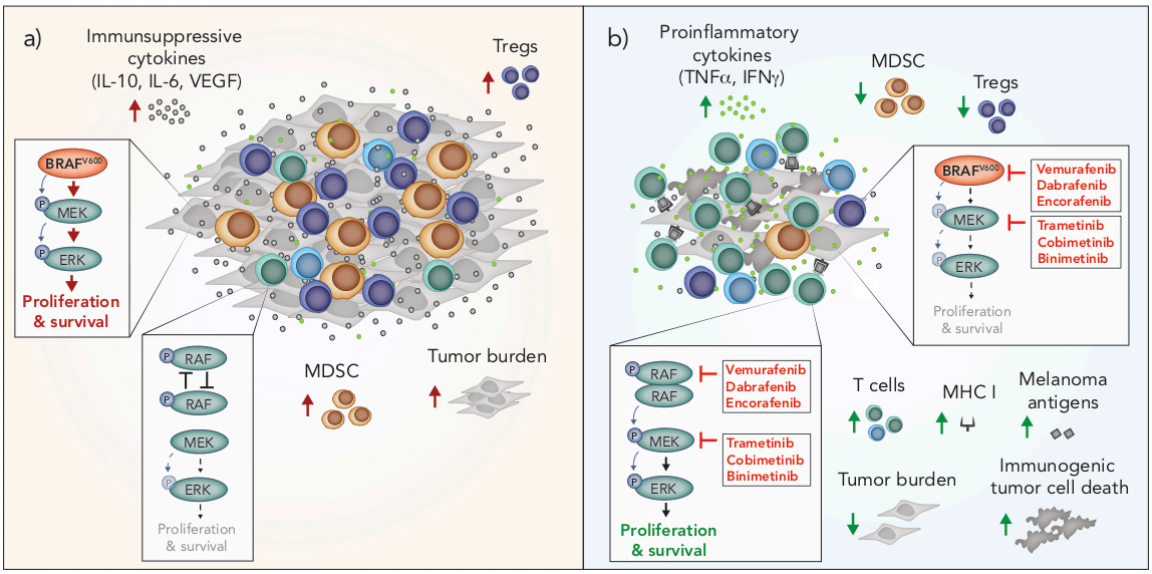

Figure 3 – Immunomodulation by oncogenic BRAF and inhibitors of BRAF/MEK in melanoma. a) *BRAF*^{V600} promotes tumor progression through tumor-intrinsic activation of MAPK/ERK signaling and increased production of immunosuppressive cytokines. MAPK/ERK signaling via oncogenic *BRAF*^{V600} is associated with increased frequencies of Tregs and MDSCs in the tumor microenvironment. In T cells, RAF is not overactive and there is no aberrant MAPK/ERK signaling. b) BRAF and MEK inhibition blocks MAPK/ERK signaling in *BRAF*^{V600} tumor cells and induces immunogenic cell death. Inhibition of MAPK/ERK promotes the upregulation of MHC I and expression of melanoma associated antigens by tumor cells, and is associated with increased frequencies of T cells and pro-inflammatory cytokines in the tumor microenvironment. BRAF inhibition is also associated with a reduction in intratumoral immunosuppressive cells including Tregs and MDSCs. In T cells and other cells with wild type BRAF, BRAF inhibition promotes paradoxical MAPK/ERK activation through RAF dimerization and dimer-dependent enzyme transactivation, enhancing the proliferation and survival of these cells. MDSC – myeloid derived suppressor cell, Treg – Regulatory T cell.

cells to regulatory T cells (205), up-regulation of MHC expression on tumor cells and enhanced presentation of melanoma-associated neo-antigens (203, 207, 208), increased production of IFN-γ and TNF-α (205) and reduced production of immunosuppressive cytokines, such as IL-6, IL-10 and VEGF (202, 207) (**Figure 3**). Interestingly, resistance to BRAF inhibition is associated with a reversal of these immune-potentiating effects, with a loss of TILs and induction of T cell exhaustion markers, including PD-1 (205, 206).

While BRAF inhibition can result in favorable changes in the tumor immune microenvironment due to tumor intrinsic effects, these inhibitors also have direct effects on lymphocytes and other immune cells. In the absence of mutant BRAF, BRAFi has been shown to paradoxically activate the MAPK/ERK pathway by promoting RAF dimerization and dimer-dependent enzyme transactivation (209-211) (**Figure 3**). This paradoxical activation has been observed in T cells (212), NK cells (213) and macrophages (214). MAPK/ERK paradoxical activation in T and NK cells is associated with a favorable anti-tumor response due to the resulting increase in proliferation of these cytotoxic lymphocytes. In contrast, paradoxical activation in macrophages leads to the production of VEGF, which promotes tumor growth and resistance to BRAF inhibition (214).

Unlike BRAFi, which are designed to selectively inhibit oncogenic BRAF in melanoma, MEK inhibitors (MEKi) are designed to target wild type MEK, which is universal across melanoma and other cell types. In cells with wild type BRAF, the addition of a MEKi reduces BRAFi-induced MAPK/ERK paradoxical activation (215). Early *in vitro* studies of the effects of MEK inhibition on the immune system raised concerns that that this inhibitor would dampen the immune response to melanoma. Specifically, MEK inhibition was shown to reduce T cell proliferation, the percentage of cytokine-producing T cells, antigen-specific T cell expansion and cross presentation by dendritic cells (216). However, clinical results of combined BRAF and MEK inhibition were striking, not only due to significantly enhanced progression free survival, but also because the addition of a MEKi unexpectedly lowered the toxicity profile compared to BRAFi monotherapy (215); a phenomenon rarely seen in combination therapy approaches. This effect has been attributed to MEKi offsetting the immune stimulatory effects of BRAF inhibition (215). Interestingly, MEK inhibition

also enhances the persistence of tumor infiltrating immune cells, prolonging anti-tumor T cell immunity (217), and may hence delay or prevent the loss of T cells seen during the development of BRAFi resistance. BRAF inhibition also causes an influx of regulatory T cells and myeloid suppressor cells into the tumor, and the addition of a MEKi appears to reverse this, leading to a more favorable tumor microenvironment (218) (**Figure 3**). Recently, dual BRAF plus MEK inhibition was also shown to induce anti-tumor immunity via the induction of pyroptosis; a type of inflammatory cell death that promotes dendritic cell activation and subsequent T cell immunity (219). Interestingly, a number of melanoma patients treated with the combination of BRAFi and MEKi have achieved durable and ongoing tumor regression (220). Given the impact of these inhibitors on the immune system, it is reasonable to question how much of this response is attributable to tumor-intrinsic effects, and how much is dependent on a favorable shift in anti-tumor immunity.

3.2 Immunomodulation by CDK4/6 inhibitors

Until recently, the immunomodulatory effects of CDK4/6 inhibition (CDK4/6i) were entirely unexplored. This changed rapidly in 2017 when a seminal study uncovered a role for CDK4/6i in augmenting anti-tumor immunity (221), prompting a spate of further studies in this area (222-225). Importantly, using various syngeneic mouse models, many of these studies showed that the efficacy of CDK4/6i is partially, or entirely abrogated, when the immune system is compromised. The immunomodulatory effects of CDK4/6i are multi-faceted and complex, and still not fully understood. Proposed mechanisms include both tumor-intrinsic effects, which indirectly modulate immunity, as well as direct effects on cells of the immune system, both of which likely contribute to significant remodeling of the tumor immune microenvironment.

3.2.1 Tumor-intrinsic immunomodulatory effects of CDK4/6 inhibition

One of the most well-defined mechanisms by which CDK4/6 inhibition augments anti-tumor immunity is through enhancing the immunogenicity of tumor cells. Most notably, CDK4/6 inhibition increases expression of antigen presenting genes (H2d1, H2k1, B2m, Erap1, Tap1, Tap2) and surface expression of MHC I and MHC II in several mouse and human breast and colon carcinoma pre-clinical models (221, 222, 226) (**Figure 4**). Likewise, elevated *CCND1* expression (encoding the CDK4/6 binding partner, Cyclin D1) is associated with lower expression of MHC I genes in breast cancer patients (221, 227). Less is known about the effects of CDK4/6 inhibition on melanoma cells, however, an increase in MHC I in the mouse melanoma cell line B16-OVA in response to CDK4/6 inhibition has been reported, which led to enhanced T cell recognition *in vitro* (221). In breast cancer preclinical models and patients, induction of tumor-intrinsic interferon signaling is observed in response to CDK4/6 inhibition, which may enhance tumor immunogenicity by promoting increased secretion of T cell chemoattractants and expression of costimulatory genes (221) (**Figure 4**). This increased interferon signaling is reportedly due to suppression of DNA methyltransferase, DNMT1, (an E2F target gene), which reduces methylation of endogenous retroviral genes, thereby promoting their expression and inducing viral mimicry (221) (**Figure 4**). Interestingly, tumor immunogenicity in response to CDK4/6 inhibition is not attributable to the induction of senescence. Cellular senescence is a state of irreversible cell cycle arrest that initiates a senescent-associated secretory phenotype (SASP), typified by the secretion of pro-inflammatory cytokines that recruit immune cells (222, 228, 229). While CDK4/6i increases B-gal staining (indicative of senescence), no other SASP genes are induced, suggesting that senescence does not contribute to CDK4/6i-induced tumor immunogenicity (221, 222).

In addition to their immune-potentiating effects, inhibitors of CDK4/6 can also dampen immunity via increased expression of PD-L1 on tumor cells (222, 223, 225, 226). PD-L1 fluctuates throughout the cell cycle and is lowest during late G1-S when CDK4/6 is most active (223). Inhibition of CDK4/6, or likewise knocking out Cyclin D1 or overexpressing $p16^{ink4a}$, leads to increased PD-L1 expression in numerous cell lines and preclinical tumor models, including B16 melanoma (222, 223, 225, 226).

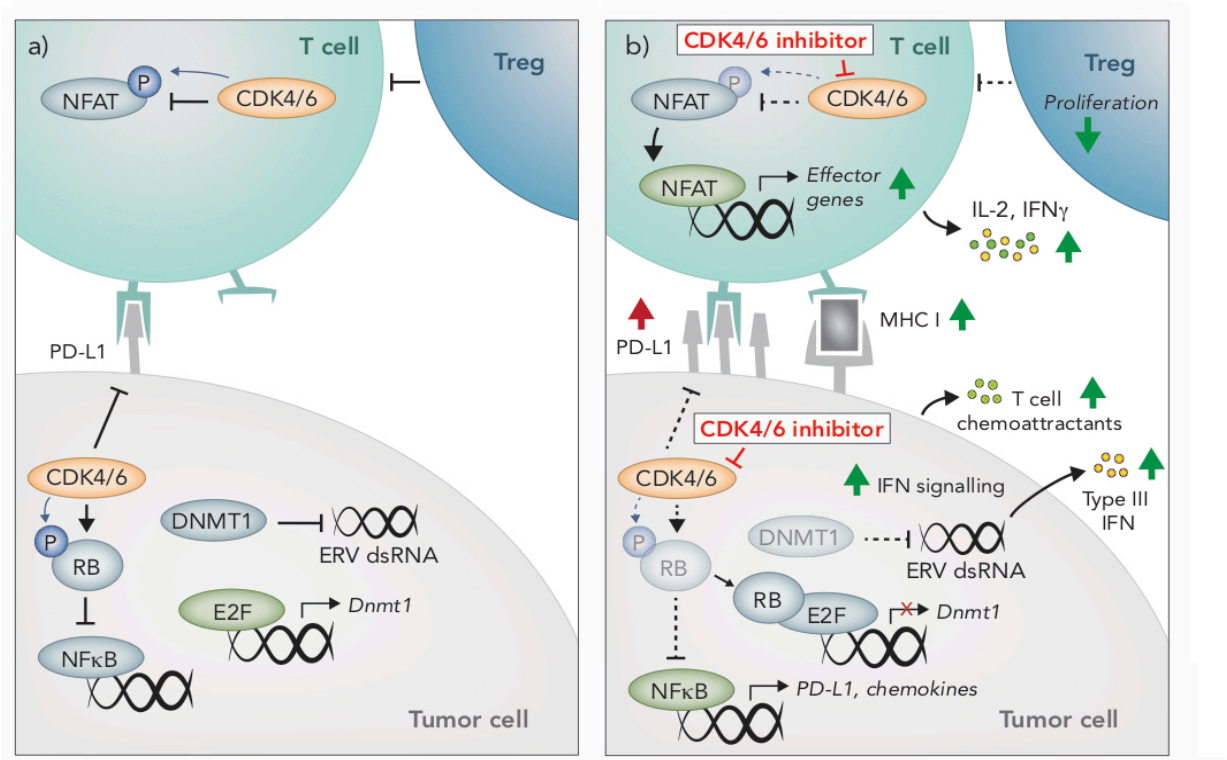

Figure 4 – Immunomodulatory effects of CDK4/6 inhibition. CDK4/6 inhibition modulates anti-tumor immunity through multiple mechanisms. a) Prior and b) post CDK4/6 inhibition. In tumors cells, CDK4/6 inhibition leads to hypophosphorylated RB, which binds to and inhibits the activity of E2F transcription factors. Reduced E2F activity leads to an induction of Type III interferons (IFN), resulting in paracrine IFN signaling and upregulation of MHC I. This induction of IFN is due to the suppression DNMT1, (an E2F target gene), which reduces methylation of endogenous retroviral (ERV) genes, thereby promoting their expression and inducing viral mimicry. Hypophosphorylated RB also promotes activation of NFκB and subsequent upregulation of T cell chemoattractants and PD-L1. CDK4/6 inhibition also prevents PD-L1 degradation, further enhancing PD-L1 protein expression on the cells surface. In T cells, NFAT activity is restrained by CDK4/6-mediated phosphorylation. Following CDK4/6 inhibition, hypophosphorylated NFAT translocates to the nucleus and upregulates expression of effector genes. Compared to other lymphocyte populations, Tregs appear particularly susceptible to the anti-proliferative effects of CDK4/6 inhibition.

3.2.2 The impact of CDK4/6 inhibition on T cells

While the majority of studies examining the immunomodulatory activity of CDK4/6 inhibition are related to tumor-intrinsic effects or effects on the tumor microenvironment more broadly, a seminal article in 2018 reported on the direct impact of CDK4/6 inhibition on T cells (224). In this study, Deng and colleagues identified CDK4/6 inhibitors in a small molecule screen aimed at uncovering enhancers of T cell activation, using IL-2 production as a readout, and subsequently identified NFAT as a novel phosphorylation substrate of CDK6 in T cells. Upon CDK4/6 inhibition, phosphorylation of NFAT is prevented, leading to its de-repression and subsequent translocation to the nucleus where it promotes the transcription of effector response genes (224). Indeed, increased NFAT signaling occurs in tumors following CDK4/6 inhibition (222), and an increase in IFNγ production by T cells in response to CDK4/6 inhibition has also been reported (221, 224). As discussed in section 2.3, in addition to enhancing T cell activation, NFAT transcription factors can also promote T cell exhaustion. Interestingly however, exhaustion markers appear to be decreased in T cells following CDK4/6 inhibition, though this has not been fully explored (221, 224). In fact, the direct effects of CDK4/6 inhibition on T cell phenotype and function is entirely unknown. Given these cells are the primary effectors of anti-tumor immunity and immunotherapies, this is an area of considerable interest and is the focus of Aim 3 (Chapter 4) of this thesis.

In addition to the regulation of NFAT, CDK4/6 may also play a role in T cell proliferation, however the mechanisms are not well defined. In human T cells, CDK4/6i has modest effects on proliferation and no impact on viability *in vitro* (222). Within the tumor microenvironment, the effects of CDK4/6 inhibition on the T cell infiltrate appear to vary depending on the tumor model and treatment schedule used. In MMTV-

Erbb2 breast, MC38 colon, and B16-F10 melanoma tumor models, CDK4/6 inhibition led to a decrease in total numbers of CD3+ tumor infiltrating T cells, encompassing CD8+ T cells and Granzyme B+ and IFNγ+ cells (223). In contrast, in the CT26 colon carcinoma model, CD3+ T cell numbers were relatively unchanged following CDK4/6 inhibition (222). While some studies have demonstrated an increase in the frequency of CD3+ T cells in the immune compartment of tumors (221, 222), it is unclear whether this is a true increase in the number of T cells, or simply a consequence of other immune populations shifting. Overall, it appears that CDK4/6 inhibition leads to less or equal absolute numbers of CD3+ T cells in the tumor microenvironment (222, 223), suggesting a possible anti-proliferative effect of CDK4/6i on these cells. Interestingly, in a syngeneic breast cancer model, CDK4/6 inhibition led to a significant reduction in the frequency and absolute number of tumor-infiltrating CD4+CD25+ Tregs, while other T cell subsets were unaffected (221), suggesting that Tregs are the most susceptible T cell subset to the anti-proliferative effects of CDK4/6 inhibition. This reduction in Tregs was attributed to cytostasis, as no changes were observed in apoptosis or the production of Tregs in the thymus (221).

Given the scarcity of studies that have investigated the direct effects of CDK4/6 inhibition on T cells, the role of CDK4 and CDK6 in these cells can be gleaned from studies that have utilized transgenic mice deficient for these kinases. Indeed, T cells from CDK6-null mice demonstrate a significant delay in proliferation and RB phosphorylation following mitogenic stimulation, indicating an important role for CDK6 in T cell proliferation following activation (230). Early studies also hinted at a role for CDK4 in T cell proliferation, as low levels of CDK4 expression correlated with reduced T cell proliferation (231). However, thymocytes from $CDK4^{-/-}$ bone marrow chimeric mice show no defects in proliferation or cytokine production (232), though

interestingly, CDK4$^{-/-}$ mice had underdeveloped thymuses and significantly increased numbers of CD8/CD4 negative thymocytes (232). A decrease in thymic mass and CD4+CD8+ thymocytes has also be observed in response to CDK4/6 inhibition (221), suggesting CDK4 may play a role in T cell development and maturation.

3.3 Targeted therapy and immune checkpoint blockade combinations

The prospect of combining targeted therapies with immune checkpoint blockade, either concurrently or consecutively, for the treatment of melanoma is attractive for two main reasons. Firstly, the clinical response profiles of these therapies are distinct, in that targeted therapies provide rapid short-term benefits for a majority of patients, while immune checkpoint blockade provides long-term benefits but for fewer patients. Assuming an additive effect, this combination strategy therefore has the potential to both increase the number of patients that respond clinically, and extend the therapeutic benefit for some. Secondly, given the profound impact targeted therapies have on anti-tumor immunity, these drugs may synergize with checkpoint blockade by creating a tumor microenvironment that is more conducive to supporting a clinically beneficial long-term response to immunotherapy. Pre-clinical studies and clinical trials examining MAPK/ERK- or CDK4/6-targeted therapy in combination with ICB will be discussed in this section.

3.3.1 Combining MAPK/ERK targeting with immune checkpoint blockade

A number of pre-clinical studies have shown promising results from combining BRAF or BRAF and MEK inhibition with immune checkpoint blockade for the treatment of melanoma. In mouse models of *BRAF*^{V600} melanoma, blockade of either PD-1 or PD-L1 synergized with BRAF inhibitor monotherapy (205) or dual inhibition of BRAF and MEK (218, 233, 234). This effect was dependent on CD8+ T cells (234),

and attributed to increased numbers and function of tumor infiltrating lymphocytes seen in response to the combination (205). Additionally, resistance to BRAF inhibitors is associated with increased expression of PD-L1 by tumor cells, further suggesting PD-1 blockade would synergize with BRAF inhibition (235). Surprisingly, preclinical studies examining the efficacy of MAPK/ERK inhibition with CTLA-4 blockade in melanoma are lacking. Interestingly however, CTLA-4 blockade synergizes with BRAF inhibition in BRAF-wildtype colon carcinoma and fibrosarcoma mouse models (236); an effect attributed to the expansion of antigen specific T cells resulting from BRAFi-induced paradoxical activation of MAPK/ERK (236), Notably, this suggests that the combined benefits of BRAF inhibition with immune checkpoint blockade may extend beyond BRAF-mutant cancers.

Given that many patients progress on targeted therapy and often receive immunotherapy as a second line of treatment, retrospective clinical data can provide insight into the potential efficacy of combining these approaches. Retrospective analysis from two clinical studies found that patients who progressed on BRAFi and MEKi, and subsequently went on to receive anti-PD-1 or anti-CTLA-4 therapy, had poor overall response rates (237, 238), possibly due to the loss of TILs associated with resistance to MAPK/ERK inhibition (205, 206). However, there are case reports where anti-CTLA-4 therapy has shown efficacy after BRAF inhibition (205, 239). Whether prior BRAF inhibition induced sensitivity to anti-CTLA-4 therapy, or whether these tumors were inherently sensitive to begin with was unclear.

Despite the conflicting data from these retrospective cases, the success of this combination in pre-clinical studies has led to the initiation of several clinical trials designed to prospectively assess the efficacy of combined MAPK/ERK targeted therapy and immune checkpoint blockade (reviewed in 240, 241). Early phase safety trials of

MAPK/ERK inhibitors co-administered with anti-CTLA-4 therapy demonstrated significant, but manageable, toxicities (242-244). Interestingly, toxicity was associated with the addition of trametinib (MEKi), and appeared worse for vemurafenib (BRAFi) than dabrafenib (BRAFi) (244), highlighting the need to consider drug-related adverse events in the design of combination therapies. MAPK/ERK targeted therapies in combination with anti-PD-1 or anti-PD-L1 therapies have shown better overall toxicity profiles than that of anti-CTLA-4 therapy, as well as more encouraging early-phase trial results (240, 241). In a phase II trial, (KEYNOTE-022), dual BRAFi/MEKi plus anti-PD-1 therapy showed a clear trend in increased PFS from 10.3 months to 16 months compared to dual BRAFi/MEKi plus placebo (245). Phase III trials (COMBI-I and TRILOGY IMspire) are currently underway to further assess this triplet combination, and the results are highly anticipated (246, 247).

3.3.2 Combining CDK4/6 inhibition with immune checkpoint blockade

The recently discovered immunomodulatory activity of CDK4/6 inhibition have made it an attractive potential adjuvant for T cell directed immunotherapies. Indeed, CDK4/6 inhibitors have demonstrated synergy with blockade of the PD-1/PD-L1 axis in a number of preclinical models (221-224), prompting evaluation of this combination therapy in clinical trials. Pre-clinically, this combination is particularly efficacious against CT26 colon carcinoma cells (221-223), which interestingly harbor a *Cdkn2a* deletion and expresses functional RB (248, 249), likely rendering it highly sensitive to the tumor-intrinsic immunomodulatory effects of CDK4/6 inhibition. In this model, the most efficacious schedule was treatment with a CDK4/6 inhibitor daily from days 6-34, with anti-PD-L1 antibody administration on days 13, 20 & 27 (222). The resulting anti-tumor efficacy of this combination schedule was attributed to CDK4/6 inhibition promoting and maintaining a T cell inflamed microenvironment (222). Efficacy of this

combination has been demonstrated in a number of other pre-clinical models, including MC38 colon carcinoma (222, 223), MMTV-Her2 breast cancer (221), EMT6 (222), as well as AT3-OVA breast cancer with the addition of a PI3K inhibitor (226). Interestingly, CDK4/6 inhibition promotes PD-L1 surface expression on tumor cells (see section 3.2.2) through both RB-dependent and RB-independent mechanisms (223, 225). This suggests CDK4/6i-induced effects on tumor PD-L1 expression, and subsequent synergy with anti-PD1/PD-L1 therapy, may also be relevant for RB-deficient tumor types.

As CDK4/6 inhibitors and PD-1/PD-L1 checkpoint inhibitors are already developed for clinical use, the combination of these two therapies has been able to rapidly enter clinical trials. In light of encouraging pre-clinical data, several clinical trials are now underway to examine the safety and efficacy of this combination. These trials are being conducted predominantly in ER^+ breast cancer, as well as other advanced solid tumors (NCT04075604, NCT02778685, NCT04118036, NCT03147287, NCT03294694, NCT02791334). As this combination is new to the clinic, examining the toxicity profile will be a crucial first step and results from these trials are eagerly anticipated. In the interim, the immunomodulatory effects of CDK4/6 inhibitors are still being elucidated and additional pre-clinical studies are required to better understand how to most effectively use CDK4/6 inhibitors to boost anti-tumor immunity.

4. Thesis aims and hypotheses

Growing evidence implicates the immune system in the anti-tumor efficacy of targeted therapies, however the impact of combined BRAF, MEK and CDK4/6 inhibition on anti-tumor immunity is entirely unexplored. Preclinical results of combined MAPK/ERK and CDK4/6 inhibition are promising, however these studies

have been restricted to *in vitro* systems and immunodeficient *in vivo* melanoma models, which preclude any analysis of the immunomodulatory activity of this therapy. This is largely due to a lack of suitable immunocompetent pre-clinical models to evaluate this combination, which is addressed in Chapter 2. Additionally, as this combination is only now recruiting for early phase clinical trials, there has been limited clinical samples to evaluate the impact on anti-tumor immunity. Understanding the immunomodulatory effects of these inhibitors is crucial to develop strategic approaches for scheduling this combination, as well as combining this class of therapeutics with immune-based therapies. As this drug combination enters the clinic for the treatment of melanoma, there is a critical need to determine how these therapies interact with the immune system and impact on the tumor microenvironment, which is the subject of Chapter 3.

In regards to individual therapies, the immune mechanisms underlying responses to BRAF and MEK inhibition have been extensively studied, however, the immunological effects of CDK4/6 inhibition are less defined. An unexpected role for CDK4/6 inhibitors as anti-tumor immunomodulatory agents recently spurred interest in their utility as adjuvants to immunotherapies. However, the clinical success of immunotherapies is contingent on the phenotypic and functional state of the lymphocytes they target. While CDK4/6 inhibitors have been shown to promote T cell activation, the subsequent effect on T cell differentiation and long-term function is unknown. This is a critical question given these are the principal effector cells targeted by immunotherapies, and is the focus of Chapter 4.

The specific aims of this project are:

Aim 1: Develop a syngeneic model of *Braf^{V600}Cdkna2$^{-/-}$* melanoma that is immunogenic and can be used to study the immunomodulatory effects of targeted inhibitors

Hypothesis: *Mouse melanoma with a clinically relevant Braf^{V600}Cdkna2$^{-/-}$ genetic background will recapitulate human melanoma in sensitivity to BRAF, MEK and CDK4/6 inhibition and will engage a therapeutically targetable immune response in vivo*

Aim 2: Assess the efficacy of BRAF, MEK and CDK4/6 inhibitors in an immunocompetent *Braf^{V600}Cdkna2$^{-/-}$* melanoma model and evaluate the effects of these inhibitors on the tumor immune microenvironment

Hypothesis: *Given the individual immunomodulatory activity of BRAF, MEK and CDK4/6 inhibitors, the combination of these will impact the tumor immune microenvironment and potentially alter tumor susceptibility to immunotherapy*

Aim 3: Evaluate the direct effects of CDK4/6 inhibition on T cells and T cell-mediated anti-tumor immunity

Hypothesis: *As CDK4/6 play a role in activation, maturation and proliferation of T cells, inhibiting these kinases will alter differentiation trajectories and the resulting phenotype and function of these cells.*

Chapter 2: A novel immunogenic mouse model of melanoma for the preclinical assessment of combination targeted and immune-based therapy

1. Preface

The aim of this chapter was to develop a syngeneic model of *Braf*^{V600}*Cdkna2*$^{-/-}$ melanoma that is immunogenic and can be used to study the immunomodulatory effects of targeted inhibitors, as well and combinations of targeted and immune-based therapies

This body of work was published in 2019 (250):

Lelliott EJ, Cullinane C, Martin CA, Walker R, Ramsbottom KM, Souza-Fonseca-Guimaraes F, Abuhammad S, Michie J, Kirby L, Young RJ, Slater A, Lau P, Meeth K, Oliaro J, Haynes N, McArthur GA, Sheppard KE. A novel immunogenic mouse model of melanoma for the preclinical assessment of combination targeted and immune-based therapy. *Sci Rep*. 2019 Feb 4;9(1):1225.

This chapter will present an introduction, the published work, and supplementary data.

2. Introduction

Over 90% of novel therapies that enter the clinic are unsuccessful in spite of promising preclinical results (251), highlighting a major challenge in translational cancer research, which is a lack of suitable preclinical models. Following evaluation in *in vitro* systems, such as cell lines and organoids, therapeutics must ideally be tested *in vivo* using animal models prior to advancing to the clinic. The most widely used *in vivo* models in cancer therapeutic research fall under one of three categories; xenografts, syngeneic models or genetically engineered mouse models (GEMMs). Each system has distinct benefits and limitations, and the most suitable model is largely dependent on the specific research question being addressed.

Xenograft models consist of human tumor cell lines or patient-derived samples engrafted into immunodeficient mice, such as nude mice (lacking T cells) or NOD-SCID gamma (NSG) mice (fully depleted immune system apart from neutrophils and monocytes). Arguably the greatest benefit of cell lines is that they provide many various, distinct and well-characterized genetic backgrounds to choose from; for example, the *Expasy Cellosaurus* encyclopedia of cell lines provides information on 2204 human melanoma cell lines with various genetic backgrounds. Cell lines can also be easily manipulated prior to engraftment, for example, by depleting specific genes or developing drug-resistant cell lines though long-term drug exposure. However, cell-derived xenograft models often fail to predict human clinical outcomes (252). This is largely attributed to artefacts introduced from interactions between human tumor cells and mouse host cells, and the fact that cell lines do not accurately recapitulate phenotypes of human tumors (253). In contrast, patient-derived xenografts (PDXs) use fresh samples of human biopsies, which can be passaged though multiple mice. These

grafts maintain the heterogeneity and genomic integrity of patient tumors, even after several passes (253-255). While PDXs are valuable preclinical models for anti-cancer drug screening (256), again the lack of an intact immune system limits the versatility of these models for studying highly immunogenic cancers such as melanoma (253).

Syngeneic models entail the engraftment of mouse tissue into a mouse of the same strain; the major benefit being that the recipient mouse has a fully functioning immune system. Further, as syngeneic models are generated from cell lines, they are easy to establish and manipulate. As such, syngeneic models are often used in cancer research to study immunotherapies, and were used for the preclinical evaluation of both CTLA-4 and PD-1 checkpoint inhibitors (56, 257). Unlike human xenografts however, there are very few syngeneic models of melanoma available. Additionally, a significant disadvantage of these models is that they lack genetic profiles inherent to human cancer, making them unsuitable for studying targeted therapies directed at human-specific oncogenic drivers.

GEMMs are developed by genetically engineering mice to harbor mutations that allow spontaneous or induced tumor development. As for syngeneic models, GEMMs offer the benefit of a fully functional immune system, however, they can be designed to carry specific mutations found in human cancers (253). A major drawback of these models is that they are developed through the introduction of only 1 or 2 specific driver mutations, and hence tumors lack the high mutational load inherent to many cancers, especially melanoma (253, 258). Consequently, these tumors do not accurately recapitulate the immunogenicity of cancers, and are therefore less useful for studying the efficacy of immunotherapies. GEMMs are also expensive, time-consuming and require extensive experience and infrastructure to house and breed multiple mouse colonies with specific genetic backgrounds (253, 258).

Developing a model to study the immune response to tumor-directed therapy presents challenges. As oncogene-targeted therapies inhibit tumor-intrinsic pathways, they are most often studied in human cancer cell lines *in vitro* and in xenograft models. In contrast, cancer immunology is commonly studied in immune-competent syngeneic models of murine cancer, which often lack human melanoma driver mutations. Studying the effect of targeted therapies on the immune response to cancer requires mouse-derived tumors harboring well-characterized human-relevant oncogenic driver mutations targeted by these therapies. The Yale University Melanoma Mouse (YUMM) (258) cell lines are derived from genetically modified C57BL/6 mice bearing genetic backgrounds relevant for studying human melanoma targeted therapies, including BRAF, MEK and CDK4/6 inhibitors. These lines enable the generation of syngeneic, transplantable models, which are fully immune competent, and significantly more experimentally tractable than GEMMs. As the YUMM models were only recently developed, their sensitivity to clinical therapies is poorly characterized. Additionally, as these lines were developed from mice genetically engineered with specific driver mutations, they lack a high mutational burden and are poorly immunogenic, unlike human melanoma. Examining the immunomodulatory effects of targeted therapies in melanoma requires a tumor model with the capacity to actively engage immune responses.

The aim of this chapter was to characterize and further develop the YUMM1.1 syngeneic model as a pre-clinical platform for examining immune modulation by targeted therapies and evaluating targeted/immune therapy combinations. This involved introducing a model antigen into the cells to enhance immunogenicity, and evaluating the sensitivity of this new tumor model to clinical targeted therapies (BRAF and MEK inhibitors) and immunotherapies (anti-PD-1 and anti-CTLA-4).

3. Publication in *Scientific Reports*, 2019

This body of work begins on the following page.

SCIENTIFIC REPORTS

OPEN

A novel immunogenic mouse model of melanoma for the preclinical assessment of combination targeted and immune-based therapy

Received: 2 August 2018
Accepted: 14 December 2018
Published online: 04 February 2019

Emily J. Lelliott[1,2], Carleen Cullinane[1,2], Claire A. Martin[1], Rachael Walker[1], Kelly M. Ramsbottom[1], Fernando Souza-Fonseca-Guimaraes[3,4], Shatha Abuhammad[1], Jessica Michie[1,2], Laura Kirby[1], Richard J. Young[1], Alison Slater[1], Peter Lau[1,2], Katrina Meeth[5], Jane Oliaro[1,2], Nicole Haynes[1,2,6], Grant A. McArthur[1,2,7] & Karen E. Sheppard[1,2,8]

Both targeted therapy and immunotherapy have been used successfully to treat melanoma, but the development of resistance and poor response rates to the individual therapies has limited their success. Designing rational combinations of targeted therapy and immunotherapy may overcome these obstacles, but requires assessment in preclinical models with the capacity to respond to both therapeutic classes. Herein, we describe the development and characterization of a novel, immunogenic variant of the *Braf*^{V600E}*Cdkn2a*$^{-/-}$*Pten*$^{-/-}$ YUMM1.1 tumor model that expresses the immunogen, ovalbumin (YOVAL1.1). We demonstrate that, unlike parental tumors, YOVAL1.1 tumors are immunogenic *in vivo* and can be controlled by immunotherapy. Importantly, YOVAL1.1 tumors are sensitive to targeted inhibitors of BRAF^{V600E} and MEK, responding in a manner consistent with human BRAF^{V600E} melanoma. The YOVAL1.1 melanoma model is transplantable, immunogenic and sensitive to clinical therapies, making it a valuable platform to guide strategic development of combined targeted therapy and immunotherapy approaches in BRAF^{V600E} melanoma.

The development of targeted therapies and immunotherapies in recent years has revolutionized the landscape of cancer treatment, particularly melanoma. The most notable clinical successes in melanoma include immune checkpoint inhibitors of PD-1 and CTLA-4[1–8], and targeted inhibitors of the MAPK/ERK pathway; specifically dual inhibition of BRAF^{V600E} and MEK[9–15]. However, resistance to targeted therapies and low response rates to immunotherapies have prompted great interest in combining these therapeutic strategies. While combination therapies are now being evaluated in clinical trials, most are performed on the basis of observed clinical success of individual therapies, with limited understanding of how these therapeutic classes interact with one another. As such, little judgement can be made about optimal combinations and scheduling, or which patients to target with various combinations. Emerging evidence suggests that therapies targeting the MAPK/ERK pathway may also impact on anti-tumor immune responses[16–18], and hence a thorough understanding of these interactions is paramount for the strategic design of efficacious targeted and immune therapy combinations.

The Yale University Mouse Melanoma (YUMM) series of cell lines can be efficiently grown and studied in immunocompetent C57BL/6 mice, and importantly, have been derived from genetically modified mice bearing mutations commonly found in human melanoma[19]. These models provide an immunocompetent and clinically relevant setting in which to study targeted and immune therapy combinations. However, as these lines were generated through the introduction of a small number of oncogenic driver mutations, they are poorly T

[1]Cancer Research Division, Peter MacCallum Cancer Centre, Melbourne, VIC, Australia. [2]Sir Peter MacCallum Department of Oncology, University of Melbourne, Melbourne, VIC, Australia. [3]Department of Medical Biology, University of Melbourne, Melbourne, VIC, Australia. [4]Division of Molecular Immunology, The Walter Eliza Hall Institute of Medical Research, Parkville, VIC, Australia. [5]Department of Pathology, Yale University School of Medicine, New Haven, CT, USA. [6]Department of Pathology, University of Melbourne, Melbourne, VIC, Australia. [7]Department of Medicine, St Vincent's Hospital, University of Melbourne, Melbourne, VIC, Australia. [8]Department of Biochemistry and Molecular Biology, University of Melbourne, Melbourne, VIC, Australia. Correspondence and requests for materials should be addressed to K.E.S. (email: karen.sheppard@petermac.org)

cell immunogenic due to a low somatic mutational burden[20–22]; a major challenge for mouse models genetically engineered in this way[23,24]. Melanoma, in particular, is a highly mutated and immunogenic cancer[25], expressing numerous neoantigens that have the capacity to stimulate strong immune responses[26–28]. The remarkable success of immunotherapies in the treatment of melanoma, in contrast to other solid cancers, is due in part to high inherent immunogenicity and acquired immunosuppressive mechanisms[29]. Hence, weakly immunogenic mouse models do not capture the full characteristics of human melanoma.

The YUMM1.1 line, derived from mice bearing a $BRAF^{V600E}$ mutation and deficient for *Cdkn2a* and *Pten*, is poorly immunogenic due to low neoantigen expression, and resistant to immunotherapy due to low inflammatory and chemotaxis gene signatures[20–22]. In the present study we show that expression of ovalbumin (OVA) was sufficient to alter the susceptibility of YUMM1.1 tumors to host T cell mediated control. The adoptive transfer of OVA-specific $CD8^+$ T cells (OT-I T cells), as well as immune checkpoint blockade therapy, further enhanced tumor control. Checkpoint inhibitors were ineffective against the parental YUMM1.1 model, indicating the expression of OVA, and enhanced T cell engagement, sensitizes this model to immunotherapy. Importantly, the response of this tumor line to standard-of-care BRAF and/or MEK inhibition was equivalent to that observed in human $BRAF^{V600E}$ melanoma, consistent with the parental YUMM1.1 line[21]. Collectively, our data highlights the utility of YOVAL1.1 as a preclinical model for examining the complex interactions of targeted therapies and the immune system, providing a valuable platform to better guide clinical application of novel and existing therapy combinations in $BRAF^{V600E}$ melanoma.

Results

Expression of the immunogen, ovalbumin, in YUMM1.1 tumor cells promotes T cell-mediated tumor control. The YUMM series of mouse melanoma cell lines are reported to be poorly T cell immunogenic *in vivo* due to low neoantigen expression[20–22]. Consistent with this, we found no significant difference in the growth kinetics or overall survival of YUMM1.1 tumors grown in immunocompetent C57BL/6 or immunodeficient NOD scid gamma (NSG) mice; which are T and B cell deficient and lack functional NK cells due to a null mutation in the IL-2 receptor common gamma chain (Fig. 1a). While these tumors induced the recruitment of IFNγ−producing NK cells (Supplementary Fig. 1a,b), this was not sufficient to control tumor growth. This was despite the fact that *in vitro*, NK cells could kill YUMM1.1 tumor cells and secrete IFNγ, which up-regulated MHC-I on the tumor cells (Supplementary Fig. 1c). Furthermore, while YUMM1.1 tumors express MHC I *in vivo* (Supplementary Fig. 1d) we speculate that, in the absence of sufficient neo-antigen expression on YUMM1.1 tumor cells, an anti-tumor T cell response was limited.

Human melanoma is inherently immunogenic due to a high neoantigen load[25]. To establish a model that would mimic the immunogenicity of melanoma, the YUMM1.1 line was retrovirally transduced to stably express OVA and GFP, and sorted for both low and high GFP expression (Fig. 1b). Both YUMM1.1 cells transduced with OVA, or an empty vector control (YV1.1), were resistant to OVA-specific OT-I T cell-mediated killing (Fig. 1c). However, pre-treatment of OVA-transduced YUMM1.1 tumor cells with IFNγ to induce $H\text{-}2K^b$ expression and presentation of the OVA peptide SIINFEKL, sensitized them to OT-I T cell killing (Fig. 1c). OVA stimulates a strong $CD8^+$ T cell response and when expressed at high levels on tumor cells, can prevent successful engraftment of tumors in C57BL/6 mice due to immune-mediated rejection[30]. Thus, we utilized the low OVA-expressing population for our *in vivo* studies, referred to here as YOVAL1.1 (**Y**UMM**1.1**-**OVA**-**L**ow).

We first examined the growth kinetics of the YOVAL1.1 tumor line in both C57BL/6 and NSG mice. Compared to that observed in NSG mice, growth of the YOVAL1.1 tumors was significantly slower in C57BL/6 mice, with a difference in median overall survival of 12 days (40 days versus 28 days; Fig. 1d). Notably, growth of the YV1.1 empty vector control tumors in C57BL/6 mice was comparable to YOVAL1.1 tumors grown in NSG mice (Fig. 1d). Furthermore, in $Rag1^{-/-}$ mice, which have a functional innate immune system but lack T and B cells, the YOVAL1.1 tumors grew out in a similar manner to that observed in NSG mice (Fig. 1e). YOVAL1.1 tumor growth in C57BL/6 mice was also significantly delayed following the adoptive transfer of OVA-specific OT-I T cells (Fig. 1f). Collectively these data support a role for T cells in mediating the control of YOVAL1.1 tumor growth *in vivo*.

Expression of the immunogen, ovalbumin, in YUMM1.1 tumor cells alters the tumor immune microenvironment. To determine the impact of OVA expression on the tumor microenvironment, we compared the immune infiltrate in parental (YUMM1.1), empty vector control (YV1.1) and OVA-expressing (YOVAL1.1) tumors 4 weeks following implant. We observed a significant increase in the frequency of major immune subsets, including $CD8^+$ T cells, $CD4^+$ T cells, T regulatory cells, NK cells, dendritic cells and macrophages, within YOVAL1.1 tumors compared to control YUMM1.1 and YV1.1 tumors (Fig. 2a and Supplementary Figs 2–4). Indeed, immunohistochemical analysis of YOVAL1.1 tumors revealed markedly higher levels of infiltrating $CD3^+$ T cells compared to YV1.1 tumors (Fig. 2b). Together these data indicate that YOVAL1.1 tumors can stimulate strong $CD8^+$ T cell activity, which appears to contribute to immune-mediated tumor growth control in C57BL/6 mice. However, the induction of an anti-tumor T cell response was insufficient to cause complete tumor rejection, which may in part have been attributed to the observed increases in tumour associated T regulatory cell and/or macrophage frequency (Fig. 2a). Notably, expression of PD-1 and PD-L1 on the $CD8^+$ TILs and YOVAL1.1 tumor cells, respectively, was also detected (Fig. 2c).

To confirm that YOVAL1.1 tumors did not escape immune control as a result of acquired resistance to T cell killing, we harvested tumors at endpoint (>1200 mm^3) and found they were sensitive to killing by *in vitro* activated OT-I T cells (Fig. 2d). Collectively these observations suggest that therapies aimed at overcoming these immunosuppressive mechanisms, such as checkpoint blockade, may be effective in this model.

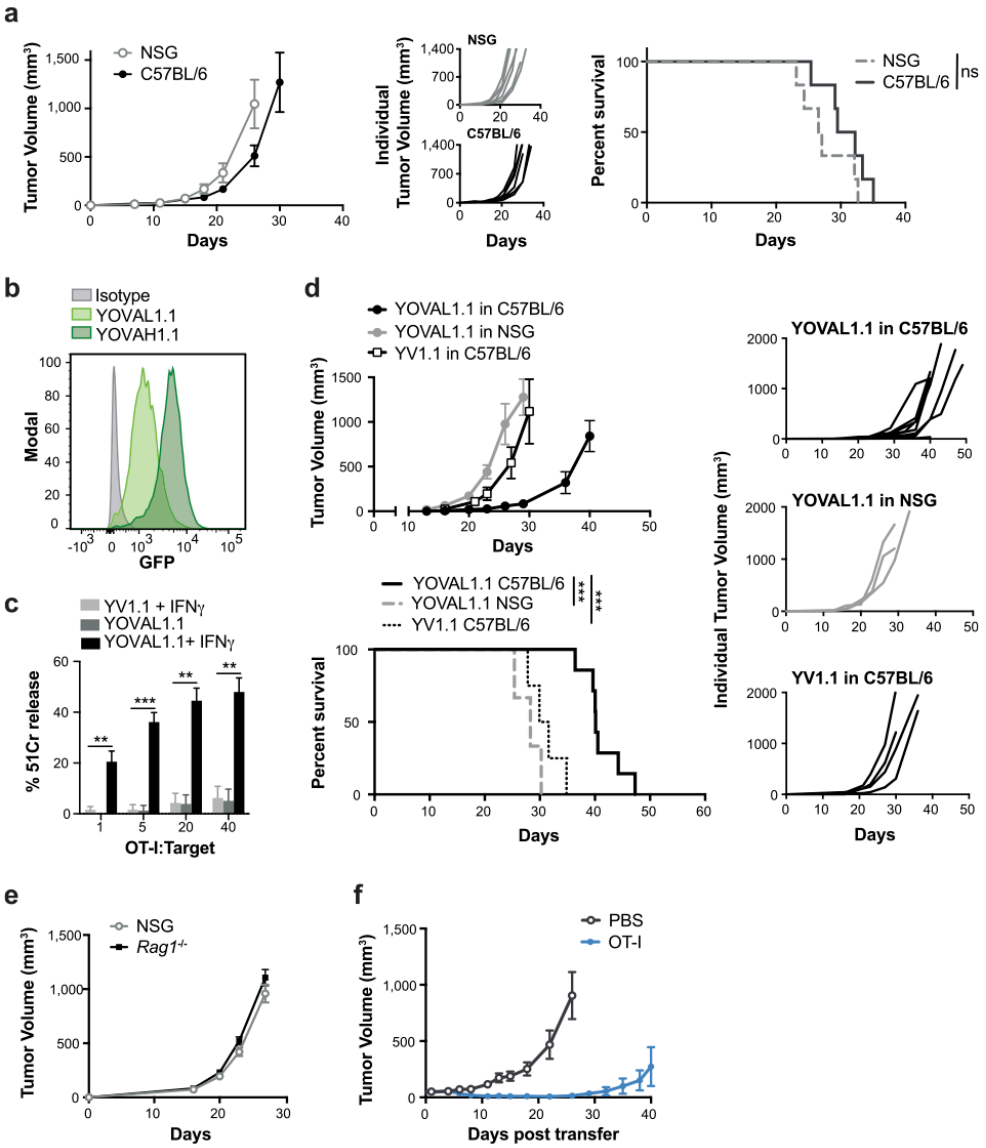

Figure 1. Expression of the immunogen, ovalbumin, in YUMM1.1 tumor cells promotes T cell-mediated tumor control. (**a**) Tumor growth and survival of 3×10^5 YUMM1.1 cells in C57BL/6 mice or NSG mice, with survival measured as time for tumors to reach >1200 mm³. ns – not significant, log-rank (Mantel-Cox) test, n = 5–8. (**b**) YUMM1.1-OVA sorted by FACS into low and high GFP-expressing populations; YOVAL1.1 and YOVAH1.1, respectively. (**c**) Killing by OT-I T cells co-cultured for 4 hours at indicated ratios with 51Cr-labelled target cells pre-stimulated +/− IFNγ. One way ANOVA, Tukey's multiple comparisons test, n = 3. (**d**) YOVAL1.1 tumor growth and survival in C57BL/6 mice or NSG mice with survival measured as time for tumors to reach >1200 mm³, log-rank (Mantel-Cox) test, n = 3–5. (**e**) Growth of YOVAL1.1 in NSG or *Rag1*$^{-/-}$ mice, n = 3. (**f**) YOVAL1.1 tumor growth and survival following transfer of activated OT-I T cells or PBS. YV1.1 – YUMM1.1 transduced with empty vector. All error bars show ±SEM. **p < 0.01, ***p < 0.001.

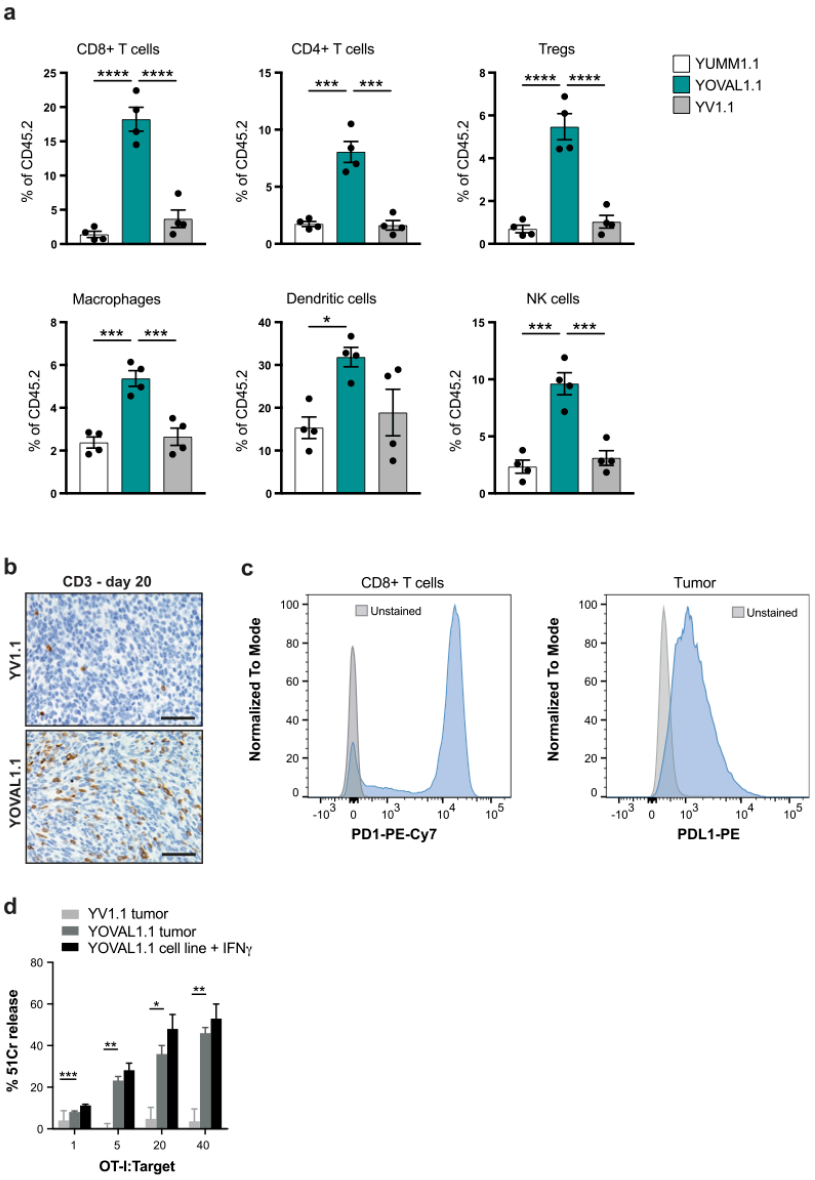

Figure 2. Expression of the immunogen, ovalbumin, in YUMM1.1 tumor cells alters the tumor immune microenvironment. Analysis of immune engagement following OVA introduction into YUMM1.1. (**a**) Flow cytometry analysis of immune infiltrate in YUMM1.1, YOVAL1.1 and YV1.1 tumors as a percentage of CD45.2$^+$ cells, 4 weeks after implant. One way ANOVA, Tukey's multiple comparisons test, n = 4. (**b**) Immunohistochemistry of CD3$^+$ infiltrate in YV1.1 and YOVAL1.1 tumors, representative of n = 3. (**c**) PD-1 and PD-L1 expression on YOVAL1.1-infiltrating CD8+ T cells and YOVAL1.1 tumor cells, respectively, representative of n = 4. (**d**) Killing by OT-I T cells co-cultured for 4 hours at indicated ratios with 51Cr-labelled targets; YOVAL1.1 and YV1.1 *ex vivo* endpoint tumors (>1200 mm^3) or YOVAL1.1 cells pre-stimulated with IFNγ. One way ANOVA, Tukey's multiple comparisons test, n = 3. YV1.1 – YUMM1.1 transduced with empty vector. All scale bars show 50 μm. All error bars show ±SEM. *p < 0.05, **p < 0.01, ***p < 0.001, ****p < 0.0001.

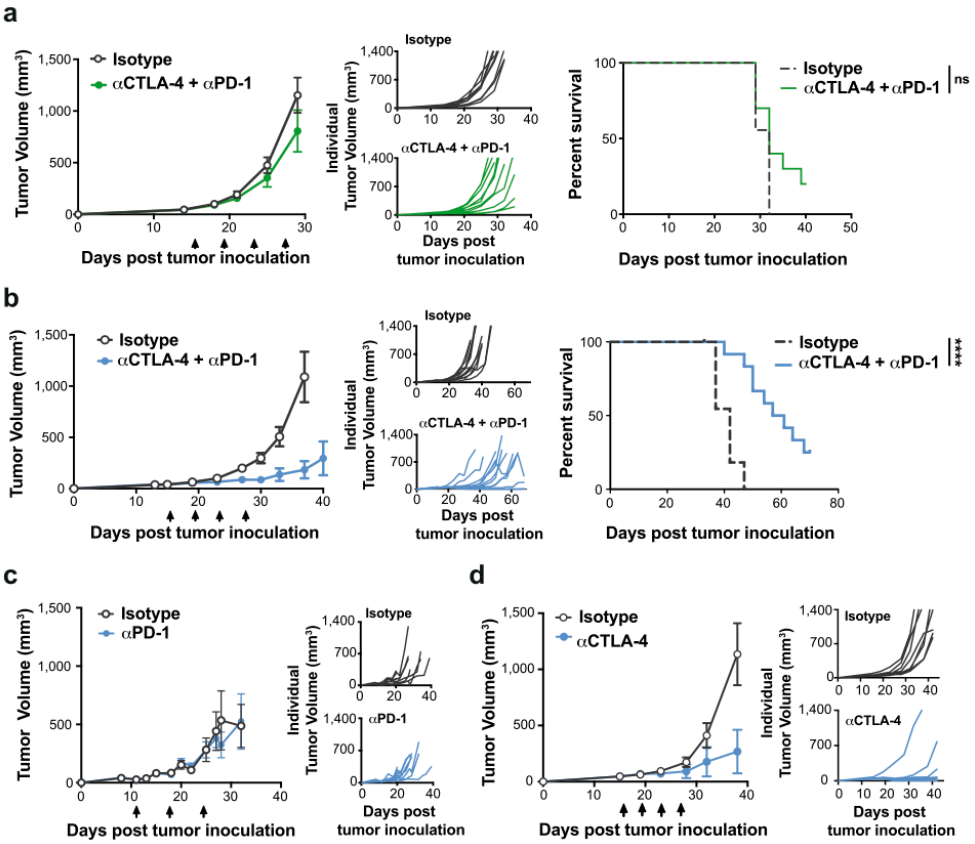

Figure 3. YOVAL1.1 tumors are responsive to immune checkpoint blockade *in vivo*. (**a**,**b**) Response of YUMM1.1 (**a**) and YOVAL1.1 (**b**) tumors to immunotherapy. Tumor growth and survival in response to combination anti-PD-1 and anti-CTLA-4 or isotype controls in C57BL/6 mice, n = 10–12. (**c**,**d**) YOVAL1.1 tumor growth in response to anti-PD-1 (**c**) or anti-CTLA-4 (**d**) or isotype controls. (**a**–**d**) Survival measured as time for tumors to reach >1200 mm^3, arrows indicate treatment days. ns – not significant, Log-rank (Mantel-Cox) test, error bars show ±SEM. ****$p < 0.0001$.

YOVAL1.1 tumors are responsive to immune checkpoint blockade *in vivo*. To determine if potential immunosuppressive mechanisms could be overcome in this model, YOVAL1.1 tumor-bearing C57BL/6 mice were treated with antibodies to the checkpoint blockade receptors PD-1 and CTLA-4. The combination of anti-PD-1 and anti-CTLA-4 checkpoint blockade is a standard-of-care therapy approach in melanoma[4–6]. Analysis of this combination strategy in C57BL/6 mice bearing parental YUMM1.1 tumors revealed that this model is poorly responsive, with no significant improvement in median survival relative to isotype control treated mice (Fig. 3a). However, we hypothesized that the enhanced capacity of YOVAL1.1 tumors to trigger an endogenous T cell response would correlate with improved response to immunotherapy.

To directly compare the two models, which grow with different kinetics *in vivo*, we inoculated mice with 2×10^6 YOVAL1.1 cells or 1.5×10^6 YUMM1.1 cells to establish tumors of the same size at day 15 post inoculation; the time at which treatment was started (Supplementary Fig. 5). In contrast to YUMM1.1 tumors, there was a significant extension of survival of YOVAL1.1-bearing C57BL/6 mice co-treated with anti-PD-1 and anti-CTLA-4 therapy compared to isotype controls, with median survival of 57 days versus 40 days post tumor inoculation, respectively (Fig. 3b). Significantly, 10/12 mice treated with the combination therapy were still alive 50 days post tumor injection, compared to 0/12 mice in the control group. Notably, the YOVAL1.1 tumors were resistant to anti-PD-1 monotherapy (Fig. 3c), but responsive to anti-CTLA-4 monotherapy (Fig. 3d), indicating that the response to the combination therapy was predominately anti-CTLA-4 driven. The immunogenicity of YOVAL1.1 tumors, and the capacity of these tumors to respond to immunotherapy *in vivo*, makes this a valuable model to dissect how these immunotherapy approaches may be enhanced by target therapies.

The response of YOVAL1.1 tumors to MAPK/ERK pathway-targeted therapy recapitulates that of human models. The YUMM series of cell lines were developed through the introduction of common mutations observed in human melanoma[21]. Specifically, YUMM1.1 has a $BRAF^{V600E}$ mutation and is sensitive to treatment with BRAF inhibitors (BRAFi) *in vitro*[21]. However, the response of YUMM1.1 to BRAFi, and standard-of-care therapy BRAFi plus MEKi, has not been reported *in vivo*, nor has the sensitivity to these inhibitors been compared to other common melanoma preclinical models. Hence, to determine the suitability of YOVAL1.1 as a model for studying targeted therapy, we examined its response to inhibitors of $BRAF^{V600E}$ and MEK. As a measure of sensitivity, we determined drug doses of PLX4720 ($BRAF^{V600E}$ inhibitor) and cobimetinib (MEK inhibitor) required for 50% growth inhibition (GI50). The PLX4720 and cobimetinib GI50s of YOVAL1.1 were not significantly different to those of the human $BRAF^{V600E}$ melanoma line, A375 (239 ± 50 nM and 4.6 ± 0.7 nM vs. 139 ± 9 nM and 4.7 ± 0.5 nM, respectively) (Fig. 4a). In contrast, B16 cells, which lack a clinically relevant genetic background, were not sensitive to these inhibitors (PLX4720 and cobimetinib GI50s $7{,}412 \pm 675$ nM and 68.3 ± 10.8 nM, respectively) (Fig. 4a).

In melanoma patients and in preclinical models using human xenografts, combined inhibition of BRAF and MEK achieves synergistic anti-cancer responses[9,12–14]. Importantly, synergy between PLX4720 and cobimetinib was also observed in the YOVAL1.1 model. *In vitro* the combination synergistically halted the proliferative activity of the YOVAL1.1 line, whereas no such synergy was observed in the B16 line (Fig. 4b). PLX4720, cobimetinib and their combination decreased P-ERK levels in YOVAL1.1 and A375 cells, but not in the non-sensitive B16 line (Fig. 4c). *In vivo*, the combination of BRAF and MEK inhibition significantly improved survival of YOVAL1.1-bearing C57BL/6 mice, with a median overall survival of 40 days on treatment, compared to 12 days for vehicle-treated mice (Fig. 4d), which was similar to the response of the parental YUMM1.1 line (Supplementary Fig. 6). Taken together, these data demonstrate that YOVAL1.1 tumors respond to MAPK/ERK pathway inhibition with similar sensitivity to that of human preclinical models. This highlights the utility of YOVAL1.1 tumors as a clinically relevant *in vivo* model for studying responses to these targeted therapies in combination with immune-based approaches.

Discussion

Immunotherapy and targeted therapy have both been immensely successful in extending the life of melanoma patients. However, the majority of patients treated with targeted therapy eventually relapse and approximately 50–70% of patients treated with immune checkpoint therapy do not respond[6,10–13,15]. In addition to inhibiting tumor intrinsic growth pathways, it is now well known that targeted therapies also impact anti-cancer immune responses[16–18]. Understanding these interactions is paramount in the strategic design of immune and targeted therapy combinations and this requires physiologically relevant, preclinical models that are both immunogenic, and responsive to standard-of-care therapies. Here, we describe YOVAL1.1 as a novel mouse model of melanoma that is suitable for evaluating *in vivo* immune interactions in response to targeted therapy.

Chicken ovalbumin (OVA) is widely used as a model antigen in T cell biology. Numerous mouse cancer models, including the commonly used B16 melanoma cell line, have been modified to express OVA to aid in enhancing and tracking tumor-specific T cell responses[31,32]; however, these models lack the genetic background commonly found in human melanoma. In contrast, the recently developed, YUMM series of cell lines carry the relevant genetic background and are fast becoming the preferred syngeneic model of melanoma[20–22,33]. In this study, we have introduced OVA into YUMM1.1 cells, to enhance *in vivo* immune interactions and thus have created a melanoma OVA model antigen system that is more clinically applicable.

Low immunogenicity is a known major challenge for genetically engineered mouse models[23,24]. Indeed, we found YUMM1.1 to be poorly immunogenic *in vivo*. The introduction of OVA to generate the YOVAL1.1 cell line was sufficient to sensitize the line to endogenous T cell control, but did not cause complete tumor rejection, supporting the presence of immunosuppressive mechanisms in this model. Consistent with this, we found an abundance of regulatory T cells within these tumors, in addition to expression of the immunosuppressive checkpoint molecules, PD-1 and PD-L1, on the T cells and tumor cells respectively. The loss of PTEN in this model is also a likely contributor to such strong immunosuppression, as PTEN loss in melanoma is associated with increased production of immunosuppressive cytokines and resistance to T cell-mediated immunotherapies[34–36]. Interestingly, the enhanced immunogenicity of YOVAL1.1 rendered the model amenable to checkpoint blockade with anti-CTLA-4, but not anti-PD-1, despite PD-1 and PD-L1 being expressed in the microenvironment, and anti-PD-1 demonstrating superior results to anti-CTLA-4 in the clinic[37]. This observed resistance to PD-1 blockade therapy is comparable to observations reported previously in a YUMM model with the same genetic background[22]. Recently, the combination of anti-CTLA-4 and anti-PD-1 was shown to be superior to anti-PD-1 monotherapy[6], and it is currently unclear whether this added benefit is due to complementary actions of the inhibitors, or a subset of anti-PD-1-resistant patients who are responsive to anti-CTLA-4. Our data suggests the latter is possible, given that this model responds equally well to anti-CTLA-4 with, and without, the addition of anti-PD-1. The primary anti-tumor mechanism of CTLA-4 checkpoint blockade remains controversial. In addition to enhancing T cell priming through blockade of inhibitory interactions between antigen presenting cells and T cells[38], anti-CLTA-4 therapy may also deplete T regulatory $FOXP3^{+}$ cells in the tumor microenvironment[39–41]. Importantly, this model provides a unique platform to dissect these mechanisms, which may provide insight into which patients are most likely to respond to anti-CTLA-4 therapy alone. Conversely, the innate resistance of the model to anti-PD-1 therapy may offer insight into mechanisms contributing to such resistance. Given the high toxicity[42] and significant monetary costs[43] of combined immune checkpoint therapies, there is great value in stratifying patients who will receive benefit from single agents or novel combination approaches.

Inhibition of BRAF and MEK is standard-of-care targeted therapy for $BRAF^{V600E}$ melanoma, and the clinical response rate of $BRAF^{V600E}$ melanoma to combined BRAF/MEK inhibition is around 70%[44]. However, there is

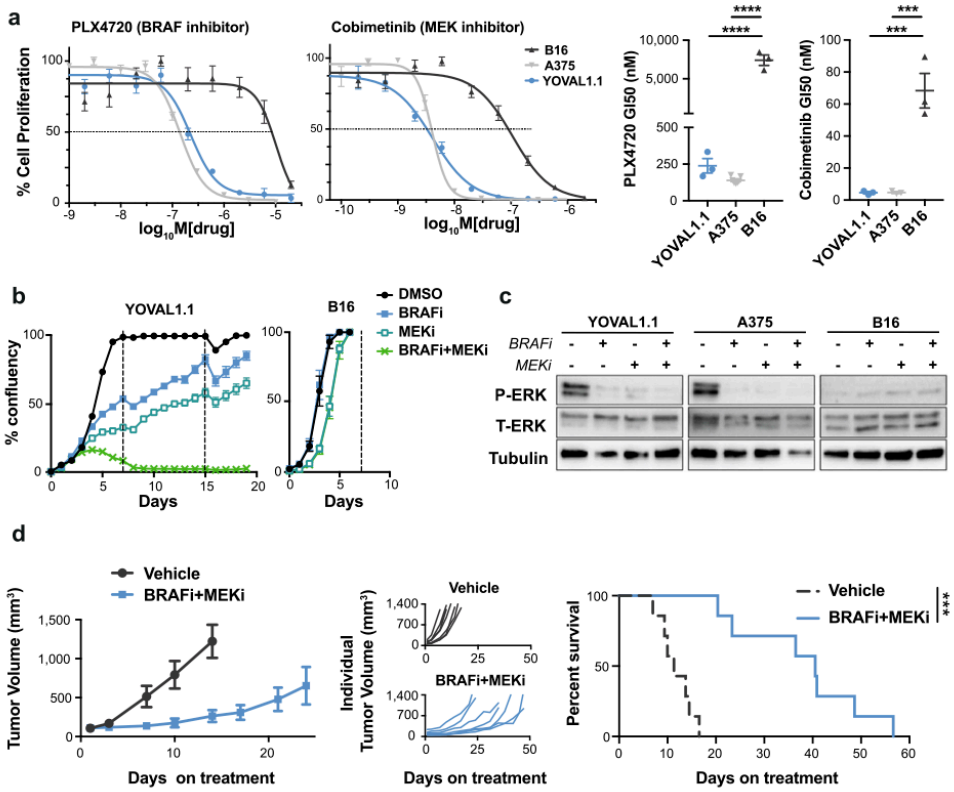

Figure 4. YOVAL1.1 is responsive to MAPK/ERK pathway-targeted therapy. Response of YOVAL1.1 to BRAF and MEK inhibition (BRAFi and MEKi). (**a**) Cell proliferation of YOVAL1.1, B16 and A375 cultured in increasing concentrations of PLX4720 (BRAFi) or cobimetinib (MEKi) for 5–6 days. Representative dose response curve shown. GI50s (right panels) were calculated as the concentration of drug leading to 50% growth inhibition. One-way ANOVA, Tukey's multiple comparisons test, n = 3. (**b**) YOVAL1.1 or B16 cells cultured with DMSO, 1 μM PLX4720 (BRAFi), 10 nM cobimetinib (MEKi) or BRAFi + MEKi and cell confluency measured every 12–24 hours using IncuCyte®ZOOM. Representative graph of n = 3. (**c**) Western blot of phospho- and total-ERK (P-ERK and T-ERK) expression in YOVAL1.1, A375 and B16 treated with DMSO, 1 μM PLX4720 (BRAFi), 10 nM cobimetinib (MEKi) or BRAFi + MEKi for 48 hours, representative blot of n = 3. All images were cropped from different parts of the same blot, with exposure times differing according to antibody and cell line (see Supplementary Fig. 7). (**d**) Tumor growth and survival in YOVAL1.1-bearing C57BL/6 mice treated daily, 6 days/week, with dabrafenib (BRAFi) plus trametinib (MEKi). Survival is measured as time for tumors to reach >1200 mm^3, log-rank (Mantel-Cox) test, n = 7. All error bars show ±SEM. ***$p < 0.001$, ****$p < 0.0001$.

now substantial evidence that these inhibitors alter anti-tumor immune responses[16–18], potentially impacting on the efficacy of immunotherapy. To comprehensively evaluate the effects of these inhibitors on the immune system using preclinical models, it is essential that the model system is sensitive to these therapies. The response of YOVAL1.1 to BRAF and MEK inhibition recapitulates that of human $BRAF^{V600E}$ A375 melanoma, demonstrating its suitability over the commonly used B16 syngeneic melanoma model. Importantly, these drugs demonstrated target specificity in YOVAL1.1, as evidenced by a reduction in P-ERK, and markedly decreased tumor progression *in vivo*. The expression of OVA in this model make it an ideal platform to evaluate the effects of these inhibitors on anti-tumor endogenous T cell responses, as well as adoptively transferred OVA-specific T cells.

In addition to being immunogenic and sensitive to clinical therapies, YOVAL1.1 tumors are transplantable, making the model a simple and effective tool to trial a range of novel and existing therapy combinations and scheduling. We therefore propose that the YOVAL1.1 melanoma model will provide a valuable platform to guide strategic development of combined targeted therapy and immunotherapy approaches in $BRAF^{V600E}$ melanoma.

Methods

Cell culture and IFNγ stimulation. YUMM1.1, YOVAL1.1 and YV1.1 were cultured in RPMI 1640 plus 20 mM HEPES containing 10% FBS, 1% GlutaMAX, 1 mM Sodium Pyruvate, 1 mM MEM Non-Essential Amino Acids and 0.1% 2-mercaptoethanol. B16 and PhoenixE cells were cultured in DMEM containing 10% FBS and 1% GlutaMAX. A375 were cultured in RPMI 1640 plus 20 mM HEPES containing 10% FBS and 1% GlutaMAX. For IFNγ stimulation, cells were cultured in 2 ng/mL recombinant mouse IFNγ for 16 hours and washed twice with PBS prior to use in assays. All cell lines were harvested using Trypsin-EDTA (0.25%). Splenocytes were cultured in RPMI 1640 plus 20 mM HEPES containing 10% FBS, 1% GlutaMAX, 1 mM Sodium Pyruvate, 1 mM MEM Non-Essential Amino Acids, 0.1% 2-mercaptoethanol and Antibiotic-Antimitotic. All cells were cultured at 37 °C in 5% CO_2.

Ovalbumin transduction. For virus production, PhoenixE cells were transfected with MSCV-IRES-GFP-OVA or MSCV-IRES-GFP in polyethylenimine (PEI), using 1 μg DNA/4.5uL PEI/mL PhoenixE media. After 16 hours, viral media was collected and combined 1:1 with YUMM1.1 media. Media was supplemented with 10 ng/mL protamine sulphate, and an additional 5% FBS before being added to YUMM1.1 cells. This was repeated three times over 20 hours. Transduced YUMM1.1 cells were sorted for GFP expression using BD FACS Aria II (BD Biosciences, North Ryde, New South Wales, Australia).

Primary T and NK cell isolation and activation. Spleens from C57BL/6.OT-I transgenic mice were filtered through a 70 μM filter and red blood cells were lysed with red cell lysis buffer (150 mM NH_4Cl, 10 mM $KHCO_3$, 0.1 mM Na_2EDTA). OT-I T cells were activated by culturing with 10 nM SIINFEKL plus 100 IU/mL IL-2 for 72 hrs, and then washed and cultured with 75 IU/mL IL-2 for a further 3–6 days prior to use in assays or for adoptive transfer studies. NK cells were isolated from spleens of C57BL/6 mice using a mouse NK cell enrichment kit (EasySep™ #19755) and cultured in 250 IU/mL IL-2 for 5–7 days prior to use in assays.

Tumor cell preparation. Tumors were digested with Collagenase IV (1.6 mg/mL) and DNase (2 U/mL) in DMEM for 45 minutes at 37 °C with agitation and filtered through a 70 μM filter to make a single cell suspension. Tumor preparations were sorted for GFP^+ cells using BD FACS Aria II.

Cytotoxic assays. Target cells were labelled with 250 μ*Ci*/mL Chromium-51 (51Cr; Perkin Elmer, VIC, Australia) for 45 minutes prior to culturing with effector cells at 37 °C. Supernatant was collected and 51Cr was measured by a gamma counter (Wallac Wizard). 51Cr release due to effector-mediated killing was calculated as $\%Release = [(51Cr_{SAMPLE} - 51Cr_{SPONT})/(51Cr_{TOTAL} - 51Cr_{SPONT})] \times 100$; where $51Cr_{SPONT}$ is spontaneous 51Cr release from target cells cultured without effector cells, and $51Cr_{TOTAL}$ is total chromium release from cells lysed with 10% Triton X-100.

Flow cytometry. Samples were blocked with 2% normal mouse serum or mouse Fc block (2.4G2, BD Biosciences). Fixable yellow (Invitrogen, L34959) was used to stain live/dead cells. Anti-mouse antibodies used were CD45.2 (104, Tonbo Biosciences), CD3 (500A2, BD Bioscience), TCRβ (H57–597, eBioscience), CD8 (53-6.7, BioLegend), CD4 (GK1.5, BioLegend), FoxP3 (FJK-16S, eBioscience), Ly6C (HK1–4, BioLegend), CD11b (M1/70, BioLegend), F4/80 (BM8, eBioscience), MHC II (M5/114.15.2, eBioscience), CD11c (N418, BioLegend), NK1.1 (PK136, BD Biosciences), IFNγ (XMG1.2, Tonbo Biosciences), H-2Db (28-14-8, eBioscience), H-2Kb (AF6–88.5.5.3, eBioscience), PD-1 (29F.1A12, BioLegend), and PD-L1 (MIH5, eBioscience). Fluorescence was measured on BD LSR Fortessa™ X-20 or BD FACSymphony™ flow cytometer (BD Biosciences, North Ryde, New South Wales, Australia) and data analysed using FlowJo, LLC software.

Cytokine bead array. IFNγ was measured with a mouse CBA inflammation kit (BD Biosciences, 552364) according to manufacturer's instructions. Samples were analyzed using a FACS Verse (BD Biosciences, North Ryde, New South Wales, Australia).

Immunohistochemistry. Tumors were fixed with 10% neutral buffered formalin and paraffin embedded. 4 μm tumor slices were immunostained with anti-CD3 (SP7, Abcam, used at 1:600) following a standard IHC protocol and utilising a DAKO Autostainer (Agilent Technologies). Slides were imaged on an Olympus BX51 microscope.

***In vivo* mouse experiments.** All animal studies were performed in accordance with the NHMRC Australian code for the care and use of animals for scientific purposes 8th edition (2013) and with approval from the Peter MacCallum Animal Experimentation Ethics Committee or the Walter and Eliza Hall and Harry Perkins Institute's Animal Ethics Committees. Male C57BL/6 and *Rag1*$^{-/-}$ mice were purchased from Walter Eliza Hall Institute and NOD scid gamma (NSG) mice were bred in-house. 6–10 week old mice were shaved 1–2 days prior to tumor implants and anaesthetised for injections. Mice were injected subcutaneous on the right flank with 2×10^6 cells in 100 μL PBS using a 27 G needle. Tumors were measured 2–3 times/week and mice were euthanized when tumor volume reached >1200 mm^3. For all therapy studies, mice were randomised according to tumor size on the day that therapy commenced. For targeted therapies, dabrafenib (30 mg/kg; Selleckchem, Houston, TX) plus trametinib (0.3 mg/kg; HY-10999 Focus Bioscience) were co-administered by a single daily oral gavage (vehicle 0.5% hydroxypropylmethyl cellulose, 0.2% Tween 80 in H_2O), 6 days/week, starting when tumors reached 50–200 mm^3. For immunotherapies, anti-PD-1 (RMP1–14) and anti-CTLA-4 (9H10), or corresponding isotypes Rat IgG2a and Syrian Hamster, respectively, were purchased from Bio X Cell (West Lebanon, NH) and administered by intraperitoneal injection. For anti-CTLA4 monotherapy and combination anti-PD-1 plus anti-CTLA-4, 200 μg/150 μg of anti PD-1/CTLA-4 or corresponding isotypes was administered to each mouse on day 15 post tumor inoculation, followed by 3 further doses of 150 μg/100 μg, 4 days apart. For anti-PD-1 monotherapy, 200 μg

of anti-PD-1 or isotype was administered once per week for 3 weeks starting 11 days post tumor inoculation. For OT-I T cell transfer, mice were given 4 Gy total body irradiation (using X-RAD iR-160; Precision X-Ray, North Branford, CT) on day 16 post tumor inoculation, followed by intravenous administration of 1×10^7 primary OT-I T cells. Mice were given 50,000 IU IL-2 by intraperitoneal injection daily for 5 days post OT-I T cell transfer.

***In vitro* drug response.** Cells were cultured in PLX4720 (Euroasian Chemicals, Mumbai, India) or cobimetinib (Selleckchem, Houston, TX, USA). For dose response curves, cells were cultured in drug for 5–6 days, then fixed with 100% methanol followed by 20 minutes in 2 N HCl + 0.5% Triton X-100, 10 minutes in 0.1 M $Na_2B_40_7.H_20$ (pH 8.5) and nuclear stained with 1 μg/mL propidium iodide. Cells were counted by Red Object Count using the Incucyte Zoom® (Essen BioScience). For proliferation assays, confluency was measured every 12–24 hours using the Incucyte Zoom®.

Western blot. Cells were lysed in buffer containing 0.5 mM EDTA, 20 mM HEPES and 2% SDS (pH 7.9), incubated at 95 °C for 10 minutes and passed through a 25 G syringe. Protein was quantified with DT™ protein kit (Bio-Rad #5000111), run on 4–20% SDS-PAGE gel and transferred by BioRad semi-dry transfer system. Immobulin-P polyvinylidene fluoride (PVDF) membrane (Millipore) was blocked with 5% skim milk in Tris-buffered saline plus 0.1% Tween-20 prior to probing with primary antibodies and HRP-conjugated secondary antibodies. ECL western blotting detection kit (GE Healthcare #45000878) was used for detection. Primary antibodies used were p44/42 (Erk1/2) Rabbit pAb (#9102 S) and phospho-p44/42 MAPK (Erk1/2) (Thr202/Tyr204) (D13.14.4E) XP® Rabbit mAb (#4370), both used at 1:1000.

Statistical analysis. One-way analysis of variance (ANOVA) with Tukey's multiple comparisons tests and unpaired *t*-tests were performed using GraphPad PRISM. Kaplan-Meier survival was compared using a log-rank (Mantel-Cox) test. All experiments were performed in at least three biological replicates. Error bars show ±SEM. Significance was determined as $^*p < 0.05$, $^{**}p < 0.01$, $^{***}p < 0.001$, $^{****}p < 0.0001$.

Data Availability

All data generated or analysed during this study are included in this published article (and its Supplementary Information files).

References

1. Ribas, A. *et al.* Association of Pembrolizumab With Tumor Response and Survival Among Patients With Advanced Melanoma. *JAMA* **315**, 1600–1609, https://doi.org/10.1001/jama.2016.4059 (2016).
2. Hodi, F. S. *et al.* Improved survival with ipilimumab in patients with metastatic melanoma. *N Engl J Med* **363**, 711–723, https://doi.org/10.1056/NEJMoa1003466 (2010).
3. Daud, A. I. *et al.* Programmed Death-Ligand 1 Expression and Response to the Anti-Programmed Death 1 Antibody Pembrolizumab in Melanoma. *J Clin Oncol* **34**, 4102–4109, https://doi.org/10.1200/JCO.2016.67.2477 (2016).
4. Larkin, J. *et al.* Combined Nivolumab and Ipilimumab or Monotherapy in Untreated Melanoma. *N Engl J Med* **373**, 23–34, https://doi.org/10.1056/NEJMoa1504030 (2015).
5. Postow, M. A. *et al.* Nivolumab and ipilimumab versus ipilimumab in untreated melanoma. *N Engl J Med* **372**, 2006–2017, https://doi.org/10.1056/NEJMoa1414428 (2015).
6. Wolchok, J. D. *et al.* Overall Survival with Combined Nivolumab and Ipilimumab in Advanced Melanoma. *N Engl J Med* **377**, 1345–1356, https://doi.org/10.1056/NEJMoa1709684 (2017).
7. Robert, C. *et al.* Nivolumab in previously untreated melanoma without BRAF mutation. *N Engl J Med* **372**, 320–330, https://doi.org/10.1056/NEJMoa1412082 (2015).
8. Robert, C. *et al.* Ipilimumab plus dacarbazine for previously untreated metastatic melanoma. *N Engl J Med* **364**, 2517–2526, https://doi.org/10.1056/NEJMoa1104621 (2011).
9. Robert, C. *et al.* Improved overall survival in melanoma with combined dabrafenib and trametinib. *N Engl J Med* **372**, 30–39, https://doi.org/10.1056/NEJMoa1412690 (2015).
10. Chapman, P. B. *et al.* Improved survival with vemurafenib in melanoma with BRAF V600E mutation. *N Engl J Med* **364**, 2507–2516, https://doi.org/10.1056/NEJMoa1103782 (2011).
11. Chapman, P. B., Solit, D. B. & Rosen, N. Combination of RAF and MEK inhibition for the treatment of BRAF-mutated melanoma: feedback is not encouraged. *Cancer Cell* **26**, 603–604, https://doi.org/10.1016/j.ccell.2014.10.017 (2014).
12. Flaherty, K. T. *et al.* Combined BRAF and MEK inhibition in melanoma with BRAF V600 mutations. *N Engl J Med* **367**, 1694–1703, https://doi.org/10.1056/NEJMoa1210093 (2012).
13. Flaherty, K. T. *et al.* Improved survival with MEK inhibition in BRAF-mutated melanoma. *N Engl J Med* **367**, 107–114, https://doi.org/10.1056/NEJMoa1203421 (2012).
14. Long, G. V. *et al.* Combined BRAF and MEK inhibition versus BRAF inhibition alone in melanoma. *N Engl J Med* **371**, 1877–1888, https://doi.org/10.1056/NEJMoa1406037 (2014).
15. Larkin, J. *et al.* Combined vemurafenib and cobimetinib in BRAF-mutated melanoma. *N Engl J Med* **371**, 1867–1876, https://doi.org/10.1056/NEJMoa1408868 (2014).
16. McArthur, G. A. & Ribas, A. Targeting oncogenic drivers and the immune system in melanoma. *J Clin Oncol* **31**, 499–506, https://doi.org/10.1200/JCO.2012.45.5568 (2013).
17. Karachaliou, N. *et al.* Melanoma: oncogenic drivers and the immune system. *Ann Transl Med* **3**, 265, https://doi.org/10.3978/j.issn.2305-5839.2015.08.06 (2015).
18. Reddy, S. M., Reuben, A. & Wargo, J. A. Influences of BRAF Inhibitors on the Immune Microenvironment and the Rationale for Combined Molecular and Immune Targeted Therapy. *Curr Oncol Rep* **18**, 42, https://doi.org/10.1007/s11912-016-0531-z (2016).
19. Boni, A. *et al.* Selective BRAFV600E inhibition enhances T-cell recognition of melanoma without affecting lymphocyte function. *Cancer Res* **70**, 5213–5219, https://doi.org/10.1158/0008-5472.CAN-10-0118 (2010).
20. Homet Moreno, B. *et al.* Response to Programmed Cell Death-1 Blockade in a Murine Melanoma Syngeneic Model Requires Costimulation, CD4, and CD8 T Cells. *Cancer Immunol Res* **4**, 845–857, https://doi.org/10.1158/2326-6066.CIR-16-0060 (2016).
21. Meeth, K., Wang, J. X., Micevic, G., Damsky, W. & Bosenberg, M. W. The YUMM lines: a series of congenic mouse melanoma cell lines with defined genetic alterations. *Pigment Cell Melanoma Res*, https://doi.org/10.1111/pcmr.12498 (2016).
22. Wang, J. *et al.* UV-induced somatic mutations elicit a functional T cell response in the YUMMER1.7 mouse melanoma model. *Pigment Cell Melanoma Res* **30**, 428–435, https://doi.org/10.1111/pcmr.12591 (2017).

23. Sanmamed, M. F., Chester, C., Melero, I. & Kohrt, H. Defining the optimal murine models to investigate immune checkpoint blockers and their combination with other immunotherapies. *Ann Oncol* **27**, 1190–1198, https://doi.org/10.1093/annonc/mdw041 (2016).
24. Kersten, K., de Visser, K. E., van Miltenburg, M. H. & Jonkers, J. Genetically engineered mouse models in oncology research and cancer medicine. *EMBO Mol Med* **9**, 137–153, https://doi.org/10.15252/emmm.201606857 (2017).
25. Alexandrov, L. B. *et al*. Signatures of mutational processes in human cancer. *Nature* **500**, 415–421, https://doi.org/10.1038/nature12477 (2013).
26. Linnemann, C. *et al*. High-throughput epitope discovery reveals frequent recognition of neo-antigens by CD4+ T cells in human melanoma. *Nat Med* **21**, 81–85, https://doi.org/10.1038/nm.3773 (2015).
27. Lu, Y. C. *et al*. Efficient identification of mutated cancer antigens recognized by T cells associated with durable tumor regressions. *Clin Cancer Res* **20**, 3401–3410, https://doi.org/10.1158/1078-0432.CCR-14-0433 (2014).
28. Verdegaal, E. M. *et al*. Neoantigen landscape dynamics during human melanoma-T cell interactions. *Nature* **536**, 91–95, https://doi.org/10.1038/nature18945 (2016).
29. van Rooij, N. *et al*. Tumor exome analysis reveals neoantigen-specific T-cell reactivity in an ipilimumab-responsive melanoma. *J Clin Oncol* **31**, e439–442, https://doi.org/10.1200/JCO.2012.47.7521 (2013).
30. Hu, D. E., Kettunen, M. I. & Brindle, K. M. Monitoring T-lymphocyte trafficking in tumors undergoing immune rejection. *Magn Reson Med* **54**, 1473–1479, https://doi.org/10.1002/mrm.20717 (2005).
31. Goldberger, O. *et al*. Exuberated numbers of tumor-specific T cells result in tumor escape. *Cancer Res* **68**, 3450–3457, https://doi.org/10.1158/0008-5472.CAN-07-5006 (2008).
32. Brown, D. M., Fisher, T. L., Wei, C., Frelinger, J. G. & Lord, E. M. Tumours can act as adjuvants for humoral immunity. *Immunology* **102**, 486–497 (2001).
33. Kaur, A. *et al*. sFRP2 in the aged microenvironment drives melanoma metastasis and therapy resistance. *Nature* **532**, 250–254, https://doi.org/10.1038/nature17392 (2016).
34. George, S. *et al*. Loss of PTEN Is Associated with Resistance to Anti-PD-1 Checkpoint Blockade Therapy in Metastatic Uterine Leiomyosarcoma. *Immunity* **46**, 197–204, https://doi.org/10.1016/j.immuni.2017.02.001 (2017).
35. Peng, W. *et al*. Loss of PTEN Promotes Resistance to T Cell-Mediated Immunotherapy. *Cancer Discov* **6**, 202–216, https://doi.org/10.1158/2159-8290.CD-15-0283 (2016).
36. Dong, Y. *et al*. PTEN functions as a melanoma tumor suppressor by promoting host immune response. *Oncogene* **33**, 4632–4642, https://doi.org/10.1038/onc.2013.409 (2014).
37. Robert, C. *et al*. Pembrolizumab versus Ipilimumab in Advanced Melanoma. *N Engl J Med* **372**, 2521–2532, https://doi.org/10.1056/NEJMoa1503093 (2015).
38. Fife, B. T. & Bluestone, J. A. Control of peripheral T-cell tolerance and autoimmunity via the CTLA-4 and PD-1 pathways. *Immunol Rev* **224**, 166–182, https://doi.org/10.1111/j.1600-065X.2008.00662.x (2008).
39. Du, X. *et al*. A reappraisal of CTLA-4 checkpoint blockade in cancer immunotherapy. *Cell Res* **28**, 416–432, https://doi.org/10.1038/s41422-018-0011-0 (2018).
40. Romano, E. *et al*. Ipilimumab-dependent cell-mediated cytotoxicity of regulatory T cells *ex vivo* by nonclassical monocytes in melanoma patients. *Proc Natl Acad Sci USA* **112**, 6140–6145, https://doi.org/10.1073/pnas.1417320112 (2015).
41. Kavanagh, B. *et al*. CTLA4 blockade expands FoxP3+ regulatory and activated effector CD4+ T cells in a dose-dependent fashion. *Blood* **112**, 1175–1183, https://doi.org/10.1182/blood-2007-11-125435 (2008).
42. Shoushtari, A. N. *et al*. Measuring Toxic Effects and Time to Treatment Failure for Nivolumab Plus Ipilimumab in Melanoma. *JAMA Oncol* **4**, 98–101, https://doi.org/10.1001/jamaoncol.2017.2391 (2018).
43. Andrews, A. Treating with Checkpoint Inhibitors-Figure $1 Million per Patient. *Am Health Drug Benefits* **8**, 9 (2015).
44. Menzies, A. M. & Long, G. V. Dabrafenib and trametinib, alone and in combination for BRAF-mutant metastatic melanoma. *Clin Cancer Res* **20**, 2035–2043, https://doi.org/10.1158/1078-0432.CCR-13-2054 (2014).

Acknowledgements

This work was supported by grants from the NHMRC of Australia to GAM, KES, CC & NH (#1100189) and from Pfizer Oncology. EL was supported by a Peter MacCallum Cancer Centre Postgraduate Scholarship, Melbourne Research Scholarship (University of Melbourne; 58616) and a Cancer Therapeutics CRC (CTx) PhD Top Up Scholarship. FSFG was supported by a NHMRC Early Career Fellowship (1088703), a National Breast Cancer Foundation (NBCF) Fellowship (PF-15-008), a NHMRC New Investigator Grant (1140406), and a grant (1120725) awarded through the Priority-driven Collaborative Cancer Research Scheme and funded by Cure Cancer Australia with the assistance of Cancer Australia.

Author Contributions

E.J.L., C.A.M., R.W., K.M.R., F.S.F.G., S.A., J.M., L.K., R.Y., A.S. and P.L. conducted experimental work. C.C., K.M., F.S.F.G. and J.O. provided reagents and advice. E.J.L., C.C., F.S.F.G., J.O., N.H., G.A.M., and K.E.S. designed the study, analysed the data and wrote the manuscript.

Additional Information

Supplementary information accompanies this paper at https://doi.org/10.1038/s41598-018-37883-y.

Competing Interests: The authors declare no competing interests.

Publisher's note: Springer Nature remains neutral with regard to jurisdictional claims in published maps and institutional affiliations.

4. Supplementary data

Supplementary data included for publication with this work begins on the following page.

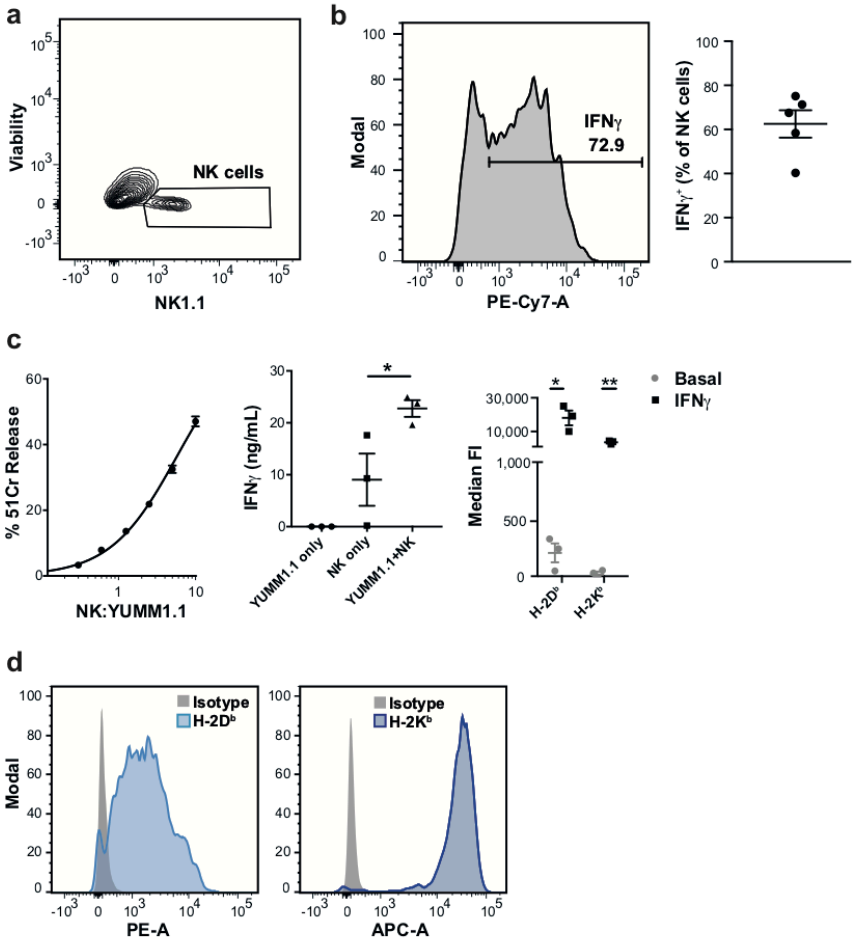

Supplementary Figure 1. a-b, NK cells **(a)** and IFNγ-expressing NK cells **(b)** in YUMM1.1 tumors harvested from C57BL/6 mice, plots representative of n=5. **c,** Left panel - Killing by splenic-derived NK cells co-cultured for 4 hours with 51Cr-labelled YUMM1.1 cells at indicated ratios, representative of n=3. Middle panel - IFNγ secretion by splenic-derived NK cells co-cultured for 4 hours with YUMM1.1 cells at a ratio of 2:1, IFNγ secretion was measured by cytokine bead array, One way ANOVA, Tukey's multiple comparisons test, n=3. Right panel - MHC I expression on unstimulated (basal) and IFNγ-stimulated YUMM1.1 cells in vitro, unpaired t test, n=3. **d,** MHC I expression on YUMM1.1 tumors harvested from C57BL/6 mice, representative of n=3. All error bars show ±SEM. *p<0.05, **p<0.01.

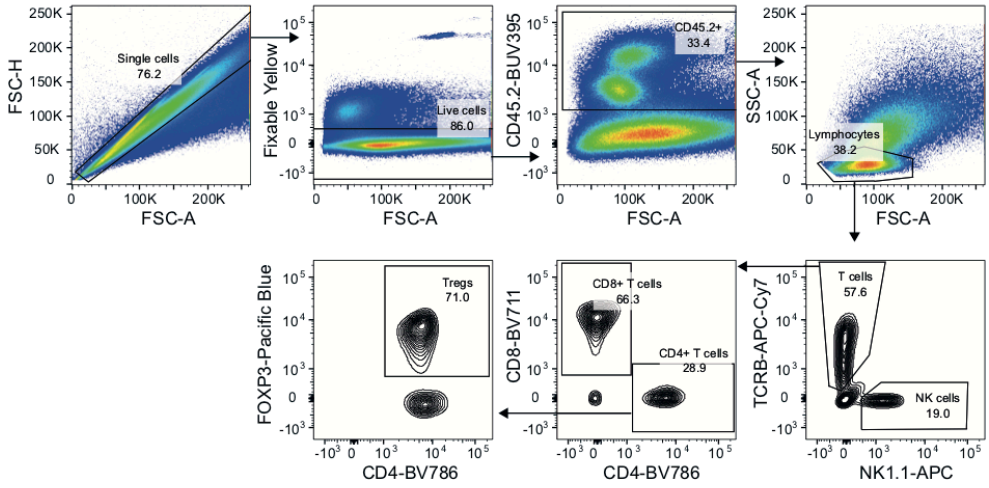

Supplementary Figure 2. Gating strategy on tumors for defining infiltrating CD8+ T cells, CD4+ T cells, regulatory T cells (Tregs) and NK cells.

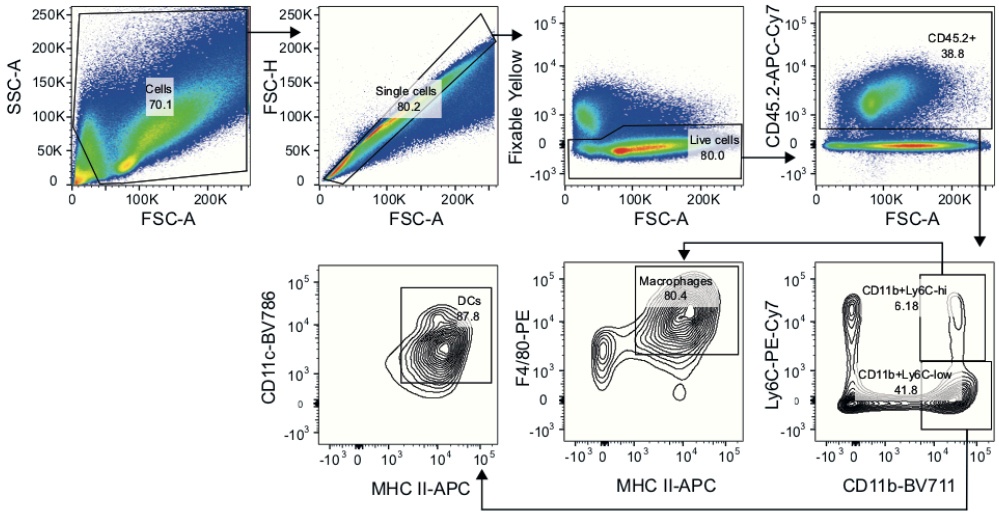

Supplementary Figure 3. Gating strategy on tumors for defining infiltrating macrophages and dendritic cells (DCs).

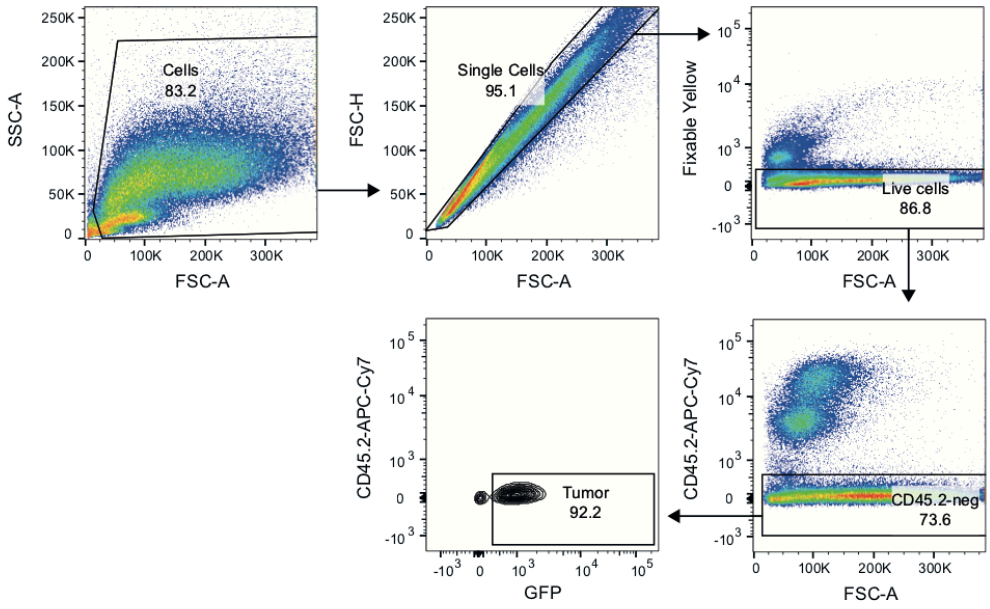

Supplementary Figure 4. Gating strategy for YOVAL1.1 tumor cells.

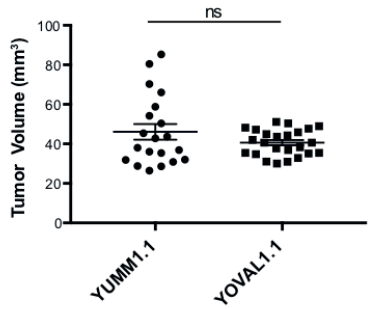

Supplementary Figure 5. Tumor volume at day 15 when immunotherapies were commenced. ns - not significant, unpaired t test, n=20-24. Error bars show ±SEM.

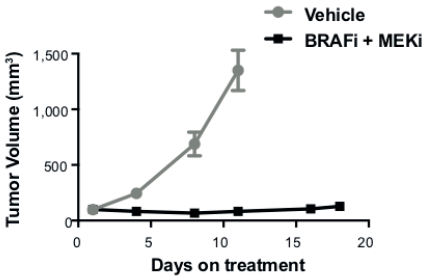

Supplementary Figure 6. YUMM1.1 tumor growth in C57BL/6 mice treated daily, 6 days/week, with dabrafenib (BRAFi) plus trametinib (MEKi). Error bars show ±SEM.

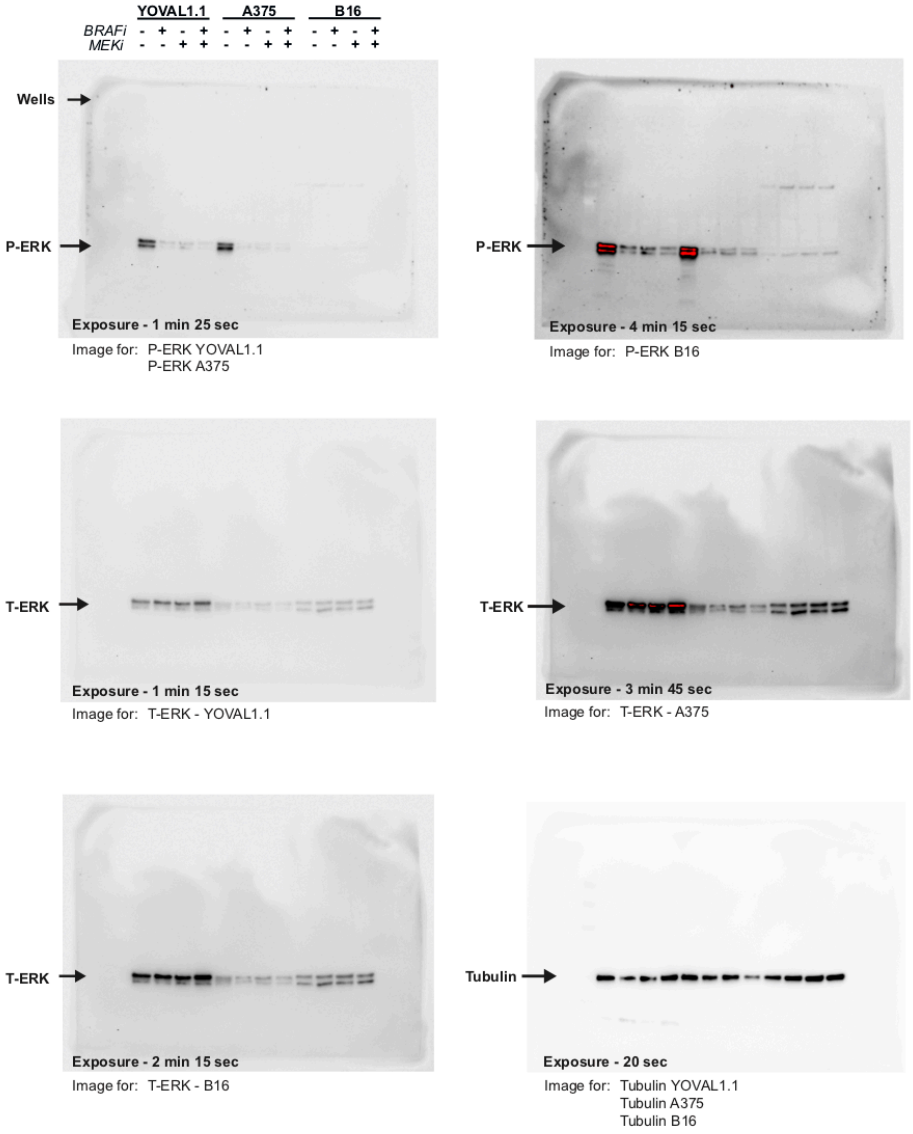

Supplementary Figure 7. Full-length blots used to compile Figure 4c. All images were cropped from different parts of the same blot at indicated exposure times. P-ERK - phosp-ERK; T-ERK - Total-ERK.

Chapter 3: Combined BRAF, MEK and CDK4/6 inhibition depletes intratumoral immune-potentiating myeloid populations in melanoma

1. Preface

The aim of this chapter was to assess the efficacy of BRAF, MEK and CDK4/6 inhibitors in an immunocompetent *Braf*^{V600}*Cdkna2*$^{-/-}$ melanoma model and evaluate the effects of these inhibitors on the tumor immune microenvironment and the response to immune checkpoint blockade.

This body of work has recently been accepted for publication:

Lelliott EJ, Mangiola S, Ramsbottom KM, Zethoven M, Lim L, Lau P, Oliver AJ, Martelotto L, Kirby L, Martin C, Patel R, Slater A, Cullinane C, Papenfuss A, Haynes NM, McArthur GA, Oliaro J, Sheppard KE. Combined BRAF, MEK and CDK4/6 inhibition depletes intratumoral immune-potentiating myeloid populations in melanoma. *Cancer Immunol Res* [in press December 2020].

This chapter will present an introduction with a summary of the key findings, the work accepted for publication, and associated supplementary data.

2. Introduction

Targeted inhibition of BRAF/MEK and CDK4/6 has shown potent anti-tumor activity in pre-clinical xenograft models of melanoma (50, 51), and is consequently undergoing evaluation in clinical trials for the treatment of *BRAF*^{V600} melanoma. However, this combination has not be tested in a syngeneic setting as, up until recently, there have been no suitable mouse melanoma models that harbor the clinically relevant oncogenic-driver mutations targeted by these drugs. As combined BRAF, MEK and CDK4/6 inhibition enters clinical trials, understanding the impact of this combination on anti-tumor immunity is essential for two key reason; (1) all three of these inhibitors have been shown to modulate anti-tumor immunity and there is strong evidence to suggest the immune system is an important component to their individual therapeutic efficacy; and (2) resistance to targeted therapies is a major clinical challenge and in some cases immune checkpoint blockade is a potential alternative treatment for patients that progress on targeted therapy.

The aim of this chapter was to use the YOVAL1.1 melanoma mouse model developed in Chapter 2 (250) to assess the efficacy of combined BRAF, MEK and CDK4/6 inhibition in the context of an intact immune system, and evaluate the effects of this combination on the tumor immune microenvironment and the response to immune checkpoint blockade. To address this, flow cytometry and single cell RNA sequencing (scRNA-seq) were used to comprehensively evaluate changes in the tumor immune compartment in response to the triple therapy combination. ScRNA-seq has revolutionized immunological analyses as it allows an unbiased evaluation of immune populations through transcriptomics, in contrast to flow cytometry, which is restricted by antibodies selected for pre-chosen surface markers. ScRNA-seq can therefore be

used as a discovery tool to identify cell types, subsets or phenotypes that one may otherwise not be looking for. Indeed, the value of scRNA-seq was illustrated in this body of work.

In this study, initial tumor growth and flow cytometric analyses showed that combined BRAF, MEK and CDK4/6 inhibition induced immunogenic cell death, enhanced expression of MHC I and caused robust *in vitro* and *in vivo* tumor control in the YOVAL1.1 model. Additionally, the triple therapy promoted T cell infiltration and depleted suppressive T regulatory cells and myeloid cells in the tumor microenvironment. However, despite these changes, the immune system did not contribute to the therapeutic response. Furthermore, tumors treated with the triple therapy unexpectedly failed to respond to immune checkpoint blockade. Further analysis by scRNA-seq revealed a marked depletion of intratumoral pro-inflammatory macrophages and cross-priming CD103+ dendritic cells in response to triple therapy, which was not identified by initial flow cytometric analyses. Reanalysis of published datasets showed that a loss of these myeloid cells significantly correlated with poor overall survival and responses to immune checkpoint blockade in melanoma patients. Accordingly, immune cells isolated from tumors following triple therapy failed to stimulate T cell responses *ex vivo*, highlighting the detrimental impact this therapy may have on anti-tumor T cell immunity.

Collectively this work demonstrates that, while combined inhibition of BRAF, MEK and CDK4/6 has potent tumor-intrinsic activity *in vivo*, this therapy combination has profound effects on the immune microenvironment that may impact on the anti-tumor efficacy of T cell-directed immunotherapies. These findings have significant implications for the clinical management of melanoma patients and decision-making

around treatment strategies and participation in trials that incorporate these targeted and/or immune-based therapies.

3. Publication accepted in *Cancer Immunology Research*

This body of work begins on the following page.

Combined BRAF, MEK and CDK4/6 inhibition depletes intratumoral immune-potentiating myeloid populations in melanoma

Emily J. Lelliott[1,2], Stefano Mangiola[3], Kelly M. Ramsbottom[1], Magnus Zethoven[1], Lydia Lim[1], Peter K. Lau[1,2], Amanda J. Oliver[1,2], Luciano G. Martelotto[4], Laura Kirby[1], Claire Martin[1], Riyaben P. Patel[1], Alison Slater[1], Carleen Cullinane[1], Anthony T. Papenfuss[1], Nicole M. Haynes[1,2], Grant A. McArthur[1,2*], Jane Oliaro[1,2,5*], Karen E. Sheppard[1,2,6*]

1. Cancer Research Division, Peter MacCallum Cancer Centre, Melbourne, VIC, Australia
2. Sir Peter MacCallum Department of Oncology, University of Melbourne, Parkville, VIC, Australia
3. The Walter and Eliza Hall Institute of Medical Research, Parkville, VIC, Australia
4. Single Cell Innovation Laboratory, The University of Melbourne, Parkville, VIC, Australia
5. Department of Immunology, Central Clinical School, Monash University, Melbourne, VIC, Australia
6. Department of Biochemistry and Molecular Biology, University of Melbourne, Parkville, VIC, Australia.

* These authors contributed equally to this work

Running title: Triple therapy depletes immune-potentiating myeloid cells

Key words: CDK4/6, MEK, BRAF, immunotherapy, melanoma

Financial support: National Health and Medical Research Council project grants to G.A.M. & K.E.S. (1100189) and J.O. (1139626); National Breast Cancer Foundation grant to J.O. (IIRS-18-151); Peter Mac Postgraduate Scholarship, Melbourne University Research Scholarship (58616) and Cancer Therapeutics CRC PhD Top Up Scholarship to E.J.L.; and Pfizer Oncology.

Correspondence: Karen E. Sheppard, the Peter MacCallum Cancer Centre, Melbourne, VIC 3000, Australia; Phone: +61 3 85596681; Fax: +61 3 8559 5039; E-mail: karen.sheppard@petermac.org

Conflict of interest: Authors declare no potential conflicts of interest

Synopsis: Combined BRAF, MEK and CDK4/6 inhibition is being tested in clinical trials for treating melanoma. The authors show this combination depletes tumor-associated myeloid cells in the tumor immune microenvironment, which renders tumors unresponsive to immune checkpoint blockade.

Abstract: 198 words (200)

Text: 3,478 words (2,500)

Figures: 4 figures (4 figures)

References: 43 (25)

Abstract

Combined inhibition of BRAF, MEK and CDK4/6 is currently under evaluation in clinical trials for patients with melanoma harboring a *BRAF*^{V600} mutation. While this triple therapy has potent tumor-intrinsic effects, the impact of this combination on anti-tumor immunity remains unexplored. Here, using a syngeneic *Braf*^{V600E}*Cdkn2a*$^{-/-}$*Pten*$^{-/-}$ melanoma model, we demonstrated that triple therapy promoted durable tumor control through tumor-intrinsic mechanisms and promoted immunogenic cell death and T-cell infiltration. Despite this, tumors treated with triple therapy were unresponsive to immune checkpoint blockade (ICB). Flow cytometric and single-cell RNA-seq analyses of tumor-infiltrating immune populations revealed that triple therapy markedly depleted pro-inflammatory macrophages and cross-priming CD103^{+} dendritic cells (DCs), the absence of which correlated with poor overall survival and clinical responses to ICB in melanoma patients. Indeed, immune populations isolated from tumors of mice treated with triple therapy failed to stimulate T-cell responses *ex vivo.* While combined BRAF, MEK and CDK4/6 inhibition demonstrates favourable tumor-intrinsic activity, these data suggest that collateral effects on tumor-infiltrating myeloid populations may impact on anti-tumor immunity. These findings have important implications for the design of combination strategies and clinical trials that incorporate BRAF, MEK and CDK4/6 inhibition with immunotherapy for the treatment of patients with melanoma.

Introduction

Inhibition of the MAPK/ERK pathway using small-molecule inhibitors of mutant $BRAF^{V600E}$ and MEK is a standard-of-care therapy for treating BRAF-mutant melanoma. Such therapy is typified by exceptional short-term clinical responses followed by the eventual emergence of resistance in most patients (1). Immune checkpoint blockade (ICB) of the inhibitory receptors PD1 and CTLA4 on T cells, is an additional treatment option for patients with melanoma (2), however the immunomodulatory effects of MAPK/ERK-targeted therapy can impact on the efficacy of this therapy. For example, short-term BRAF inhibition can enhance tumor susceptibility to ICB by increasing the immunogenicity of tumors (3, 4), while resistance to long-term BRAF inhibition correlates with a loss of tumor-infiltrating lymphocytes essential for ICB efficacy (4-6).

Cyclin-dependent kinases 4 and 6 (CDK4/6), are aberrantly activated in approximately 90% of melanomas (7), and inhibiting these kinases improves the efficacy of dual BRAF and MEK inhibition (8, 9). As a result, triple inhibition of BRAF, MEK and CDK4/6 is now being evaluated in clinical trials for the treatment of melanoma (NCT01820364, NCT02065063). Similar to BRAF- and MEK-targeted therapies, CDK4/6 inhibitors also have immunomodulatory effects (10, 11). However, the impact of the triple therapy on anti-tumor immunity remains unexplored.

Here, we used our recently developed syngeneic mouse model of $Braf^{V600E}Cdkn2a^{-/-}Pten^{-/-}$ melanoma (12), to examine the immunomodulatory effects of BRAF, MEK and CDK4/6 inhibition. While superior to dual BRAF and MEK inhibition in controlling tumour growth, we found that continuous administration of triple therapy depleted the tumor microenvironment of pro-inflammatory macrophages and cross-priming $CD103^{+}$ DCs that may be required for optimal anti-tumor T cell immunity. These data have

important clinical implications for therapy scheduling and the stratification of melanoma patients between trials of this triple therapy and available immunotherapy options.

Methods

Mice and in vivo growth and therapy studies

Animal work was performed in agreement with the National Health and Medical Research Council (NHMRC) Australian code for care and use of animals for scientific purposes 8th edition (2013) with approval from the Peter MacCallum Animal Experimentation Ethics Committee. $2x10^6$ YOVAL1.1 cells in PBS were injected subcutaneously on the right flank of C57BL/6 (purchased from Walter and Eliza Hall Institute of Medical Research) or C57BL/6-Rag2$\gamma c^{-/-}$ (bred in house) male mice (6-10 weeks old) and tumors were measured twice per week. Tumor volumes were calculated as 0.5 x tumor length x (tumor width)^2. NOD scid gamma (NSG) mice were bred in house and C57BL/6.OT-II were obtained from the Peter Doherty Institute. For survival, end-point tumor volume was >1200mm^3. Unless otherwise indicated, mice were randomized for treatment when tumors reached approximately 100mm^3. For targeted therapies, mice were dosed with dabrafenib/trametinib (Ark Pharm cat. #AK174048 and Focus Bioscience cat. #HY-10999, respectively) (30/0.3mg/kg in 0.5% hydroxypropylmethyl cellulose, 0.2% Tween 80 in H_2O), palbociclib (Pfizer; 80mg/kg in 50mM sodium lactate), or the combination. The targeted therapies were administered daily by oral gavage 6–7 days per week. Anti-PD1 (Bio X Cell, clone RMP1-14, cat. #BE0146), anti-CTLA4 (Bio X Cell , clone 9H10, cat. #BE0131), or corresponding isotype controls (Bio X Cell, clone 2A3, cat. #BE0089, or polyclonal Syrian hamster, cat #BE0087, respectively) were given by intraperitoneal injection 4 days apart (first dose 200µg/150µg, subsequent doses 150µg/100µg). CD8 and NK depleting antibodies, anti-

CD8 (Bio X Cell, clone YTS169.4, cat. #BE0117) and anti-asialo GM1 (Novachem, cat. #986-10001), respectively, were administered at 250μg/mouse on day -1 & 0 and 150μg/mouse on day 4, 8 and weekly ongoing, with day 0 being the day of tumor inoculation.

Tumor preparation, flow cytometry and sorting

Tumors were harvested, weighed, and diced with a scalpel followed by incubation with Collagenase IV (1.6mg/mL; Worthington Biochemical Corporation, cat. #LS004188) + DNase (2U/mL; Merck, cat. #11284932001) in DMEM, high glucose, pyruvate (Thermo Fisher Scientific, cat. #11965092) for 45 minutes at 37^{o}C with agitation. Digests were then filtered through a 70μm filter and washed before staining with relevant antibodies for flow cytometry analysis or fluorescence activated cell (FAC) sorting. Immune cells were isolated from tumors by FAC sorting on live CD45.2+ cells using BD FACSAria Fusion. Antibodies were sourced from Thermo Fisher eBioscience—H-2Kb (AF6-88.5.5.3), CD3 (17A2), CD4 (GK1.5), FOXP3 (FJK-16s), Ly6C (HK1.4), Ly6G (1A8), and CD103 (2E7)—Biolegend—CD8 (53-6.7), CD19 (6D5), NK1.1 (PK136), CD11b (M1/70), MHC-II (1-A/1-E; M5/114.15.2), F4/80 (BM8), CD24 (M1/69), CD44 (IM7), CD69 (H1.2F3), and CD25 (PC61)—Tonbo Biosciences CD45.2 (104)—and Abcam—CRT (EPR3924). Fixable yellow (Invitrogen, L34959) was used to stain live/dead cells. Fluorescence was measured on a BD FACSymphony flow cytometer or a BD LSR Fortessa X-20 cytometer (BD Biosciences) and data analysed using FlowJo, LLC software. For t-distributed stochastic neighbor embedding (tSNE) analysis, subpopulations of equal numbers of CD45.2 cells were generated from representative samples using the DownSample V3 plugin. Subpopulations from all groups were then concatenated into one file for dimensionality reduction using the tSNE function, with all

antibody markers plus FSC and SSC as parameters. Different groups within the concatenated file were then re-delineated based on pre-assigned sample IDs.

Cell lines and in vitro drug assays

YOVAL1.1 cells were developed in-house (described in ref. 12; 2019) and used for *in vivo* work within 8 days (2 passages) of thawing, or for *in vitro* work within 14 days (4 passages) of thawing. YOVAL1.1 cells were cultured in RPMI-1640 (Thermo Fisher Scientific, cat. #11875093) supplemented with 10% FBS (Thermo Fisher Scientific, cat. #10100147), 20 mM HEPES (Merck, cat. #H0887), 1% GlutaMAX (Thermo Fisher Scientific, cat. #35050061), 1 mM Minimal Essential Medium Non-Essential Amino Acids (Thermo Fisher Scientific, cat. #11140050), 0.1% 2-mercaptoethanol (Merck, cat. #M6250) and 1 mM Sodium Pyruvate (Thermo Fisher Scientific, cat. #11360070), at 37 °C in 5% CO_2. Cells were confirmed negative for mycoplasma by polymerase chain reaction and used within 1 week of testing. For proliferation assays, cells were cultured in various combinations of 2nM dabrafenib, 0.2nM trametinib, or 2μM palbociclib. For flow cytometry and western blot cells were cultured in various combinations of 20nM dabrafenib, 2nM trametinib or 1μM palbociclib for 72 hours. Dimethylsulfoxide (DMSO) was used as a vehicle for all *in vitro* drug assays.

Proliferation assays

YOVAL1.1 cells were seeded at a density of 500 cells/well in 96 well plates and allowed to adhere for 24 hours. After 24 hours, confluency was measured using Incucyte Zoom (Essen Biosciences). Targeted therapies were then added to each well using 5 technical replicates per treatment group. Assay plates were then incubated under standard cell culture conditions. Live cell confluency was measured every 12–24 hours for two weeks

using Incucyte Zoom. Media was removed and replaced with fresh media plus drugs after one week.

Immunoblot

Cells were lysed in 2% SDS buffer containing 0.5 mM EDTA and 20 mM HEPES, boiled for 5 minutes, and quantified using DC protein assay (Bio-Rad, cat. #5000112) as per the manufacturer's protocol. Equal amounts of protein in 5X SDS sample buffer (0.05% (w/v) 313 mM Tris HCl pH 6.8, 10% (w/v) SDS, 50% (v/v) glycerol, 10% (v/v) β-mercaptoethanol, bromophenol blue) were boiled for 5 minutes and resolved via SDS-PAGE using precast gels (Bio-Rad) with running buffer (25 mM Tris (VWR), 190 mM glycine (Astral Scientific), 0.1% (w/v) SDS). Precision-plus protein dual color standard (Bio-Rad, cat. #1610374) was used as a molecular weight marker. Proteins were transferred onto methanol-activated PVDF membranes (Millipore) using the Trans-Blot Turbo semi-dry transfer system (Bio-Rad) with tris-glycine transfer buffer (50 mM Tris, 0.375% (w/v) SDS, 40 mM glycine, 20% (v/v) methanol). Membranes were blocked in 5% skim milk (Diploma Instant) in TBS-T (TBS+0.1% Tween-20 (Sigma-Aldrich)) for 1 hour prior to probing with primary antibody overnight at 4^{o}C, and horse-radish peroxidase (HRP)-conjugated secondary antibody for one hour at room temperature. Immunoblots were washed for 10 minutes in TBS-T three times after each antibody incubation. Proteins were detected using ECL western blotting substrate (Amersham GE Healthcare) and imaged using the ChemiDoc Imaging System (Bio-Rad). Antibodies used were: anti-phospho-44/42 MAPK (Erk1/2) (Thr202/Tyr204) (D13.14.4E) XP® (Cell Signalling Technology, cat. #4370S), anti-p44/42 MAPK (ERK1/2) (Cell Signalling Technology, cat. #9102S), anti-Phospho-RB (Ser807/811) (Cell Signalling Technology, cat. #9308S), anti-RB1 (G3-245) (BD Pharmingen, cat. #554136), anti-α-Tubulin

(DM1A) (Merck Millipore, cat. #05-829), anti-Mouse IgG (H + L)-HRP Conjugate (Bio-Rad, cat. #1706516), anti-Rabbit IgG (H + L)-HRP Conjugate (Bio-Rad, cat. #1706515).

Immunohistochemistry

Tumors were fixed in 10% neutral buffered formalin (NBF) overnight and paraffin embedded, followed by 4μm–thick sectioning onto glass slides. Slides were dewaxed in xylene, followed by antigen-retrieval in 10 mmol/L citrate buffer (Sigma; pH 6) at 125ºC for 3 minutes. Perkin Elmer OPAL reagents were used for staining as per the manufacturer's protocol (Opal 7-Color Manual IHC Kit, cat. #NEL811001KT). Anti-CD3 (clone SP7, Abcam) with Opal 690 Fluorophore and Dapi (Invitrogen, cat. #D1306) were used for staining. Perkin Elmer Vectra 3 microscope was used to obtain images. Analysis was performed with InForm v2.4.0 (Perkin Elmer) and HALO v2.3 (Indica).

Primary cell isolation, CTV labelling and co-cultures

Spleens from C57BL/6.OT-II transgenic mice were filtered through a 70μm filter and red blood cells were lysed with red cell lysis buffer (150mM NH_4Cl, 10mM $KHCO_3$, 0.1mM Na_2EDTA). Naïve $CD4^+$ T cells were isolated using a mouse Naïve $CD4^+$ T cell Isolation Kit (EasySep cat. #19765) and incubated with CellTrace Violet (CTV; Thermo Fisher Scientific) 1:1000 in PBS for 20 minutes. CTV-labelled cells were washed with PBS and cultured 10:1 with CD45.2+ cells isolated from tumors. Co-cultures were performed in 96-well plates (1 well per biological replicate) at 37 °C in 5% CO_2 RPMI-1640 supplemented with 10% FBS, 20 mM HEPES, 1% GlutaMAX, 1 mM Minimal Essential Medium Non-Essential Amino Acids, 0.1% 2-mercaptoethanol, and 1 mM Sodium Pyruvate.

Single-cell RNA-sequencing and TCR-sequencing

Sorted cells were washed with PBS, counted, and diluted to approximately 1000 cells/µl in PBS supplemented with 1% molecular grade bovine serum albumin (Thermo Fisher Scientific, cat. #B14) and 200U/mL RNase inhibitor (Merck, cat. #3335399001). Cells were then loaded onto the 10x Chromium instrument (10x Genomics, Pleasanton, CA, USA) to generate single-cell Gel Beads-in-Emulsion (GEMs) and capture/barcode cells. Samples were processed and libraries prepared using 10x Genomics Single Cell V(D)J kit as per the manufacturer's instructions (10x Genomics, cat. #PN-1000014). T-cell receptor (TCR) libraries were prepared using the 10x Chromium Single Cell V(D)J Enrichment Kit (10x Genomics cat. #PN-1000071).

Single-cell RNA sequencing and TCR sequencing analysis

For RNA analysis, sequencing reads were harmonised, mapped to the mm10 mouse genome and gene transcription abundance was quantified using the CellRanger suite 3.0 (10x Genomics) with default parameters. The software suite Seurat3 (13) was used for the analysis and manipulation of gene transcript abundance data. Droplets were excluded from further analyses if including less than 200 detected transcripts and if including a fraction of mitochondrial derived reads higher than 0.1. Cell-cycle state was inferred for each cell using the CellCycleScoring function with default parameters. Principal component analysis (PCA) was used to reduce the dimensionality of the data. PCA revealed the presence of unwanted variation generated from the cell-cycle phase. Transcript abundance was normalized and the unwanted variation was removed using regularized negative binomial regression (SCT algorithm) (13). Cells were assigned to clusters using the shared-nearest neighbor method (SNN) using default resolution. The algorithm SingleR (14) with Blueprint reference was used to label each cell cluster with

a cell-type identity. All differential transcript abundance analyses were conducted using FindMarkers function with the parameters min.pct=0.1 and only.pos=TRUE. Heatmaps were drawn using tidyHeatmapwrapper for the ComplexHeatmap algorithm (15). For TCR analyses, sequencing reads were trimmed for adapters using trimgalore, and aligned to the mm10 mouse genome using STAR (16) with default parameters. Mixrc (17) was used to quantify TCR proportions for each sample pool. The software suite tidyverse from R was used to perform all data manipulation and visualisation. All sequencing data has been deposited into the Gene Expression Omnibus (GEO) under the access number GSE162467.

For analyses of Sade-Feldman et al. dataset (18), transcripts per million (TPM) values were downloaded from the Gene Expression Omnibus (GEO; accession ID GSE120575) and processed using the *R* statistical software language (version 3.6.1) with the *Seurat* package (version 3.1.2) (13). The top 2000 variable genes were selected using the *FindVariableFeatures* function with the variance stabilizing transformation (VST) method. The selected genes were then scaled using the *ScaleData* function, using the fraction of total counts belonging to mitochondrial genes and the log total UMI counts for each cell as variables to regress out. PCA of the scaled genes was then calculated using the *RunPCA* function. The top 20 principal components were used to calculate Uniform Manifold Approximation and Projection (UMAP) (19) values using the *uwot* R package (version 0.1.5). Cells were clustered using the Louvain algorithm (with resolution parameter 0.8) using the *FindClusters* function applied to the SNN network calculated using the *FindNeighbors* function. Cosine distance metric and 30 nearest neighbors were used for both UMAP and SNN algorithms. Signature area-under-curve (AUC) scores were calculated using the AUC R package (version 1.8.0). Clusters were labelled with putative cell types informed by the scMatch algorithm (20). Patients where

total myeloid cells were less than 1% were excluded from analysis. Cells in the monocyte cluster with $CD103^+$ DC AUC score greater than 0.2 were classified as $CD103^+$ DCs.

TCGA analysis

RNA-Seq by Expectation Maximization (RSEM) (21) scaled expression values for TCGA were downloaded from the GDAC Firehose website (22). Counts were normalised to transcripts-per-million (TPM) values with a pseudo-count of 2. Entrez gene IDs were mapped to HGNC gene symbols using the biomaRt R package (version 2.42.0) (23) and collapsed to unique values per gene symbol by selecting the most variable entrez ID among all samples for each gene symbol. Primary and, where a primary sample was unavailable, metastatic tumour samples from the SKCM dataset (n=469, Table S1) were selected using the TCGAbiolinks R package (version 2.14.0) (24) and were matched with overall survival (OS) endpoints from the TCGA Pan-Cancer Clinical Data Resource (25). *WDFY4* and *XCR1* expression was separated in 'low' (bottom quartile) and 'int-high' (top 3 quartiles) categories, then used to fit Kaplan-Meier and Cox regression models using the *survival* R package (version 3.1-8) (26).

Statistical analysis

One-way analysis of variance (ANOVA) with Tukey's multiple comparisons tests, log-rank (Mantel-Cox) test and unpaired *t*-tests were performed using GraphPad PRISM. All experiments other than single-cell RNA-seq were performed in at least three biological replicates and error bars show ±SEM. Significance was determined as *$p<0.05$, **$p<0.01$, ***$p<0.001$, **** $p<0.0001$.

Results and Discussion

Combined BRAF, MEK and CDK4/6 inhibition has anti-tumor and immunomodulatory activity

To determine if the CDK4/6 inhibitor, palbociclib, enhances the efficacy of dual BRAF and MEK inhibition in a syngeneic setting, we first tested the *in vitro* activity of this triple therapy on our immunogenic *Braf*^{V600E}*Cdkn2a*$^{-/-}$*Pten*$^{-/-}$ mouse melanoma cell line, YOVAL1.1 (12). Consistent with human melanoma cell lines (8, 9), triple therapy potently suppressed both phosphorylation of RB (**Fig. S1A**) and proliferation of YOVAL1.1 cells compared to dual BRAF and MEK (BRAFi+MEKi) or CDK4/6 (CDK4/6i) inhibition alone (**Fig. 1A**). Triple therapy also led to significant upregulation of the MHC Class I molecule H-2K^{b} (**Fig. 1B, Fig. S1B),** which presents the YOVAL1.1 immunogenic peptide derived from ovalbumin (12), and induced surface exposure of calreticulin (CRT), an indicator of immunogenic cell death (27) (**Fig. 1C, Fig. S1B**). These effects were predominately mediated through BRAFi+MEKi, consistent with previous reports (28). *In vivo*, triple therapy resulted in immediate tumor regression and significantly improved survival compared with BRAFi+MEKi or CDK4/6i alone (**Fig. 1D, Fig. S1C**). Notably, treatment of YOVAL1.1 tumors with triple therapy recapitulated the potent and prolonged tumor control observed with dual BRAFi and CDK4/6i in xenograft models of human *Braf*^{V600}*Cdkn2a*$^{-/-}$ melanoma (8, 9).

To examine the immunomodulatory effects of triple therapy, mice bearing YOVAL1.1 tumors were treated with vehicle, BRAFi+MEKi, CDK4/6i, or triple therapy for 7 days, after which the tumors were harvested and the immune compartment analysed by flow cytometry. No significant difference in the total number of tumor-associated CD45.2+ immune cells was observed across groups (**Fig. S1D-E**), however, there was a notable shift in the distribution of the lymphoid and myeloid compartments in response to the

triple therapy (**Fig. 1E–J, Fig. S1D–I**). Specifically, these tumors contained a significantly higher frequency of both $CD4^+$ and $CD8^+$ T cells compared to all other treatment groups (**Fig. 1F–G, Fig, S1F**), while the frequency of natural killer (NK) and B cells remained relatively unchanged (**Fig. S1G–H**). Interestingly, despite a significant increase in $CD4^+$ T cells following triple therapy, the frequency of $CD4^+$ Tregs was not increased (**Fig. 1F**), likely due to the reported anti-proliferative effects of CDK4/6 inhibitors on this T-cell subset (10). Indeed, tumors treated with CDK4/6i alone had significantly fewer Tregs than all other treatment groups (**Fig. 1F**).

The increase in lymphocyte frequency following triple therapy was coupled with a concurrent decrease in the frequency of myeloid cells. We observed a significant loss of tumor-associated $CD11b^+$ cells, which was exclusive to tumors treated with triple therapy (**Fig. 1H–J**). This encompassed a reduction in all myeloid subsets analyzed, including monocytes ($CD11b^{high}Ly6C^{high}$) and mononuclear myeloid-derived suppressor cells (M-MDSCs; $CD11b^{high}Ly6C^{high}Ly6G^{low}$), DCs ($Ly6C^{low}CD11c^+MHC\text{-}II^+F480^{low\text{-}int}$) and tumor-associated macrophages (TAMs; $Ly6C^{low}CD11c^+MHC\text{-}II^+F480^{high}$) (**Fig. 1J, S1D**). No changes were seen in polymorphonuclear (PMN)-MDSCs ($CD11b^{high}Ly6C^{high}Ly6G^{high}$), although the frequency of these cells across all groups was negligible (**Fig. S1I**). Collectively these data highlight that, in addition to potent tumor-intrinsic activity, triple therapy leads to profound remodelling of the tumor immune microenvironment.

Tumors treated with BRAF, MEK and CDK4/6 inhibition are unresponsive to ICB

To investigate the contribution of host immunity to the anti-tumor activity of triple therapy, we treated tumors grown in fully immunodeficient NSG mice, $Rag2\gamma c^{-/-}$ mice, which lack functional T, B and NK cells, and wild-type mice depleted of $CD8^+$ T or NK

cells. We observed no difference in the efficacy of triple therapy in these mice compared with immunocompetent mice, suggesting that the *in vivo* anti-tumor activity of this combination was predominately mediated by tumor-intrinsic mechanisms (**Fig. S2A-B**), likely due to selective and potent inhibition of the clinically relevant oncogenic drivers in these tumor cells (12). While triple therapy was superior at controlling YOVAL1.1 tumor growth and delayed the emergence of drug resistance compared with dual BRAFi+MEKi, tumors did eventually escape approximately 80 days into treatment in a third of the mice (**Fig. 1D, Fig. S2C**). Another third demonstrated complete tumor clearance for several weeks, but tumors rapidly re-established upon therapy withdrawal (**Fig. S2C**). Therapy resistance and the need for continued treatment are two common clinical challenges of targeted therapies. Consequently, several clinical trials are currently examining the benefits of combining MAPK/ERK or CDK4/6 targeted therapies with ICB as a strategy to overcome such challenges (NCT02130466, NCT04075604). ICB is reportedly more efficacious in settings where tumor burden is low (29), tumor-lymphocyte infiltration is high (30) and immunosuppressive populations, such as Tregs and MDSCs, are low (31, 32) (**Fig. 2A**). Notably, all these factors shifted favorably following triple therapy (**Fig. 2B-C**). We have previously shown the YOVAL1.1 model is amenable to anti-PD1+anti-CTLA4 (12), and as such we sought to determine whether ICB could be used to promote immune-mediated clearance or control of tumors following withdrawal from triple therapy. To investigate this, mice with established YOVAL1.1 tumors were treated short-term (1–2 weeks) with triple therapy ± ICB (anti-CTLA4+anti-PD1). Multiple scheduling combinations were tested (**Fig. 2D–G**) to examine both the capacity of ICB to enhance triple-therapy-mediated tumor regression up front, or to promote clearance of residual tumors following triple therapy. However, in all instances, tumors failed to respond to ICB, with no significant difference in tumor growth or survival (**Fig. 2D–G**). To

determine whether triple therapy had induced tumor-intrinsic resistance to ICB, residual tumors were harvested from mice treated with triple therapy and re-implanted into treatment naïve recipients (**Fig. 2H**). Once the tumors reached an equivalent size at which they were resistant to ICB following triple therapy, mice were treated with either ICB or an isotype control (**Fig. 2H)**. In this setting, ICB led to complete tumor clearance in 8/9 mice (**Fig. 2H).** Taken together, these findings suggest that the immunomodulatory activity of triple therapy promotes a host tumor microenvironment that is unresponsive to ICB.

Triple therapy depletes tumor-associated pro-inflammatory macrophages and CD103$^+$ DCs

To investigate changes in the tumor immune microenvironment that might account for the unresponsiveness of triple therapy–treated YOVAL1.1 tumors to ICB, we further analysed the tumor-associated immune compartment using single-cell RNA-seq (scRNA-seq) and paired TCR sequencing. YOVAL1.1 tumors were harvested from mice after 7 days of treatment with either vehicle or triple therapy, followed by isolation and droplet encapsulation of the CD45.2$^+$ cells for sequencing (**Fig. 3A**). Dimensionality reduction t-SNE analysis delineated 10 broad immune subsets including B cells, DCs, innate lymphoid cells, macrophages, monocytes, neutrophils, NK cells, CD4$^+$ and CD8$^+$ T cells, and Tregs (**Fig. 3B-C**). In accordance with our earlier analyses (**Fig. 1**), we detected an almost complete loss of myeloid populations following triple therapy, coupled with a corresponding increase in the lymphoid compartment (**Fig. 3C-D**). Both CD8$^+$ and CD4$^+$ T cells were transcriptionally and clonally similar across untreated and treated samples, with comparable expression of genes associated with effector function (e.g., *Ifng, Prf1*) (**Fig. 3E-F**). However, T cells from tumors treated with triple therapy expressed slightly lower levels of exhaustion-associated genes (e.g., *Lag3, Pdcd1, Tigit, Tox*) and higher

levels of memory/stem-like-associated genes (e.g., *Tcf7, Il7r*) (**Fig. 3E**), and exhibited greater numbers of unique TCR clones and overall clonal diversity (**Fig. 3F-G, Fig. S3A)**; all features favourable for ICB efficacy (33). By flow cytometry, there was no change in the overall frequency of $PD1^{+}CD8^{+}$ T cells following triple therapy, suggesting that the unresponsiveness of these tumors to anti-PD1 is not due to a lack of PD1 expression on tumor-infiltrating T cells (**Fig. S3B**). Taken together, these data indicate that the functional capacity of T cells to respond to ICB is not impaired, but potentially enhanced, following triple therapy.

Transcriptional profiling of the intratumoral myeloid compartment revealed that both immunosuppressive (defined by expression of *Mrc1* (34)) and pro-inflammatory (defined by expression of *Cxcl10 and Cxcl9* (35)) macrophage subsets were depleted following triple therapy (**Fig. 3H**). Pro-inflammatory macrophages underpin the success of T-cell-directed therapies, including ICB, as these cells cooperate with T cells to promote tumor clearance through phagocytosis and the production of inflammatory cytokines, such as TNFα (36). Additionally, macrophage-derived CXCL10 and CXCL9 are essential for the recruitment of T cells to the tumor site following ICB (35), and while tumors treated with triple therapy were host to an abundance of lymphocytes, clonal replacement of intratumoral T cells is suggested to be critical for the success of ICB (37). Indeed, pro-inflammatory $CXCL9^{+}$ and $CXCL10^{+}$ macrophages are associated with improved survival and clinical responses to ICB in melanoma patients (35). Hence, the absence of this cellular subset following triple therapy may impact on the efficacy of ICB through reduced capacity to stimulate both existing and new anti-tumor T cell responses.

DCs are another critical component of anti-tumor immunity, including that mediated by dual BRAFi+MEKi (28). Our t-SNE analysis delineated four distinct DC clusters, of which cluster 2 was most markedly depleted by triple therapy (**Fig. 3I**). This DC subset

expressed high levels of genes associated with antigen cross-presentation (e.g., *Wdfy4*, *Xcr1)* (38, 39) (**Fig. 3J**), suggesting that triple therapy may strip the tumor immune compartment of the ability to cross-present antigens and stimulate T-cell activity. Indeed, a specific subset of antigen-presenting $CD103^+$ DCs is critical for promoting intratumoral T-cell immunity (40), and for enhancing the therapeutic efficacy of combined BRAFi and anti-PDL1 therapy (41). To investigate whether $CD103^+$ DCs were impacted by triple therapy, we applied a previously published gene signature for this specific subset (40) to our scRNA-seq analyses and found enrichment of this signature specifically in the *Wdfy4*$^+$*Xcr1*$^+$ DC cluster (**Fig. 3K**), identifying this cluster as $CD103^+$ DCs. The intratumoral ratio of $CD103^+$ DCs to other myeloid populations is strongly prognostic for survival across a range of cancers (40), and importantly our scRNA-seq analyses showed this ratio was diminished in tumors treated with triple therapy (**Fig. 3L**). This suggested that triple therapy may impair anti-tumor immunity and responses to ICB via potent depletion of $CD103^+$ DCs.

Tumor-associated myeloid cells are prognostic for clinical responses to ICB and required for inducing T-cell immunity

To investigate the potential clinical impact of depleting *Wdfy4*$^+$*Xcr1*$^+$$CD103^+$ DCs we analyzed TCGA datasets, and found that low expression of *WDFY4* and *XCR1* significantly correlated with poor survival in melanoma patients (**Fig. 4A, Fig. S4A**). To examine this more specifically in the context of ICB, we analyzed a published scRNA-seq dataset of tumor-infiltrating immune populations from melanoma patients taken prior to or during ICB (18). Using the $CD103^+$ DC signature that was applied to our scRNA-seq analyses (**Fig. 3K**) (40), we identified a rare population within the myeloid compartment of patient samples that was enriched for this gene set (**Fig. 4B, Fig. S4B–D**). In accordance with our scRNA-seq dataset, this population was also enriched for

WDFY4 and *XCR1* expression, with *XCR1* expression exclusive to this immune subset (**Figure 4B, S4D**). Importantly, a significantly higher proportion of this $CD103^+$ DC subset was present within the myeloid population in patients that responded to ICB compared to non-responders, as defined by RECIST criteria (42) (**Fig. 4C**). Likewise, patients with low levels of intratumoral $CD103^+$ DCs (less than 5% of the myeloid population) had much poorer response rates than patients with higher $CD103^+$ DC frequencies (20% vs 50% response rate, respectively) (**Fig. 4D**). This correlation appeared stronger for patients treated with anti-CTLA4 or anti-CTLA4+anti-PD1, than anti-αPD1 alone (**Fig. 4C**). In contrast to anti-PD1 therapy, which blocks inhibitory interactions between T cells and tumor cells, anti-CTLA4 functions primarily through de-repressing cross-priming interactions between T cells and DCs (43). $CD103^+$ DCs might therefore be expected to correlate more strongly with ICB responses in the context of anti-CTLA4 therapy, consistent with our findings. Furthermore, we have previously shown that treatment-naïve YOVAL1.1 tumors are responsive to anti-CTLA4 and anti-CTLA4+ anti-PD1, but not anti-PD1 alone (12). This suggests that poor responsiveness to ICB in this model is mediated through mechanisms that infer resistance to anti-CTLA4, such as a loss of $CD103^+$ DCs following triple therapy.

To further validate whether $CD103^+$ DCs were among the dominant myeloid subsets depleted following triple therapy, YOVAL1.1 tumors were harvested from mice after 7 days of triple therapy and analyzed by flow cytometry using surface markers specific for this population (**Fig. S4E**) (40). Unsupervised tSNE clustering delineated a distinct cluster expressing MHC II, CD11c, CD24 and CD103, which we identified to be $CD103^+$ DCs using published gating strategies (**Fig. 4E-F, Fig. S4E**) (40). In support of our scRNA-seq analyses, both $CD103^+$ DCs and macrophages were markedly depleted in tumors treated with the triple therapy compared to vehicle controls (**Fig. 4F–G**), with a

significant reduction in the frequency and total number of these myeloid populations (**Fig. 4G, Fig. S4F**). Importantly, the frequency of both populations was significantly higher in treatment-naïve tumors of an equivalent size (**Fig. 4G**), which were previously confirmed to be responsive to ICB (**Fig. 2H**) (12). This further indicated that depletion of these myeloid subsets by triple therapy may be contributing to the poor responsiveness of these tumors to ICB. Interestingly, depletion of these subsets was not seen after only 2 days of triple therapy, while MDSCs were still depleted efficiently in this timeframe (**Fig. S5A-B**). Further, following 7 days of triple therapy, depleted MDSCs rapidly repopulated tumors when therapy was withdrawn, while antigen-presenting subsets failed to recover in the 5 days following therapy withdrawal (**Fig. S5C-D**). This suggests that short intermittent dosing of triple therapy may be needed to preserve immune-potentiating myeloid populations within tumors.

As tumor-associated $CD103^+$ DCs and pro-inflammatory macrophages were depleted following triple therapy, and are critical components of anti-tumor T-cell immunity (35, 40), we hypothesized that the $CD45.2^+$ immune population from these tumors would fail to stimulate optimal T-cell responses. To test this, $CD45.2^+$ immune cells isolated from tumors treated with vehicle or triple therapy were pulsed with the cognate antigen, $OVA_{323-399}$, and co-cultured with CTV-labelled naïve $CD4^+$ OT-II T cells (**Fig. 4H**). Strikingly, OT-II T cells co-cultured with $CD45.2^+$ cells from tumors treated with the triple therapy failed to proliferate or upregulate activation markers (CD44, CD69 and CD25) (**Fig. 4I-J**). Taken together, these data suggested that tumor-associated myeloid populations depleted by triple therapy are important for the induction of optimal T-cell responses.

In conclusion, we demonstrate that combined inhibition of BRAF, MEK and CDK4/6 leads to profound remodelling of the tumor immune microenvironment. The changes

observed are reminiscent of those reported in tumors that respond to ICB (such as low tumor burden, increased lymphocyte frequency and a reduction in immunosuppressive cells) (**Fig. 4K**). However, our data demonstrates that this triple combination also depletes immune-potentiating myeloid populations, including pro-inflammatory macrophages and cross-priming $CD103^+$ DCs, and in doing so may render these tumors unresponsive to ICB (**Fig. 4K**). As a result, this promising therapy, while effective due to potent tumor intrinsic activity, may impede the ability of the immune system to contribute to the overall anti-tumor response.

Acknowledgements

We thank Benjamin Blyth, Susan Jackson, Kerry Warren, Jeannette Schreuders and Rachael Walker of the Peter MacCallum Cancer Centre Translational Research Laboratory for technical support with animal work.

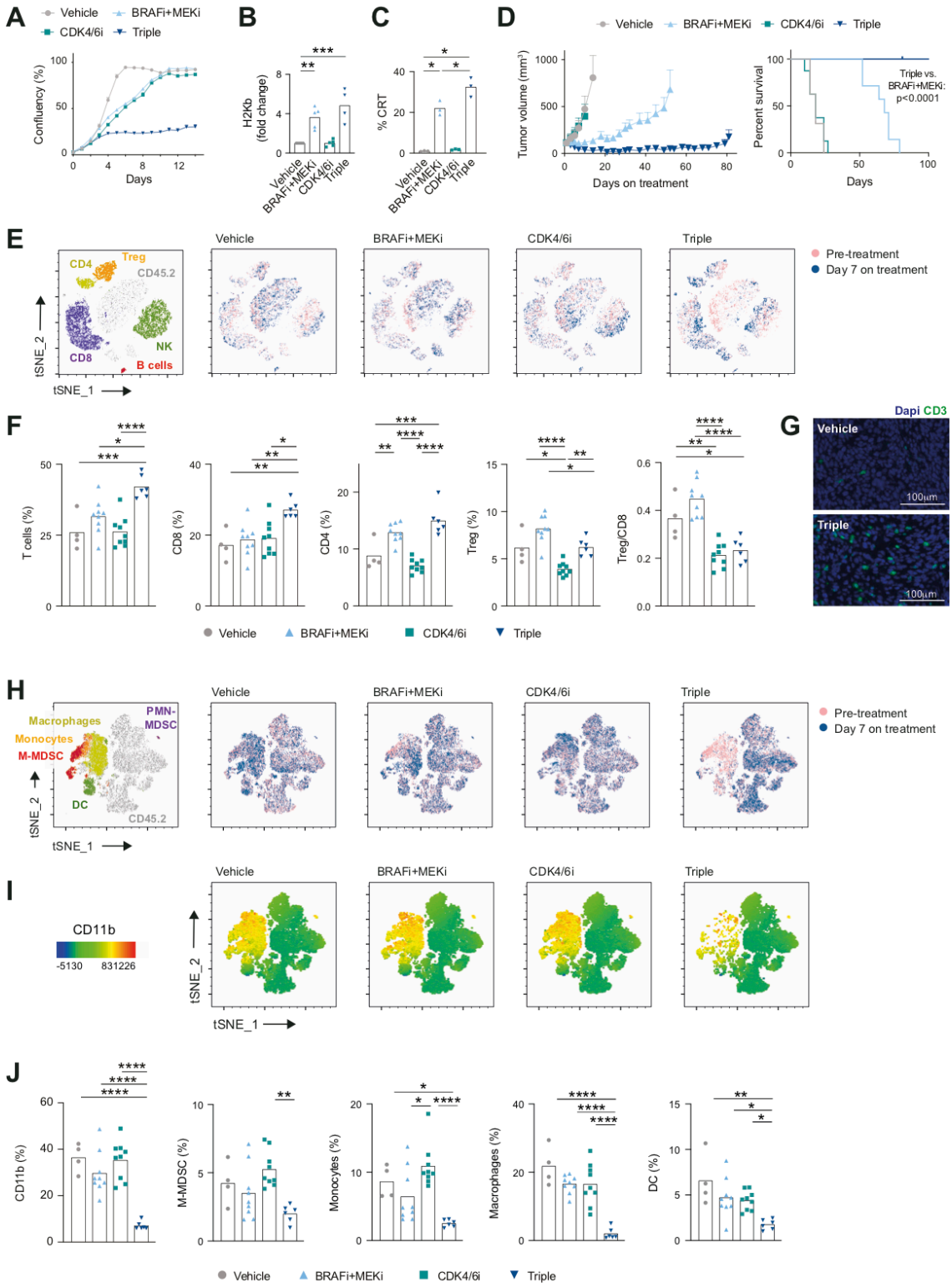
A
Vehicle
BRAFi+MEKi
CDK4/6i
Triple
Confluency (%)
Days
B
H2Kb (fold change)
C
% CRT
D
Tumor volume (mm³)
Days on treatment
Percent survival
Triple vs. BRAFi+MEKi: p<0.0001
E
CD4
Treg
CD45.2
NK
CD8
B cells
tSNE_1
tSNE_2
Pre-treatment
Day 7 on treatment
F
T cells (%)
CD8 (%)
CD4 (%)
Treg (%)
Treg/CD8
G
Dapi CD3
100µm
H
Macrophages
Monocytes
M-MDSC
PMN-MDSC
DC
I
CD11b
-5130
831226
J
CD11b (%)
M-MDSC (%)
Monocytes (%)
Macrophages (%)
DC (%)

Figure 1. Triple therapy has anti-tumor and immunomodulatory activity. (**A**) YOVAL1.1 cell confluency measured over time *in vitro* in the presence of vehicle or the indicated drug(s), this experiment is representative of n=3. (**B-C**) YOVAL1.1 cells analyzed by flow cytometry after 72h of treatment, One-way ANOVA Tukey's multiple comparisons test, n=3-5. (**D**) YOVAL1.1 tumor growth and survival in C57BL/6 mice, n=7-9 per group, log rank (Mantel-Cox) test. (**E-J**) Analysis of YOVAL1.1 tumors by flow cytometry (**E-F, H-J**) and immunohistochemistry (**G**) pre-treatment or after 7 days of treatment. (**E, H–I**) tSNE clustering based on equal numbers of $CD45.2^+$ cells pooled from all treatment groups, plots are representative of n=4 concatenated samples per group. (**F, J**) Indicated population frequency of $CD45.2^+$, One-way ANOVA Tukey's multiple comparisons test, n=4-9. (**G**) Representative of n=3, quantification in **Fig. S1F**. All gating strategies are shown in **Fig. S1B, D**. Error bars show +/- SEM. *p<0.05, **p<0.01, ***p<0.001, ****p<0.0001. BRAFi – dabrafenib; MEKi -trametinib; CDK4/6i – palbociclib; Triple – BRAFi+MEKi-+CDK4/6i.

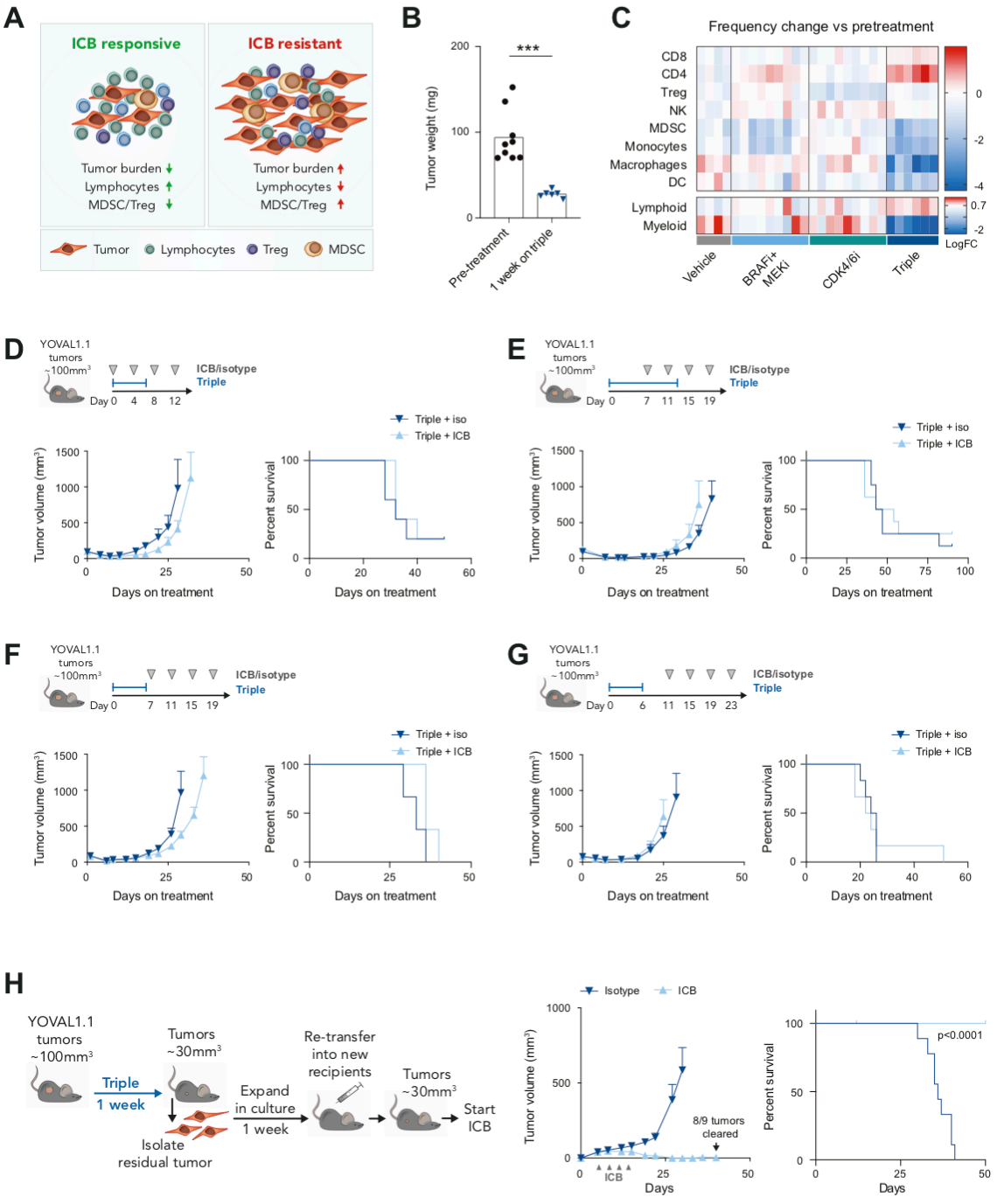
A
ICB responsive
ICB resistant
Tumor burden ↓
Lymphocytes ↑
MDSC/Treg ↓
Tumor burden ↑
Lymphocytes ↓
MDSC/Treg ↑
Tumor
Lymphocytes
Treg
MDSC
B
Tumor weight (mg)
***
Pre-treatment
1 week on triple
C
Frequency change vs pretreatment
CD8
CD4
Treg
NK
MDSC
Monocytes
Macrophages
DC
Lymphoid
Myeloid
LogFC
Vehicle
BRAFi+ MEKi
CDK4/6i
Triple
D
YOVAL1.1 tumors ~100mm³
ICB/isotype
Triple
Day 0 4 8 12
Triple + iso
Triple + ICB
Tumor volume (mm³)
Percent survival
Days on treatment
E
YOVAL1.1 tumors ~100mm³
ICB/isotype
Triple
Day 0 7 11 15 19
Triple + iso
Triple + ICB
Tumor volume (mm³)
Percent survival
Days on treatment
F
YOVAL1.1 tumors ~100mm³
ICB/isotype
Triple
Day 0 7 11 15 19
Triple + iso
Triple + ICB
Tumor volume (mm³)
Percent survival
Days on treatment
G
YOVAL1.1 tumors ~100mm³
ICB/isotype
Triple
Day 0 6 11 15 19 23
Triple + iso
Triple + ICB
Tumor volume (mm³)
Percent survival
Days on treatment
H
YOVAL1.1 tumors ~100mm³
Triple 1 week
Tumors ~30mm³
Isolate residual tumor
Expand in culture 1 week
Re-transfer into new recipients
Tumors ~30mm³
Start ICB
Isotype
ICB
Tumor volume (mm³)
8/9 tumors cleared
ICB
Days
Percent survival
p<0.0001
Days

Figure 2. Tumours treated with triple therapy are unresponsive to immune checkpoint blockade. (**A**) Schematic showing tumor features associated with response/resistance to ICB (29-32). (**B**) Tumor weights after 7 days of treatment, unpaired t-test, n=6-9. (**C**) Indicated population frequency of $CD45.2^+$ cells compared to pre-treatment samples from **Fig. 1E-J**, columns show individual mice. (**D-G**) YOVAL1.1 tumor growth and survival in C57BL/6 mice, n=3-6 per group. (**H**) Residual YOVAL1.1 tumors were isolated following one week of triple therapy, transferred into naive C57BL/6 recipients, and treated with ICB when tumors reached an equivalent size at which they were harvested, graphs show tumor growth and survival from time of tumor inoculation, with ICB administered where indicated, n=9-10 per group, log rank (Mantel-Cox) test. Error bars show +/- SEM. ***p<0.001. BRAFi – dabrafenib; MEKi - trametinib; CDK4/6i – palbociclib; Triple – BRAFi+MEKi-+CDK4/6i; ICB; anti-CTLA4+anti-PD1.

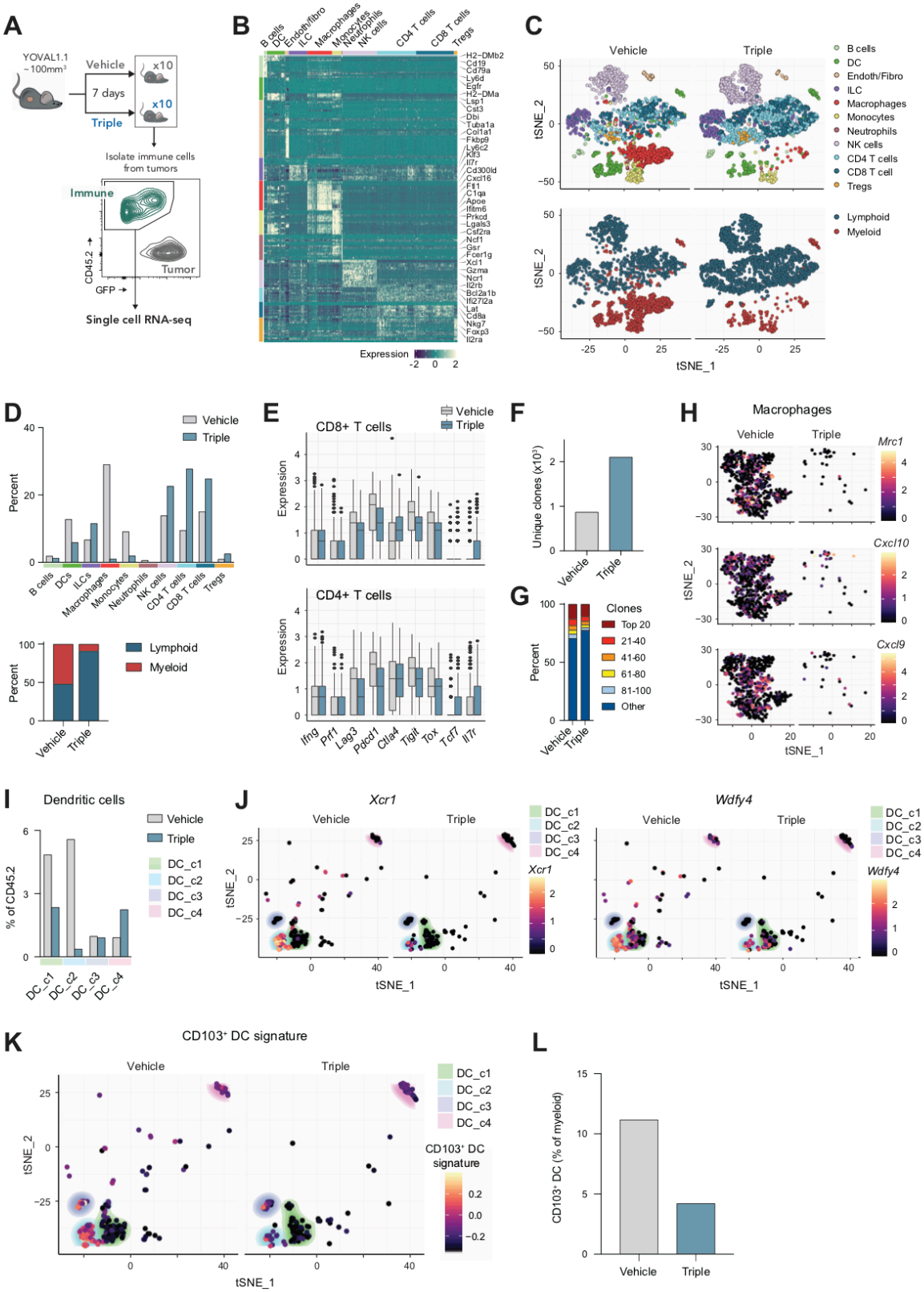
A
YOVAL1.1
~100mm³
Vehicle
7 days
Triple
x10
x10
Isolate immune cells
from tumors
Immune
Tumor
CD45.2
GFP
Single cell RNA-seq
B
B cells
DC
Endoth/fibro
ILC
Macrophages
Monocytes
Neutrophils
NK cells
CD4 T cells
CD8 T cells
Tregs
Expression
C
Vehicle
Triple
tSNE_2
tSNE_1
B cells
DC
Endoth/Fibro
ILC
Macrophages
Monocytes
Neutrophils
NK cells
CD4 T cells
CD8 T cell
Tregs
Lymphoid
Myeloid
D
Vehicle
Triple
Percent
B cells
DCs
ILCs
Macrophages
Monocytes
Neutrophils
NK cells
CD4 T cells
CD8 T cells
Tregs
Lymphoid
Myeloid
E
CD8+ T cells
CD4+ T cells
Expression
Ifng
Prf1
Lag3
Pdcd1
Ctla4
Tigit
Tox
Tcf7
Il7r
F
Unique clones (x10³)
G
Clones
Top 20
21-40
41-60
61-80
81-100
Other
H
Macrophages
Mrc1
Cxcl10
Cxcl9
I
Dendritic cells
% of CD45.2
DC_c1
DC_c2
DC_c3
DC_c4
J
Xcr1
Wdfy4
K
CD103⁺ DC signature
L
CD103⁺ DC (% of myeloid)

Figure 3. Triple therapy depletes pro-inflammatory macrophages and CD103$^+$ dendritic cells. Single-cell RNA-seq on CD45.2$^+$ cells isolated from YOVAL1.1 tumors following 7 days of treatment with vehicle or triple, n=10 mice per group pooled. (**A**) Schematic of experimental set up, tumors from 10 mice per treatment group were pooled, and CD45.2$^+$ immune cells were isolated by FACS for single-cell RNA-seq (**B-C**) tSNE clustering and annotation based on gene expression. (**D**) Cluster frequencies. (**E**) Gene expression of CD8$^+$ and CD4$^+$ T cells. (**F**) Number of unique TCR rearrangements and (**G**) frequency of top 100 abundant clones, plus remaining clones (other). (**H**) Gene expression of macrophages. (**I**) Frequency and (**J**) gene expression of DC clusters 1-4 (DC_c1-4) delineated from analysis in **(C)**. (**K**) Expression of CD103$^+$ DC gene signature (40) in DC clusters. (**L**) Frequency of CD103$^+$ DCs (DC_c2) as a percent of all myeloid cells identified by single-cell RNA-seq. Triple – BRAFi (dabrafenib) + MEKi (trametinib) + CDK4/6i (palbociclib).

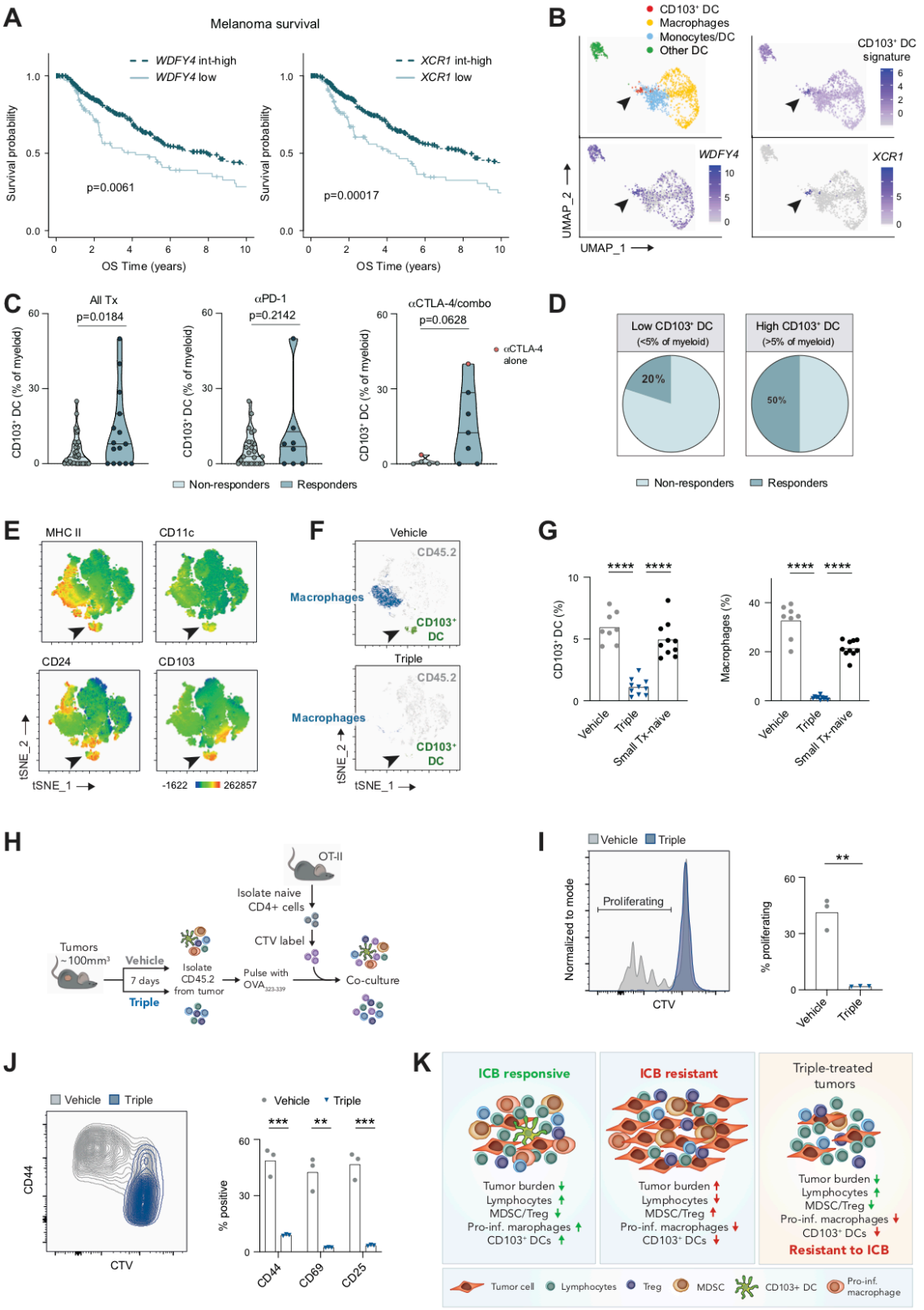
A
Melanoma survival
WDFY4 int-high
WDFY4 low
XCR1 int-high
XCR1 low
Survival probability
p=0.0061
p=0.00017
OS Time (years)
B
CD103+ DC
Macrophages
Monocytes/DC
Other DC
CD103+ DC signature
WDFY4
XCR1
UMAP_2
UMAP_1
C
All Tx
p=0.0184
αPD-1
p=0.2142
αCTLA-4/combo
p=0.0628
αCTLA-4 alone
CD103+ DC (% of myeloid)
Non-responders
Responders
D
Low CD103+ DC
(<5% of myeloid)
High CD103+ DC
(>5% of myeloid)
20%
50%
Non-responders
Responders
E
MHC II
CD11c
CD24
CD103
tSNE_2
tSNE_1
-1622
262857
F
Vehicle
Triple
CD45.2
Macrophages
CD103+ DC
tSNE_2
tSNE_1
G
CD103+ DC (%)
Macrophages (%)
****
Vehicle
Triple
Small Tx-naive
H
OT-II
Isolate naive CD4+ cells
CTV label
Tumors ~100mm3
Vehicle
7 days
Triple
Isolate CD45.2 from tumor
Pulse with OVA323-339
Co-culture
I
Vehicle
Triple
Proliferating
Normalized to mode
CTV
% proliferating
**
J
Vehicle
Triple
CD44
CTV
% positive
***
**
CD44
CD69
CD25
K
ICB responsive
Tumor burden ↓
Lymphocytes ↑
MDSC/Treg ↓
Pro-inf. marophages ↑
CD103+ DCs ↑
ICB resistant
Tumor burden ↑
Lymphocytes ↓
MDSC/Treg ↑
Pro-inf. macrophages ↓
CD103+ DCs ↓
Triple-treated tumors
Tumor burden ↓
Lymphocytes ↑
MDSC/Treg ↓
Pro-inf. macrophages ↓
CD103+ DCs ↓
Resistant to ICB
Tumor cell
Lymphocytes
Treg
MDSC
CD103+ DC
Pro-inf. macrophage

Figure 4. Intratumoral myeloid populations depleted by triple therapy are required for optimal T cell immunity. (**A**) Kaplan-Meier overall survival of 469 melanoma patients from TCGA stratified by top 75% (int-high) vs bottom 25% (low) expression of indicated gene, logrank p-values are indicated. (**B-D**) Analysis of single cell RNA-seq on tumor-infiltrating immune cells from melanoma patients treated with ICB (18). (**B**) UMAP clustering based on gene expression, showing myeloid populations only, (full plots in **Fig. S4B-D**), $CD103^+$ DCs identified using signature from **Fig. 3J** (40). (**C**) $CD103^+$ DCs frequency of all myeloid cells in responders vs non-responders, unpaired T test. (**D**) Proportion of responders among patients with low (<5% of myeloid population) or high (>5% of myeloid population) $CD103^+$ DCs. (**E-G**) Analysis of YOVAL1.1 tumors by flow cytometry after 7 days of treatment, gating strategy shown in **Fig. S4E**. (**E-F**) tSNE clustering based on equal numbers of $CD45.2^+$ cells pooled from both treatment groups, plots are representative of n=8 concatenated samples per group. (**G**) Frequency of indicated population, One-way ANOVA Tukey's multiple comparisons test, n=8-10. (**H**) Schematic of experimental set up, $CD45.2^+$ cells were isolated from tumors treated with vehicle or triple for 7 days, pulsed with $OVA_{323-339}$, and co-cultured with cell-trace violet (CTV)-labelled $CD4^+$ T cells from transgenic OT-II mice. (**I**) Representative plot of CTV measured after 90h of co-culture (left) and percent proliferating based on CTV dilution (right), unpaired t-test, n=3. (**J**) Representative plot and flow cytometric analysis of activation markers, One-way ANOVA Tukey's multiple comparisons test, n=3. (**I-J**) n=3 independent co-cultures with $CD45.2^+$ cells pooled from 3 mice for each co-culture. (**K**) Schematic showing tumor features associated with response/resistance to ICB, and the microenvironment of tumors following treatment with triple. **p<0.01, ***p<0.001, ****p<0.0001. Triple – BRAFi (dabrafenib) + MEKi (trametinib) + CDK4/6i (palbociclib).

References

1. Flaherty KT, *et al.* (2012) Combined BRAF and MEK inhibition in melanoma with BRAF V600 mutations. *N Engl J Med* 367(18):1694-1703.
2. Larkin J, *et al.* (2015) Combined Nivolumab and Ipilimumab or Monotherapy in Untreated Melanoma. *N Engl J Med* 373(1):23-34.
3. Boni A, *et al.* (2010) Selective BRAFV600E inhibition enhances T-cell recognition of melanoma without affecting lymphocyte function. *Cancer Res* 70(13):5213-5219.
4. Frederick DT, *et al.* (2013) BRAF inhibition is associated with enhanced melanoma antigen expression and a more favorable tumor microenvironment in patients with metastatic melanoma. *Clin Cancer Res* 19(5):1225-1231.
5. Cooper ZA, *et al.* (2014) Response to BRAF inhibition in melanoma is enhanced when combined with immune checkpoint blockade. *Cancer Immunol Res* 2(7):643-654.
6. Wilmott JS, *et al.* (2012) Selective BRAF inhibitors induce marked T-cell infiltration into human metastatic melanoma. *Clin Cancer Res* 18(5):1386-1394.
7. Sheppard KE & McArthur GA (2013) The cell-cycle regulator CDK4: an emerging therapeutic target in melanoma. *Clin Cancer Res* 19(19):5320-5328.
8. Martin CA, *et al.* (2018) Palbociclib synergizes with BRAF and MEK inhibitors in treatment naive melanoma but not after the development of BRAF inhibitor resistance. *Int J Cancer* 142(10):2139-2152.
9. Yadav V, *et al.* (2014) The CDK4/6 inhibitor LY2835219 overcomes vemurafenib resistance resulting from MAPK reactivation and cyclin D1 upregulation. *Mol Cancer Ther* 13(10):2253-2263.

10. Goel S, *et al.* (2017) CDK4/6 inhibition triggers anti-tumour immunity. *Nature* 548(7668):471-475.

11. Deng J, *et al.* (2018) CDK4/6 Inhibition Augments Antitumor Immunity by Enhancing T-cell Activation. *Cancer Discov* 8(2):216-233.

12. Lelliott EJ, *et al.* (2019) A novel immunogenic mouse model of melanoma for the preclinical assessment of combination targeted and immune-based therapy. *Sci Rep* 9(1):1225.

13. Stuart T, *et al.* (2019) Comprehensive Integration of Single-Cell Data. *Cell* 177(7):1888-1902 e1821.

14. Aran D, *et al.* (2019) Reference-based analysis of lung single-cell sequencing reveals a transitional profibrotic macrophage. *Nat Immunol* 20(2):163-172.

15. Gu Z, Eils R, & Schlesner M (2016) Complex heatmaps reveal patterns and correlations in multidimensional genomic data. *Bioinformatics* 32(18):2847-2849.

16. Dobin A, *et al.* (2013) STAR: ultrafast universal RNA-seq aligner. *Bioinformatics* 29(1):15-21.

17. Bolotin DA, *et al.* (2017) Antigen receptor repertoire profiling from RNA-seq data. *Nat Biotechnol* 35(10):908-911.

18. Sade-Feldman M, *et al.* (2019) Defining T Cell States Associated with Response to Checkpoint Immunotherapy in Melanoma. *Cell* 176(1-2):404.

19. Becht E, *et al.* (2018) Dimensionality reduction for visualizing single-cell data using UMAP. *Nat Biotechnol*.

20. Hou R, Denisenko E, & Forrest ARR (2019) scMatch: a single-cell gene expression profile annotation tool using reference datasets. *Bioinformatics* 35(22):4688-4695.

21. Li B & Dewey CN (2011) RSEM: accurate transcript quantification from RNA-Seq data with or without a reference genome. *BMC Bioinformatics* 12:323.

22. TCGA (2016) Firehose stddata_2016_01_28 run. (Broad Institute of MIT and Harvard).

23. Durinck S, Spellman PT, Birney E, & Huber W (2009) Mapping identifiers for the integration of genomic datasets with the R/Bioconductor package biomaRt. *Nat Protoc* 4(8):1184-1191.

24. Colaprico A, *et al.* (2016) TCGAbiolinks: an R/Bioconductor package for integrative analysis of TCGA data. *Nucleic Acids Res* 44(8):e71.

25. Liu J, *et al.* (2018) An Integrated TCGA Pan-Cancer Clinical Data Resource to Drive High-Quality Survival Outcome Analytics. *Cell* 173(2):400-416 e411.

26. Therneau T (2015) A Package for Survival Analysis in S. version 2.38.

27. Obeid M, *et al.* (2007) Calreticulin exposure dictates the immunogenicity of cancer cell death. *Nat Med* 13(1):54-61.

28. Erkes DA, *et al.* (2020) Mutant BRAF and MEK Inhibitors Regulate the Tumor Immune Microenvironment via Pyroptosis. *Cancer Discov* 10(2):254-269.

29. Huang AC, *et al.* (2017) T-cell invigoration to tumour burden ratio associated with anti-PD-1 response. *Nature* 545(7652):60-65.

30. Tumeh PC, *et al.* (2014) PD-1 blockade induces responses by inhibiting adaptive immune resistance. *Nature* 515(7528):568-571.

31. Gebhardt C, *et al.* (2015) Myeloid Cells and Related Chronic Inflammatory Factors as Novel Predictive Markers in Melanoma Treatment with Ipilimumab. *Clin Cancer Res* 21(24):5453-5459.

32. Maj T, *et al.* (2017) Oxidative stress controls regulatory T cell apoptosis and suppressor activity and PD-L1-blockade resistance in tumor. *Nat Immunol* 18(12):1332-1341.

33. Miller BC, *et al.* (2019) Subsets of exhausted CD8(+) T cells differentially mediate tumor control and respond to checkpoint blockade. *Nat Immunol* 20(3):326-336.

34. Noy R & Pollard JW (2014) Tumor-associated macrophages: from mechanisms to therapy. *Immunity* 41(1):49-61.

35. House IG, *et al.* (2020) Macrophage-Derived CXCL9 and CXCL10 Are Required for Antitumor Immune Responses Following Immune Checkpoint Blockade. *Clin Cancer Res* 26(2):487-504.

36. Thoreau M, *et al.* (2015) Vaccine-induced tumor regression requires a dynamic cooperation between T cells and myeloid cells at the tumor site. *Oncotarget* 6(29):27832-27846.

37. Yost KE, *et al.* (2019) Clonal replacement of tumor-specific T cells following PD-1 blockade. *Nat Med* 25(8):1251-1259.

38. Theisen DJ, *et al.* (2018) WDFY4 is required for cross-presentation in response to viral and tumor antigens. *Science* 362(6415):694-699.

39. Bachem A, *et al.* (2012) Expression of XCR1 Characterizes the Batf3-Dependent Lineage of Dendritic Cells Capable of Antigen Cross-Presentation. *Front Immunol* 3:214.

40. Broz ML, *et al.* (2014) Dissecting the tumor myeloid compartment reveals rare activating antigen-presenting cells critical for T cell immunity. *Cancer Cell* 26(5):638-652.

41. Salmon H, *et al.* (2016) Expansion and Activation of CD103(+) Dendritic Cell Progenitors at the Tumor Site Enhances Tumor Responses to Therapeutic PD-L1 and BRAF Inhibition. *Immunity* 44(4):924-938.

42. Eisenhauer EA, *et al.* (2009) New response evaluation criteria in solid tumours: revised RECIST guideline (version 1.1). *Eur J Cancer* 45(2):228-247.

43. Wei SC, Duffy CR, & Allison JP (2018) Fundamental Mechanisms of Immune Checkpoint Blockade Therapy. *Cancer Discov* 8(9):1069-1086.

4. Supplementary data

Supplementary data included for publication with this work begins on the following page.

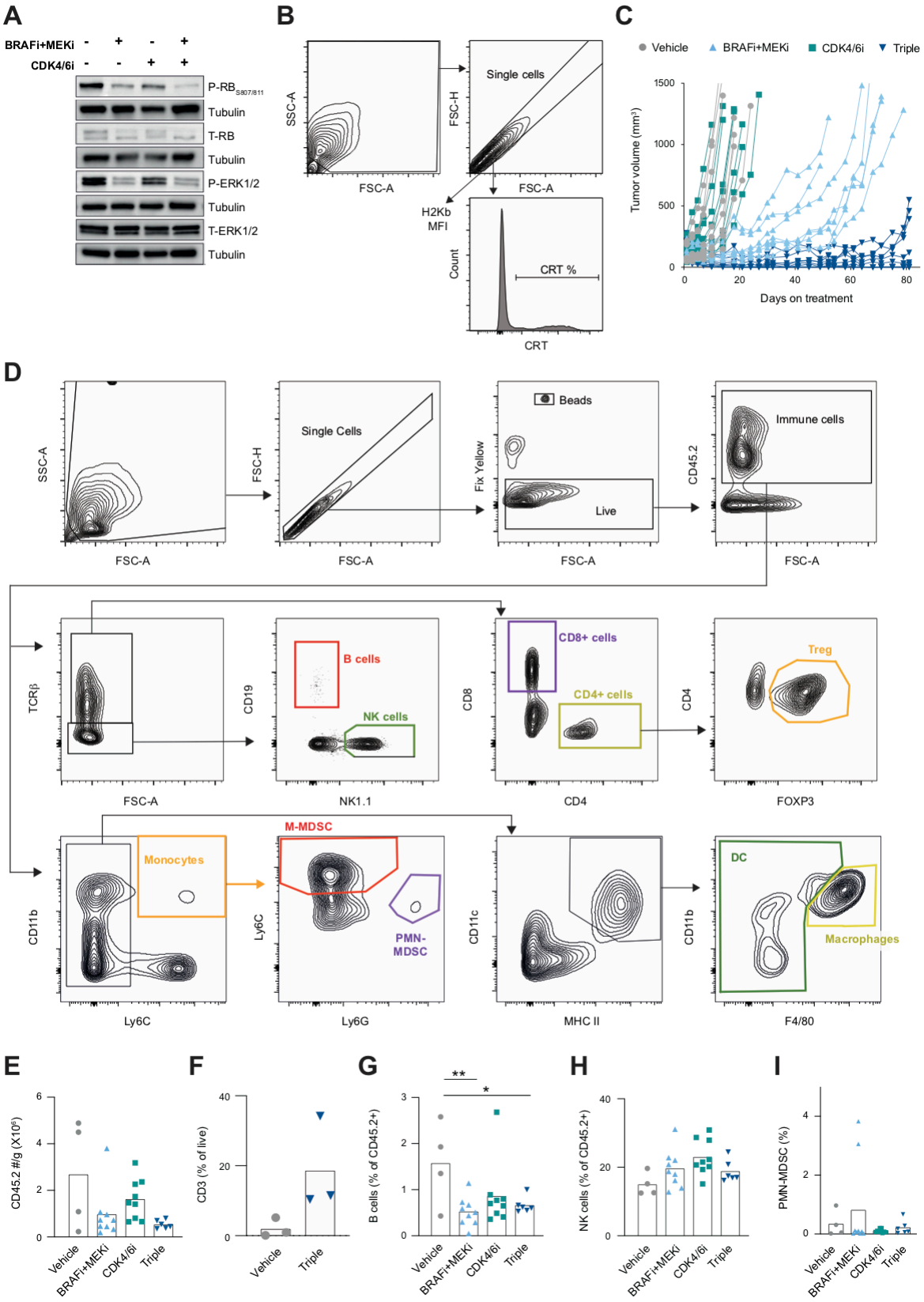
A
BRAFi+MEKi - + - +
CDK4/6i - - + +
P-RB S807/811
Tubulin
T-RB
Tubulin
P-ERK1/2
Tubulin
T-ERK1/2
Tubulin
B
SSC-A
FSC-A
FSC-H
Single cells
H2Kb MFI
Count
CRT %
CRT
C
Vehicle
BRAFi+MEKi
CDK4/6i
Triple
Tumor volume (mm³)
Days on treatment
D
SSC-A
FSC-A
Single Cells
FSC-H
Beads
Fix Yellow
Live
CD45.2
Immune cells
TCRβ
CD19
B cells
NK cells
NK1.1
CD8
CD8+ cells
CD4+ cells
CD4
Treg
FOXP3
CD11b
Monocytes
Ly6C
M-MDSC
PMN-MDSC
Ly6G
CD11c
MHC II
DC
Macrophages
F4/80
E
CD45.2 #/g (X10⁶)
F
CD3 (% of live)
G
B cells (% of CD45.2+)
H
NK cells (% of CD45.2+)
I
PMN-MDSC (%)
Vehicle
BRAFi+MEKi
CDK4/6i
Triple

Figure S1. (A) YOVAL1.1 cells analysed by immunoblot after 72h of treatment. **(B)** Gating strategy for **Fig. B-C**. **(C)** YOVAL1.1 individual growth curves from **Fig. 1D**, n=7-9 per group. **(D)** Gating strategy for **Fig. 1E-F, H, J**. **(E-I)** Analysis of YOVAL1.1 tumors by flow cytometry **(D-E, G-I)** and immunohistochemistry **(F)** pre-treatment or after 7 days of treatment, One-way ANOVA Tukey's multiple comparisons test, n=4-9. **(F)** Quantification of immunohistochemistry in **Fig. 1G**. *p<0.05, **p<0.01. BRAFi – dabrafenib; MEKi -trametinib; CDK4/6i – palbociclib; Triple – BRAFi+MEKi-+CDK4/6i.

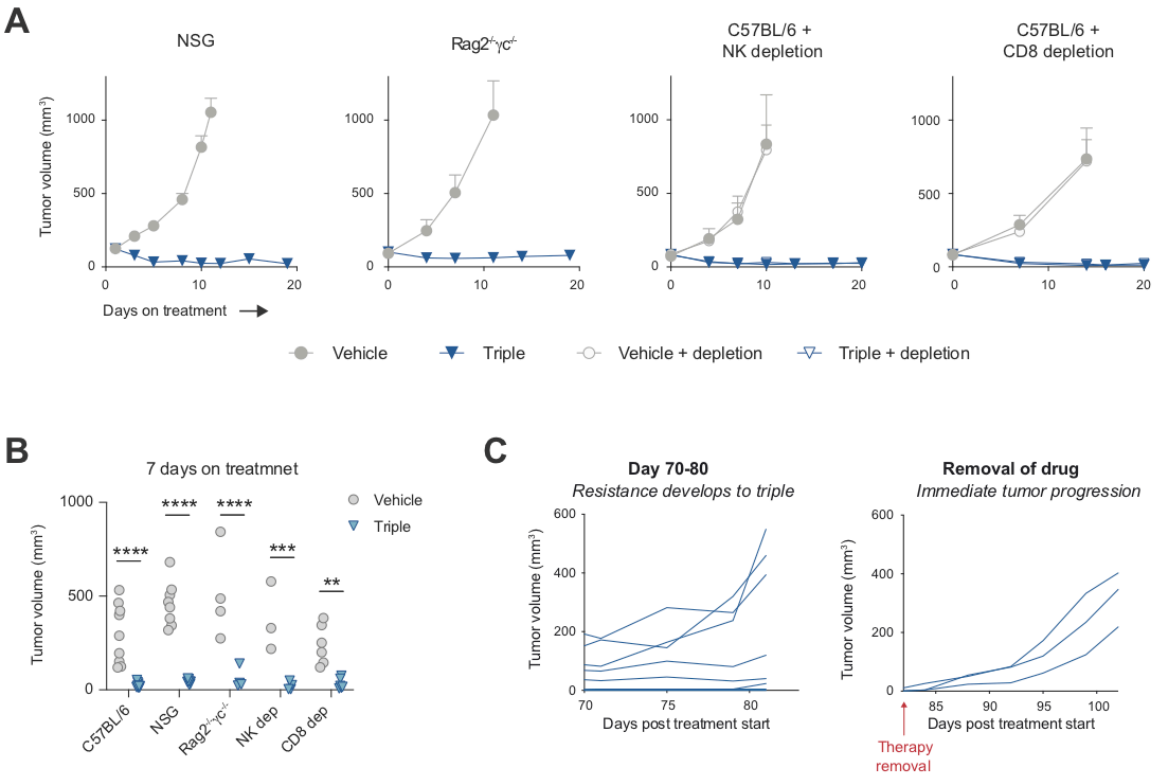
A
NSG
Rag2-/-γc-/-
C57BL/6 +
NK depletion
C57BL/6 +
CD8 depletion
Tumor volume (mm3)
1000
500
0
0
10
20
Days on treatment
Vehicle
Triple
Vehicle + depletion
Triple + depletion
B
7 days on treatmnet
Vehicle
Triple
****
****
****
***
**
C57BL/6
NSG
Rag2-/-γc-/-
NK dep
CD8 dep
C
Day 70-80
Resistance develops to triple
Removal of drug
Immediate tumor progression
600
400
200
70
75
80
85
90
95
100
Days post treatment start
Therapy
removal

Figure S2. (A) YOVAL1.1 tumor growth in NSG mice, $Rag2^{-/-}\gamma c^{-/-}$ mice, or C57BL/6 mice depleted of NK cells or CD8+ cells, randomised for treatment when tumors reached ~100mm^3. **(B)** Tumor volume following 7 days of treatment with vehicle or triple, One-way ANOVA Tukey's multiple comparisons test, n=3-9. **(C)** Individual growth curves for mice treated with triple therapy, showing day 70-82 on treatment (left panel; from Figure 1D, S1B, n=9), and following therapy removal on day 82, showing those mice that had cleared tumors prior to day 82 (right panel, n=3). Error bars show +/- SEM. *p<0.05, **p<0.01, ****p<0.0001. Triple – BRAFi (dabrafenib) + MEKi (trametinib) + CDK4/6i (palbociclib).

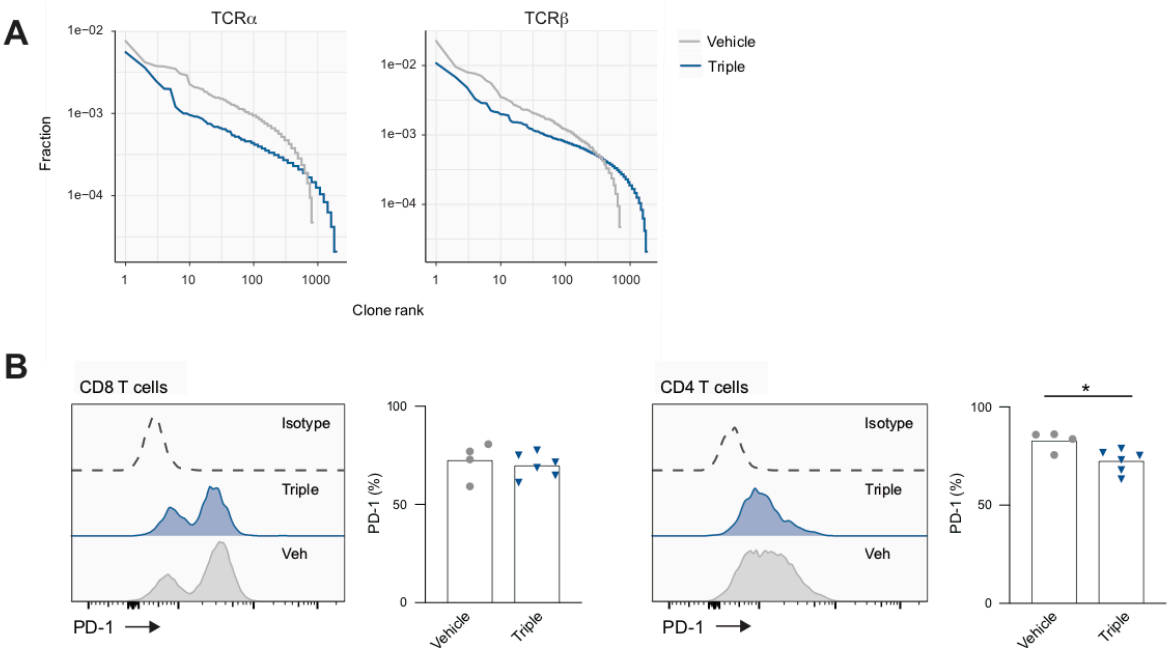
A
TCRα
TCRβ
Vehicle
Triple
Fraction
1e−02
1e−03
1e−04
1
10
100
1000
Clone rank
B
CD8 T cells
CD4 T cells
Isotype
Triple
Veh
PD-1
PD-1 (%)
100
50
0
Vehicle
Triple
*

Figure S3. (A) TCR clonal diversity delineated in to TCRa and TCRb from single-cell RNA-seq on T cells isolated from YOVAL1.1 tumors following 7 days of treatment, n=10 mice per group pooled. **(B)** Flow cytometric analysis of T cells from YOVAL tumors after 7 days of treatment, gating strategy for CD8+ T cells and CD4+ T cells is shown in **Fig. S1D**, unpaired t-test, n=4-6, plots are representative. Error bars show +/- SEM. *p<0.05. Triple – BRAFi (dabrafenib) + MEKi (trametinib) + CDK4/6i (palbociclib).

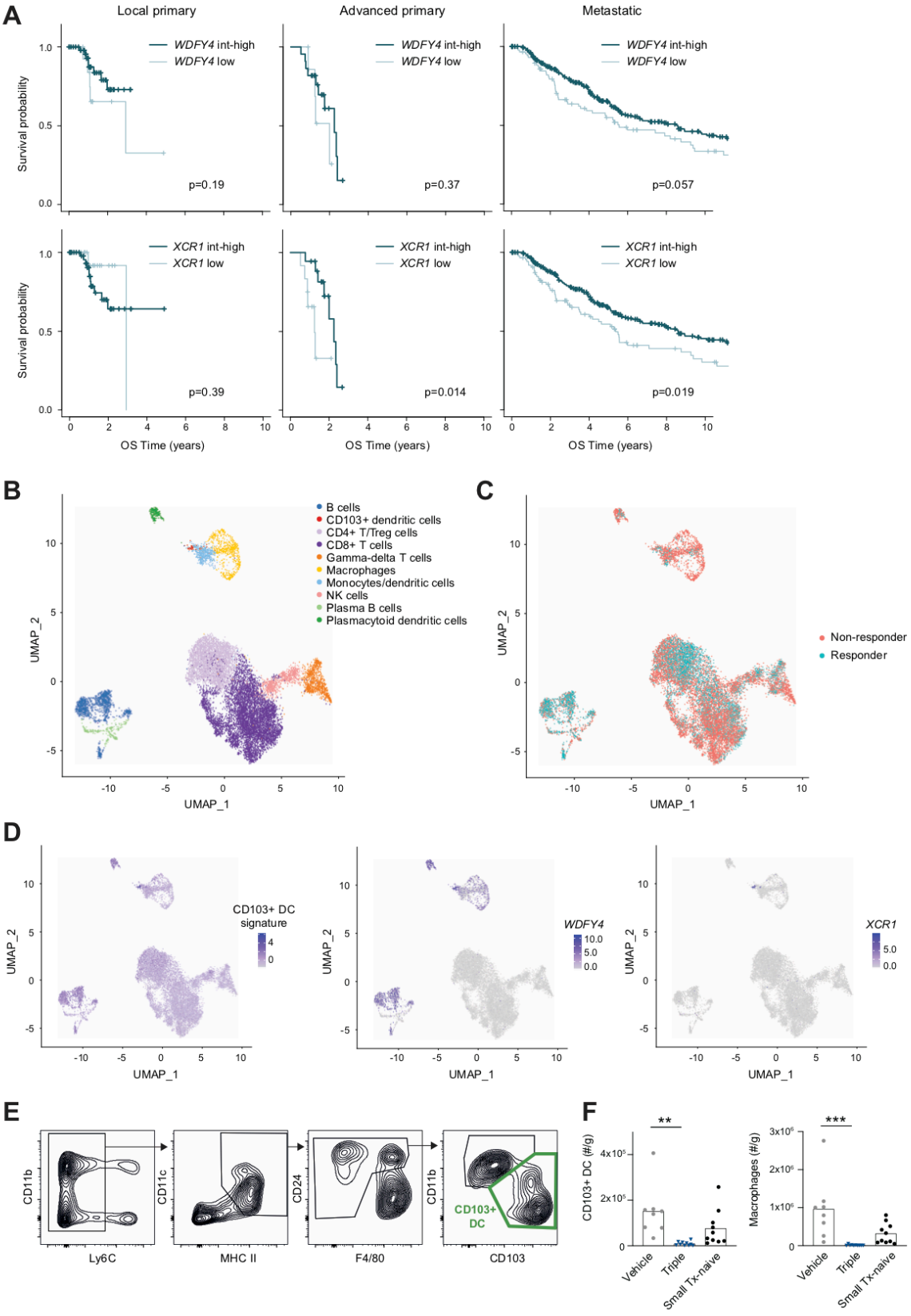
A
Local primary
Advanced primary
Metastatic
WDFY4 int-high
WDFY4 low
XCR1 int-high
XCR1 low
Survival probability
p=0.19
p=0.37
p=0.057
p=0.39
p=0.014
p=0.019
OS Time (years)
B
B cells
CD103+ dendritic cells
CD4+ T/Treg cells
CD8+ T cells
Gamma-delta T cells
Macrophages
Monocytes/dendritic cells
NK cells
Plasma B cells
Plasmacytoid dendritic cells
UMAP_1
UMAP_2
C
Non-responder
Responder
D
CD103+ DC signature
WDFY4
XCR1
E
CD11b
Ly6C
CD11c
MHC II
CD24
F4/80
CD103+ DC
CD103
F
CD103+ DC (#/g)
Macrophages (#/g)
Vehicle
Triple
Small Tx-naive

Figure S4. (A) Kaplan-Meier overall survival of melanoma patients with different stages of disease, stratified by expression level of indicated gene; top 75% (int-high) vs bottom 25% (low), logrank p-values are indicated. **(B-D)** Analysis of published single cell RNA-seq on tumor-infiltrating immune cells from melanoma patients treated with ICB (31), UMAP clustering based on gene expression, $CD103^+$ DCs identified using signature from Figure 1K (29). **(E)** Gating strategy used to define $CD103^+$ DCs, gated from $CD45.2^+$ cells (as in **Fig. S1D**). **(F)** Total number of indicated population after 7 days of treatment, One-way ANOVA Tukey's multiple comparisons test, n=8-10. Triple – BRAFi (dabrafenib) + MEKi (trametinib) + CDK4/6i (palbociclib).

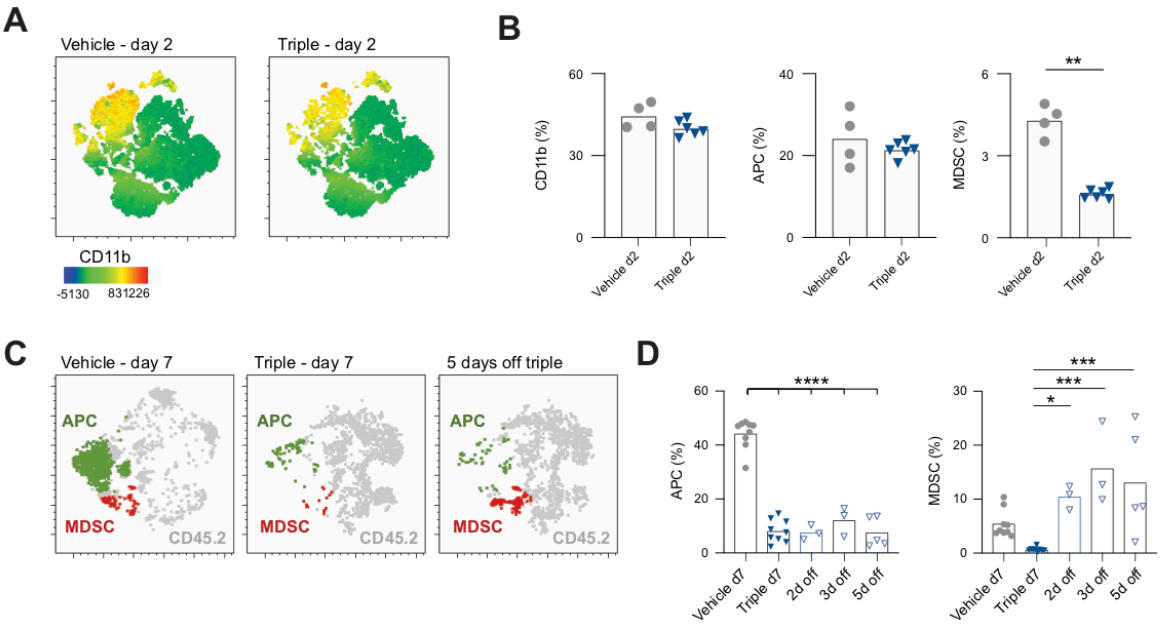
A
Vehicle - day 2
Triple - day 2
CD11b
-5130
831226
B
CD11b (%)
APC (%)
MDSC (%)
Vehicle d2
Triple d2
**
C
Vehicle - day 7
Triple - day 7
5 days off triple
APC
MDSC
CD45.2
D
APC (%)
MDSC (%)
****
***
*
Vehicle d7
Triple d7
2d off
3d off
5d off

Figure S5. Analysis of YOVAL1.1 tumors by flow cytometry. **(A, C)** tSNE clustering based on equal numbers of CD45.2^{+} cells pooled from all treatment groups, plots are representative of n=5 concatenated samples per group. **(B, D)** Indicated population as a percent of CD45.2^{+}, **(B)** unpaired t-test, n=4-6, **(D)** One-way ANOVA Tukey's multiple comparisons test, n=3-9. **(C-D)** For 2d off, 3d off and 5d off samples, mice were treated with triple therapy for 7 days, then therapy was withdrawn and tumors were harvested for analysis 2, 3 or 5 days after therapy cessation. Antigen presenting cells (APCs) include macrophages and DCs, MDSCs include M-MDSC and PMN-MDSC, gating strategy for these populations is shown in **Fig. S1D**. Error bars show +/- SEM. *p<0.05, **p<0.01, ***p<0.001, ****p<0.0001. Triple – BRAFi (dabrafenib) + MEKi (trametinib) + CDK4/6i (palbociclib).

Chapter 4: Pharmacological inhibition of CDK4/6 augments long-term anti-tumor immunity through the induction of T cell memory

1. Preface

The aim of this chapter was to evaluate the direct effects of CDK4/6 inhibition on T cells and T cell-mediated anti-tumor immunity

This body of work is currently under peer review for publication:

Lelliott EJ, Kong I, Zethoven M, Ramsbottom KM, Martelotto L, Meyran D, Zhu JJ, Costacurta M, Kirby L, Sandow J, Lim L, Dominguez P, Todorovski I, Haynes NM, Beavis PA, Neeson PJ, Hawkins ED, McArthur GA, Parish IA, Johnstone RW, Oliaro J, Sheppard KE, Kearney CJ, Vervoort SJ. Pharmacological inhibition of CDK4/6 augments long-term anti-tumor immunity through the induction of T cell memory. *Cancer Discovery* [under review Nov 2020].

This chapter will present an introduction with a summary of the key findings, the work submitted for publication, and associated supplementary data.

2. Introduction

As discussed in Chapter 1, there is strong evidence that CDK4/6 inhibition would be an attractive adjuvant to immunotherapies, and this is reflected in the number of clinical trials now underway to evaluate the efficacy of combined CDK4/6 inhibition and anti-PD-1/PD-L1 blockade. However, while a number of studies have addressed the impact of CDK4/6 inhibition on tumor-intrinsic immune modulation and the overall tumor immune microenvironment (discussion in section 1.3.2) (221-223), very little is known about the direct influence of inhibiting CDK4/6 within T lymphocytes, which are the principal effector cells that mediate responses to immune checkpoint therapy. One seminal study recently identified NFAT as a direct target of CDK6 in T lymphocytes (*39*). In this context, CDK4/6 inhibition enhanced T cell activation via the de-repression of NFAT. However, while essential for initial T cell activation, NFAT also drives transcriptional programs of T cell exhaustion (*50, 51*), and the impact of CDK4/6 inhibitors on the longevity of anti-tumor T cell responses remains unclear. The aim of this chapter was therefore to evaluate the direct impact of inhibiting CDK4/6 in T cells.

To address this, a series of integrated multi-omic approaches, combined with immunological assays and model systems, was used to comprehensively examine the effect of CDK4/6 inhibition on T cells. Integral to the work in this chapter was the application of Cellular Indexing of Transcriptomes and Epitopes by Sequencing (CITE-seq) technology; a method that combines multiplexed antibody detection of surface proteins together with transcriptome profiling at a single cell level (259). This enabled the interrogation of T cell phenotype based on cellular protein expression and the transcriptome. CITE-seq was applied in parallel with bulk RNA-seq, ATAC-seq and

flow cytometry to comprehensively analyze tumor infiltrating T cells following CDK4/6 inhibition. Further analyses were performed *in vitro* to examine isolated effects of CDK4/6 inhibition on activated T cells. This was coupled with a series of adoptive transfer experiments in both tumor and infection models to evaluate the subsequent *in vivo* characteristics of T cells that had been pre-exposed to a CDK4/6 inhibitor.

This body of work identified a critical role for CDK4/6 in regulating T cell fate. Specifically, CDK4/6 inhibition led to the emergence of memory-like T cells within the tumor microenvironment, which correlated with long-term tumor control following therapy removal. Importantly, CDK4/6 inhibition acted intrinsically on T cells, directly promoting transcriptional and epigenetic signatures that drive T cell stemness, which resulted in long-term *in vivo* persistence of memory cells that rapidly responded to antigen re-encounter. T cell stemness is a property that is clinically appealing in the application of adoptive cellular therapies, including chimeric antigen receptor (CAR) T cell therapy. CAR T cell therapy is highly efficacious for the treatment of blood cancers (260, 261), but is much less successful for the treatment of solid cancers (262-264), in part due to the lack of persistence of the adoptively transferred CAR T cells (265, 266). As such, research is currently focused on identifying therapies that improve the longevity of CAR T cells following transfer into patients (267). Here, exposure of *in-vitro* generated human CAR T cells to a CDK4/6 inhibitor induced stem-like attributes in these cells, which significantly enhanced their persistence and survival *in vivo*, and led to superior suppression of tumor growth upon re-challenge. Further analysis of patient samples and published data sets revealed that CDK4/6 inhibition promotes a T cell phenotype that is associated with better responses to immune checkpoint blockade, and hence may be used to prime the cellular pool for responses to immunotherapy. Taken together, these data implicate CDK4/6 as critical regulators of T cell memory

formation, while providing mechanistic insight and rationale for the clinical application of combination therapies incorporating CDK4/6 inhibition with immunotherapy.

3. Publication under peer review by *Cancer Discovery*

This body of work begins on the following page.

Pharmacological inhibition of CDK4/6 augments long-term anti-tumor immunity through the induction of T cell memory

Emily J. Lelliott[1,2], Isabella Kong[3,4], Magnus Zethoven[1,5], Kelly M. Ramsbottom[1,6], Luciano Martelotto[7], Deborah Meyran[1,6,8], Joe Jiang Zhu[1,2,6], Matteo Costacurta[1,9], Laura Kirby[1], Jarrod Sandow[3], Lydia Lim[1], Pilar Dominguez[1,9], Izabela Todorovski[1,9], Nicole M. Haynes[1,2,10], Paul A. Beavis[1,2,6], Paul J. Neeson[1,2,6], Edwin D. Hawkins[3,4], Grant A. McArthur[1,2], Ian A. Parish[1,6], Ricky W. Johnstone[1,2,9], Jane Oliaro[1,2,6,11], Karen E. Sheppard[1,2,12#*], Conor J. Kearney[1,2,9,#*] and Stephin J. Vervoort[1,2,9,#*]

1. Cancer Research Division, Peter MacCallum Cancer Centre, Melbourne, VIC, Australia
2. Sir Peter MacCallum Department of Oncology, University of Melbourne, Parkville, VIC, Australia
3. The Walter and Eliza Hall Institute of Medical Research, Parkville, VIC, Australia
4. Department of Medical Biology, The University of Melbourne, Parkville, VIC, Australia
5. Bioinformatics Core Facility, Peter MacCallum Cancer Centre, Melbourne, VIC, Australia
6. Cancer Immunology Program, Peter MacCallum Cancer Centre, Melbourne, VIC, Australia
7. Single Cell Innovation Laboratory, The University of Melbourne, Parkville, VIC, Australia
8. Université de Paris, Inserm, U976 HIPI Unit, Institut de Recherche Saint-Louis, Paris, France
9. Translational Haematology Program, Peter MacCallum Cancer Centre, Melbourne, VIC, Australia

10. Department of Pathology, University of Melbourne, Parkville, VIC, Australia
11. Department of Immunology, Central Clinical School, Monash University, Melbourne, VIC, Australia
12. Department of Biochemistry and Molecular Biology, University of Melbourne, Parkville, VIC, Australia.

Equal senior author

*Correspondence to: conor.kearney@petermac.org, karen.sheppard@petermac.org, stephin.vervoort@petermac.org

Running title: CDK4/6 inhibition promotes T cell memory and anti-tumor immunity.

Abstract

Small molecule inhibitors of cyclin dependent kinases 4 and 6 (CDK4/6) are an approved treatment for hormone receptor-positive breast cancer and are currently under evaluation across hundreds of clinical trials for other cancer types. The clinical success of these inhibitors is largely attributed to well-defined tumor-intrinsic cytostatic mechanisms, while their emerging role as immunomodulatory agents is less understood. Using integrated epigenomic, transcriptomic and proteomic analyses, we demonstrated a novel action of CDK4/6 inhibitors in promoting the phenotypic and functional acquisition of immunological T cell memory. Short-term priming with a CDK4/6 inhibitor promoted long-term endogenous anti-tumor T cell immunity in mice, enhanced the persistence and therapeutic efficacy of chimeric antigen receptor (CAR)-T cells, and induced an RB-dependent T cell phenotype supportive of favorable responses to immune checkpoint blockade in melanoma patients. Taken together, these mechanistic insights significantly broaden the prospective utility of CDK4/6 inhibitors as clinical tools to boost anti-tumor T cell immunity.

Significance: Immunological memory is critical for sustained anti-tumor immunity. Our discovery that CDK4/6 inhibitors drive T cell memory fate commitment sheds new light on their clinical activity, which is essential for the design of clinical trial protocols incorporating these agents, particularly in combination with immunotherapy, for the treatment of cancer.

Introduction

Aberrant cell cycling via disruption of the cyclin-dependent kinases 4 and 6 (CDK4/6)/retinoblastoma (RB) tumor suppressor pathway is observed in many cancers and has spurred the clinical development of inhibitors that specifically target these kinases (1, 2). CDK4/6 inhibitors (CDK4/6i) are now an approved treatment for hormone receptor-positive breast cancer, and under investigation in clinical trials as a therapeutic for a wide array of cancer types (3). In addition to inducing tumor cell cytostasis, recent studies have highlighted a role for CDK4/6 inhibitors in promoting anti-tumor immunity (4-8); an effect that has been attributed to both tumor-intrinsic mechanisms, such as increasing tumor expression of major histocompatibility complex (MHC) class I, (4) as well as direct effects on the immune system, such as enhancing T cell activation (6). Indeed, CDK4/6i have shown remarkable synergy with blockade of the PD-1/PD-L1 axis in preclinical models (4, 6-8), prompting evaluation of this combination therapy in a number of clinical trials (e.g. NCT04075604, NCT02778685, NCT04118036).

T cell dysfunction in the tumor microenvironment is a major barrier to effective anti-tumor immunity. The advent of modern technologies, such as single-cell transcriptomics, has provided unprecedented molecular insights into the heterogenous nature of tumor infiltrating T cells (9-11), revealing a diverse spectrum of phenotypic states with varying effector capacity. Notably, such technology has enabled the identification of T cells with stem or memory-like properties as the primary responders to immune checkpoint blockade (ICB) and the key mediators of long-term anti-tumor immunity (11-17). These intratumoral memory-like subsets demonstrate superior capacity for self-renewal and longevity, and can reconstitute and maintain a phenotypically diverse T cell compartment (15). Indeed, strategies to preserve stem-like properties of autologous T cells and chimeric antigen receptor (CAR)-T cells have resulted in superior anti-tumor efficacy following

adoptive transfer (14, 18-20). Such cell states are governed by diverse transcriptional and epigenetic regulatory networks (21-23), and targeting these networks to direct immune cell fate is of great clinical interest.

Here, using integrated single cell multi-omics, whole genome CRISPR/Cas9 screening and functional-based *in vitro* and *in vivo* analyses, we identify CDK4/6 as a critical regulator of T cell fate. Specifically, short-term pharmacological inhibition of CDK4/6 led to direct T cell-intrinsic RB-dependent induction of immunological memory, which correlated with long-term endogenous anti-tumor immune control following therapy removal. Further, pre-conditioning mouse or human CAR-T cells with CDK4/6i enhanced their persistence and anti-tumor efficacy in murine models. Finally, we showed that the T cell-intrinsic gene signature induced by CDK4/6 inhibition is associated with favourable responses to ICB in melanoma patients, and validated these findings through serial sample collection from a melanoma patient over the course of their treatment with CDK4/6i and subsequent ICB. Together, our results comprehensively and mechanistically detail the influence of pharmacological CDK4/6 inhibition on the phenotype and function of T lymphocytes – the key mediators of anti-tumor immunity. These findings provide essential insight into the utility of these inhibitors as immunomodulatory agents and as adjuvants to a range of T cell-directed immunotherapies.

Results

Emergence of intratumoral memory-like CD8+ T cells in response to CDK4/6 inhibition

To comprehensively evaluate the effect of CDK4/6 inhibition on anti-tumor T cell immunity, we used multimodal single cell sequencing (CITE-seq) (24, 25) to analyze the intratumoral T cell population in MC38-OVA tumors from mice treated with the CDK4/6 inhibitor, palbociclib, or a vehicle control (**Fig. 1A**). This approach allowed us to

simultaneous measure surface protein expression and cellular transcripts, while de-multiplexing pooled treatment conditions (**Fig. 1A**). Dimensional analysis revealed 10 distinct T cell clusters within MC38-OVA tumors (**Fig. 1B**), and antibody-derived tags delineated discrete populations of CD4+ and CD8+ tumor infiltrating lymphocytes (TILs) (**Fig. S1A).** Notably, tumors treated with CDK4/6i had a lower frequency of CD4+ regulatory T cells (*Foxp3*+ Tregs), consistent with previous reports (4), and a higher frequency of CD8+ memory-like T cells, marked by high expression of *Tcf7*, *Sell*, *Bcl2* and *Cd7* (**Fig. 1B-D, S1B**). Further analyses of gene expression dynamics of the CD8+ T cellular pool across a pseudotime trajectory (a measure of how far a cell has moved through a biological process) revealed CD8+ TILs from CDK4/6i-treated mice were skewed towards an earlier, and more stem-like differentiation state (**Fig. 1E-F, S1C**). Consistent with this, cells earlier on the pseudotime trajectory expressed higher levels of memory-associated genes (*Tcf7*, *Sell*, *Il7r*), and lower levels of effector-associated genes (*Prf1*, *Gzmb*) and exhaustion markers (PD-1, TIM3) (**Fig. 1G, S1D**). Similarly, inferred transcription factor (TF) activity analysis (SCENIC) revealed that memory-associated TFs, including TCF1 and FOXP1, were highly active in 'earlier' T cell clusters, while the effector-associated TFs, IRF8 and NFATc1, were most active in cells further along the pseudotime trajectory (**Fig. S1E-G**). Published gene signatures of memory versus effector cells derived from lymphocytic choriomeningitis virus (LCMV) infection (26) also correlated with early and late pseudotime, respectively (**Fig. S1H**). Accordingly, cells within the CD8+ memory T cell cluster, which was increased following CDK4/6i treatment, were enriched for a memory versus effector gene signature (**Fig. S1I-J**). We further characterized the CD8+ T cell population by *ex vivo* bulk 3'RNA-seq and, in accordance with our single cell analyses, found enrichment of memory versus effector signatures following CDK4/6i treatment (**Fig. S2A-C**), with increased expression of

several memory-associated genes (*Sell, Il7r, Tcf7*) (**Fig. S2C**). To validate these findings with a second pharmacological inhibitor of CDK4/6, we re-analysed previously published single cell RNA-seq data on tumor-infiltrating T cells from lung tumors of mice treated with trilaciclib (6). Here, we also found an increase in memory-associated genes (**Fig. S2D**), which was not discovered or reported in the previous study. In support of our transcriptional analyses, further investigation by flow cytometry demonstrated a significantly higher proportion of CD8+ TILs with a central memory (Tcm) phenotype (CD44+CD62L+) (**Fig. 1H**), which was consistent across various tumor models (**Fig S2E**). CD8+ TILs from CDK4/6i-treated mice also had higher expression of memory markers, TCF1 and CD127, and lower expression of exhaustion markers, PD-1 and TIM3 (**Fig. S2F-G).** Notably, this CDK4/6i-mediated induction of memory was also observed in the tumor-specific OVA-reactive CD8+ T cell population **(Fig. S2H).**

We next assessed whether these phenotypic and transcriptional changes were associated with stable epigenetic alterations using Assay for Transposase-Accessible Chromatin sequencing (ATAC-seq) to assess chromatin accessibility in CD8+ T cells from vehicle- or CDK4/6i-treated MC38-OVA tumors. Indeed, *ex vivo* bulk ATAC-seq revealed a global reduction in chromatic accessibility in the CD8+ T cell population (**Fig. S2I-J**), consistent with the more quiescent nature of memory T cells (27). Furthermore, gene set enrichment analysis (GSEA) of genes associated with regions of increased chromatin accessibility confirmed significant enrichment for T cell memory signatures (**Fig. S2K-L**), suggesting that CDK4/6i-driven phenotypic and transcriptional changes stem from stable epigenetic underpinnings.

To examine the long-term functional effect of CDK4/6 inhibition on anti-tumor T cell immunity, we next treated MC38-OVA tumor-bearing mice with CDK4/6i over a short window (days 3-13 when the anti-tumor T cell response is most active) followed by

therapy withdrawal. Strikingly, CDK4/6i treatment resulted in complete tumor clearance in 21/22 mice, compared to 9/22 for vehicle-treated mice (**Fig. 1I-J**). Depletion of CD4+ and CD8+ T cells abrogated the efficacy of CDK4/6i, indicating the response was T cell-mediated (**S2M-N**). Importantly, at the time of therapy cessation, tumor volumes were equivalent in both vehicle- and CDK4/6i-treated mice (**Fig. 1K**), and CDK4/6i-treated mice also showed an overall reduction in tumor-filtrating T cells prior to therapy withdrawal (**Fig. S2O**). Together, this suggested T cells present in CDK4/6i treated tumors exhibited a greater capacity for ongoing anti-tumor activity than those from vehicle-treated tumors. Collectively, these data demonstrate that pharmacological inhibition of CDK4/6 promotes T cell memory and generates an intratumoral T cell compartment capable of driving a potent and sustained anti-tumor response.

CDK4/6i-mediated acquisition of CD8+ T cell memory is cell-intrinsic

Lymphocyte differentiation is tightly regulated during cell proliferation (28-30), though it is unknown whether acute manipulation of cell cycle machinery has a directional influence on cell fate. To determine if the emergence of T cell memory observed in CDK4/6i-treated tumors was due to the direct inhibition of CDK4/6 within these cells, we exposed activated primary mouse CD8+ T cells to CDK4/6i *in vitro* and monitored Tcm acquisition and division number. CDK4/6i exposure 0, 24 and 72 h after activation decreased the mean division number and concurrently increased the proportion of Tcm cells in a dose dependent manner, occurring in as little as 24 h after drug exposure (**Fig. 2A, S3A-B**). Notably, exposing cells to CDK4/6i 72 h after activation not only prevented further differentiation of Tcm into effector cells (Tem), but redirected differentiation of Tem into Tcm (**Fig. S3C**), with Tcm acquisition occurring independently of cell division (**Fig. S3D**). This indicated that CDK4/6i was not simply restraining differentiation, but rather directly promoting memory formation, demonstrating a directional relationship

between cell cycle machinery and differentiation. Further analysis by 3'RNA-seq revealed an increase in memory-associated transcripts following CDK4/6i, and GSEA analysis confirmed enrichment of memory-associated signatures coupled with a decrease in cell-cycle associated signatures, including E2F targets (**Fig. 2B-E, S3E**). Paradoxically, CDK4/6 inhibition also induced effector-associated transcripts, including *Gzma*, *Gzmc* and *Pdcd1* (**Fig. 2B-C**), consistent with previous reports that CDK4/6i promotes T cell activation (6). Indeed, CDK4/6i-treated cells expressed higher levels of T cell activation markers (CD25, CD69) and demonstrated enhanced effector function (**Fig. S3F-H**). To determine if acute *in vitro* treatment with CDK4/6i resulted in epigenetic changes that may account for these effects, we performed Chromatin Immunoprecipitation sequencing (ChIP-seq) for H3K27 acetylation. Following acute (6 h) treatment, we observed a dramatic reduction in H3K27 acetylation at cell cycle-related gene regions, including E2F TFs (**Fig. S3I-J**). Accordingly, motif analysis identified significant enrichment in E2F TF motifs at regions associated with decreased acetylation, and an increase in acetylation at motifs associated with drivers of T cell memory, including forkhead-box-containing factors (31) (**Fig. 2F**). To determine if these changes were followed by long term epigenetic commitment to a distinct cellular state, we performed ATAC-seq on *in vitro*-activated T cells following CDK4/6 inhibition. Concordant with our *ex vivo* ATAC-seq (**Fig. S2I-J**), we observed a global reduction in chromatin accessibility, with an increase in accessibility at regions of genes involved in T cell memory, including *Tcf7, Ccr7* and *Sell* (**Fig. 2G, S3K**).

To unravel the apparent dichotomy of both memory and effector features in response to CDK4/6 inhibition, we performed single cell RNA-seq on *in vitro*-activated T cells following 24 h exposure to CDK4/6i. This analysis revealed the existence of distinct T cell subpopulations that were altered upon CDK4/6i treatment, with increases in clusters

2, 4, 5 and 8, decreases in cluster 0, and a global G1 cell cycle arrest (**Fig. 2H-I, S3L-M**). We next generated memory and effector gene signatures and, using AUCell to compare enrichment scores, identified distinct memory-like and effector-like clusters within the cellular pool (**Fig. 2I-J, S3N-O**). Interestingly, of those clusters that increased in frequency following CDK4/6i, clusters 2 and 5 were memory-like, and cluster 8 was effector-like (**Fig. 2I**), demonstrating that CDK4/6 inhibition promotes memory differentiation and enhances effector function in phenotypically distinct subsets in a heterogenous T cell pool.

CDK4/6 inhibition promotes memory formation in an RB-dependent manner

To determine the molecular drivers of CDK4/6i-induced memory, we performed a genome wide CRISPR/Cas9 screen for genes that regulate the memory marker, CD62L (*SELL*), in response to CDK4/6 inhibition. Cas9-expressing Jurkat T cells (which up-regulate CD62L upon CDK4/6 inhibition) were transduced with a genome wide sgRNA library, followed by treatment with CDK4/6i and fluorescence-activated cell sorting for cells that failed to upregulate CD62L (**Fig. 3A**). Sequencing of the sorted population revealed that sgRNAs targeting RB transcriptional corepressor 1 (*RB1)* were significantly enriched only in the treated condition (**Fig. 3B**), suggesting that RB is required for CDK4/6i-induced CD62L upregulation. To identify potential screen hits that are direct phosphorylation substrates of CDK4/6 kinase activity, we performed global phospho-proteomics on both Jurkat cells and activated primary mouse CD8+ T cells upon acute (2 h) exposure to CDK4/6i (**Fig. 3C**). We detected a significant loss of specific phosphorylation sites on multiple peptides in both Jurkat and mouse T cells, including the canonical CDK4/6 targets, RB and RBL1/2 (**Fig. 3D-F, S4A-D**). Notably, RB was an overlapping hit across the phospho-proteomic analysis and the genome wide CRISPR/Cas9 screen (**Fig. 3G, S4C-D**), suggesting that CDK4/6i-mediated memory

formation is mediated through RB. Accordingly, targeted deletion of *RB1* in Jurkat cells abrogated the induction of CD62L and dampened the anti-proliferative effects of CDK4/6i (**Fig. 3H, S4E-F**). Further analyses by 3'RNA-seq showed RB loss likewise abrogated the transcriptional response to CDK4/6i, with global CDK4/6i-induced transcriptional changes, including *SELL*, largely attenuated in the absence of RB (**Fig. 3I, S4G**). Consistent with this, targeted deletion of *Rb1* also abrogated Tcm formation in activated primary mouse CD8+ T cells (**Fig. 3J**). To determine if CDK4/6i-induced memory formation occurs through an RB-dependent block in G1 of the cell cycle, we treated cells with the G1 blocking agent, thymidine. Indeed, thymidine phenocopied CDK4/6 inhibition, transcriptionally and phenotypically, and largely rescued Tcm formation in *Rb1* KO cells (**Fig. 3J, S4H-J**). Further analysis of *Rb1* KO cells by 3'RNA-seq revealed a downregulation of memory associated genes and an increase in effector signatures **(Fig. 3K-L, S4K),** which failed to be reversed upon CDK4/6 inhibition **(Fig. 3M-N, S4L)**. Taken together, these data suggest that CDK4/6 inhibition induces memory formation through RB-mediated transcriptional changes, which concurrently regulate G1 cell cycle arrest and differentiation.

CDK4/6i preconditioning enhances the persistence of functional memory CD8+ T cells.

The capacity for long-term survival is a fundamental characteristic of T cell memory (32). To determine whether CDK4/6i-treated cells demonstrated superior survival *in vivo*, untreated and CDK4/6i-pre-treated *in vitro*-activated CD45.1 OT-I T cells were transferred into congenic CD45.2 mice, and their persistence and phenotype was evaluated overtime by flow cytometry (**Fig. 4A**). A significantly higher frequency of pre-treated OT-I T cells was detected in both the blood and the spleen over 30 days (**Fig. 4B, S5A-B**). After 30 days, untreated and pre-treated OT-I T cells that persisted in the blood and spleen were phenotypically similar (**Fig. S5C-F**), with characteristics of memory

precursors (MPECs; KLRG1-CD127+) (**Fig. 4C**). Upon antigen re-encounter, bona fide MPECs rapidly proliferate and differentiate into KLRG1+ short-lived effectors (SLECs) (33). To evaluate the recall capacity of CDK4/6i-treated cells, untreated or pre-treated *in vitro*-activated CD45.1 OT-I T cells were again transferred into congenic CD45.2 hosts. After 30 days, OT-I T cells were isolated and re-transferred at equal numbers into new hosts that were simultaneously infected with *Listeria*-OVA (LM-OVA) (**Fig. 4D**). Both untreated and pre-treated OT-I T cells expanded and differentiated in response to LM-OVA infection, rapidly acquiring a functional, cytokine-producing SLEC phenotype (KLRG1+CD127-) (**Fig. 4E-F, S6A-F**). This confirmed that CDK4/6 inhibition drives both the phenotypic and functional acquisition of T cell memory.

We next used single cell RNA-seq to characterize the transcriptional profile of those T cells that persisted in the spleen 30 days after transfer (**Fig. 4G**). Consistent with our flow cytometry data, the transferred T cells from both untreated and pre-treated conditions were phenotypically similar (**Fig. S7A-C**) and were predominately resting in G1 (**Fig. S7D**). Using pseudobulk RNA-seq analysis and gene comparison with our pre-transfer *in vitro* cultures, we generated a gene signature for persisting cells, which was marked by high expression of memory-associated genes (*Sell, Foxp1, Tcf7, Cd7, Il7r, Klf2, Ccl5*) and low expression of effector-associated genes (*Gzmd, Ifng, Prf1, Gzma, Gzmb*) (**Fig. 4H-I**). Further analysis of our previous *in vitro* single cell data (**Fig. 2H-J**) revealed an increase in the frequency of cells with this persistence signature, from 7.5% to 26.8%, following CDK4/6i treatment (**Fig. 4J-K, S7E**). Together, these data indicate that CDK4/6 inhibition promotes differentiation of T cells towards a bona fide memory phenotype, characteristic of functional long-term persistence.

CDK4/6i preconditioning enhances the persistence and efficacy of CAR-T cells

We next tested whether treatment with CDK4/6i would induce a memory phenotype in chimeric antigen receptor (CAR)-T cells, and overcome two major impediments to successful CAR-T cell therapy – T cell exhaustion and lack of persistence (34). Using clinical protocols, we generated human CAR-T cells targeting the Lewis Y (LeY) antigen (35) (**Fig. 5A**) and found that exposure to CDK4/6i yielded an enrichment of CD4+ and CD8+ stem cell memory (Tscm) CAR-T cells (**Fig. 5B, S8A-B**). These stem-like CAR-T cells are reported to have superior survival and self-renewal capacities (36, 37). 3'RNA-seq of the CAR-T cells revealed significant changes in gene expression following CDK4/6 inhibition, with GSEA analyses confirming enrichment of memory versus effector signatures, and an expected downregulation of E2F target genes (**Fig. 5C, S8C-D**). To examine *in vivo* persistence, LeY CAR-T cells, generated using PBMC from two independent donors, were pre-treated with CDK4/6i and transferred into NSG mice (**Fig. 5D**). Compared to untreated controls, we observed a significant increase in both the frequency and number of CD8+ and CD4+ pre-treated CAR-T cells in the blood in the weeks following transfer (**Fig. 5E, S8E-F**). To assess the functional recall capacity of these CAR-T cells we challenged mice 30 days after CAR-T cell transfer with the LeY+ ovarian cancer cell line, OVCAR-3 (**Fig. 5D**) and observed a significant increase in the expansion of pre-treated CAR-T cells in the blood of mice compared to the untreated CAR group (**Fig. 5F**). This translated to a significant and striking enhancement in tumor control in mice that had previously received pre-treated CAR-T cells (**Fig. 5G-H, S8G)**. Notably, there was a significant negative correlation between tumor size at day 30 and the number of CD3+ T cells in the blood prior to tumor challenge (**Fig. 5I)**, suggesting that the enhanced persistence of CDK4/6i-treated CAR-T cells was a critical factor driving tumor control. Indeed, mice that received pre-treated CAR-T cells had

significantly higher numbers of tumor infiltrating CD4+ and CD8+ CAR-T cells 40 days post tumor inoculation (**Fig. 5J**). To validate our findings, we examined a second CAR-T cell model, using mouse T cells transduced with a CAR targeting HER2. Consistent with our previous observations, CDK4/6 inhibition induced Tcm formation in these CAR-T cells, leading to increased persistence *in vivo* (**Fig. S8H-N**). Together, these data demonstrate that *in vitro* treatment with CDK4/6i is a robust strategy to improve the phenotype, persistence and functional longevity of CAR-T cells.

CDK4/6 inhibition induces a T cell phenotype associated with favourable responses to immune checkpoint blockade in melanoma patients

CDK4/6 inhibitors have shown remarkable synergy with ICB in preclinical mouse models (4, 6-8), prompting investigation of this combination in clinical trials. However, the mechanisms underpinning the synergy of these therapies are incompletely understood. Given that recent studies highlight stem-like T cells in the tumor microenvironment as the key mediators of ICB responses (12, 16, 17), we hypothesised that CDK4/6i-mediated induction of T cell memory generates a more favourable T cell pool for immune checkpoint targeting, and will thus contribute to the efficacy of this combination in the clinic. To explore this, we analysed single cell RNA-seq data on the tumor infiltrating CD8+ T cell compartment from melanoma patients who either responded or did not respond to ICB (9). Utilising our *ex vivo* transcriptomic datasets on CD8+ TILs from mice treated with CDK4/6i, we generated a T cell-intrinsic CDK4/6i response signature and used AUCell to determine the enrichment of this signature in patient samples. Indeed, this CDK4/6i response signature was enriched in CD8+ TILs from patients who responded to ICB, accurately stratifying responders and non-responders at both a single cell and patient level (**Fig. 6A-D, S9A-B**). Together, this demonstrated that CDK4/6i

induces a T cell-intrinsic gene signature that is associated with favourable responses to ICB in patients.

To investigate this further, we collected and analysed serial blood samples from a melanoma patient over the course of their treatment, during which they received CDK4/6i in combination with a targeted MEK inhibitor, followed by subsequent treatment with combination PD-1 and CTLA-4 ICB (**Fig. 6E**). Notably, MEK inhibition did not alter T cell memory formation in primary mouse CD8+ T cells alone or in combination with CDK4/6i (**Fig. S10A**), suggesting this inhibitor does not confound the CDK4/6i-mediated phenotype. Using CITE-seq technology to evaluate the series of patient samples, we observed a time dependent increase in the frequency of the CD8+ T cell memory population following CDK4/6i+MEKi therapy, characterized by high expression of *SELL, IL7R* and *TCF7* (**Fig. 6F-I, S10B-D**), consistent with our preclinical analyses. The identity of these CD8+ clusters was further confirmed using SCENIC analysis (**Fig. S10E-F**). Importantly, upon ICB the patient achieved a clinical and immunological response in which this CD8+ memory cluster diminished, suggesting these cells mounted a response by differentiating into functional effectors, (**Fig. 6G-I**), which is consistent with the reported role of stem-like T cell subsets following ICB (12). Indeed, pseudotime analyses revealed a differentiation trajectory from memory-like populations through to effector cells, with CDK4/6i restraining CD8+ T cells early on this trajectory, and subsequent ICB therapy accelerating differentiation (**Fig. 6J-K, S10G-I**). TCR clonotype tracking across this time series also revealed that CDK4/6 inhibition increased the frequency of rare T cell clones, predominantly existing within the memory population, followed by amplification of these clones upon ICB **(Fig. 6L, S10J**). This suggested that ICB therapy liberates the use of a greater variety of T cell receptors in peripheral blood, consistent with published data (38). Collectively, these data provide evidence that

CDK4/6i may be utilised as priming tool to promote a more favourable T cell phenotype prior to the administration of ICB.

Discussion

In this study we demonstrated that pharmacological inhibition of CDK4/6 in cytotoxic T cells promotes the acquisition of a memory phenotype and significantly potentiates the long-term anti-tumor activity of these cells. While CDK4/6i are emerging as a promising new cancer therapeutic, currently the majority of clinical trials incorporating CDK4/6i are restricted to cancer types in which RB is functional, as CDK4/6i-induction of cell cycle arrest requires RB-mediated inactivation of E2F transcription factors (39, 40). Indeed, the clinical success of CDK4/6i is primarily attributed to the inhibition of tumor cell proliferation, coupled with immunomodulation that occurs downstream of tumor-intrinsic cytostasis (3, 4, 8). Unexpectedly however, CDK4/6i recently demonstrated efficacy in triple negative breast cancer (where RB loss is common), as part of a phase 2 trial where CDK4/6i was incorporated only as a tool to transiently arrest cycling of healthy cells to protect from chemotherapy-induced myelotoxicity (41). Such an example highlights the potential of CDK4/6i beyond cancers with targetable tumor-intrinsic pathways, but the mechanisms underpinning their clinical efficacy in this setting remain unclear. Here, our discovery that CDK4/6i directly influence cytotoxic T cell differentiation sheds new light on their clinical activity and substantially broadens the prospective utility of these therapeutic agents, which may be employed strategically as clinical tools to augment anti-tumor immunity in a wide array of cancer types.

Despite a well-established role for CDK4/6 in cellular proliferation, previous reports have indicated CDK4/6i does not compromise expansion of tumor-specific CD8+ T cells (4, 6). In contrast, through comprehensive analysis of the direct T cell-intrinsic effects of

CDK4/6i, we demonstrated clear CDK4/6i-mediated anti-proliferative activity in these cells. Importantly, while rapid clonal expansion of antigen specific lymphocytes is often an assumed requirement for optimal T cell immunity, here we demonstrate that controlled regulation of the cell cycle may in fact promote a more robust and long-term anti-tumor immune response. Interestingly, in addition to memory formation, we also observed enhanced T cell effector function in response to CDK4/6i, consistent with previous reports that CDK4/6i mediates the de-repression of NFAT (6). Using single cell RNA-seq, we demonstrated that this enhancement in both memory and effector functions occurred in transcriptionally distinct subsets. Thus CDK4/6i appears to serve a dual function in a heterogenous T cell population, enhancing acute cytotoxic effector function while simultaneously promoting differentiation of memory subsets that are capable of maintaining ongoing anti-tumor immunity.

Strategies to preserve or induce stem-like properties of T cells to promote sustained immunity is of significant clinical interest. Thus, the capacity for CDK4/6i to promote T cell memory makes them an attractive clinical tool, both as immunomodulatory agents in their own right and as adjuvants to T cell-directed immunotherapies. Indeed, in this study we demonstrated that short-term priming with CDK4/6i enhanced endogenous anti-tumor T cell immunity, significantly improved the persistence and efficacy of adoptively transferred CAR-T cells, and induced a T cell intrinsic gene signature that correlated with favourable responses to ICB in melanoma patients. CDK4/6 inhibitors have already demonstrated synergy with blockade of the PD-1-PD-L1 axis in a number of preclinical models (4, 6-8), through mechanisms that are incompletely understood. While the efficacy of this combination is largely attributed to tumor-intrinsic immunomodulatory activity of CDK4/6 inhibitors, our data suggests a novel mechanism whereby CDK4/6 inhibitors promote a more favourable T cell pool for immune checkpoint targeting. This

suggests that CDK4/6 inhibition may be used to prime the T cell pool prior to the application of ICB. Notably, as CDK4/6 inhibition also reduces expansion of CD8+ T cells, using CDK4/6 inhibition as a priming tool may be an optimal approach as is removes the potential complication of restricted T cell expansion following ICB administration, which is likely to occur if CDK4/6 inhibition is continuously co-administered. Certainly, our results, as well as recent reports, demonstrate that transient CDK4/6 inhibition is sufficient to promote anti-tumor immunity (42, 43), though further investigation is needed to inform the optimal scheduling of CDK4/6 inhibitors with immune-based therapies.

In summary, using integrated multi-omics approaches, we uncover a novel mechanism of action of CDK4/6i in promoting long-term anti-tumor immunity through the induction of T cell memory. We show that direct pharmacological inhibition of CDK4/6 in T cells redirects cell fate, and may be clinically leveraged to improve a variety of T-cell directed anti-tumor immunotherapies, including CAR-T cell therapy and immune checkpoint blockade. As CDK4/6i undergo investigation in hundreds of clinical trials, our findings have direct and widespread implications, with potential to inform current and future design of trial protocols incorporating CDK4/6i, particular in combination with immunotherapy, for the treatment of cancer.

Materials and methods

In vivo experiments

Animal work was conducted with approval from the Peter MacCallum Animal Experimentation Ethics Committee in accordance with the NHMRC Australian code for the use of animals for research purposes 8th edition (2013). C57BL/6 mice were purchased from Walter Eliza Hall Institute, and C57BL/6-Tg(OT-I) and NOD scid

gamma (NSG) mice were bred in-house. All tumors were injected subcutaneously on the right flank and mice were randomized and treated with 80mg/kg palbociclib daily by oral gavage, starting 3 days after tumor inoculation. Palbociclib (6-acetyl-8-cyclopentyl-5-methyl-2-((5-(piperazin-1-yl)pyridin-2-yl)amino)pyrido[2, 3-d]pyrimidin-7(8H)-one) was provided by Pfizer (New York, NY). Mice were treated for 7 days or 10 days for tumor harvests or survival studies, respectively. CD8+ (YTS 169.4) or CD4+ (GK1.5) depletion antibodies were administered at 250ug/mouse on day -1 & 0 and 150ug/mouse on day 4, 8 and weekly ongoing, with day 0 being the day of tumor inoculation. Tumor growth was measured either as volume (calculated as 0.5 x tumor length x (tumor width)^2) or size (tumor length x tumor width). For survival studies, mice were euthanized when tumors reached ethical endpoint of 1200mm^3 or no tumor could be seen 100 days after inoculation. For transfer studies (excluding LM-OVA), mice received 5x10^6 OT-I T cells or 10x10^6 LeY/Her2 CAR-T cells by intravenous administration. For LM-OVA studies, spleens were harvested from mice that had 30 days previously received 1x10^6 OT-I T cells intravenously, then splenocytes containing 5x10^5 transferred OT-I cells were re-transferred into recipient mice, simultaneously with 10^5 c.f.u. LM-OVA.

Ex vivo mouse sample processing for analysis and cell sorting

Tumors were digested with Collagenase IV (1.6 mg/mL) and DNase (2 U/mL) in DMEM for 45 minutes at 37 °C with agitation and filtered through a 70 μM filter. Spleens were processed through a 70 μM filter and lysed with red cell lysis buffer (150 mM NH_4Cl, 10 mM $KHCO_3$, 0.1 mM Na2-EDTA). Lymphocytes were isolated from blood using Histopaque Density Gradient Media (Sigma-Aldrich),

Flow cytometry and cell sorting

Mouse T cells were isolated from tumors by FAC sorting on CD3+TCRB+CD90.2+CD11b- cells, plus CD8a+ where indicated. Human T cells were

isolated from PBMCs by FAC sorting CD3+CD14-CD16-CD19- cells. Fixable yellow (Invitrogen, L34959) or PI was used to stain live/dead cells. Anti-mouse antibodies used were: CD3 (17A2), TCRB (H57-597), CD11b (M1/70), CD90.2 (53-2.1), CD8α (clone 53-6.7), CD4 (GK1.5), CD44 (clone IM7), CD62L (clone MEL14), CD45.1 (clone A20), CD45.2 (clone 104), KLRG1 (clone 2F1), CD127 (clone A7R34), TCF1 (C63D9), PD-1 (29F.1A12), TIM3 (B8.2C12), CD25 (clone PC61), CD69 (H1.2F3), Bim (Cat. No. 2819; Cell Signaling Technology), Bcl2 (3F11]), CD27 (LG.3A10), CXCR3 (CXCR3-173), IRF4 (IRF4.3E4), Ki67 (B56), EOMES (W17001), TBET (4B10), GZMB (GRB04), CD107a (1D4B), IFN-γ (XMG1.2), TNF-α (MP6-XT22), IL-2 (JES6-5H4). Anti-human antibodies used were: CD62L (SK11), CD45RA (HI100), CD45RO (UCHL1), CCR7 (G043H7), CD8 (RPA-T8), CD4 (OKT4), CD3 (OKT3), CD14 (HCD14), CD16 (3G8), CD19 (HIB19). Cell sorting was conducted using BD FACSAria™ Fusion and analysis was performed on BD LSR Fortessa™ X-20 or BD FACSymphony™ flow cytometer (BD Biosciences, North Ryde, New South Wales, Australia). Data was analysed using FlowJo, LLC software.

Cell lines

MC38-OVA and B16-OVA cell lines were cultured in DMEM containing 10%FBS and cultured at 37 °C in 10% CO_2. YOVAL1.1 were cultured in RPMI 1640 plus 20 mM HEPES containing 10% FBS, 1% GlutaMAX, 1 mM Sodium Pyruvate, 1 mM MEM Non-Essential Amino Acids and 0.1% 2-mercaptoethanol and cultured at 37 °C in 5% CO_2. Jurkats and OVCAR-3 were cultured in RPMI 1640 containing 10% FBS and 1% GlutaMAX.

Primary mouse T cell isolation and culture

Naïve $CD8^+$ T cells were isolated from C57BL/6 mouse spleens using EasySep™ Mouse $CD8^+$ T cell isolation kit (Stemcell Technologies) and labelled with division tracking dye,

Cell Trace Violet (CTV). Purity of T cell population was verified as >95% CD8+ CD4- by flow cytometry. Labelled $CD8^+$ T cells were stimulated with plate-bound αCD3 antibody, αCD28 antibody (clone 37.51) (2µg/mL; WEHI) and mIL-2 (100U/mL; WEHI). To obtain OT-I T cells, splenocytes from C57BL/6.OT-I transgenic mice were cultured with 10 nM SIINFEKL plus 100 IU/mL IL-2 for 72 hrs.All primary mouse cells were cultured in RPMI 1640 plus 20 mM HEPES containing 10% FBS, 1% GlutaMAX, 1 mM Sodium Pyruvate, 1 mM MEM Non-Essential Amino Acids, 0.1% 2-mercaptoethanol and Antibiotic-Antimitotic and cultured at 37 °C in 5% CO^2 and supplemented with 100IU/mL IL-2.

In vitro drug treatments and quantitative analysis

For all assays, primary mouse cells were activated for 72h followed by 24h treatment with 1uM palbociclib, unless otherwise specified. Absolute cell numbers were determined with the addition of $1x10^4$ calibration beads directly to cells prior to analysis. 0.2µM Propidium iodide (PI) was used to identify dead cells by exclusion. Ratio of live cells to beads was measured by flow cytometry to determine the absolute live cell number. Mean division number calculations were performed as previously described (44).

Single cell RNA-seq, CITE-seq and TCR-seq

Cells were 'stained' with Cell Hashing antibodies and CITE-seq antibodies as previously described (24, 25). 'Stained' and washed cells were counted, bought to ~1000 cells/uL and loaded onto the 10x Chromium instrument (10x Genomics, Pleasanton, CA, USA) to generate single-cell Gel Beads-in-Emulsion (GEMs) and capture/barcode cells. All samples followed the 10x Genomics Single Cell 3′ v3 according to the manufacturer's instructions up until the cDNA amplification step (10x Genomics, USA). Two picomoles of HTO and ADT additive oligonucleotides were spiked into the cDNA amplification PCR, and cDNA was amplified according to the 10x Single Cell 3′ v3 protocol (10x

Genomics, USA). Following cDNA amplification, 0.6X SPRI was used to separate the large cDNA fraction derived from cellular mRNAs (retained on beads) from the ADT- and Cell Hashtag (HTO)-containing fraction (in supernatant). The cDNA fraction was processed according to the 10x Genomics Single Cell 3′ v3 protocol to generate the transcriptome library; indexing was done using Chromium i7 Multiplex Kit. An additional 1.4X reaction volume of SPRI beads was added to the ADT/HTO fraction to bring the ratio up to 2.0X. The beads were washed with 80% ethanol, eluted in water, and an additional round of 2.0X SPRI performed to remove excess single-stranded oligonucleotides from cDNA amplification. After final elution, separate PCRs were set up to generate the CITE-seq ADT library (SI-PCR and RPI-x primers) and the HTO library (SI-PCR and D7xx_s). For 5' multi-omics including gene expression, TCR-sequencing and Hashing/CITE-Seq we used the 10x Single Cell V(D)J kit with Feature Barcoding (enabled for **5′** Gene Expression, TCR and Feature Barcoding for Cell Surface Protein) protocol following the manufacturer's instructions. TCR libraries were prepared using the 10x Chromium Single Cell V(D)J Enrichment Kit, Human (or Mouse) T Cell. 5' HTO/ADT (one library) was prepared using Chromium Single Cell 5' Feature Barcode Library Kit and indexed using the Chromium i7 Multiplex Kit N, Set A. Cell Ranger: Reads were aligned to the mm10 or hg19 reference genome, cellular barcodes were demultiplexed and unique molecular identifiers (UMI) and antibody capture (Antibody Derived Tags (ADT) and Hashtag oligos (HTO)) were quantified using 10x Genomics' Cell Ranger software (version 3.1.0). Cell barcodes containing RNA or antibody counts from cells from more than one sample (inter-sample doublets) were identified using Seurat's HTODemux function. Barcodes containing counts from more than one cell within the same sample (intra-sample doublets) were identified using the Scrublet python package (version 0.2.1) (45). A cutoff of more than one median absolute deviation (MAD)

value above the median Scrublet score was chosen. Cells identified as either type of doublet were removed from the analysis. Relative transcription factor activity in each cell was estimated using the Single-Cell Regulatory Network Inference And Clustering (SCENIC) method (46). Area-under-curve (AUC) scores for transcription factors were calculated based on inferred gene regulatory networks using the pyscenic python package (version 0.9.19). Gene expression and antibody count matrices were processed in R (version 3.6.1) using the Seurat R package (version 3.1.0) (47). RNA transcript counts for barcodes identified as cells by Cell Ranger were normalized using sctransform via Seurat's SCTransform function. The counts were first transformed with no covariates in the sctransform model then cell cycle phase scores were estimated using Seurat's CellCycleScoring function with mouse homologues of the cell cycle gene sets provided by Seurat. The sctransform normalization was then rerun with the cell cycle phase scores and the percent of raw RNA counts belonging to mitochondrial genes for each cell as variables to be regressed out in the model.ADT counts were normalized using centered log ratio (CLR) transformation.Principal component analysis (PCA) was then performed on the sctransform scaled RNA expression values for genes with residual variance in the sctransform model greater than 1.3. A shared-nearest-neighbours (SNN) network was calculated using the top 10 principal components using the FindNeighbors function with k-nearest neighbors set to 50 and cosine distance metric. The SNN network was then used to identify cell populations using the FindClusters function using the Louvain algorithm with resolution parameter 0.6. Uniform Manifold Approximation and Projection (UMAP) values were also calculated using the RunUMAP function with the top 10 principal components as input and parameters n.neighbors=50 and metric="cosine". Monocle3 was utilized for pseudotime analysis using default setting.

Whole genome CRISPR screen

Jurkat cells were transduced with mCherry-Cas9 using the (FUCas9Cherry) and cell sorted for cherry+ cells. mCherry-Cas9-expressing cells were then transduced with lentivirus containing a custom cloned genome-wide sgRNA library. Forty-eight hours after transduction, successfully transduced cells were selected with puromycin (1 mg/mL; Millipore) for one 5 days. After selection at the commencement of screen, a reference sample at time point zero, T0, was snap frozen and stored at -80C. For the screen, library-containing cells ($20x10^6$) were left untreated or treated with palbociclib (1uM) for three days. Cells were then stained with anti-human CD62L and FACS sorted on the lowest 10% percentile of CD62L expression. Cell were put back in culture for 5 days then this process repeated. Genomic DNA was extracted from screen and control samples using the DNeasy Blood & Tissue Kit (QIAGEN) according to the manufacturer's instructions. sgRNA sequences were then amplified for next generation sequencing by PCR using specific adaptor sequences. PCR products were pooled and cleaned up using the AMPure XP-PCR purification system (Beckman Coulter) according to the manufacturer's instructions. Samples were subsequently multiplexed and sequenced on the NextSeq 500 (Illumina) in-house at the Peter MacCallum Molecular Genomics Core Facility generating 75 base pair single-end reads. After demultiplexing with CASAVA (v1.8), adaptor sequences were removed using Cutadapt (v1.7), leaving the 20 base pair sgRNA sequence. Model-based Analysis of Genome-wide CRISPR/Cas9 Knockout, v0.5.9 (MAGeCK count and MAGeCK test) software was subsequently used to count the reads and perform sgRNA enrichment and statistical analyses between treated/sorted and control samples. Screen data were visualized using the R package, ggplot2, v2.2.1.

CRISPR/Cas9 knockout

Targeted gene deletion was performed by electroporation of Cas9 nuclease/synthetic guide RNA (Synthego) into target cells using Amaxa™ 4D-Nucleofector™ electroporation system (Lonza #AAF-1002B) as per manufacturers protocol. Primary mouse naïve CD8+ T cells were isolated and electroporated with Cas9/sgRNA using P3 Primary Cell 4D-Nucleofector X kit (Lonza #V4XP-3024) prior to activation with CD3/CD28. Jurkat cells were electroporated using SE Cell Line 4D-Nucleofector X Kit (Lonza #V4XC-1032).

LeY Chimeric Receptor Construction and Retroviral Vector Production

DNA encoding the anti-LeY chimeric receptor was generated with standard molecular biology techniques, using a scFv (48) generated from the humanized monoclonal antibody Hu3S193 (49). A truncated human CD34 was inserted as an extracellular domain in the current second-generation construct (anti-LeY scFv- CD3ζ-CD28) as previously described (35). Human CD34 was cloned from cDNA (50) and a truncated (extracellular domain) form was amplified using PCR and cloned into the LeY retroviral plasmid using appropriate restriction digest and ligations.

Human T cell isolation and CAR generation

Human peripheral blood mono- nuclear cells (PBMCs) were isolated from normal donor buffy coats and retrovirally transduced with an anti-human LeY chimeric receptor. PBMCs were stimulated with anti-human CD3 (OKT3 30 ng/ml, Ortho Biotech) and IL-2 (600 units/ ml), followed 3 and 4 days later by incubation with supernatant from the PG13 retroviral producer cell line on a Retronectin (Takara Bio, Otsu, Japan) matrix as per the manufacturer's instructions. Briefly, Retronectin was coated at a concentration of 6 mg/cm^2 in non-tissue culture six-well plates (Becton Dickinson, Franklin Lakes, NJ, USA) and incubated with 5 ml of retroviral supernatant. After 4 h, supernatant was removed and 2.5 x10^6 T cells in 5 ml of complete media added for 12 h. The transduced

T cells were expanded for up to 8 days in culture with IL-2 (600 units/ml) +/- 1uM palbociclib.

Mouse CAR-T cell generation

Splenocytes from C57BL/6 mice were activated with anti-CD3 (0.5 mg/mL) and anti-CD28 (0.5 mg/mL) in the presence of IL-2 (100 IU/mL) and IL-7 (2 ng/mL), followed by transduction with retrovirus encoding the CAR (comprised of an extracellular scFv specific for human HER2, a CD8 hinge region and transmembrane CD28 and CD3z domains) as previously described (51, 52).

Western blot

Cell pellets were lysed in 2% Sodium Dodecyl Sulfate (SDS) buffer (0.5 mM EDTA, 20 mM HEPES), boiled (95^{o}C, 5 mins), and quantified using the DCTM protein assay (Bio-Rad) as per manufacturer's protocol. Equal amounts of total protein in 5X SDS sample buffer (313 mM Tris HCl pH 6.8, 50% (v/v) Glycerol, 10% (v/v) β-mercaptoethanol, 10% (w/v) SDS, 0.05% (w/v) Bromophenol blue) were boiled (95^{o}C, 5 mins), loaded into precast gels (Bio-Rad) and resolved via SDS-PAGE with running buffer containing 25 mM Tris, 190 mM Glycine, 0.1% (w/v) SDS. Precision-plus protein^{TM} dual colour standard (Bio-Rad) was used as a molecular weight marker. Proteins were transferred onto methanol-activated PVDF membranes (Millipore) using the Trans-Blot Turbo semi-dry transfer system (Bio-Rad) for 20-30 minutes with tris-glycine transfer buffer (50 mM Tris, 40 mM Glycine, 0.375% (w/v) SDS, 20% (v/v) methanol). Membranes were blocked in 5% skim milk made up in TBS containing 0.1% Tween-20 (TBS-T) for 1 hour before probing with primary antibody overnight at 4^{o}C, followed by corresponding horse-radish peroxidase (HRP)-conjugated secondary antibody for one hour at RT. Immunoblots were washed thrice with TBS-T (10 mins each) after each antibody

incubation and proteins were detected using ECL western blotting substrate (Amersham GE Healthcare). Antibody details: Anti-RB1 (G3-245), Anti-α-Tubulin (DM1A).

3'RNA-seq

Cells were collected and washed once with ice-cold PBS prior to resuspension in TRIzol™ (ThermoFisher Scientific, 15596026). RNA was isolated using the Direct-zol RNA MiniPrep kit (Zymo Research, R2052) according to the manufacturer's instructions. Sequencing libraries were prepared using the QuantSeq 3'-mRNA Seq Library Prep Kit for Ilumina (Lexogen, Vienna, Austria). Libraries were sequenced on the Illumina NextSeq 500 to obtain 75 b.p. single-end reads. Sequencing files were demultiplexed using Bcl2fastq (v2.17.1.14) to generate FASTQ files on which QC was performed using FASTQC (v0.11.5). Sequencing reads were trimmed using cutadapt (v1.7) and aligned to the human reference genome (Hg19) using HISAT2 (v2.1.0). Read counting across genomic features was performed using FeatureCounts (from the Subread package, v1.5.0) prior to differential gene expression analysis using Voom/Limma. Gene set enrichment analyses were performed using GSEA software (Broad Institute) and barcode plots were plotted using ReplotGSEA.R (part of the Rtoolbox R package).

ATAC-seq

Cells were washed once in ice-cold PBS and lysed in ATAC lysis buffer (0.1% Tween-20, 0.1% NP-40, 3mM MgCl2, 10mM NaCl, 10mM Tris HCl pH 7.4). Tagmentation was performed with Tn5 transposase and 2x TD Buffer (Nextera DNA Library Prep Kit, Ilumina) for 30 minutes at 37°C. Tagmented DNA was purified using a MinElute colum (Qiagen, 28004) and amplified for 12 cycles using 2x KAPA HiFi HotStart ReadyMix (Kapa Biosystems, KK2602). The amplified libraries were purified using MinElute columns (Qiagen) and sequenced on an Ilumina NextSeq 500 with 75 bp single-end reads. Library QC and quantification was performed using D1000 high-sensitivity screen tape

with 4200 TapeStation Instrument (Agilent Technologies) and size selected for between 200 bp and 700 bp using a Pippin Prep system (Sage Science).

ChIP-seq

T cells were cross-linked with 2% formaldehyde for 10 minutes at room temperature and quenched with addition of 1.25M glycine. Cells were washed twice (5% BSA, 800g, 5min, 4˚C) and lysed in nuclear extraction buffer three times. Nuclei resuspended in sonication buffer and sonicated with a Covaris S220 sonicator (peak power, 105; duty factor, 20; cycle/burst, 200; duration, 600s). Samples were cleared by centrifugation at 12,000g for 20 min, and one volume of dilution buffer was added to cleared chromatin. 1% chromatin was taken as input. Immunoprecipitation was performed overnight at 4°C with rotation with 2µg anti-H3K27ac antibody (Abcam). Immunoprecipitated samples were captured by incubation with 20µl Dynabeads Protein G (Life Technologies) blocked with 0.1% BSA for 2 hours. Beads were then washed twice each with wash buffer 1, wash buffer 2, wash buffer 3 and TE buffer. DNA was eluted with 100µL elution buffer for 30 minutes twice and reverse crosslinked. DNA product was purified using Zymo ChIP DNA Clean and Concentrator Kit. Libraries were generated using the NEBNext Ultra II DNA library prep kit from NEB. For sequencing, libraries were pooled and sequenced on a NextSeq 500 (Illumina) and 15 to 20 million single-end 50 bp reads were generated per sample.

ChIP-seq and ATAC-seq analysis

Bcl2fastq v2.17.1.14 was used for demultiplexing. The Fastq files generated by sequencing were aligned to the mouse reference genome (GRCm38/mm10) using bowtie (v2.2.3). Samtools (v1.8) was used for manipulation of SAM and BAM files, after which MACS (v2.0.10) was used for peak calling. Browser viewable TDF files were generated using IGVTools (v2.3.72) and ChIP-Seq tracks were visualized using IGV (v2.3.55).

Differentially accessible regions were quantitative analyzed using Rsubread featureCounts on merged reference bed file containing all peaks identified across treatment conditions after which the limma-voom package was used for statistical analysis of differentially accessible regions. Subsequently, = HOMER (v4.8.3) was used for motif analysis on MACS2 peak summits using FindMotifGenome.pl for differentially accessible regions using all summits as a background set with the -bg option. ChIP-seq and ATAC-seq peaks were annotated to genes using the AnnotatePeaks.pl function after which R was used for visualization.

Statistical analysis

Statistical tests were performed using GraphPad PRISM. All error bars show ±SEM. Significance was determined as *p < 0.05, **p < 0.01, ***p < 0.001, ****p < 0.0001.

Acknowledgements: We thank A/Prof Shahneen Sandhu and the Peter MacCallum Cancer Centre Melanoma Biomarker Project for provision of patient samples, and the Peter MacCallum Cancer Centre Translation Research Laboratory (Carleen Cullinane, Susan Jackson, Kerry Warren and Jeannette Schreuders) for technical support with animal work. This work was supported by the National Health and Medical Research Council: project grants (to G.A.M. & K.E.S.-1100189; J.O.-1139626; R.J.W.; E.D.H.-1140187, 1165591), program grants (to R.J.W.-454569; P.J.N.) and fellowships (to S.J.V.-EL1,GNT1178339; C.J.K.-ECF; R.J.W-SPRF; E.D.H.-CDF2,159488), Peter Mac Foundation grant (to S.J.V); Cancer Council Victoria project grants (to G.A.M.; R.J.W.); National Brest Cancer Foundation – grants (to J.O.-IIRS-18-151) and fellowships (to P.A.B.- ECF-17-005); Netherlands Organization for Scientific Research (to S.J.V, Rubicon Fellowship, NWO, 019.161LW.017); PeterMac Postgraduate Scholarship (to E.J.L.); Melbourne University Research Scholarship (to E.J.L.-58616); Cancer Therapeutics CRC (CTx) PhD Top Up Scholarship (to E.J.L.); The Kids' Cancer Project (to R.W.J. and S.J.V.); Leukemia & Lymphoma Society grant (to E.D.H.-6552-18); Plan Cancer 2014-2019, l'Institut Servier and Fondation Nuovo-Soldati (to D.M.) and Pfizer Oncology.

Author contributions: Initiated study- S.J.V., C.J.K., K.E.S., Conceptualized research- E.J.L., C.J.K., S.J.V. Directed the project - C.J.K., S.J.V. Designed methodology - E.J.L., I.A.P., J.O., C.J.K., S.J.V. Performed bioinformatics - M.Z., S.J.V. Performed experiments - E.J.L., I.K., K.M.R., L.M., D.M., J.J.Z., L.K., L.L., P.D., I.A.P., C.J.K., S.J.V. Analysed data - E.J.L., I.K., M.Z., I.T., C.J.K., S.J.V. Validated findings - E.J.L., I.K., K.M.R., P.D., I.A.P., C.J.K., S.J.V. Provided resources – L.M., N.M.H., P.A.B., P.J.N., E.D.H., G.A.M., I.A.P., R.W.J., J.O., K.E.S. Acquired patient samples – K.E.S. Wrote the manuscript - E.J.L., C.J.K., S.J.V. Edited the manuscript - R.W.J., J.O.

Prepared Figures - E.J.L., C.J.K., S.J.V. Acquired funding - G.A.M., R.W.J., J.O., K.E.S., S.J.V. All authors discussed the results and commented on the manuscript.

Conflict of Interest Statement

The Johnstone laboratory receives research support from Roche, BMS, Astra-Zeneca and MecRx. RWJ is a scientific consultant and shareholder in MecRx. The McArthur laboratory receives non-financial support from Pfizer Oncology for supply of palbociclib.

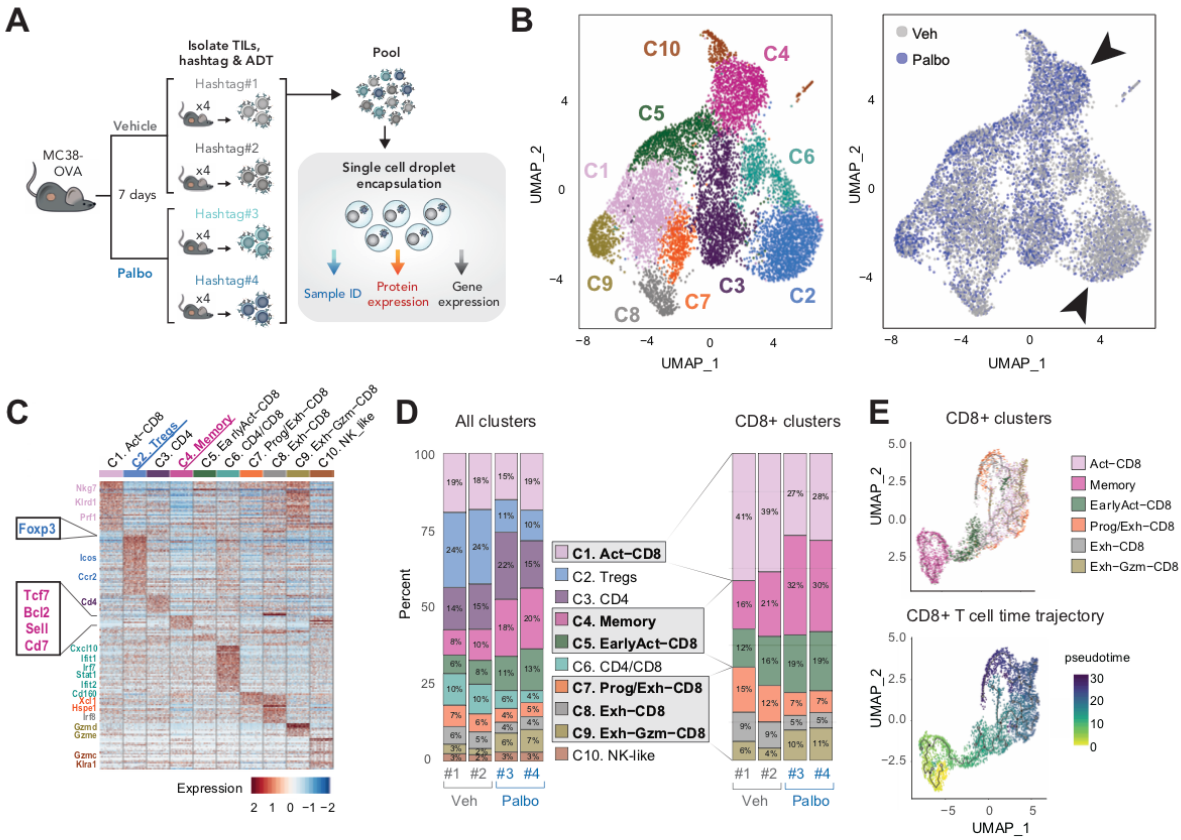
A
Isolate TILs, hashtag & ADT
Pool
Vehicle
MC38-OVA
7 days
Palbo
Hashtag#1
Hashtag#2
Hashtag#3
Hashtag#4
x4
Single cell droplet encapsulation
Sample ID
Protein expression
Gene expression
B
C10
C4
C5
C6
C1
C9
C8
C7
C3
C2
UMAP_1
UMAP_2
Veh
Palbo
C
C1. Act-CD8
C2. Tregs
C3. CD4
C4. Memory
C5. EarlyAct-CD8
C6. CD4/CD8
C7. Prog/Exh-CD8
C8. Exh-CD8
C9. Exh-Gzm-CD8
C10. NK-like
Foxp3
Tcf7
Bcl2
Sell
Cd7
Icos
Ccr2
Cd4
Expression
D
All clusters
CD8+ clusters
Percent
Veh
Palbo
E
CD8+ clusters
Act-CD8
Memory
EarlyAct-CD8
Prog/Exh-CD8
Exh-CD8
Exh-Gzm-CD8
CD8+ T cell time trajectory
pseudotime
F
Pseudotime
>20
13-20
<13
G
Gene expression - CD8+ TIL
Tcf7
Sell
Prf1
Gzmb
Il7r
Value
Pseudotime
H
MC38-OVA CD8+ TILs
Vehicle
Palbo
Tcm
12.6
25.2
84.9
72.5
CD62L
CD44
Tcm (% of CD8+ TIL)
***
I
Vehicle
Palbo
Tumor volume (mm³)
Therapy stopped
palbo
Days
J
Percent survival
21/22
9/22
***
K
Last day of therapy
ns

Figure 1 - Emergence of intratumoral memory-like CD8+ T cells in response to CDK4/6 inhibition. (A) Schematic of CITE-seq experimental set up. (B) Intratumoral T cell clusters based on RNA expression. (C) Cluster gene expression and annotation. (D) Frequency of all clusters (left panel) and CD8+ clusters (right panel). (E) CD8+ clusters (top panel) and CD8+ pseudotime trajectory (bottom panel). (F) Distribution of CD8+ clusters over pseudotime. (G) Gene expression in CD8+ clusters over pseudotime. (H) Flow cytometry on CD8+ T cells from MC38-OVA tumors, Mann-Whitney test, pooled data from 3 independent experiments. (I-J) MC38-OVA tumor growth and survival, n=22 pooled from 3 independent experiments, log rank (Mantel-Cox) test. (K) Size of tumors on the day therapy was stopped. Tcm – central memory T cells. Error bars show +/- SEM, ***$p<0.001$.

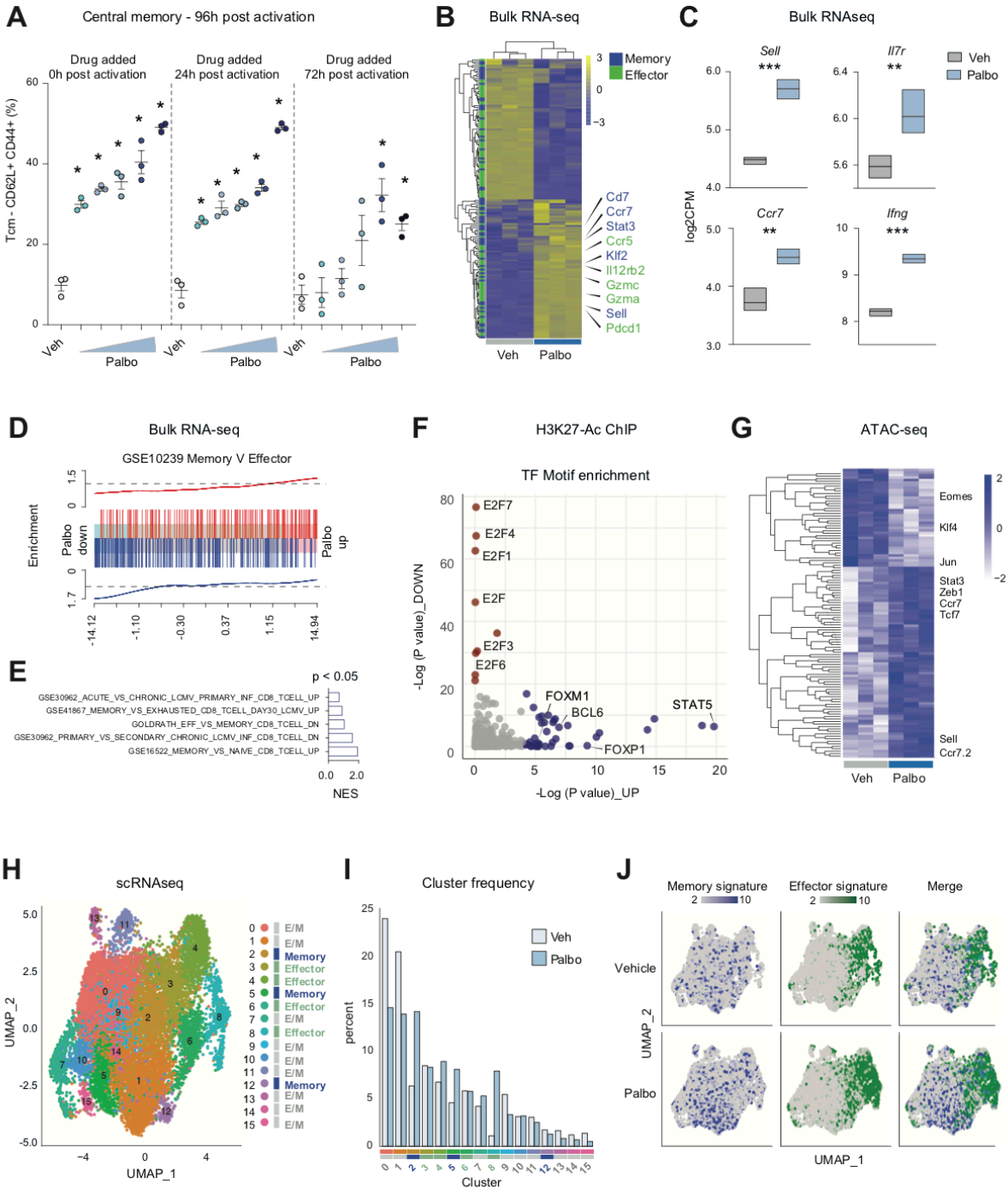
A
Central memory - 96h post activation
Drug added 0h post activation
Drug added 24h post activation
Drug added 72h post activation
Tcm - CD62L+ CD44+ (%)
Veh
Palbo
B
Bulk RNA-seq
Memory
Effector
Cd7
Ccr7
Stat3
Ccr5
Klf2
Il12rb2
Gzmc
Gzma
Sell
Pdcd1
C
Bulk RNAseq
Sell
Il7r
Ccr7
Ifng
log2CPM
Veh
Palbo
D
Bulk RNA-seq
GSE10239 Memory V Effector
Enrichment
Palbo down
Palbo up
E
p < 0.05
GSE30962_ACUTE_VS_CHRONIC_LCMV_PRIMARY_INF_CD8_TCELL_UP
GSE41867_MEMORY_VS_EXHAUSTED_CD8_TCELL_DAY30_LCMV_UP
GOLDRATH_EFF_VS_MEMORY_CD8_TCELL_DN
GSE30962_PRIMARY_VS_SECONDARY_CHRONIC_LCMV_INF_CD8_TCELL_DN
GSE16522_MEMORY_VS_NAIVE_CD8_TCELL_UP
NES
F
H3K27-Ac ChIP
TF Motif enrichment
E2F7
E2F4
E2F1
E2F
E2F3
E2F6
FOXM1
BCL6
FOXP1
STAT5
-Log (P value)_DOWN
-Log (P value)_UP
G
ATAC-seq
Eomes
Klf4
Jun
Stat3
Zeb1
Ccr7
Tcf7
Sell
Ccr7.2
Veh
Palbo
H
scRNAseq
UMAP_1
UMAP_2
E/M
Memory
Effector
I
Cluster frequency
Veh
Palbo
percent
Cluster
J
Memory signature
Effector signature
Merge
Vehicle
Palbo
UMAP_1
UMAP_2

Figure 2 – CDK4/6i-mediated acquisition of CD8+ T cell memory is cell-intrinsic. (A) Tcm (CD44+CD62L+) frequency of *in vitro* CD8+ T cells analysed by flow cytometry 96h after activation, following treatment with palbociclib (125nM-2μM; 2-fold serial dilution) added at indicated time points post activation. (B-E) Bulk RNA-seq, (F) ChIP-seq, (G) ATAC-seq and (H-J) single cell RNA-seq on *in vitro* activated OT-I following 24h of 1μM palbociclib treatment added 72h post-activation. (B-C) Differential gene expression. (D-E) Gene set enrichment analysis. Error bars show +/- SEM, *p<0.05, p****>0.0001.

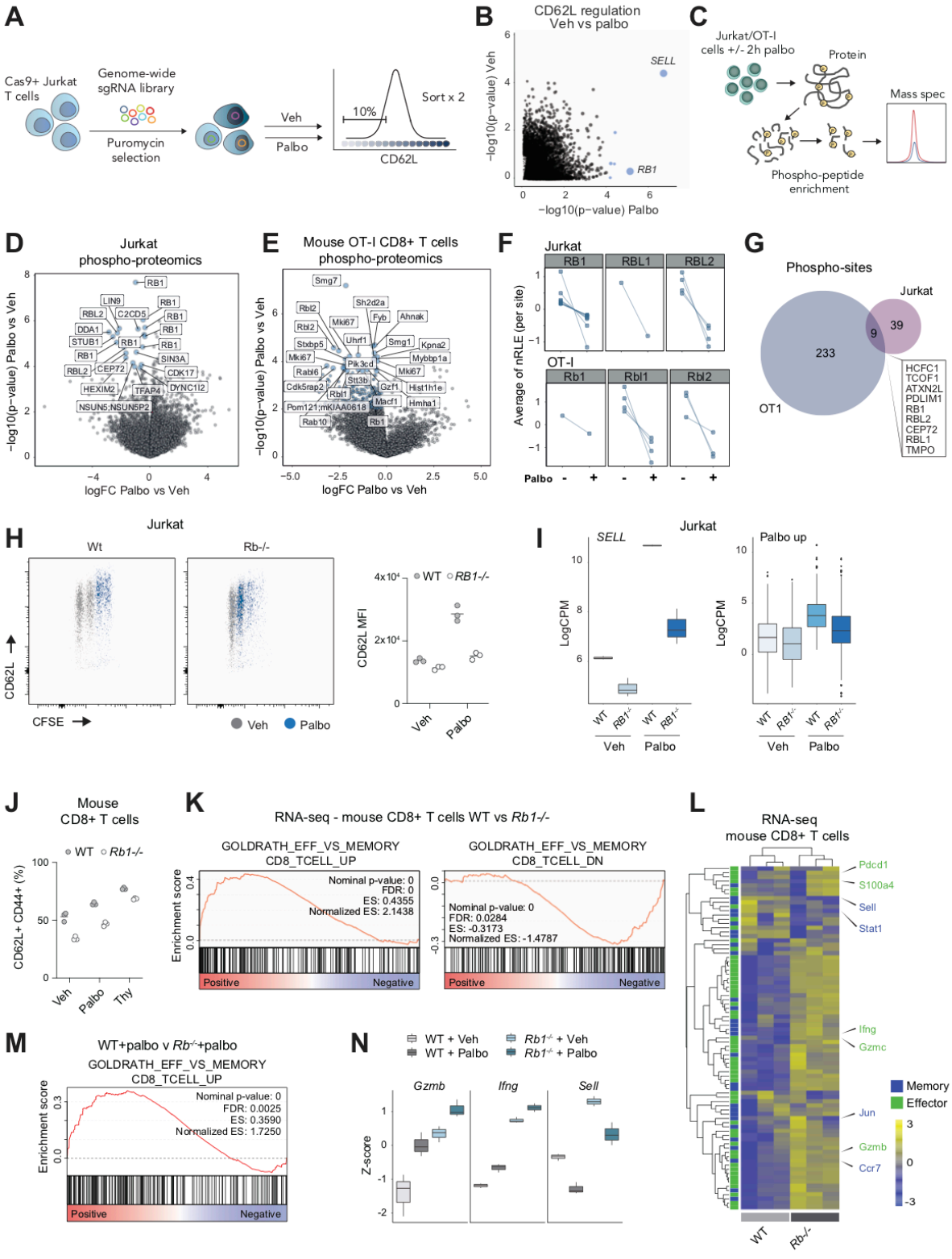
A
Cas9+ Jurkat T cells
Genome-wide sgRNA library
Puromycin selection
Veh
Palbo
10%
Sort x 2
CD62L
B
CD62L regulation Veh vs palbo
SELL
RB1
−log10(p−value) Veh
−log10(p−value) Palbo
C
Jurkat/OT-I cells +/- 2h palbo
Protein
Mass spec
Phospho-peptide enrichment
D
Jurkat phospho-proteomics
−log10(p−value) Palbo vs Veh
logFC Palbo vs Veh
E
Mouse OT-I CD8+ T cells phospho-proteomics
F
Jurkat
RB1
RBL1
RBL2
OT-I
Rb1
Rbl1
Rbl2
Average of nRLE (per site)
Palbo
G
Phospho-sites
Jurkat
OT1
233
9
39
HCFC1
TCOF1
ATXN2L
PDLIM1
RB1
RBL2
CEP72
RBL1
TMPO
H
Jurkat
Wt
Rb-/-
CD62L
CFSE
Veh
Palbo
CD62L MFI
WT
RB1-/-
I
Jurkat
SELL
Palbo up
LogCPM
J
Mouse CD8+ T cells
CD62L+ CD44+ (%)
Thy
K
RNA-seq - mouse CD8+ T cells WT vs Rb1-/-
GOLDRATH_EFF_VS_MEMORY CD8_TCELL_UP
Nominal p-value: 0
FDR: 0
ES: 0.4355
Normalized ES: 2.1438
GOLDRATH_EFF_VS_MEMORY CD8_TCELL_DN
Nominal p-value: 0
FDR: 0.0284
ES: -0.3173
Normalized ES: -1.4787
Enrichment score
Positive
Negative
L
RNA-seq mouse CD8+ T cells
Pdcd1
S100a4
Sell
Stat1
Ifng
Gzmc
Jun
Gzmb
Ccr7
Memory
Effector
M
WT+palbo v Rb-/-+palbo
GOLDRATH_EFF_VS_MEMORY CD8_TCELL_UP
Nominal p-value: 0
FDR: 0.0025
ES: 0.3590
Normalized ES: 1.7250
N
WT + Veh
WT + Palbo
Rb1-/- + Veh
Rb1-/- + Palbo
Gzmb
Ifng
Sell
Z-score

Figure 3 - CDK4/6 inhibition promotes memory formation in an RB-dependent manner. (A) Experimental set up of CRISPR/Cas9 screen in Jurkat cells. (B) Enriched sgRNA in untreated and palbociclib-treated Jurkat cells. (C) Experimental set up of phospho-proteomics. (D-F) Significantly regulated phospho-peptides in Jurkat cells and mouse OT-I T cells following 2 h treatment with 1uM palbociclib, OT-I cells treated 3 days post *in vitro* activation. (G) Overlapping significantly regulated phospho-peptides from (D-F). (H) Flow cytometry and (I) RNA-seq on Jurkat T cells following 72h palbociclib treatment. (J) Flow cytometry and (K-N) bulk RNA-seq on *in vitro*-activated CD8+ mouse cells treated for 24h with 1μM palbociclib, cells were treated 48h after activation, Cas9/*Rb1* sgRNA was electroporated into naïve cells immediately prior to activation.

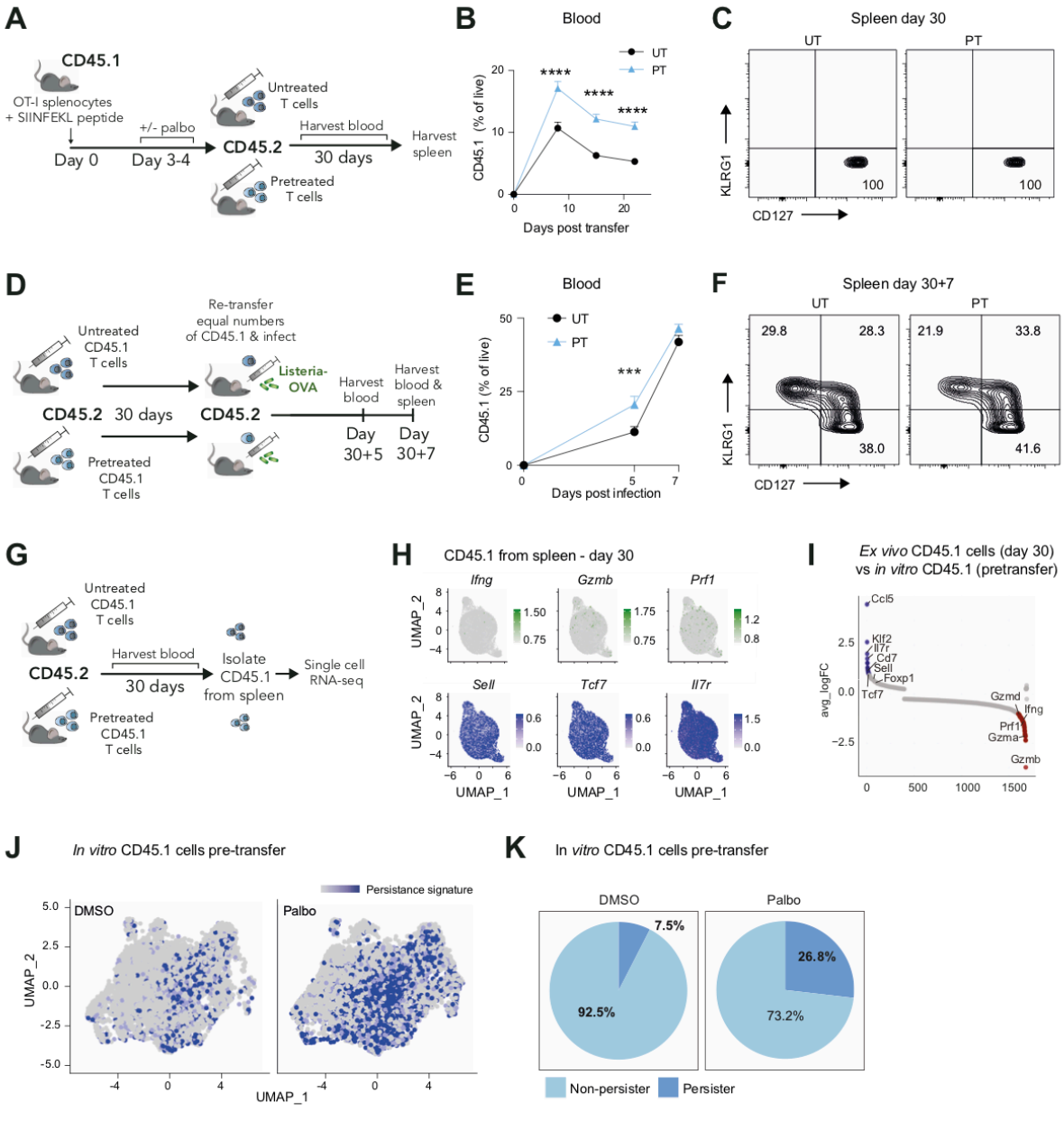
A
CD45.1
OT-I splenocytes
+ SIINFEKL peptide
Day 0
+/- palbo
Day 3-4
Untreated
T cells
CD45.2
Pretreated
T cells
Harvest blood
30 days
Harvest
spleen
B
Blood
UT
PT
CD45.1 (% of live)
Days post transfer
****
C
Spleen day 30
UT
PT
KLRG1
CD127
100
D
Untreated
CD45.1
T cells
Re-transfer
equal numbers
of CD45.1 & infect
Listeria-
OVA
CD45.2
30 days
Harvest
blood
Harvest
blood &
spleen
Day
30+5
Day
30+7
Pretreated
CD45.1
T cells
E
Blood
***
Days post infection
F
Spleen day 30+7
29.8
28.3
21.9
33.8
38.0
41.6
G
Isolate
CD45.1
from spleen
Single cell
RNA-seq
H
CD45.1 from spleen - day 30
Ifng
Gzmb
Prf1
Sell
Tcf7
Il7r
UMAP_1
UMAP_2
I
Ex vivo CD45.1 cells (day 30)
vs in vitro CD45.1 (pretransfer)
Ccl5
Klf2
Il7r
Cd7
Sell
Foxp1
Tcf7
Gzmd
Ifng
Prf1
Gzma
Gzmb
avg_logFC
J
In vitro CD45.1 cells pre-transfer
Persistance signature
DMSO
Palbo
K
In vitro CD45.1 cells pre-transfer
DMSO
Palbo
7.5%
92.5%
26.8%
73.2%
Non-persister
Persister

Figure 4 – CDK4/6 preconditioning enhances the persistence of functional memory CD8+ T cells. (A) Experimental set up to track *in vivo* persistence of CD8+ OT-I cells following *in vitro* palbociclib exposure. (B) Frequency of OT-I cells in blood following adoptive transfer. (C) Phenotype of OT-I cells in spleen 30 days after transfer. (D) Experimental set up to determine recall response of persisting OT-I cells. (E) Expansion of OT-I cells in blood following LM-OVA infection. (F) Phenotype of OT-I cells in spleens 7 days post infection. (G) Experimental set up for single cell RNA-seq on persisting cells. (H) Gene expression of persisting cells. (I) Persistence gene signature determined by genes enriched in *ex vivo* persisting cells versus *in vitro* cells pre-transfer. (J-K) Persistence signature in pre-transfer cell populations. (B, E) Multiple t-tests. (B-F) Data pooled from 2 independent experiments, n=10, error bars show +/- SEM, ***p<0.001, ****p<0.0001.

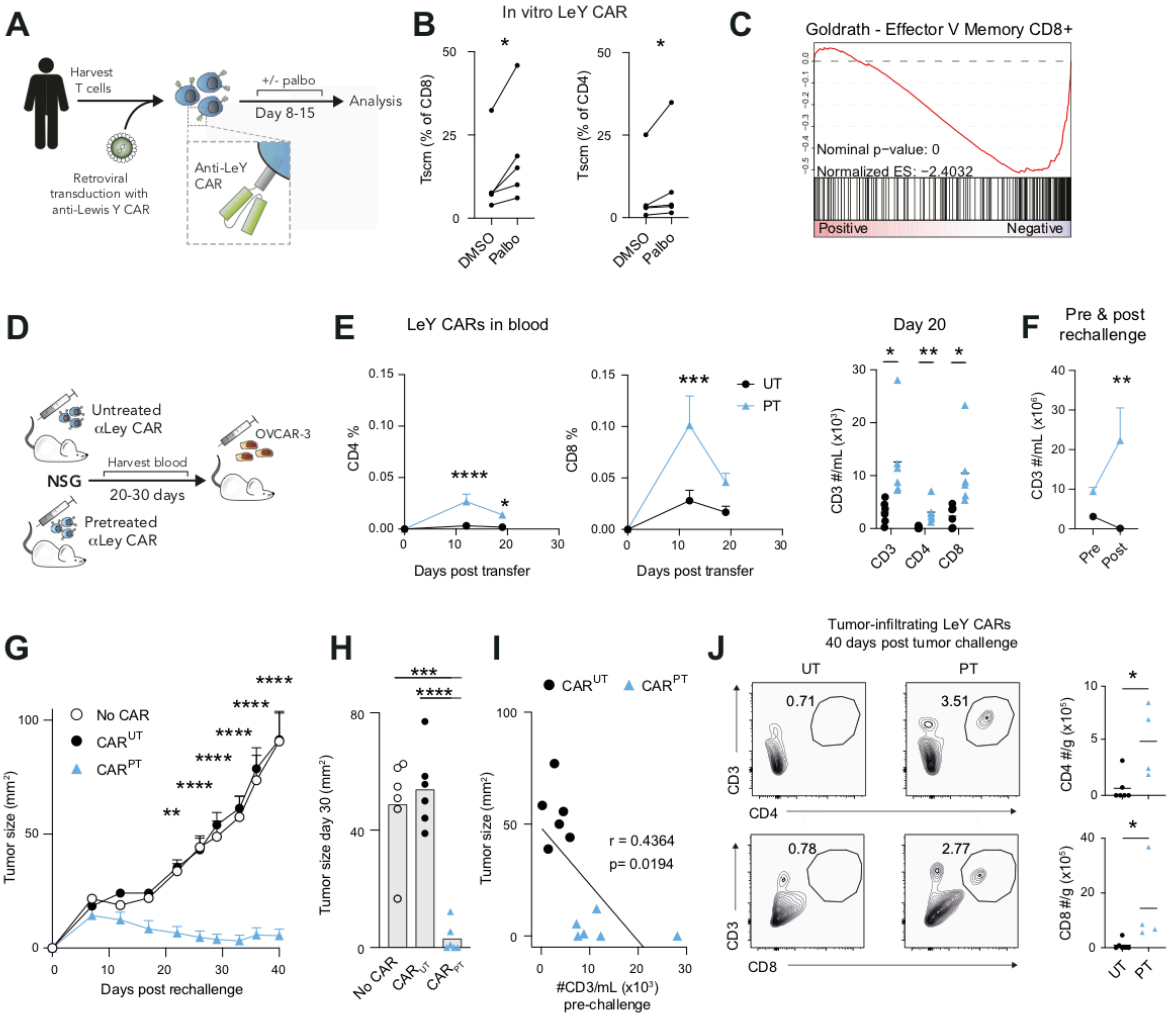
A
Harvest T cells
Retroviral transduction with anti-Lewis Y CAR
+/- palbo
Day 8-15
Analysis
Anti-LeY CAR
B
In vitro LeY CAR
Tscm (% of CD8)
Tscm (% of CD4)
DMSO
Palbo
C
Goldrath - Effector V Memory CD8+
Nominal p-value: 0
Normalized ES: -2.4032
Positive
Negative
D
Untreated αLey CAR
Pretreated αLey CAR
NSG
Harvest blood
20-30 days
OVCAR-3
E
LeY CARs in blood
CD4 %
CD8 %
Days post transfer
UT
PT
Day 20
CD3 #/mL (x10³)
CD3
CD4
CD8
F
Pre & post rechallenge
CD3 #/mL (x10⁶)
Pre
Post
G
No CAR
CAR^UT
CAR^PT
Tumor size (mm²)
Days post rechallenge
H
Tumor size day 30 (mm²)
No CAR
CAR_UT
CAR_PT
I
CAR^UT
CAR^PT
Tumor size (mm²)
r = 0.4364
p= 0.0194
#CD3/mL (x10³) pre-challenge
J
Tumor-infiltrating LeY CARs
40 days post tumor challenge
UT
PT
0.71
3.51
0.78
2.77
CD3
CD4
CD8
CD4 #/g (x10⁵)
CD8 #/g (x10⁵)

Figure 5. CDK4/6i pre-conditioning enhances persistence and efficacy of CAR-T cells. (A) Generation of human LeY CAR-T cells. (B) Flow cytometry and (C) RNA-seq of LeY CAR-T cells expanded *in vitro* with/without palbociclib, paired t-test. (D) Experimental set up to examine persistence and function of LeY CAR-T cells *in vivo* following *in vitro* exposure to palbociclib. (E) Frequency and number of LeY CAR-T cells in blood overtime and 20 days post transfer, 2way ANOVA Sidak's multiple comparisons test, and (F) expansion one week post challenge with OVCAR-3 tumors, multiple t-tests, n=5-6. (G) Growth of OVCAR-3 tumors implanted in mice 30 days after receiving untreated or pre-treated LeY CARs, multiple t-tests, n=5-6. (H) Tumor size 30 days post inoculation. (I) Tumor size at day 30 post tumor inoculation versus the total number of CD3 cells in the blood prior to inoculation. (J) Tumor-infiltrating T cells 40 days post tumor inoculation. Error bars show +/- SEM, *p<0.05, **p<0.01, ****p<0.0001.

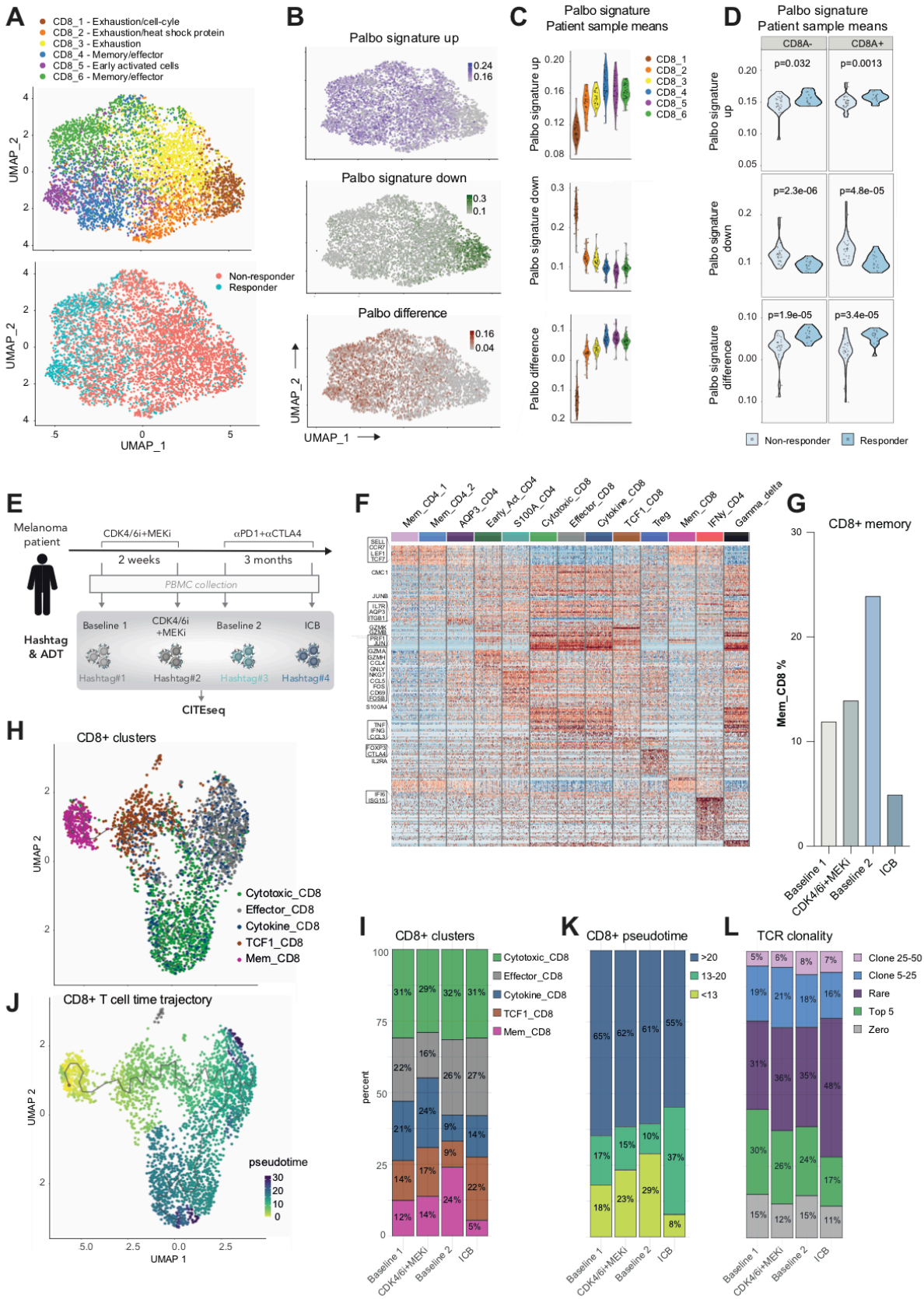
A
CD8_1 - Exhaustion/cell-cyle
CD8_2 - Exhaustion/heat shock protein
CD8_3 - Exhaustion
CD8_4 - Memory/effector
CD8_5 - Early activated cells
CD8_6 - Memory/effector
UMAP_2
UMAP_1
Non-responder
Responder
B
Palbo signature up
Palbo signature down
Palbo difference
C
Palbo signature
Patient sample means
Palbo signature up
Palbo signature down
Palbo difference
D
Palbo signature
Patient sample means
CD8A-
CD8A+
p=0.032
p=0.0013
p=2.3e-06
p=4.8e-05
p=1.9e-05
p=3.4e-05
Non-responder
Responder
E
Melanoma patient
CDK4/6i+MEKi
αPD1+αCTLA4
2 weeks
3 months
PBMC collection
Baseline 1
CDK4/6i +MEKi
Baseline 2
ICB
Hashtag & ADT
Hashtag#1
Hashtag#2
Hashtag#3
Hashtag#4
CITEseq
F
Mem_CD4_1
Mem_CD4_2
AQP3_CD4
Early_Act_CD4
S100A_CD4
Cytotoxic_CD8
Effector_CD8
Cytokine_CD8
TCF1_CD8
Treg
Mem_CD8
IFNγ_CD4
Gamma_delta
G
CD8+ memory
Mem_CD8 %
Baseline 1
CDK4/6i+MEKi
Baseline 2
ICB
H
CD8+ clusters
Cytotoxic_CD8
Effector_CD8
Cytokine_CD8
TCF1_CD8
Mem_CD8
UMAP 2
I
CD8+ clusters
percent
Cytotoxic_CD8
Effector_CD8
Cytokine_CD8
TCF1_CD8
Mem_CD8
K
CD8+ pseudotime
>20
13-20
<13
L
TCR clonality
Clone 25-50
Clone 5-25
Rare
Top 5
Zero
J
CD8+ T cell time trajectory
pseudotime
UMAP 1
UMAP 2

Figure 6. CDK4/6 inhibition induces an ICB-responsive T cell phenotype. (A) Single cell RNA-seq data on CD8+ TILs from melanoma patients evaluated by Sade-Feldmann et al.(9) (B) A T cell-intrinsic palbociclib response gene signature was derived from ex vivo RNA-seq analysis of CD8+ TILs from palbociclib-treated MC38-OVA tumors (Fig. S2A-C), and AUCell was used to apply this signature to patients samples in (A). (C-D) Palbociclib up/down AUCell signature scores for (C) each cluster in (A), and (D) all pooled clusters in (A) segregated on responding/non-responding patients to ICB. (E) Time course of patient samples collected for CITE-seq. (F, H) Cluster annotation. (G, I) Frequencies as a percent of CD8+ clusters. (J-K) CD8+ T cell pseudotime trajectory. (L) TCR clonal frequencies.

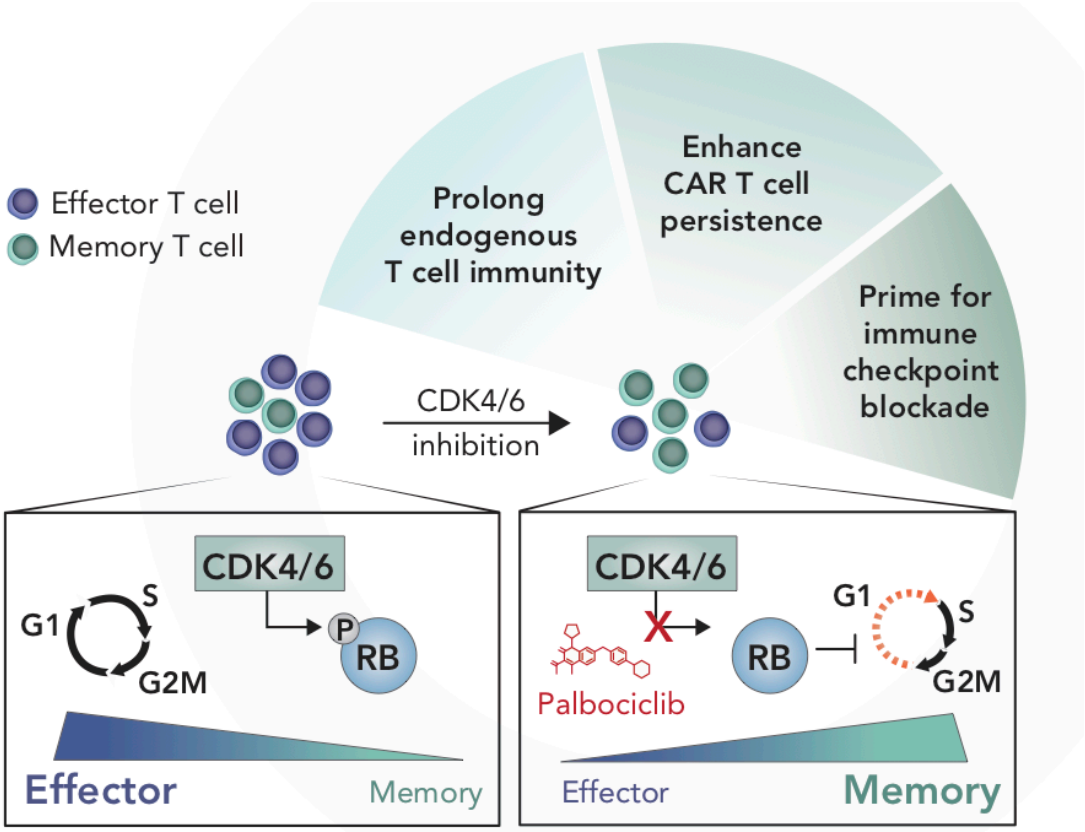

Figure 7. Model demonstrating CD8+ T cell-intrinsic immune-potentiating effects of CDK4/6 inhibitors. CDK4/6 inhibition promotes RB-mediated induction of T cell memory, which enhances the efficacy of endogenous T cell immunity, CAR-T cells and immune checkpoint blockade.

References

1. Hanahan D & Weinberg RA (2011) Hallmarks of cancer: the next generation. *Cell* 144(5):646-674.
2. Garcia-Bates TM, *et al.* (2016) Enhanced Cytotoxic CD8 T Cell Priming Using Dendritic Cell-Expressing Human Papillomavirus-16 E6/E7-p16INK4 Fusion Protein with Sequenced Anti-Programmed Death-1. *J Immunol* 196(6):2870-2878.
3. Sherr CJ, Beach D, & Shapiro GI (2016) Targeting CDK4 and CDK6: From Discovery to Therapy. *Cancer Discov* 6(4):353-367.
4. Goel S, *et al.* (2017) CDK4/6 inhibition triggers anti-tumour immunity. *Nature* 548(7668):471-475.
5. Jin X, *et al.* (2019) Phosphorylated RB Promotes Cancer Immunity by Inhibiting NF-kappaB Activation and PD-L1 Expression. *Mol Cell* 73(1):22-35 e26.
6. Deng J, *et al.* (2018) CDK4/6 Inhibition Augments Antitumor Immunity by Enhancing T-cell Activation. *Cancer Discov* 8(2):216-233.
7. Zhang J, *et al.* (2018) Cyclin D-CDK4 kinase destabilizes PD-L1 via cullin 3-SPOP to control cancer immune surveillance. *Nature* 553(7686):91-95.
8. Schaer DA, *et al.* (2018) The CDK4/6 Inhibitor Abemaciclib Induces a T Cell Inflamed Tumor Microenvironment and Enhances the Efficacy of PD-L1 Checkpoint Blockade. *Cell Rep* 22(11):2978-2994.
9. Sade-Feldman M, *et al.* (2019) Defining T Cell States Associated with Response to Checkpoint Immunotherapy in Melanoma. *Cell* 176(1-2):404.
10. Li H, *et al.* (2019) Dysfunctional CD8 T Cells Form a Proliferative, Dynamically Regulated Compartment within Human Melanoma. *Cell* 176(4):775-789 e718.

11. Brummelman J*, et al.* (2018) High-dimensional single cell analysis identifies stem-like cytotoxic CD8(+) T cells infiltrating human tumors. *J Exp Med* 215(10):2520-2535.
12. Miller BC*, et al.* (2019) Subsets of exhausted CD8(+) T cells differentially mediate tumor control and respond to checkpoint blockade. *Nat Immunol* 20(3):326-336.
13. Gattinoni L, Speiser DE, Lichterfeld M, & Bonini C (2017) T memory stem cells in health and disease. *Nat Med* 23(1):18-27.
14. Hurton LV*, et al.* (2016) Tethered IL-15 augments antitumor activity and promotes a stem-cell memory subset in tumor-specific T cells. *Proc Natl Acad Sci U S A* 113(48):E7788-E7797.
15. Jansen CS*, et al.* (2019) An intra-tumoral niche maintains and differentiates stem-like CD8 T cells. *Nature* 576(7787):465-470.
16. Siddiqui I*, et al.* (2019) Intratumoral Tcf1(+)PD-1(+)CD8(+) T Cells with Stem-like Properties Promote Tumor Control in Response to Vaccination and Checkpoint Blockade Immunotherapy. *Immunity* 50(1):195-211 e110.
17. Gide TN*, et al.* (2019) Distinct Immune Cell Populations Define Response to Anti-PD-1 Monotherapy and Anti-PD-1/Anti-CTLA-4 Combined Therapy. *Cancer Cell* 35(2):238-255 e236.
18. Garfall AL*, et al.* (2019) T-cell phenotypes associated with effective CAR T-cell therapy in postinduction vs relapsed multiple myeloma. *Blood Adv* 3(19):2812-2815.
19. Blaeschke F*, et al.* (2018) Induction of a central memory and stem cell memory phenotype in functionally active CD4(+) and CD8(+) CAR T cells produced in an automated good manufacturing practice system for the treatment of CD19(+) acute lymphoblastic leukemia. *Cancer Immunol Immunother* 67(7):1053-1066.

20. Alizadeh D*, et al.* (2019) IL15 Enhances CAR-T Cell Antitumor Activity by Reducing mTORC1 Activity and Preserving Their Stem Cell Memory Phenotype. *Cancer Immunol Res* 7(5):759-772.
21. Chen Y, Zander R, Khatun A, Schauder DM, & Cui W (2018) Transcriptional and Epigenetic Regulation of Effector and Memory CD8 T Cell Differentiation. *Front Immunol* 9:2826.
22. Rodriguez RM*, et al.* (2017) Epigenetic Networks Regulate the Transcriptional Program in Memory and Terminally Differentiated CD8+ T Cells. *J Immunol* 198(2):937-949.
23. Yu B*, et al.* (2017) Erratum: Epigenetic landscapes reveal transcription factors that regulate CD8(+) T cell differentiation. *Nat Immunol* 18(6):705.
24. Stoeckius M*, et al.* (2017) Simultaneous epitope and transcriptome measurement in single cells. *Nat Methods* 14(9):865-868.
25. Stoeckius M*, et al.* (2018) Cell Hashing with barcoded antibodies enables multiplexing and doublet detection for single cell genomics. *Genome Biol* 19(1):224.
26. Wherry EJ*, et al.* (2007) Molecular signature of CD8+ T cell exhaustion during chronic viral infection. *Immunity* 27(4):670-684.
27. Tough DF, Rioja I, Modis LK, & Prinjha RK (2020) Epigenetic Regulation of T Cell Memory: Recalling Therapeutic Implications. *Trends Immunol* 41(1):29-45.
28. Kretschmer L*, et al.* (2020) Differential expansion of T central memory precursor and effector subsets is regulated by division speed. *Nat Commun* 11(1):113.
29. Lin WW*, et al.* (2016) CD8(+) T Lymphocyte Self-Renewal during Effector Cell Determination. *Cell Rep* 17(7):1773-1782.

30. Singh A, *et al.* (2010) Regulation of memory CD8 T-cell differentiation by cyclin-dependent kinase inhibitor p27Kip1. *Mol Cell Biol* 30(21):5145-5159.
31. Kaech SM & Cui W (2012) Transcriptional control of effector and memory CD8+ T cell differentiation. *Nat Rev Immunol* 12(11):749-761.
32. Martin MD & Badovinac VP (2018) Defining Memory CD8 T Cell. *Front Immunol* 9:2692.
33. Plumlee CR, Sheridan BS, Cicek BB, & Lefrancois L (2013) Environmental cues dictate the fate of individual CD8+ T cells responding to infection. *Immunity* 39(2):347-356.
34. MacKay M, *et al.* (2020) The therapeutic landscape for cells engineered with chimeric antigen receptors. *Nat Biotechnol* 38(2):233-244.
35. Westwood JA, *et al.* (2005) Adoptive transfer of T cells modified with a humanized chimeric receptor gene inhibits growth of Lewis-Y-expressing tumors in mice. *Proc Natl Acad Sci U S A* 102(52):19051-19056.
36. Biasco L, *et al.* (2015) In vivo tracking of T cells in humans unveils decade-long survival and activity of genetically modified T memory stem cells. *Sci Transl Med* 7(273):273ra213.
37. Fraietta JA, *et al.* (2018) Determinants of response and resistance to CD19 chimeric antigen receptor (CAR) T cell therapy of chronic lymphocytic leukemia. *Nat Med* 24(5):563-571.
38. Yost KE, *et al.* (2019) Clonal replacement of tumor-specific T cells following PD-1 blockade. *Nat Med* 25(8):1251-1259.
39. Kato J, Matsushime H, Hiebert SW, Ewen ME, & Sherr CJ (1993) Direct binding of cyclin D to the retinoblastoma gene product (pRb) and pRb phosphorylation by the cyclin D-dependent kinase CDK4. *Genes Dev* 7(3):331-342.

40. Dyson N (1998) The regulation of E2F by pRB-family proteins. *Genes Dev* 12(15):2245-2262.
41. Tan AR*, et al.* (2019) Trilaciclib plus chemotherapy versus chemotherapy alone in patients with metastatic triple-negative breast cancer: a multicentre, randomised, open-label, phase 2 trial. *Lancet Oncol* 20(11):1587-1601.
42. Lai AY*, et al.* (2020) CDK4/6 inhibition enhances antitumor efficacy of chemotherapy and immune checkpoint inhibitor combinations in preclinical models and enhances T-cell activation in patients with SCLC receiving chemotherapy. *J Immunother Cancer* 8(2).
43. Roberts PJL, A. Y.; Sorrentino, J. A.; Malik, R. K. (2018) Trilaciclib (G1T28), a CDK4/6 inhibitor, enhances the efficacy of combination chemotherapy and immune checkpoint inhibitor treatment in preclinical models. *Ann Oncol* 29.
44. Hawkins ED*, et al.* (2007) Measuring lymphocyte proliferation, survival and differentiation using CFSE time-series data. *Nat Protoc* 2(9):2057-2067.
45. Wolock SL, Lopez R, & Klein AM (2019) Scrublet: Computational Identification of Cell Doublets in Single-Cell Transcriptomic Data. *Cell Syst* 8(4):281-291 e289.
46. Aibar S*, et al.* (2017) SCENIC: single-cell regulatory network inference and clustering. *Nat Methods* 14(11):1083-1086.
47. Stuart T*, et al.* (2019) Comprehensive Integration of Single-Cell Data. *Cell* 177(7):1888-1902 e1821.
48. Power BE*, et al.* (2001) Construction, expression and characterisation of a single-chain diabody derived from a humanised anti-Lewis Y cancer targeting antibody using a heat-inducible bacterial secretion vector. *Cancer Immunol Immunother* 50(5):241-250.

49. Scott AM, *et al.* (2000) Construction, production, and characterization of humanized anti-Lewis Y monoclonal antibody 3S193 for targeted immunotherapy of solid tumors. *Cancer Res* 60(12):3254-3261.
50. Norell H, *et al.* (2010) CD34-based enrichment of genetically engineered human T cells for clinical use results in dramatically enhanced tumor targeting. *Cancer Immunol Immunother* 59(6):851-862.
51. Haynes NM, *et al.* (2002) Single-chain antigen recognition receptors that costimulate potent rejection of established experimental tumors. *Blood* 100(9):3155-3163.
52. Wang LX, *et al.* (2010) Tumor ablation by gene-modified T cells in the absence of autoimmunity. *Cancer Res* 70(23):9591-9598.

4. Supplementary data

Supplementary data included for publication with this work begins on the following page.

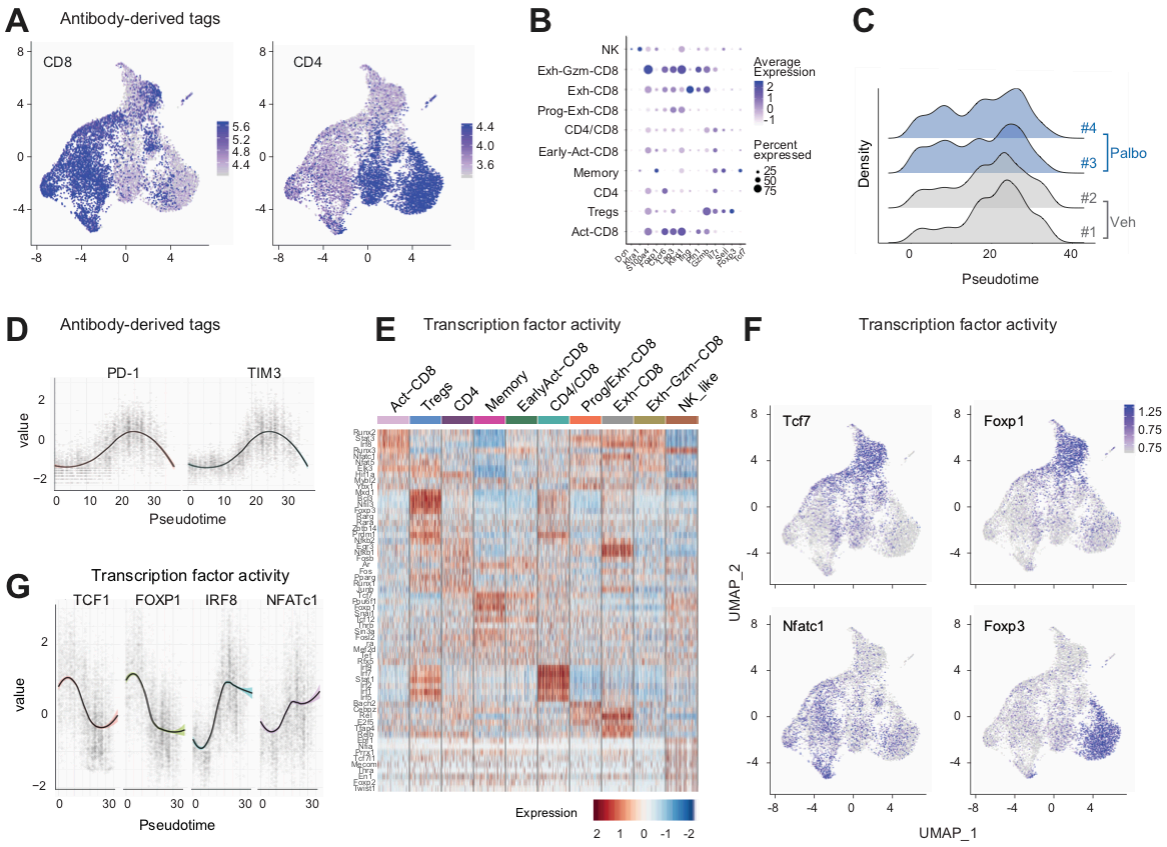
A
Antibody-derived tags
CD8
CD4
B
NK
Exh-Gzm-CD8
Exh-CD8
Prog-Exh-CD8
CD4/CD8
Early-Act-CD8
Memory
CD4
Tregs
Act-CD8
Average Expression
Percent expressed
C
Density
#4
#3
#2
#1
Palbo
Veh
Pseudotime
D
Antibody-derived tags
PD-1
TIM3
value
Pseudotime
E
Transcription factor activity
Act-CD8
Tregs
CD4
Memory
EarlyAct-CD8
CD4/CD8
Prog/Exh-CD8
Exh-CD8
Exh-Gzm-CD8
NK_like
Expression
F
Transcription factor activity
Tcf7
Foxp1
Nfatc1
Foxp3
UMAP_2
UMAP_1
G
Transcription factor activity
TCF1
FOXP1
IRF8
NFATc1
value
Pseudotime
H
Goldrath effector
Goldrath memory
value
Pseudotime
I
Goldrath memory
Goldrath effector
UMAP_2
UMAP_1
J
Goldrath memory vs effector
Memory signature
Effector signature
Act-CD8
Memory
EarlyAct-CD8
Prog/Exh-CD8
Exh-CD8
Exh-Gzm-CD8

Figure S1. (A) CD4 and CD8 antibody-derived tags. (B) Expression of key genes across clusters. (C) Distribution of CD8+ clusters over pseudotime. (D) Anti-body derived tags in CD8+ clusters over pseudotime. (E-G) Inferred transcription factor activity of all clusters (E-F) and CD8+ clusters (G). (H-J) Published Goldrath effector and memory signatures in CD8+ clusters.

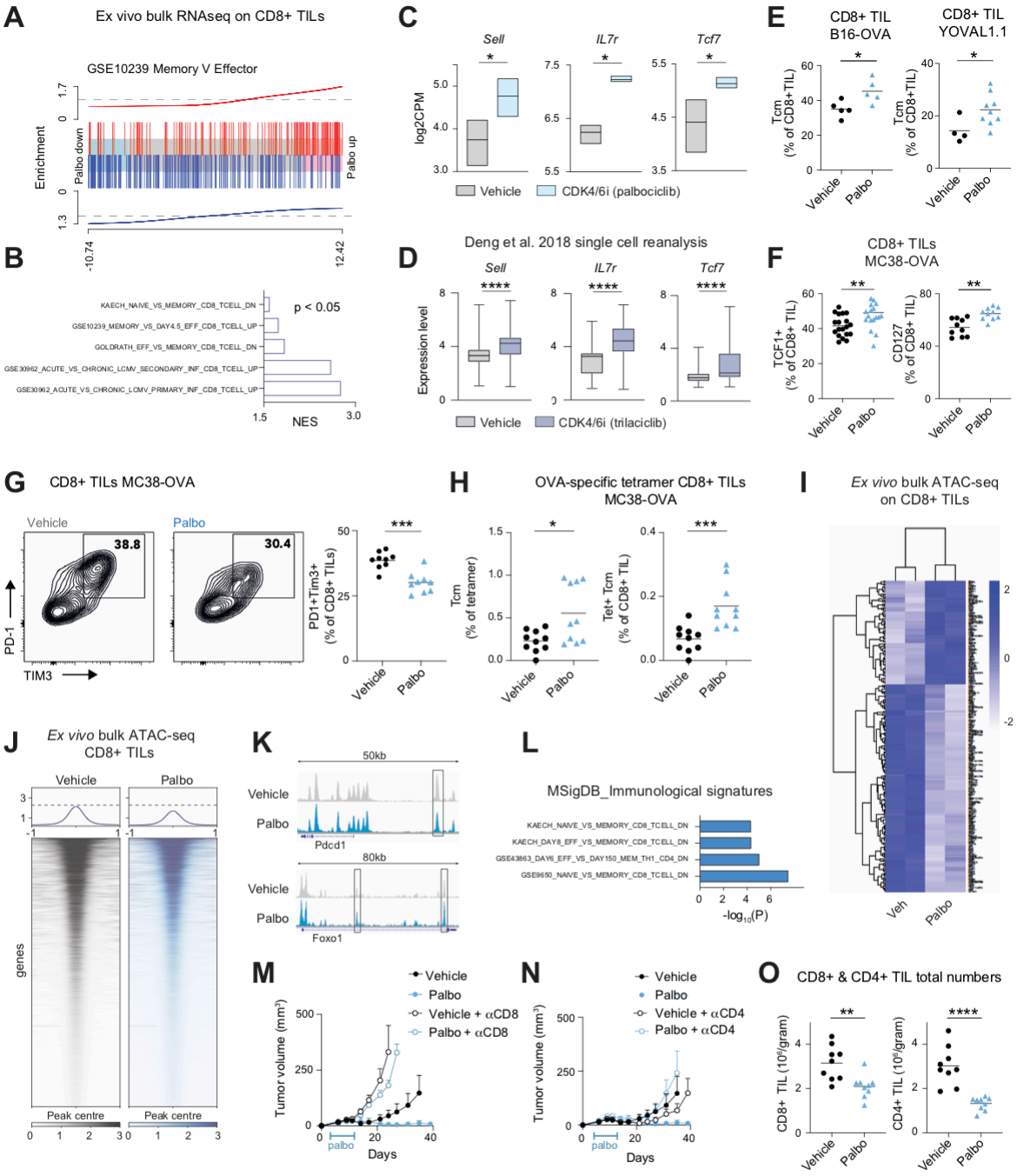
A
Ex vivo bulk RNAseq on CD8+ TILs
GSE10239 Memory V Effector
Enrichment
Palbo down
Palbo up
-10.74
12.42
B
p < 0.05
KAECH_NAIVE_VS_MEMORY_CD8_TCELL_DN
GSE10239_MEMORY_VS_DAY4.5_EFF_CD8_TCELL_UP
GOLDRATH_EFF_VS_MEMORY_CD8_TCELL_DN
GSE30962_ACUTE_VS_CHRONIC_LCMV_SECONDARY_INF_CD8_TCELL_UP
GSE30962_ACUTE_VS_CHRONIC_LCMV_PRIMARY_INF_CD8_TCELL_UP
NES
C
Sell
IL7r
Tcf7
log2CPM
Vehicle
CDK4/6i (palbociclib)
D
Deng et al. 2018 single cell reanalysis
Expression level
Vehicle
CDK4/6i (trilaciclib)
E
CD8+ TIL B16-OVA
CD8+ TIL YOVAL1.1
Tcm (% of CD8+TIL)
Vehicle
Palbo
F
CD8+ TILs MC38-OVA
TCF1+ (% of CD8+ TIL)
CD127 (% of CD8+ TIL)
G
CD8+ TILs MC38-OVA
Vehicle
Palbo
38.8
30.4
PD-1
TIM3
PD1+Tim3+ (% of CD8+ TILs)
H
OVA-specific tetramer CD8+ TILs MC38-OVA
Tcm (% of tetramer)
Tet+ Tcm (% of CD8+ TIL)
I
Ex vivo bulk ATAC-seq on CD8+ TILs
Veh
Palbo
J
Ex vivo bulk ATAC-seq CD8+ TILs
Vehicle
Palbo
genes
Peak centre
K
50kb
Pdcd1
80kb
Foxo1
L
MSigDB_Immunological signatures
KAECH_NAIVE_VS_MEMORY_CD8_TCELL_DN
KAECH_DAY8_EFF_VS_MEMORY_CD8_TCELL_DN
GSE43863_DAY6_EFF_VS_DAY150_MEM_TH1_CD4_DN
GSE9650_NAIVE_VS_MEMORY_CD8_TCELL_DN
-log10(P)
M
Vehicle
Palbo
Vehicle + αCD8
Palbo + αCD8
Tumor volume (mm3)
palbo
Days
N
Vehicle
Palbo
Vehicle + αCD4
Palbo + αCD4
Tumor volume (mm3)
palbo
Days
O
CD8+ & CD4+ TIL total numbers
CD8+ TIL (10^6/gram)
CD4+ TIL (10^6/gram)
Vehicle
Palbo

Figure S2. (A-C) *Ex vivo* bulk RNA-seq on CD8+ TILs from MC38-OVA tumors. (D) Re-analysis of published data (6) on CD3+ cells isolated from trilaciclib-treated *Kras*$^{LSL\text{-}G12D}$*Trp53*$^{fl/fl}$ lung tumors. (E-H) Flow cytometry on CD8+ TILs from (E) B16-OVA or YOVAL1.1(53), or (F-H) MC38-OVA mouse tumor models following one week of palbociclib treatment. (I-L) *Ex vivo* bulk ATACseq on CD8+ TILs from MC38-OVA tumors. (M-N) MC38-OVA tumor growth, n=6, in response to palbociclib treatment with CD8 or CD4 depletion antibodies. (J) Total number of CD8+ or CD4+ TILs in MC38-OVA tumors following one week of palbociclib treatment. All statistics use Mann-Whitney test. Error bars show +/- SEM, *p<0.05, **p<0.01, ***p<0.001, ****p<0.0001.

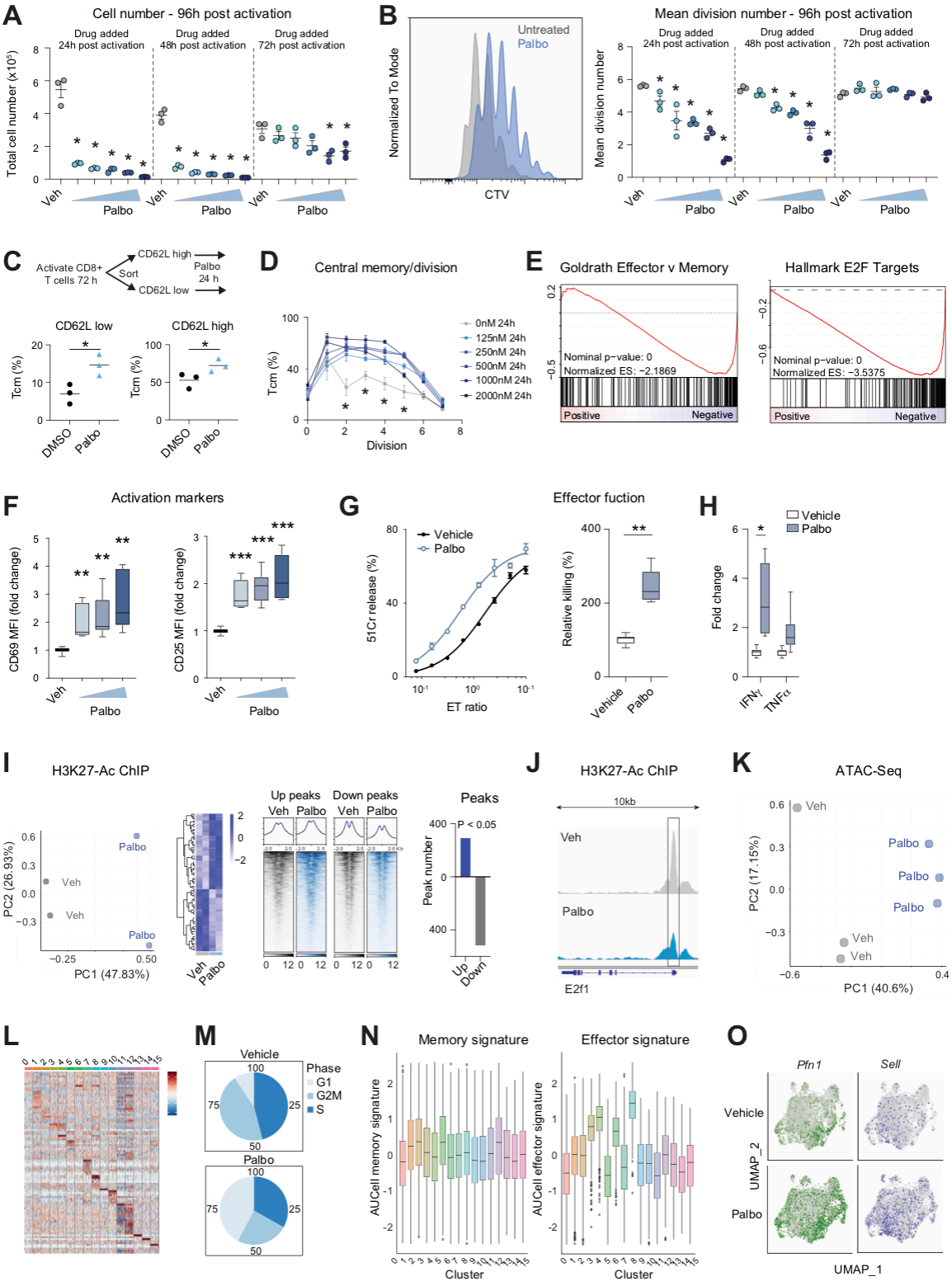
A
Cell number - 96h post activation
Drug added 24h post activation
Drug added 48h post activation
Drug added 72h post activation
Total cell number (x10⁵)
Veh
Palbo
B
Untreated
Palbo
Normalized To Mode
CTV
Mean division number - 96h post activation
Mean division number
C
Activate CD8+ T cells 72 h
Sort
CD62L high
CD62L low
Palbo 24 h
CD62L low
CD62L high
Tcm (%)
DMSO
Palbo
D
Central memory/division
Tcm (%)
Division
0nM 24h
125nM 24h
250nM 24h
500nM 24h
1000nM 24h
2000nM 24h
E
Goldrath Effector v Memory
Hallmark E2F Targets
Nominal p-value: 0
Normalized ES: −2.1869
Normalized ES: −3.5375
Positive
Negative
F
Activation markers
CD69 MFI (fold change)
CD25 MFI (fold change)
G
Effector fuction
Vehicle
Palbo
51Cr release (%)
ET ratio
Relative killing (%)
H
Fold change
IFNγ
TNFα
I
H3K27-Ac ChIP
PC2 (26.93%)
PC1 (47.83%)
Up peaks
Down peaks
Peaks
P < 0.05
Peak number
Up
Down
J
H3K27-Ac ChIP
10kb
E2f1
K
ATAC-Seq
PC2 (17.15%)
PC1 (40.6%)
L
M
Vehicle
Palbo
Phase
G1
G2M
S
N
Memory signature
Effector signature
AUCell memory signature
AUCell effector signature
Cluster
O
Pfn1
Sell
UMAP_2
UMAP_1

Figure S3. (A-B) *In vitro*-activated CD8 T cells analysed 96hr post activation, following treatment with palbociclib (125nM-2uM; 2 fold serial dilution) added at indicated timepoints post activation. (C) CD8+ T cells were activated for 72 h and then sorted based on high or low expression of CD62L. Sorted cells were then treated with 1uM palbociclib for 24 h and analysed by flow cytometry. (D) Tcm percentage in each division shown in (B). (E) Bulk RNA-seq and (F) flow cytometry on *in vitro*-activated OT-I following 24h of 1uM palbociclib treatment added 72h post-activation. (G) *In vitro* killing of MC38-OVA by OT-I cells pre-treated for 24h with 1uM palbociclib. (H) Cytokines in supernatants in co-cultures from (G). (I-J) H3K27Ac ChIP on *in vitro* activated OT-I following 6h of 1uM palbociclib treatment added 72h post-activation. (K) ATAC-seq on *in vitro* activated OT-I following 24h of 1uM palbociclib treatment added 72h post-activation. (L-O) Single cell RNA-seq on *in vitro* activated OT-I following 24h of 1uM palbociclib treatment added 72h post-activation.

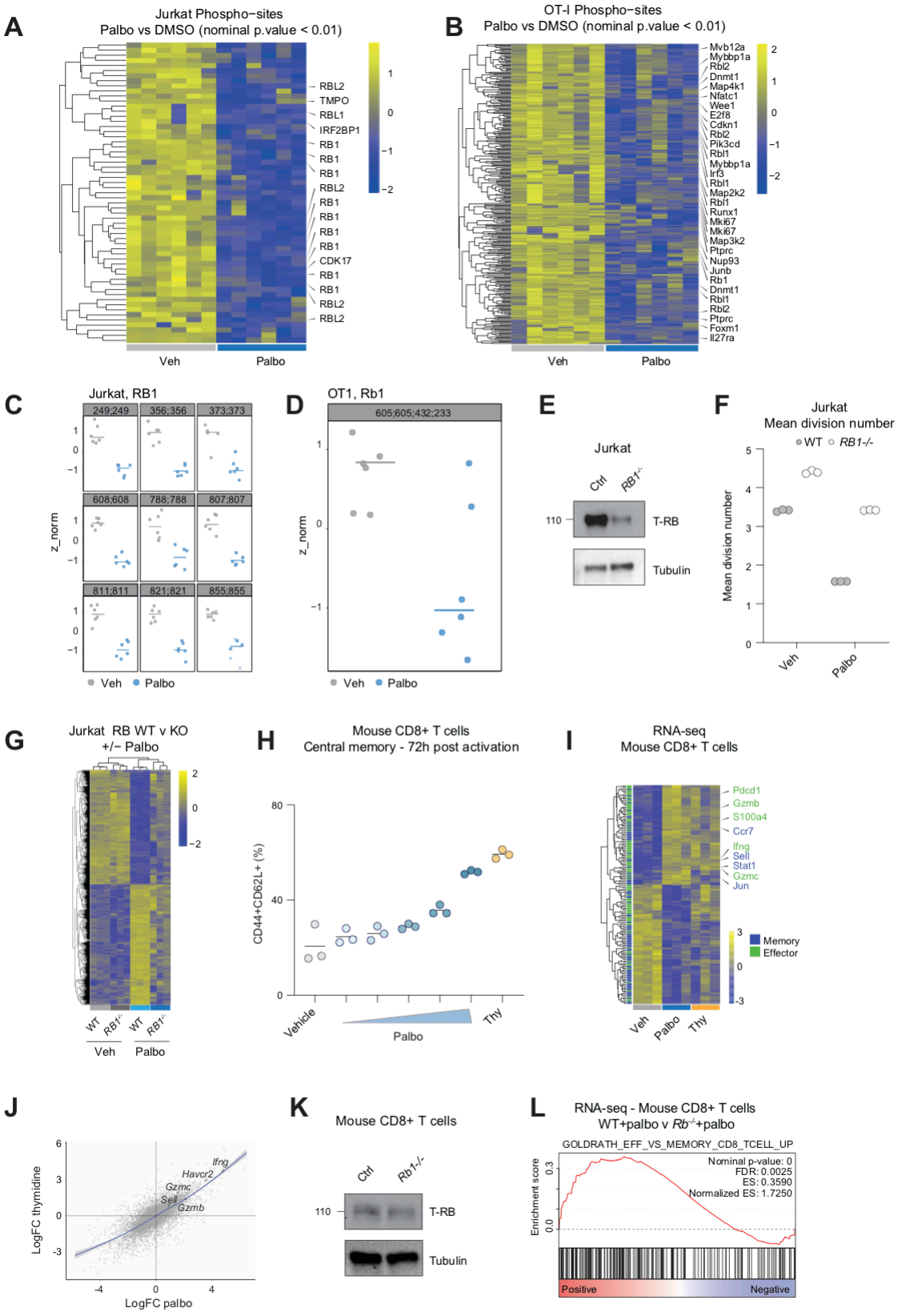
A
Jurkat Phospho−sites
Palbo vs DMSO (nominal p.value < 0.01)
RBL2
TMPO
RBL1
IRF2BP1
RB1
RB1
RB1
RBL2
RB1
RB1
RB1
RB1
CDK17
RB1
RB1
RBL2
RBL2
Veh
Palbo
B
OT-I Phospho−sites
Palbo vs DMSO (nominal p.value < 0.01)
Mvb12a
Mybbp1a
Rbl2
Dnmt1
Map4k1
Nfatc1
Wee1
E2f8
Cdkn1
Rbl2
Pik3cd
Rbl1
Mybbp1a
Irf3
Rbl1
Map2k2
Rbl1
Runx1
Mki67
Mki67
Map3k2
Ptprc
Nup93
Junb
Rb1
Dnmt1
Rbl1
Rbl2
Ptprc
Foxm1
Il27ra
Veh
Palbo
C
Jurkat, RB1
249;249
356;356
373;373
608;608
788;788
807;807
811;811
821;821
855;855
z_norm
Veh
Palbo
D
OT1, Rb1
605;605;432;233
z_norm
Veh
Palbo
E
Jurkat
Ctrl
RB1-/-
110
T-RB
Tubulin
F
Jurkat
Mean division number
WT
RB1-/-
Mean division number
Veh
Palbo
G
Jurkat RB WT v KO
+/− Palbo
WT
RB1-/-
WT
RB1-/-
Veh
Palbo
H
Mouse CD8+ T cells
Central memory - 72h post activation
CD44+CD62L+ (%)
Vehicle
Palbo
Thy
I
RNA-seq
Mouse CD8+ T cells
Pdcd1
Gzmb
S100a4
Ccr7
Ifng
Sell
Stat1
Gzmc
Jun
Memory
Effector
Veh
Palbo
Thy
J
LogFC thymidine
LogFC palbo
Ifng
Havcr2
Gzmc
Sell
Gzmb
K
Mouse CD8+ T cells
Ctrl
Rb1-/-
110
T-RB
Tubulin
L
RNA-seq - Mouse CD8+ T cells
WT+palbo v Rb-/-+palbo
GOLDRATH_EFF_VS_MEMORY_CD8_TCELL_UP
Nominal p-value: 0
FDR: 0.0025
ES: 0.3590
Normalized ES: 1.7250
Enrichment score
Positive
Negative

Figure S4. (A-D) Phospho-proteomics on Jurkat cells or OT-I cells following 2 h of treatment with 1uM palbociclib, OT-I cells treated 3 days post *in vitro* activation. (E) Immunoblot, (F) flow cytometry and (G) RNA-seq on WT and *Rb1*$^{-/-}$ Jurkat T cells following 72h of 1uM palbociclib treatment, CSFE used to measure division number. (H) Tcm (CD44+CD62L+) frequency of *in vitro* CD8+ T cells analyzed by flow cytometry following 48h treatment with palbociclib (125nM-2μM; 2-fold serial dilution) or 2mM thymidine, treated 24h post activation. (I-J) Bulk RNA-seq on *in vitro* activated mouse CD8+ T cells following 48h treatment with 1uM palbociclib or 2mM thymidine, treated 48h post-activation. (K) Immunoblot on *in vitro* activated mouse CD8+ T cells. (L) Bulk RNA-seq on *in vitro*-activated CD8+ mouse cells treated for 24h with 1μM palbociclib, treated 48h post-activation, Cas9/*Rb1* sgRNA was electroporated into naïve cells immediately prior to activation.

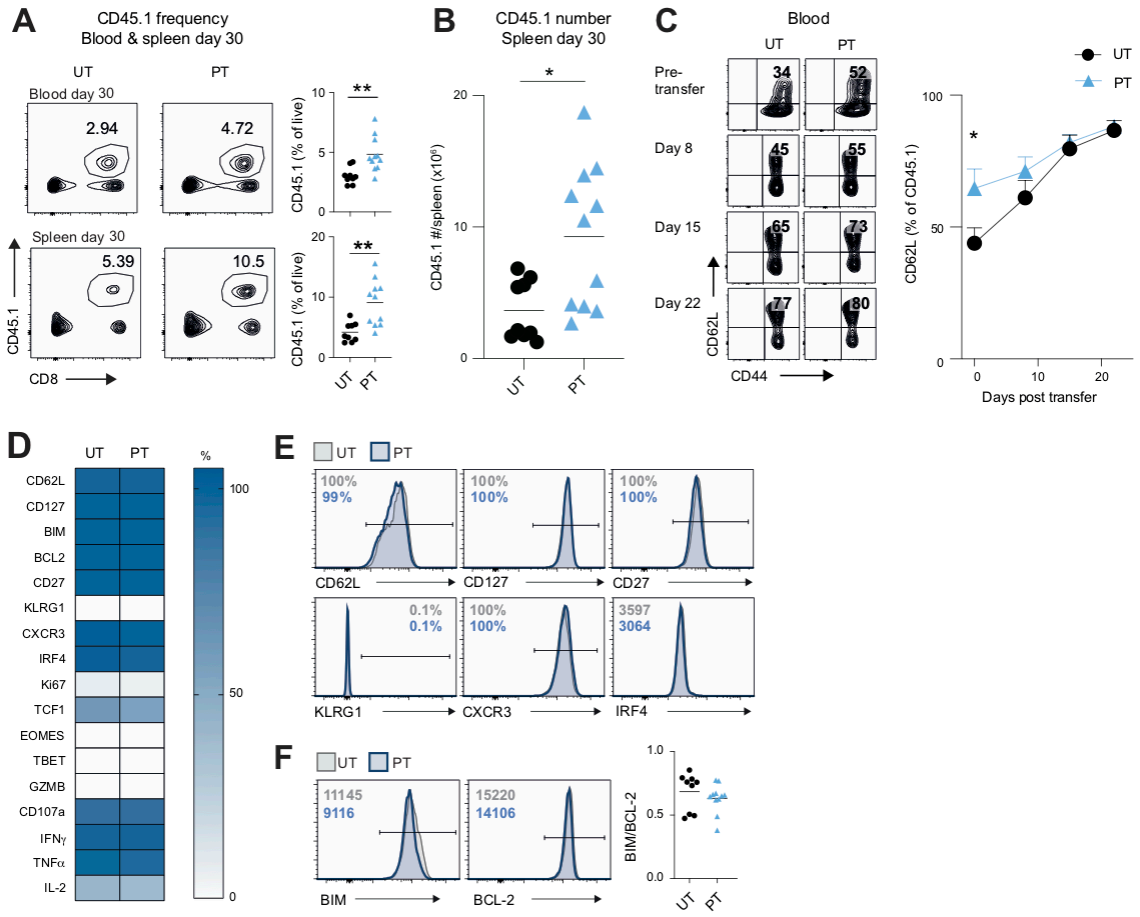
A
CD45.1 frequency
Blood & spleen day 30
UT
PT
Blood day 30
2.94
4.72
Spleen day 30
5.39
10.5
CD45.1
CD8
CD45.1 (% of live)
**
**
B
CD45.1 number
Spleen day 30
*
CD45.1 #/spleen (x10⁶)
C
Blood
Pre-transfer
Day 8
Day 15
Day 22
34
52
45
55
65
73
77
80
CD62L
CD44
CD62L (% of CD45.1)
*
Days post transfer
D
CD62L
CD127
BIM
BCL2
CD27
KLRG1
CXCR3
IRF4
Ki67
TCF1
EOMES
TBET
GZMB
CD107a
IFNγ
TNFα
IL-2
%
E
100%
99%
100%
100%
100%
100%
0.1%
0.1%
100%
100%
3597
3064
CD62L
CD127
CD27
KLRG1
CXCR3
IRF4
F
11145
9116
15220
14106
BIM
BCL-2
BIM/BCL-2

Figure S5. (A-B) OT-I frequency and number in blood and spleen, and (C-F) phenotype of OT-I cells in spleen 30 days-post transfer, Mann-Whitney test. Heatmap represents percent of cells positive for the indicated marker. Data pooled from 2 independent experiments, n=10. *$p<0.05$, **$p<0.01$.

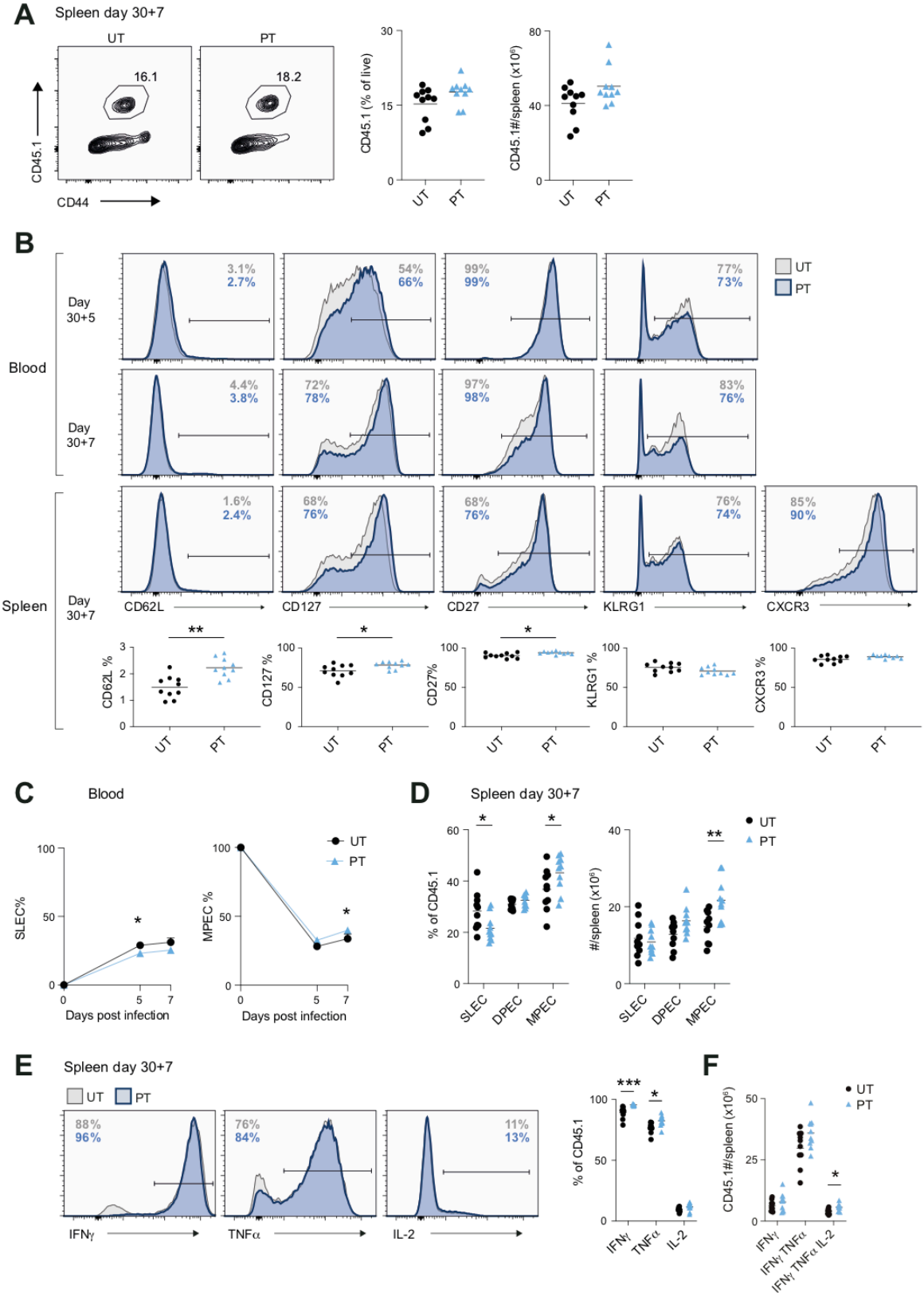
A
Spleen day 30+7
UT
PT
16.1
18.2
CD45.1
CD44
CD45.1 (% of live)
CD45.1#/spleen (x10⁶)
B
Blood
Spleen
Day 30+5
Day 30+7
3.1%
2.7%
54%
66%
99%
99%
77%
73%
4.4%
3.8%
72%
78%
97%
98%
83%
76%
1.6%
2.4%
68%
76%
68%
76%
76%
74%
85%
90%
CD62L
CD127
CD27
KLRG1
CXCR3
CD62L %
CD127 %
CD27%
KLRG1 %
CXCR3 %
C
Blood
SLEC%
MPEC %
Days post infection
D
Spleen day 30+7
% of CD45.1
#/spleen (x10⁶)
SLEC
DPEC
MPEC
E
Spleen day 30+7
88%
96%
76%
84%
11%
13%
IFNγ
TNFα
IL-2
% of CD45.1
F
CD45.1#/spleen (x10⁶)
IFNγ
IFNγ TNFα
IFNγ TNFα IL-2

Figure S6. (A) OT-I frequency and total number in spleen 7 days post-infection. (B) Phenotype of OTI in blood and spleen following infection, Mann-Whitney test. (C-D) Phenotype of OT-I in blood following infection, SLEC ($KLRG1^{high}CD127^{low}$), DPEC ($KLRG1^{high}CD127^{high}$) and MPEC ($KLRG1^{low}CD127^{high}$), multiple t test. (E-F) Cytokine production of OT-I cells in spleens 7 days post infection following *ex vivo* re-stimulation with OVA peptide. Data pooled from 2 independent experiments, n=10, error bars show +/- SEM, *p<0.05, **p<0.01, ***p<0.001.

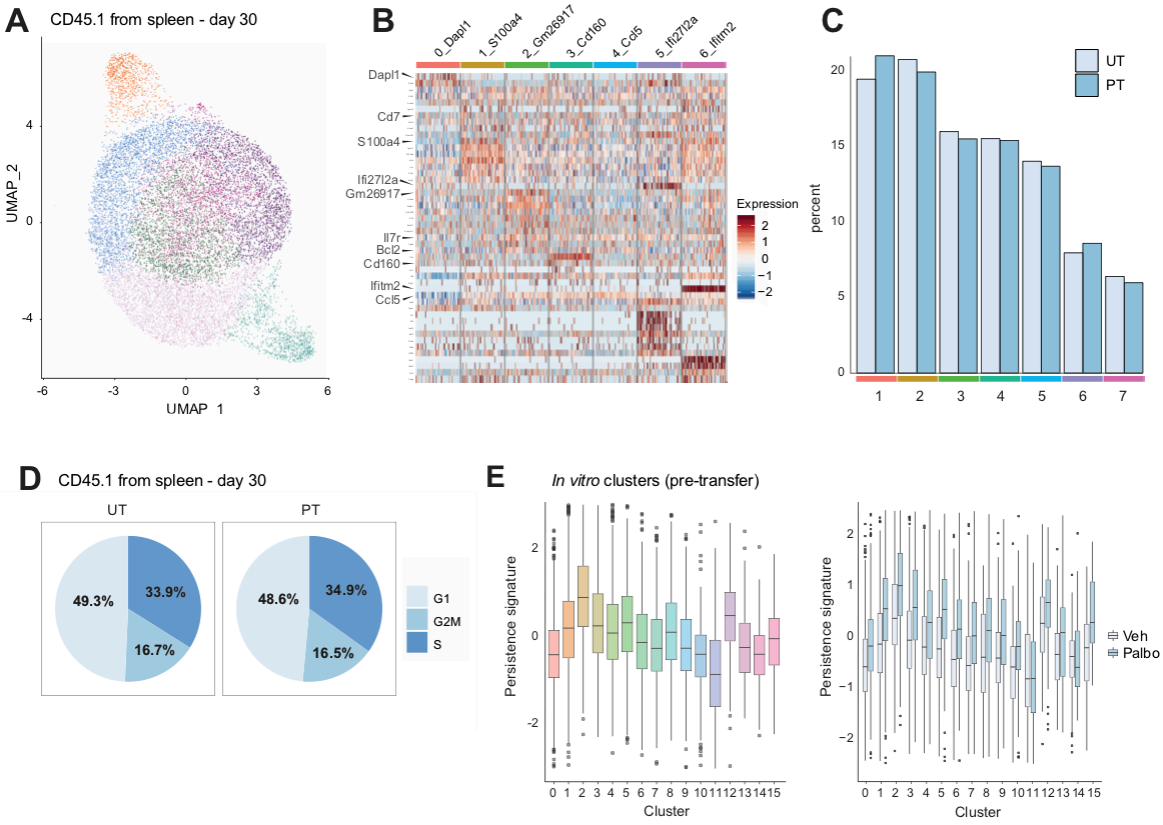
A
CD45.1 from spleen - day 30
UMAP_2
UMAP_1
B
0_Dapl1
1_S100a4
2_Gm26917
3_Cd160
4_Ccl5
5_Ifi27l2a
6_Ifitm2
Dapl1
Cd7
S100a4
Ifi27l2a
Gm26917
Il7r
Bcl2
Cd160
Ifitm2
Ccl5
Expression
C
UT
PT
percent
D
CD45.1 from spleen - day 30
UT
PT
49.3%
33.9%
16.7%
48.6%
34.9%
16.5%
G1
G2M
S
E
In vitro clusters (pre-transfer)
Persistence signature
Cluster
Veh
Palbo

Figure S7. (A) Clustering of day 30 *ex vivo* persisting OT-I cells based on gene expression. (B) Cluster gene expression and annotation and (C) cluster frequency. (D) Cell cycle stage of persisting day 30 OT-I cells based on gene expression. (E) Persistence signature among *in vitro* pre-transfer OT-I cell clusters.

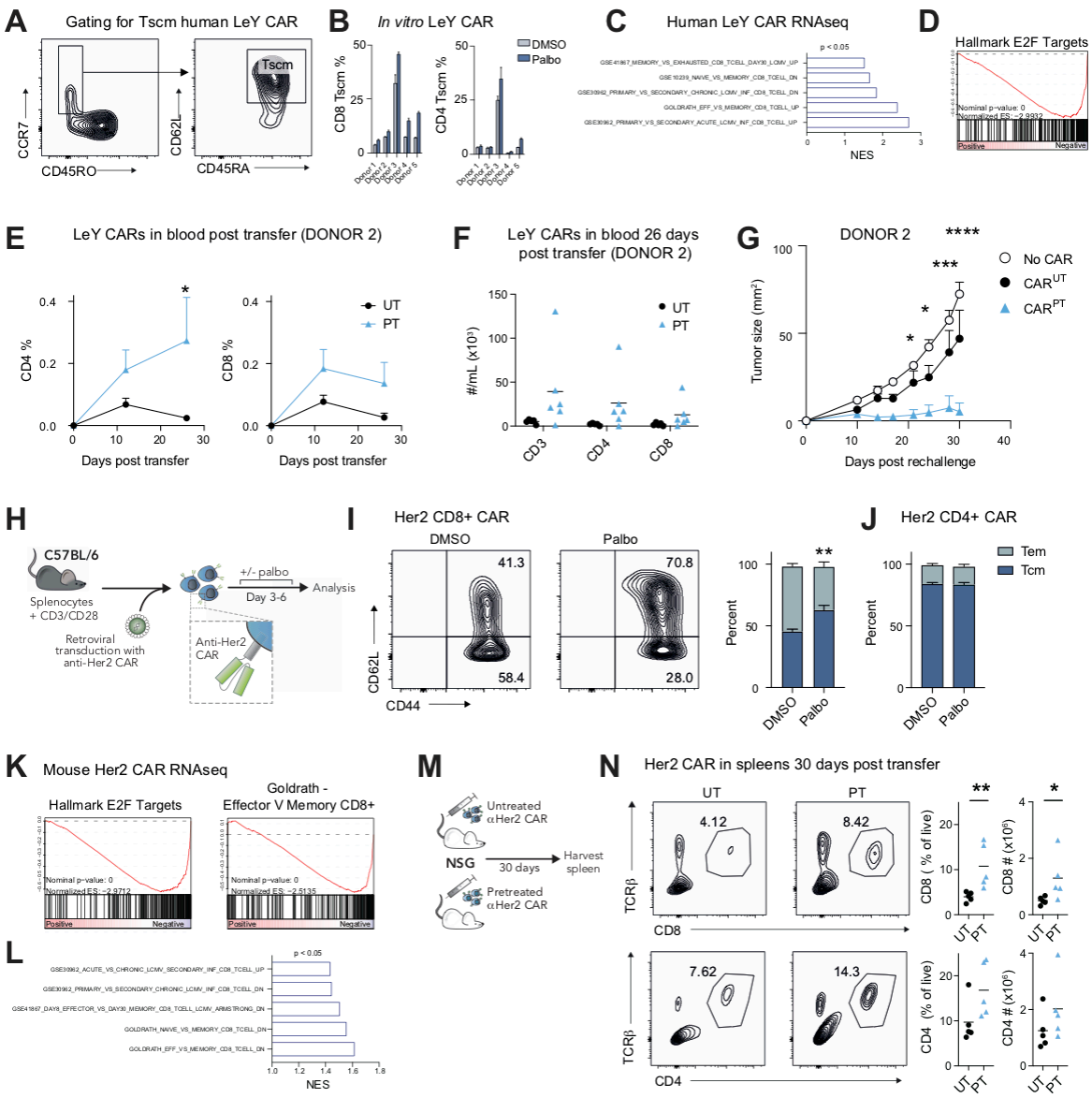
A
Gating for Tscm human LeY CAR
CCR7
CD45RO
CD62L
CD45RA
Tscm
B
In vitro LeY CAR
CD8 Tscm %
CD4 Tscm %
DMSO
Palbo
C
Human LeY CAR RNAseq
p < 0.05
NES
D
Hallmark E2F Targets
Nominal p-value: 0
Positive
Negative
E
LeY CARs in blood post transfer (DONOR 2)
CD4 %
CD8 %
UT
PT
Days post transfer
F
LeY CARs in blood 26 days post transfer (DONOR 2)
#/mL (x10³)
CD3
CD4
CD8
G
DONOR 2
Tumor size (mm²)
No CAR
CAR^UT
CAR^PT
Days post rechallenge
H
C57BL/6
Splenocytes + CD3/CD28
Retroviral transduction with anti-Her2 CAR
+/- palbo
Day 3-6
Analysis
Anti-Her2 CAR
I
Her2 CD8+ CAR
DMSO
Palbo
41.3
58.4
70.8
28.0
CD62L
CD44
Percent
J
Her2 CD4+ CAR
Tem
Tcm
K
Mouse Her2 CAR RNAseq
Hallmark E2F Targets
Goldrath - Effector V Memory CD8+
L
NES
M
Untreated αHer2 CAR
NSG
30 days
Harvest spleen
Pretreated αHer2 CAR
N
Her2 CAR in spleens 30 days post transfer
UT
PT
4.12
8.42
7.62
14.3
TCRβ
CD8
CD4
CD8 (% of live)
CD8 # (x10⁶)
CD4 (% of live)
CD4 # (x10⁶)

Figure S8. (A) Gating for Tscm cells. (B) Frequency of Tscm CAR from five independent PBMC donors. (C-D) RNA-seq of LeY CAR-T cells expanded *in vitro* with/without palbociclib. (E) Frequency of LeY CAR-T cells in blood following transfer. (F) Number of LeY CARs in blood 26 days after transfer. (G) Growth of OVCAR-3 tumors implanted in mice 30 days after receiving untreated or pre-treated LeY CARs. (H) Generation of HER2 mouse CAR-T cells. (I-J) Flow cytometry of (I) CD8+ Her2 CAR-T cells and (J) CD4+ Her2 CAR-T cells treated *in vitro* with palbociclib. (K-L) RNA-seq on Her2 CAR-T cells following palbociclib treatment *in vitro*. (M) Experimental set up to examine persistence of Her2 CAR-T cells *in vivo* following *in vitro* exposure to palbociclib. (N) Frequency and total number of CD8+ and CD4+ in spleens of mice 30 days after transfer.

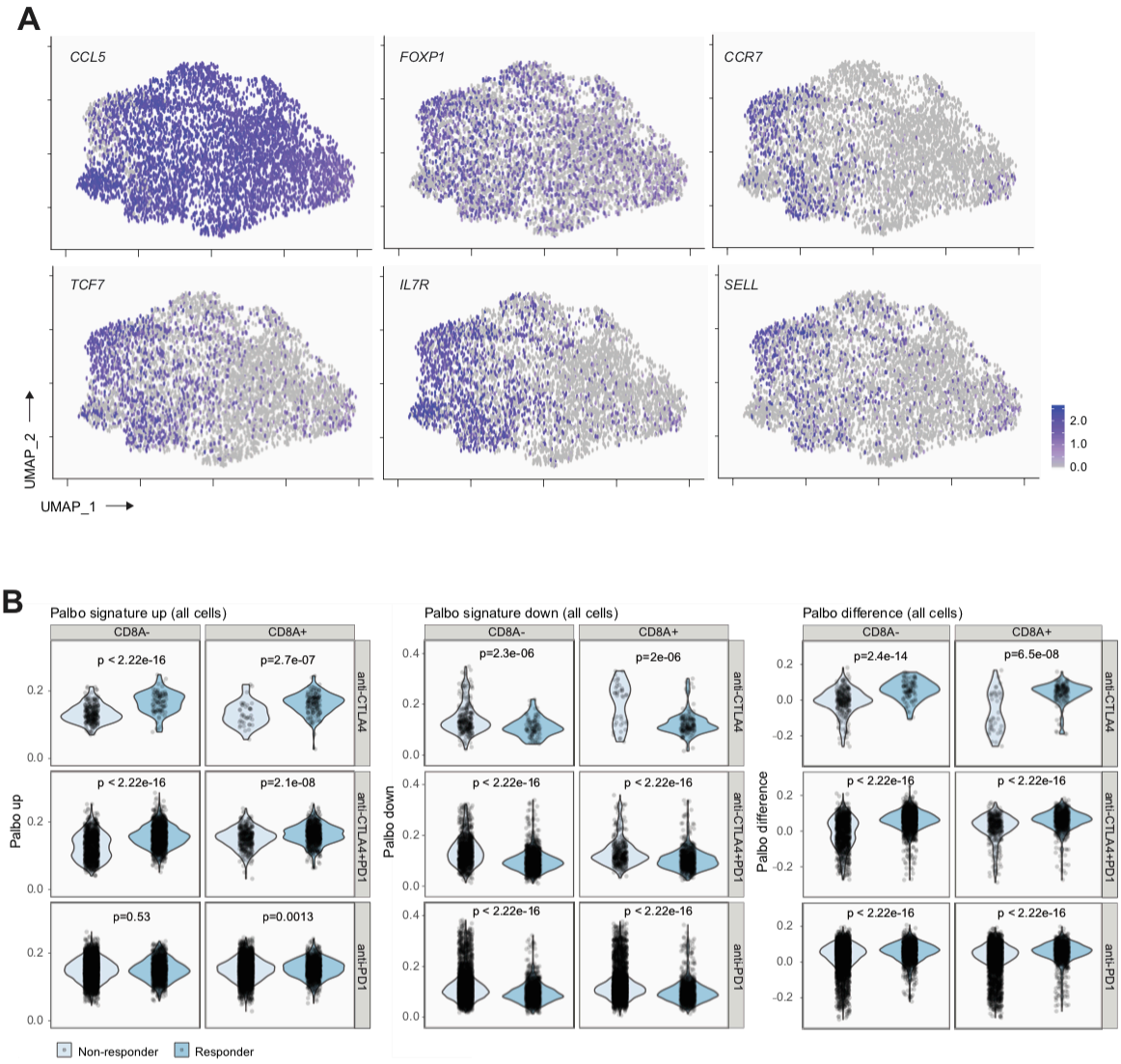
A
CCL5
FOXP1
CCR7
TCF7
IL7R
SELL
UMAP_2
UMAP_1
2.0
1.0
0.0
B
Palbo signature up (all cells)
Palbo signature down (all cells)
Palbo difference (all cells)
CD8A-
CD8A+
anti-CTLA4
anti-CTLA4+PD1
anti-PD1
Palbo up
Palbo down
Palbo difference
p < 2.22e-16
p=2.7e-07
p=2.1e-08
p=0.53
p=0.0013
p=2.3e-06
p=2e-06
p=2.4e-14
p=6.5e-08
Non-responder
Responder

Figure S9. (A) Single cell RNA-seq data on CD8+ TILs from melanoma patients evaluated by Sade-Feldmann et al.(9) (B) Gene markers defining ICB-responsive CD8+ TIL clusters in Figure 6A. (E) Palbociclib AUCell score segregated on CD8+ T cells derived from responding/non-responding patients to ICB.

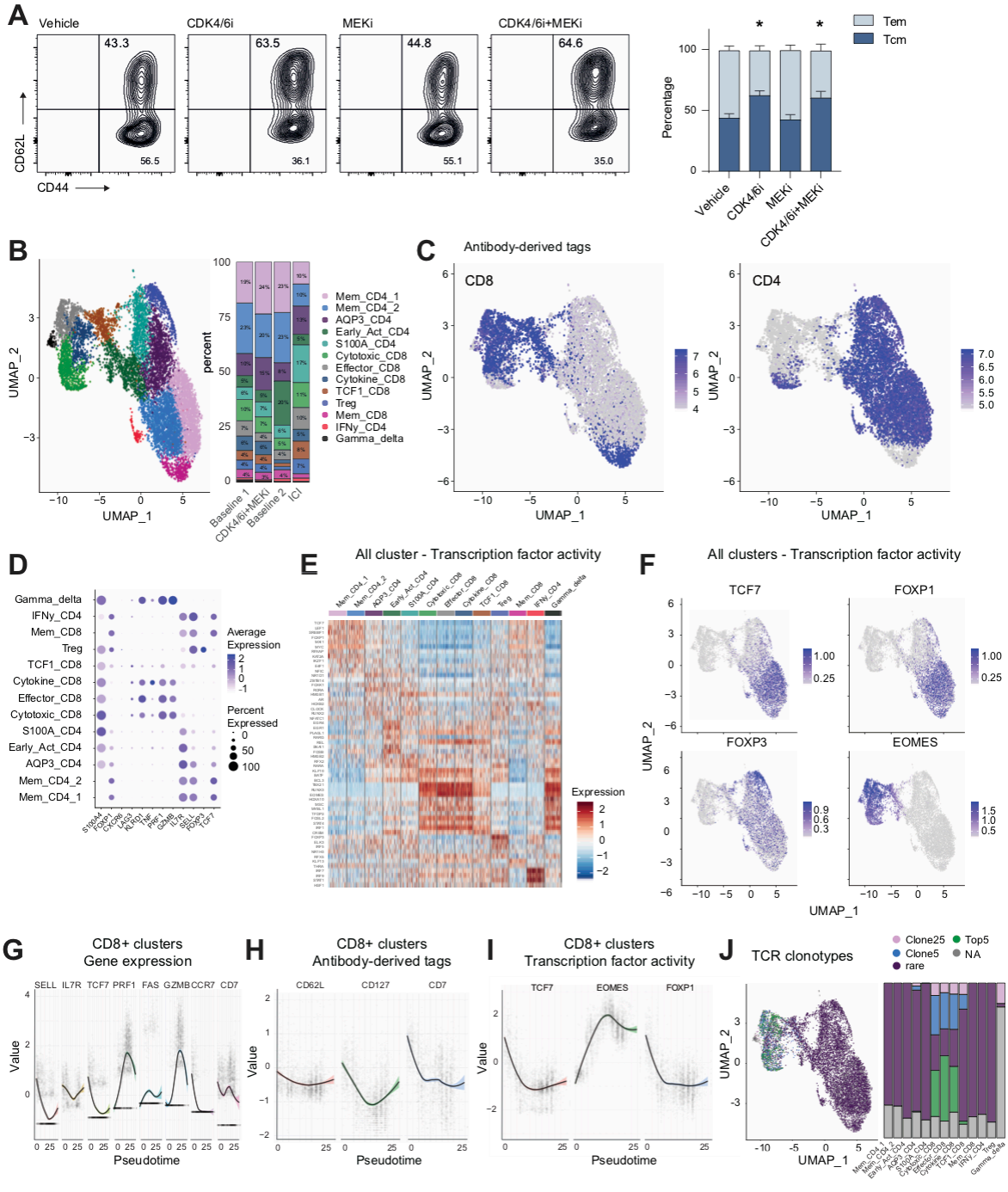
A
Vehicle
CDK4/6i
MEKi
CDK4/6i+MEKi
43.3
56.5
63.5
36.1
44.8
55.1
64.6
35.0
CD62L
CD44
Tem
Tcm
Percentage
Vehicle
CDK4/6i
MEKi
CDK4/6i+MEKi
B
UMAP_1
UMAP_2
percent
Baseline 1
CDK4/6i+MEKi
Baseline 2
ICI
Mem_CD4_1
Mem_CD4_2
AQP3_CD4
Early_Act_CD4
S100A_CD4
Cytotoxic_CD8
Effector_CD8
Cytokine_CD8
TCF1_CD8
Treg
Mem_CD8
IFNγ_CD4
Gamma_delta
C
Antibody-derived tags
CD8
CD4
D
Average Expression
Percent Expressed
E
All cluster - Transcription factor activity
Expression
F
All clusters - Transcription factor activity
TCF7
FOXP1
FOXP3
EOMES
G
CD8+ clusters
Gene expression
SELL
IL7R
TCF7
PRF1
FAS
GZMB
CCR7
CD7
Value
Pseudotime
H
CD8+ clusters
Antibody-derived tags
CD62L
CD127
CD7
I
CD8+ clusters
Transcription factor activity
J
TCR clonotypes
Clone25
Top5
Clone5
NA
rare

Figure S10. (A) Flow cytometry on *in vitro*-activated OT-I following 72h of 1uM palbociclib +/- cobimetinib (MEK inhibitor; MEKi), treatment added 72h post-activation. (B) Peripheral T cell clusters in patient blood based on RNA expression. (C) CD8 and CD4 clusters determined by antibody-derived tags. (D) Cluster gene expression. (E-F) Inferred transcription factor activity in all clusters. (G) Gene expression, (H) antibody-derived markers and (I) inferred transcription factor activity of CD8 clusters over pseudotime. (J) TCR clonality within all cluster.

Chapter 5: Discussion

1. Summary and discussion

The overarching aim of the research presented in this thesis was to evaluate the impact of BRAF, MEK and CDK4/6 inhibition on anti-tumor immunity in melanoma. BRAF and MEK inhibitors have been extensively studied in pre-clinical models and used in the clinic for several years, and hence the novelty of this research was centred around CDK4/6. As such, two key questions were central at the outset of the project; 1) what are the immune-related effects of adding a CDK4/6 inhibitor to the current standard-of-care BRAF/MEK inhibition in *BRAF*^{V600} melanoma, and 2) what are the immune-related effects of CDK4/6 inhibition as a monotherapy? In order to address the first question, a suitable melanoma mouse model was developed and characterized, and is presented in Chapter 2. This model provided the foundation for exploring the impact of BRAF, MEK and CDK4/6 inhibition on the tumor immune microenvironment, which is presented in Chapter 3. The immunomodulatory activity of CDK4/6 inhibition on T-cells was addressed in Chapter 4. Despite a spate of publications on this topic 18 months into the project, a clear gap remained in this literature in regard to our understanding of the direct effect of CDK4/6 inhibition on cytotoxic T lymphocytes – the key immune subset required for effective anti-tumor immunity and success of immune checkpoint blockade. Targeted and immune-based therapies are both current treatment options for melanoma patients. The incorporation of new targets, and the rational design of combinations of these therapeutic approaches, requires a fundamental understanding of the complex crosstalk between these drugs and the immune system.

1.1 The YOVAL1.1 syngeneic melanoma model

The first aim of this work was to develop a mouse model suitable for evaluating the immunomodulatory activity of combined BRAF, MEK and CDK4/6 inhibition in melanoma. An optimal model for this study required four key features; it needed to 1) be a model of mouse melanoma, rather than human melanoma, in order to perform studies in an immunocompetent host, 2) have the capacity to engage the immune system (e.g. express neoantigens and MHC I) in order to study the effects of therapy on anti-tumor immunity, 3) have a genetic background common to human melanoma and relevant for studying these specific inhibitors (e.g. $Braf^{V600}$ for overactive MAPK/ERK signaling targeted by BRAF inhibitors, $Cdkn2a^{-/-}$ for overactive CDK4/6 activity targeted by CDK4/6 inhibitors) and 4) be transplantable for more rapid and cost-effective studies.

Prior to the development of the YUMM series of congenic mouse melanoma cell lines (258), the most widely available transplantable mouse melanoma models were B16 and SM1. Both of these lines are resistant to BRAF inhibition (though SM1 has amplified $BRAF^{V600E}$ activity) and neither have a loss of $p16^{INK4A}$ (encoded by the *CDKN2A* gene), which enhances sensitivity to CDK4/6 inhibitors. The YUMM lines harbor various genetic backgrounds found in human melanoma, and were recently established with the goal of providing more clinically relevant syngeneic melanoma models for pre-clinical analyses (258). In addition to being a more clinically applicable platform to study targeted therapies, these models are also likely to better recapitulate the tumor immune microenvironment of human melanoma. This is because many mutations found in the clinic have been shown to modulate immunity, for example, the production of immunosuppressive cytokines resulting from activation of immunomodulatory cytokine networks by oncogenic BRAF (202). However, despite

their advantages, the YUMM cell lines were notoriously poorly immunogenic due to a lack of neoantigen expression (268), and this was confirmed in our studies. Shortly after sourcing the YUMM cell line for this project, an immunogenic variant of the YUMM1.7 model was developed, coined YUMMER1.7 (268). This model was derived through irradiating YUMM1.7 cells to promote neoantigen expression through UV-induced DNA damage, followed by single-cell cloning to generate a uniform population. This approach to generating an immunogenic cell line was particularly attractive, as it recapitulates the process by which melanoma acquires immunogenic mutations via UV exposure. In our study we used an alternative approach by introducing a model immunogenic antigen, OVA, into the YUMM1.1 cell line. While this system of immunogenicity is more artificial than that of YUMMER1.7, it has distinct benefits, the major one being it allows evaluation of tumor-specific T cell responses, both endogenous and adoptively transferred. Indeed, OVA is widely used as a model antigen in T cell biology and cancer immunology, and examining antigen-specific T cell responses has been made possible with the development of H-2K^{b}-OVA tetramer technology and OT-I transgenic mice, which have an engineered T cell receptor specific for OVA (269, 270).

Though different, YOVAL1.1 and YUMMER1.7 draw some interesting parallels that give insight into these model systems. As expected in the setting of an immunogenic cancer, both models appear to have a highly immunosuppressive tumor microenvironment. T cells were implicated in tumor growth control in both models through examining growth kinetics in mice with various immunocompromised backgrounds (268). However, interestingly depletion of CD8+ T cells alone was not sufficient to change the growth kinetics of these tumors (268, data not shown), suggesting that CD8+ T cells are likely already being suppressed at the time of

depletion. Consistent with this, our data demonstrated that YOVAL1.1 tumors express PD-L1 and have a high frequency of immunosuppressive Tregs and macrophages. Additionally, both YOVAL1.1 and YUMMER1.7 models have a *Pten* deletion, which has been associated with increased expression of immunosuppressive cytokines and resistance to T cell-directed immunotherapies (271-273). Hence, the immunosuppressive microenvironment of these tumors is likely the key contributor to their immune escape, making them ideal models to examine immunotherapeutic strategies that aim to overcome immunosuppression. In OVA models, tumor escape can also be due to selective growth of a small OVA-negative population, however we circumvented this issue by performing several sequential cell sorts to eliminate OVA-negative cell contamination. Indeed, we confirmed antigen expression in escaped tumors by demonstrating that the tumor cells remained sensitive to OT-I T cell killing *ex vivo*, confirming that tumor escape was a result of immunosuppressive mechanisms, rather than a loss in tumor intrinsic sensitivity to T cell control. This ability to detect antigen loss and intrinsic T cell susceptibility highlights an advantage of using the OVA model system. The dynamic tumor-immune interactions observed in YOVAL1.1 tumors, coupled with sensitivity to both immune checkpoint blockade and BRAF/MEK-inhibitors confirmed this to be an optimal model for evaluating any immunomodulatory activity of targeted therapies, which was the next aim of this thesis.

1.2 Immunomodulatory effects of combined BRAF, MEK and CDK4/6 inhibition

The second aim presented in this thesis was to examine changes in the tumor immune microenvironment in response to BRAF, MEK and CDK4/6 inhibition in *BRAF*^{V600} melanoma. This was achieved using the YOVAL1.1 model developed in the first aim. The key question was to examine the immune-related impacts of adding a

CDK4/6 inhibitor to a current standard-of-care treatment in human melanoma, dual BRAF plus MEK inhibition. As such, the treatment groups examined under this aim were vehicle, dual BRAFi+MEKi, CDK4/6i alone or the triple combination.

Combined inhibition of BRAF and CDK4/6 has shown striking synergy in human xenograft models of *BRAF*^{V600} melanoma, with long-term tumor control of over 100 days (50, 51). The triple combination of BRAF, MEK and CDK4/6 has not previously been evaluated *in vivo*, however *in vitro* the anti-proliferative effects of the triple therapy are comparable to that of BRAFi plus CDK4/6i (50). Here, we used the YOVAL1.1 model to evaluate the efficacy of the triple combination *in vivo* in the context of an intact immune system. The anti-tumor efficacy was similar to BRAFi plus CDK4/6i in human models, however resistance began to develop after around 80 days of treatment, which was not seen in human models (50, 51). This may be due to tumor-intrinsic differences between these models. Resistance to dual MEKi and CDK4/6i has been attributed to aberrant NRAS activity as well as increased mTOR signaling (274). In early clinical trials of the triple combination, high levels of phosphorylated S6 (a readout of mTOR activity) were associated with worse clinical outcomes, though the number of patients in this study was low (n=9) and these results were not statistically significant (274). Whether enhanced mTOR activity is a mechanism of resistance to the triple therapy in the YOVAL1.1 model requires further investigation. It is also interesting to note that YOVAL1.1 tumors were not as sensitive to CDK4/6i monotherapy as human models. *In vitro*, CDK4/6i demonstrated anti-proliferative activity and a modest reduction in phosphorylated RB and ERK in the YOVAL1.1 cell line, however, *in vivo* there was no single agent activity. While the combination of CDK4/6i with dual BRAFi+MEKi showed clear synergy *in vivo*, the low sensitivity of YOVAL1.1 tumors to CDK4/6i monotherapy may contribute to the early emergence of

resistance in this model. Indeed, resistance to dual MEK and CDK4/6 inhibition has been associated with E2F reactivation (274), suggesting low sensitivity to CDK4/6i may be a contributing factor to early resistance.

When examining therapies in immunocompetent models, treatment start time is a critical factor to consider. Tumor inoculation triggers an immediate innate immune inflammatory response. During this response DCs uptake antigen, traffic to the lymph node to activate naïve T cells, which then traffic to the tumor site (104, 105, 275). In immunogenic models this is often reflected in the growth kinetics of the tumor, which grows slowly for around seven days, and then plateaus for several days in response to T cell-mediated tumor control. At this point tumors are either spontaneously rejected, or escape T cell control and enter an exponential growth phase. Immune checkpoint blockade (ICB) is most effective in mouse tumor models when used during the first two weeks following tumor inoculation, while tumor burden is low and active T cell engagement is taking place. However, the more clinically applicable time to start treatment is when tumors are well established and have escaped immune control, as this is the scenario faced in the clinic. Hence in addressing aim 2, targeted therapy was started around three to four weeks post tumor inoculation, when tumors were at an established size of ~100mm^3. This is a time at which ICB is less effective and targeted therapies are needed to control tumor growth, allowing us to examine the capacity for targeted therapies to engage immunity, rather than augment a pre-existing response.

The *in vivo* response of YOVAL1.1 tumors to the triple therapy highlighted two critical challenges that parallel those seen in the clinic. Firstly, tumors developed resistance to the therapy. Secondly, tumors that had been macroscopically cleared, re-established rapidly upon therapy removal. This is also observed in human pre-clinical models, and indeed targeted therapy is administered continually in the clinic for this

reason. Together this indicated that triple therapy alone was not sufficient to elicit cures via tumor-intrinsic or immune-mediated mechanisms. However, we predicted that the dramatic reduction in tumor burden coupled with the T cell inflamed microenvironment seen in response to triple therapy would sensitize these tumors to ICB-mediated clearance or tumor control. However, this was not the case, most likely due the collateral effects of the triple therapy on tumor infiltrating myeloid populations that are critical for supporting an optimal T cell response.

Several of the changes observed in the tumor immune microenvironment in response to therapy in the YOVAL1.1 model were consistent with existing literature. Specifically, in accordance with our findings, dual BRAFi/MEKi has previously been reported to induce expression of MHC I (203, 207, 208), cause immunogenic cell death (219), increase tumor infiltrating T cells (TILs) (205-207), and decrease MDSCs (276). Similarly, we observed a decrease in Tregs in response to CDK4/6i monotherapy, which is also consistent with previous reports (221). Notably, these changes were also seen in tumors treated with the triple therapy, indicating the drugs were not antagonistic in regards to these effects. In contrast to these changes, which appeared mostly driven by one or more of the individual therapies, depletion of the myeloid compartment was specific to the triple therapy. Importantly this was not simply an artefact of a lower tumor burden as treatment naïve tumors of the same size were not depleted of these cellular subsets. It is unclear whether the depletion of myeloid subsets was via direct cell-intrinsic cytotoxic actions of the drug combination, or an indirect effect driven by factors secreted from dying tumor cells or other immune or stromal cells in the tumor microenvironment. The MAPK/ERK and CDK4/6/RB signaling pathways targeted by BRAF, MEK and CDK4/6 have been implicated in the downstream production of numerous cytokines and chemokines (202-204, 221). Therefore, inhibiting these

pathways in tumor cells and immune cells is likely to profoundly shift the tumor secretome and, consequently, the immune microenvironment (277). For example, an induction in inflammatory cytokines, such as TNFα, may promote death of tumor infiltrating myeloid subsets, or a reduction in chemoattractants, such as CCL2 and CCL5, may affect the recruitment of migratory DCs and monocytic precursors (150, 278). The tumor secretome was not evaluated in this study but is an area of interest for future research. The combination may also cause systemic depletion of these subsets through direct cytotoxicity. Indeed, CDK4/6 inhibition induces neutropenia in patients (279), suggesting it may systemically deplete subsets of a similar lineage. However, CDK4/6 alone did not reduce the frequency of any myeloid subsets examined. In a small pilot study, we did observe a trend toward lower myeloid precursors in the spleens of mice treated with triple therapy, but this did not reach significance due to significant variation between biological replicates (data not shown). The direct and systemic effects of triple therapy on myeloid subsets requires further investigation to elucidate the mechanisms driving a depletion of these subsets within tumors.

Initial flow cytometric analysis of the tumor immune compartment suggested that triple therapy induced a favorable microenvironment for ICB. Specifically, triple therapy reduced tumor burden, increased lymphocyte infiltration and decreased immunosuppressive populations, including Tregs and MDSCs; all of which are factors associated with favorable responses to ICB (280-283). However, subsequent analysis by scRNA-seq revealed more detailed insight into the immune populations affected by triple therapy, thus providing a more comprehensive understanding of the potential impact of these changes on anti-tumor immunity. These findings highlighted the value of scRNA-seq as a discovery tool. Technologies for sequencing the transcriptome at a single cell level were first described in 2009 (284), and are now revolutionizing the way

in which we approach immunological studies. Flow cytometry has long been the principal technique for identifying and characterizing immune populations, but is restricted by a small number of candidate markers. Mass cytometry was recently developed as a next generation flow cytometry platform that allows for the inclusion of significantly more markers (285), but is still restricted by pre-determined candidates. In contrast, scRNA-seq is a valuable discovery tool for uncovering novel cell types or phenotypes, or for gaining a broad picture of immune populations in an unbiased manner. However, scRNA-seq technology is expensive, which restricts the number of samples that can be analyzed, thereby reducing statistical power. This is particularly problematic when analyzing tumor-infiltrating immune populations, which can be highly variable between biological replicates. To circumvent this in our study, we pooled cells from 10 mice for each sample, thereby diluting noise from biological replicates and making our single sample a more valid representation of the treatment group. 'Hashtagging' technology can also be utilized to reduce sequencing costs (286), and this technique was applied in chapter 4. In this approach, individual samples are barcoded with an oligo-tagged antibody, which allows samples to be pooled for sequencing and then delineated using downstream bioinformatic analyses. An additional challenge of scRNA-seq is gene 'dropout', as highly expressed transcripts are preferentially detected (287). However, even abundant transcripts may dropout from the analysis due to technical limitations, thus complicating downstream cell identification and phenotyping (287, 288). Gene dropout can be partly resolved through deeper sequencing, but this adds substantially to the cost. Despite these limitations, scRNA-seq is a powerful technology that is advancing rapidly and will likely become more affordable and more widely accessible in the coming years.

Our scRNA-seq analyses revealed that the myeloid cells depleted by triple therapy included subsets that are potentially critical for supporting T cell immunity, such as antigen presenting dendritic cells (DCs) (108). Unbiased tSNE clustering revealed four distinct DC populations in the microenvironment of YOVAL1.1 tumors, which were not equally impacted by the triple therapy. Interestingly, the DC population most dramatically depleted was characterized by high expression of genes associated with cross presentation (*Wydf4*, *Xcr1*) (289, 290), and which we identified to be CD103+ DCs based on published transcriptome data (108). To further evaluate the importance of these CD103+ DCs in responses to ICB in melanoma patients, we analyzed published TCGA and single cell datasets (131). Sequencing technology has rapidly advanced in the past two decades, and as a result, large published datasets are readily available for reanalysis to support research hypotheses and findings. Here we analyzed data from a study by Sade-Feldmann and colleagues that applied scRNA-seq to analyze the tumor infiltrating immune compartment from melanoma patients treated with ICB (131). We found the presence of CD103+ DCs correlated with responses to ICB in these patients. Interestingly, in this dataset and our own, *Xcr1* expression was restricted to this rare CD103+ DC population, and is also not expressed by the majority of cancers, including melanoma (291). It is therefore a useful marker to identify these cells in bulk tumor samples. Previously, the prognostic value of CD103+DCs in bulk tumor samples was determined by applying a ratio of a CD103+DC signature to a signature of other myeloid cells in TCGA datasets (108). This approach is complicated by the inclusion of multiple genes that may be expressed by many cells present in bulk tumor samples. Therefore, *Xcr1* expression may better reflect the presence of CD103+ DCs, and hence may be a superior prognostic marker. Indeed, we found Xcr1

expression to be strongly prognostic for survival in melanoma patients, which has not been shown using previously published CD103+ DC and myeloid signatures.

In the dataset published by Sade-Feldman and colleagues (108), surprisingly B cells were the most prognostic immune subset for positive clinical responses, and interestingly, the majority of responding patients with low CD103+ DCs had higher levels of B cells (data not shown). Similar to CD103+ DCs, B cells can augment anti-tumor immunity via antigen cross-presentation and stimulation of T cell responses within the tumor microenvironment (130). It is therefore possible that the role of CD103+ DCs and B cells demonstrate overlapping redundant roles within the tumor, however this requires further investigation. Notably, YOVAL1.1 tumors are mostly devoid of B cells, suggesting CD103+ DCs may be of particular importance in supporting anti-tumor T cell immunity in this model. Further, the correlation of CD103+ DCs with ICB responses in melanoma patients was stronger for those patients treated with anti-CTLA-4 than anti-PD-1 therapy. This is consistent with the proposed mechanism of action of CTLA-4, which functions primarily through de-repressing cross-priming interactions between T cells and DCs (57). Notably, in the chapter 2 of this thesis, we showed that treatment-naïve YOVAL1.1 tumors were responsive to anti-CTLA-4, but not anti-PD-1 therapy. This suggests that poor responsiveness to ICB in this model is likely to be mediated through mechanisms that infer resistance to anti-CTLA-4 therapy, such as this loss of CD103+ DCs following triple therapy.

DCs, and in particularly CD103+ DCs, are implicated as a key immune subset in promoting the anti-tumor immune activity of dual BRAF and MEK inhibition, alone and in combination with ICB (219, 292). Dual inhibition of BRAF and MEK reportedly induces immunogenic cell death (219), which is consistent with our findings. Immunogenic cell death sheds tumor antigens into the microenvironment, and immune

engagement requires DCs to uptake these antigens in order to initiate a T cell response (293). It is likely the immunogenic cell death we observed following triple therapy promoted the recruitment of T cells, explaining the increased frequency of lymphocytes in these tumors seven days after therapy. Indeed, our TCR analysis suggested a broadening of the TCR repertoire in response to therapy, rather than an expansion of specific T cell clones, indicating engagement of a new T cell response. However, by the time these T cells reached the tumor, immune-supportive macrophages and DC populations had been depleted. Without the presence of pro-inflammatory cytokines and cross priming stimulation within tumors, the T cell response was likely restricted. Further, it is suggested that ICB efficacy relies on recruitment of T cells to the tumor (177), which requires migratory CD103+ DCs and chemokine-producing macrophages (94, 275, 294). Hence, the loss of these myeloid populations likely impacted on the efficacy of ICB through reduced capacity of these tumors to stimulate both existing and new anti-tumor T cell responses.

1.3 Induction of T cell memory in response to CDK4/6 inhibition

The third aim of the research presented in this thesis was to evaluate the direct impact of CDK4/6 inhibition on T cells. Several recent studies demonstrated immune-potentiating effects of CDK4/6 inhibition, and subsequent synergy with immune checkpoint blockade (221-224). However, T cells are the primary target of these immunotherapies, and an understanding of the direct effects of CDK4/6 inhibition on this cellular subset was lacking. The data presented in chapter 3 showed that CDK4/6 inhibition as a monotherapy had little effect on the YOVAL1.1 tumor immune microenvironment, apart from a reduction in the frequency of Tregs. However, our scRNA-seq analyses revealed that the T cells in tumors treated with triple therapy had lower levels of exhaustion markers and higher levels of memory markers. Further,

preliminary *in vitro* and *in vivo* analysis examining changes in CD62L expression (a memory marker) on T cells, in response to various drug combinations, suggested this shift in phenotype was mediated by CDK4/6 inhibition (data not shown). Indeed, it is well appreciated that lymphocyte fate decisions are intricately linked to cell cycle (295-298). The precise mechanisms underpinning this relationship are complex and difficult to elucidate, but it is likely that the cell cycle machinery plays a dual function in driving cell cycle progression, while simultaneously suppressing differentiation pathways. Such differentiation pathways are most often activated in G1; the decision point for exiting the cell cycle (295, 296). Given the critical role of CDK4/6 in regulating G1 to S cell cycle transition, coupled with our preliminary findings, we hypothesized that CDK4/6 inhibition would modulate T cell fate.

A recent study by Deng and colleagues identified NFAT as a target of negative regulation by CDK6 in T cells and hence suggested that CDK4/6 inhibition promotes T cell activation (224). However, 'T cell activation' alone does not address subsequent functional consequences, and many transcription factors that initiate T cell activity, including NFAT, are also involved in feedback loops that limit this activity. Notably, in addition to driving transcription of genes associated with effector function, NFAT is also associated with the regulation of T cell dysfunctional states, including anergy, tolerance and exhaustion (188, 299). In contrast, transcription factors that promote T cell memory or stemness, such as TCF1, are associated with superior functional capacity (196, 300, 301). Given the reported role for CDK4/6 inhibition in promoting NFAT activity, it was perhaps surprising that a decrease in T cell exhaustion markers was observed following CDK4/6 inhibition in two independent studies, neither of which emphasized this finding (221, 224). However, consistent with our hypothesis that CDK4/6 inhibition modulates T cell differentiation, our re-analysis of datasets

published by Deng and colleagues (224) revealed an increase in expression of memory-associated genes (*Sell, Il7r, Tcf7*) in T cells isolated from mouse *Kras*-driven lung tumors following CDK4/6 inhibition; remarkably a phenotype that was unreported in this study. Using a comprehensive range of approaches and various mouse tumor models, we subsequently demonstrated that CDK4/6 inhibition did indeed promote the acquisition of intratumoral T cell memory.

Our discovery that directly inhibiting CDK4/6 in T cells promotes memory differentiation was somewhat in contrast to the reported role for CDK4/6 inhibitors in enhancing NFAT activity (222, 224). However, perhaps one of the most intriguing findings from our study was confirmation that CDK4/6 inhibition indeed also promoted T cell effector function, such as enhanced killing and IFNγ secretion; features known to be dampened in memory T cells (302). To unravel this dichotomy, we applied scRNA-seq and discovered that effector features and memory features driven by CDK4/6 inhibition occur in distinct cell populations within a heterogenous T cell pool. While the effector fate may be attributable to enhanced NFAT activity (224), this was not confirmed in our study. We did, however, identify a requirement for RB in the CDK4/6-mediated induction of T cell memory through a genome wide CRISPR/Cas9 screen using the human T cell lymphoma line, Jurkat. Jurkat cells were employed for this screen as primary mouse T cells rapidly shift their phenotype in culture over time, potentially introducing artefacts, and are difficult to manipulate as they are only suitable for use in assays for approximately five days. Similar to primary T cells, we found that Jurkat cells upregulated the memory marker CD62L in response to CDK4/6 inhibition, thus presenting an ideal model to screen for CDK4/6-mediated regulators of this marker. Indeed, in accordance with our screen, RB deletion in primary mouse T cells promoted enrichment of effector gene sets, confirming a role for RB in memory

formation. However, whether RB promotes bona fide T cell memory in the form of a long-term persistent phenotype *in vivo*, still needs to be determined.

RB is the most well characterized substrate of CDK4/6, and indeed was also the top hit in our phosphoproteomics data for both Jurkat and primary mouse T cells. The idea that RB may be a molecular rheostat governing T cell differentiation is perhaps not surprising, as RB has long been known to play a pivotal role in cellular differentiation and proliferation in tumor cells (reviewed in 303); although its exact role in lymphocytes is unclear. A 1993 study by Chen and colleagues (304) found that RB is not required for normal lymphocyte development, or T cell activation and proliferation, perhaps deterring further interest in studying RB in these cells. Interestingly however, lymphocytes express high levels of RB protein (305), and thus its seemingly redundant role suggests it is constitutively inhibited, likely by CDK4/6. The role of RB in its differing phosphorylation states has not been previously explored in T cells, and our findings suggest that in its active hypophosphorylated form (following CDK4/6 inhibition) it mediates exit from the cell cycle and memory formation. However, the precise downstream mechanisms linking hypophosphorylated RB to T cell differentiation requires further investigation, and is likely extremely complex.

Terminally differentiated lymphocytes exhibit a stable epigenetic landscape (306). Here, we showed that CDK4/6 inhibition promotes epigenetic remodeling and subsequent commitment to a memory phenotype, which is sustained long after drug removal. This was demonstrated through the long-term *in vivo* persistence of bona fide memory cells that were generated through a short *in vitro* exposure to a CDK4/6 inhibitor. Cell-fate commitment requires complex epigenetic remodeling during G1, prior to DNA synthesis in S phase (307). The induction of G1 arrest by CDK4/6i-mediated activation of RB likely allows epigenetic remodeling to take place, which

would otherwise be repressed by rapid cell cycle progression. Further, in addition to RB, hundreds of other CDK4/6 substrates have been identified (308), several of which were detected in our phosphoproteomics analysis and are implicated in differentiation. This highlights the complicated mechanisms underpinning the relationship between cell cycle machinery and cell fate. The acquisition of memory in response to CDK4/6 inhibition is likely a result of multiple complex regulatory mechanisms taking place during an RB-mediated G1 arrest.

The activated T cell pool comprises a spectrum of phenotypic states (302, 309), and distinct subpopulations of cells with stem or memory-like properties are implicated as the critical subsets required for sustained immunity (180, 193, 194). Our finding that CDK4/6 inhibition promotes T cell stemness offers critical insight into the immune-potentiating function of these inhibitors. This discovery broadens the prospective utility of CDK4/6 inhibitors, which may in fact be used as clinical tools to promote a wide range of T cell directed therapies in addition to potentiating endogenous anti-tumor immunity. Potential future applications of CDK4/6 inhibitors will be discussed in the next section.

2. Future perspectives

2.1 CDK4/6 inhibitors as adjuvants to ICB

CDK4/6 inhibitors have demonstrated synergy with blockade of the PD-1-PD-L1 axis in a number of preclinical models (221-224), prompting evaluation of this combination therapy in clinical trials. While the efficacy of this combination is largely attributed to tumor-intrinsic immunomodulatory activity of CDK4/6 inhibitors, our data suggests a novel mechanism whereby CDK4/6 inhibitors promote a more favorable T

cell pool for immune checkpoint targeting. Indeed, our re-analysis of published data on TILs from melanoma patients indicated that the gene signature induced by the clinical CDK4/6 inhibitor, palbociclib, significantly correlated with better responses to immune checkpoint blockade. Accordingly, our analysis of peripheral T cells from a melanoma patient indicated an expansion of the memory T cell pool in response to dual CDK4/6 and MEK inhibition, followed by an immunological response to subsequent immune checkpoint therapy, demonstrated by effector differentiation and a broadening of the TCR repertoire. This suggests that CDK4/6 inhibition may be used to prime the T cell pool prior to the application of immune checkpoint blockade. In contrast to this approach, using preclinical mouse models Schaer and colleagues (222) demonstrated the most efficacious schedule for this combination was continuous administration of a CDK4/6 inhibitor before, throughout and after ICB, based on the rationale that CDK4/6 inhibition is required to maintain a T cell-inflamed microenvironment. In their study, a consecutive schedule of ICB after CDK4/6i demonstrated poor anti-tumor efficacy. However, this is likely because CDK4/6 inhibition was administered for 15 days and demonstrated no single agent activity, thus allowing tumors to grow almost 10-fold in size prior to the administration of ICB. As mentioned earlier, large established tumors are often poorly responsive to ICB in preclinical models. In our studies, we found a mere 24h exposure to CDK4/6 inhibition was sufficient to redirect T cell phenotype, and hence it would be interesting to determine whether preconditioning tumors with a once-off dose of CDK4/6i would improve the sensitivity to ICB. In our study, we also demonstrated that CDK4/6 inhibition reduces expansion of CD8+ T cells, which was not previously described in the literature. Hence, using CDK4/6 inhibition as a priming tool removes the potential complication of restricted T cell expansion in response to ICB, which is likely to occur if CDK4/6 inhibition is continuously administered.

2.2 Using CDK4/6 inhibitors to improve CAR T cell therapy

The capacity for CDK4/6 inhibitors to promote T cell memory makes them an attractive potential tool to improve the efficacy of CAR T cell therapy, where one of the major challenges is a lack of persistence of the adoptively transferred T cells (265, 266). Our analysis of human CAR T cells revealed an increase in the frequency of less differentiated stem cell-like memory T cells (Tscm) in response to CDK4/6 inhibition. This subset has been shown to be capable of reconstituting a phenotypically diverse T cell compartment while retaining the capacity for self-renewal (310). Strategies to preserve stem-like properties of autologous T cells and CAR T cells have resulted in superior anti-tumor efficacy following adoptive transfer (311-314). Such cell states are governed by diverse transcriptional and epigenetic regulatory networks (315-317), and targeting these networks to direct immune cell fate is of great clinical interest. Hence, here we present a potential strategy to enhance the efficacy of CAR T therapy through exposure to a CDK4/6 inhibitor during *in vitro* manufacturing. However, there are several potential caveats to this approach. Notably, CDK4/6 inhibition compromises T cell expansion, and clinical CAR T cell protocols rely on *in vitro* expansion of a therapeutically optimal number of cells for patient administration. It would hence need to be determined whether any enhanced efficacy from CDK4/6i exposure outweighs potential limitations imposed by suboptimal *in vitro* expansion. Several other agents have also been shown to induce T cell memory without compromising expansion. For example, AKT inhibitors promote T cell memory without anti-proliferative effects, and hence have also been proposed as a potential tool to prime T cells *in vitro* to improve adoptive cell therapies (318). Expanding CAR T cells in the cytokines, IL-7/IL-15, can also enhance memory formation, and under these conditions CAR T cells exhibit higher proliferation and reduced apoptosis than cells expanded in IL-2 (267). Accordingly, T

cells expanded in the presence of an AKT inhibitor or IL-7/IL-15 have shown superior anti-tumor efficacy when transferred *in vivo* (267, 318). The mechanisms underpinning memory formation in these different settings are likely complex and possibly distinct. Hence, to evaluate the feasibility of using CDK4/6 inhibitors to enhance CAR T cell therapy, manufacturing protocols incorporating a CDK4/6 inhibitor would need to be compared to alternative approaches that are currently being evaluated for clinical use.

2.3 CDK4/6 inhibitors as adjuvants to other therapies

CDK4/6 inhibitors are showing promise in combination with a range of other cancer therapies (reviewed in 319). The role of these inhibitors in promoting T cell memory provides additional insight into their potential role in these combinations. For example, CDK4/6 inhibitors have shown synergy with PI3Kα inhibitors in combination with immune checkpoint blockade in preclinical syngeneic breast cancer models (226). Interestingly, inhibition of mTOR (downstream of PI3K) has also been shown to overcome resistance to dual MEK and CDK4/6 inhibition (274). A role for mTOR in T cell memory is well established, with mTOR signaling reportedly dampening memory formation (320). Hence, while the approach of combining CDK4/6 and PI3K/mTOR inhibitors was formed on the basis of their dual tumor-intrinsic activity, these combinations may further support the development of T cell memory. Although T cell memory enhances survival and persistence of T cells, therapeutically beneficial anti-tumor T cell responses also require expansion and effector differentiation of these cells. Hence appropriate scheduling of CDK4/6 and PI3K/mTOR inhibitors must be considered to avoid restraining T cells in a quiescent state.

Perhaps one of the most intriguing combinations incorporating a CDK4/6 inhibitor was evaluated in a recent clinical trial for triple negative breast cancer (TNBC)

(321). CDK4/6 inhibitors are not used to treat TNBC, as these tumors often exhibit a functional loss of RB (322), making the CDK4/6/RB axis a seemingly redundant target. However, in this trial, a single high dose of a CDK4/6 inhibitor was given intravenously prior to the administration of chemotherapy, with the goal of transiently arresting immune cells in G1 to reduce myelotoxicity (321). Indeed, CDK4/6 administration had previously been employed to protect chemotherapy-induced immune suppression in this way (180, 323, 324). Strikingly, in this TNBC trial patients receiving trilaciclib achieved better overall survival. While the mechanism behind this is unclear, it is speculated to be a possible result of the immune-potentiating role of CDK4/6 inhibitors (321, 325). This is particularly intriguing in the wake of our findings that transient exposure to a CDK4/6 inhibitor can promote long-lasting immunity via the induction of T cell memory. Indeed, recent preliminary evidence suggests that transient CDK4/6 inhibition is sufficient to promote immunity, through mechanisms that are not entirely clear (326, 327).

Another clinical scenario in which short-term exposure to a CDK4/6 inhibitor may prove efficacious is vaccine administration. The current COVID-19 pandemic is a pertinent example of the critical need for effective vaccines to control potentially lethal infectious diseases. Vaccines use attenuated pathogens or peptides to initiate an immune response and create antibody responses and immunological T cell memory to protect against future encounters with the pathogen. Adjuvants are often added to vaccines to promote more robust immunity (328), however, long-lasting immunological memory is not always achieved (329, 330). Indeed, in the case of COVID-19, promoting long lasting immunity is a major anticipated challenge in vaccine development. Therefore, the capacity for CDK4/6 inhibitors to boost T cell memory following antigen exposure makes them an attractive adjuvant to enhance immunological memory following

vaccine administration. However, further studies are required to determine if this is an efficacious clinical approach.

2.4 Optimizing scheduling for combined BRAF, MEK and CDK4/6 inhibition

In this study, combined inhibition of BRAF, MEK and CDK4/6 depleted intratumoral immune subsets critical for supporting a therapeutically beneficial T cell response. Therefore, while this therapy combination is effective due to potent tumor intrinsic activity, it may impede the ability of the immune system to contribute to the overall anti-tumor response. As immunotherapy is an alternative treatment option for melanoma patients, these findings have significant implications for the stratification of patients between ongoing clinical trials of combined BRAFi, MEKi and CDK4/6i, and available immunotherapy options. For example, the triple combination may be more beneficial as a next line of treatment for patients that first fail to respond to immunotherapy, or conversely, patients switching from triple therapy to immunotherapy may benefit from a therapy break to potentially allow depleted immune populations to recover. Alternatively, the negative immunomodulatory impacts of triple therapy may be managed with optimal therapy scheduling. Indeed, our findings, coupled with existing literature, offer insight into the best approach to incorporate and schedule these therapies. In xenograft models, the combination of MEK and CDK4/6 inhibition is more efficacious when the CDK4/6 inhibitor is administered intermittently, which reportedly delays the onset of tumor-intrinsic resistance (274). This schedule is also attractive because 1) continuous CDK4/6 inhibition is associated with higher clinical toxicities (331) and 2) our findings suggest that continuous CDK4/6 inhibition will restrain T cell expansion and hence limit an optimal immune response. Further evidence suggests MEK inhibition is also more efficacious when administered intermittently, which is reportedly due to enhancing anti-tumor T cell activity rather

than a tumor-intrinsic effect (332). Our findings, and others, demonstrated that dual BRAF/MEK inhibition causes immunogenic cell death and activation of a T cell response (219), and transient CDK4/6 inhibition appears to be sufficient to promote immunity and T cell memory. Therefore, it is possible that a single dose of CDK4/6i given upfront with dual BRAFi/MEKi would be sufficient to further enhance and prolong BRAFi/MEKi-induced anti-tumor T cell immunity without depleting myeloid populations critical for supporting this response. Indeed, our preliminary findings suggested that depletion of myeloid cells by the triple therapy occurred after two days of treatment, suggesting this combination may not induce negative collateral effects on the tumor immune compartment if used transiently. Determining optimal combinations of BRAF, MEK and CDK4/6 requires further investigation. However, evaluating these schedules in preclinical mouse models is difficult because without continuous therapy most of these tumors grow aggressively, and the window for immunotherapies to be effective rapidly closes due to unmanageable tumor burden. Examining the tumor immune microenvironment in preclinical models and patient samples in response to various schedules may offer some insight into optimal immune-potentiating approaches.

3. Conclusion

In summary, this thesis details the development of a novel immunogenic mouse *BRAF*^{V600} melanoma model for preclinical assessment of the immunomodulatory activity of BRAF, MEK and CDK4/6 inhibitors. In this model, the triple therapy combination promoted immunogenic cell death and robust tumor regression *in vivo*, which was accompanied by an influx of lymphocytes into the tumor microenvironment. However, the triple therapy also depleted intratumoral myeloid subsets critical for supporting a T cell response, and as a result, rendered tumors unresponsive to immune

checkpoint blockade. This finding has important implications for scheduling combinations of targeted therapies with immunotherapy in the clinic. Further comprehensive analysis of the individual immunomodulatory activity of CDK4/6 inhibitors revealed that transient CDK4/6 inhibition in T cells promotes acquisition of a memory phenotype. This highlights CDK4/6 inhibitors as a valuable clinical tool to promote endogenous T cell immunity, improve the persistence of CAR T cells and enhance the efficacy of immune checkpoint blockade by priming the endogenous T cell pool. The induction of T cell memory in response to transient CDK4/6 inhibition also suggests that, with optimal scheduling to prevent depletion of critical myeloid subsets, CDK4/6 inhibitors may be used to enhance and prolong BRAFi/MEKi-induced anti-tumor T cell immunity. Taken together, these findings offer essential new insights into the immunomodulatory activity and utility of melanoma targeted therapies. Defining the mechanisms that underpin the clinical efficacy of available therapies is a critical step forward for optimising novel combination and scheduling approaches to combat this deadly disease.

Chapter 6: References

1. MacKie RM, Hauschild A, & Eggermont AM (2009) Epidemiology of invasive cutaneous melanoma. *Ann Oncol* 20 vi1-7.
2. Gandini S*, et al.* (2005) Meta-analysis of risk factors for cutaneous melanoma: I. Common and atypical naevi. *Eur J Cancer* 41(1):28-44.
3. Markovic SN*, et al.* (2007) Malignant melanoma in the 21st century, part 1: epidemiology, risk factors, screening, prevention, and diagnosis. *Mayo Clin Proc* 82(3):364-380.
4. Melanoma Institute Australia (2020) Melanoma facts and statistics.
5. Cancer Council Victoria (2019) Curing Australia's National Cancer.
6. de Vries E*, et al.* (2007) Up-to-date survival estimates and historical trends of cutaneous malignant melanoma in the south-east of The Netherlands. *Ann Oncol* 18(6):1110-1116.
7. American Cancer Society (2020) Survival Rates for Melanoma Skin Cancer.
8. Song X*, et al.* (2015) Overall survival in patients with metastatic melanoma. *Curr Med Res Opin* 31(5):987-991.
9. Wang HT, Choi B, & Tang MS (2010) Melanocytes are deficient in repair of oxidative DNA damage and UV-induced photoproducts. *Proc Natl Acad Sci U S A* 107(27):12180-12185.
10. Chow AY (2010) Cell Cycle Control by Oncogenes and Tumor Suppressors: Driving the Transformation of Normal Cells into Cancerous Cells. *Nat Education* 3:7.
11. Weinstein IB (2002) Cancer. Addiction to oncogenes--the Achilles heal of cancer. *Science* 297(5578):63-64.

12. Davies H, *et al.* (2002) Mutations of the BRAF gene in human cancer. *Nature* 417(6892):949-954.

13. Cantwell-Dorris ER, O'Leary JJ, & Sheils OM (2011) BRAFV600E: implications for carcinogenesis and molecular therapy. *Mol Cancer Ther* 10(3):385-394.

14. Garnett MJ & Marais R (2004) Guilty as charged: B-RAF is a human oncogene. *Cancer Cell* 6(4):313-319.

15. Colombino M, *et al.* (2012) BRAF/NRAS mutation frequencies among primary tumors and metastases in patients with melanoma. *J Clin Oncol* 30(20):2522-2529.

16. Wan PT, *et al.* (2004) Mechanism of activation of the RAF-ERK signaling pathway by oncogenic mutations of B-RAF. *Cell* 116(6):855-867.

17. Downward J (2003) Targeting RAS signalling pathways in cancer therapy. *Nat Rev Cancer* 3(1):11-22.

18. Sensi M, *et al.* (2006) Mutually exclusive NRASQ61R and BRAFV600E mutations at the single-cell level in the same human melanoma. *Oncogene* 25(24):3357-3364.

19. Tsai J, *et al.* (2008) Discovery of a selective inhibitor of oncogenic B-Raf kinase with potent antimelanoma activity. *Proc Natl Acad Sci U S A* 105(8):3041-3046.

20. Chapman PB, *et al.* (2011) Improved survival with vemurafenib in melanoma with BRAF V600E mutation. *N Engl J Med* 364(26):2507-2516.

21. Banzi M, *et al.* (2016) Dabrafenib: a new opportunity for the treatment of BRAF V600-positive melanoma. *Onco Targets Ther* 9:2725-2733.

22. Koelblinger P, Thuerigen O, & Dummer R (2018) Development of encorafenib for BRAF-mutated advanced melanoma. *Curr Opin Oncol* 30(2):125-133.

23. Chapman PB (2013) Mechanisms of resistance to RAF inhibition in melanomas harboring a BRAF mutation. *Am Soc Clin Oncol Educ Book*.

24. Luebker SA & Koepsell SA (2019) Diverse Mechanisms of BRAF Inhibitor Resistance in Melanoma Identified in Clinical and Preclinical Studies. *Front Oncol* 9:268.

25. Flaherty KT*, et al.* (2012) Combined BRAF and MEK inhibition in melanoma with BRAF V600 mutations. *N Engl J Med* 367(18):1694-1703.

26. Flaherty KT*, et al.* (2012) Improved survival with MEK inhibition in BRAF-mutated melanoma. *N Engl J Med* 367(2):107-114.

27. Matsushime H*, et al.* (1992) Identification and properties of an atypical catalytic subunit (p34PSK-J3/cdk4) for mammalian D type G1 cyclins. *Cell* 71(2):323-334.

28. Burkhart DL & Sage J (2008) Cellular mechanisms of tumour suppression by the retinoblastoma gene. *Nat Rev Cancer* 8(9):671-682.

29. Giacinti C & Giordano A (2006) RB and cell cycle progression. *Oncogene* 25(38):5220-5227.

30. Dyson N (1998) The regulation of E2F by pRB-family proteins. *Genes Dev* 12(15):2245-2262.

31. Sherr CJ (1996) Cancer cell cycles. *Science* 274(5293):1672-1677.

32. Kato J, Matsushime H, Hiebert SW, Ewen ME, & Sherr CJ (1993) Direct binding of cyclin D to the retinoblastoma gene product (pRb) and pRb phosphorylation by the cyclin D-dependent kinase CDK4. *Genes Dev* 7(3):331-342.

33. Ewen ME*, et al.* (1993) Functional interactions of the retinoblastoma protein with mammalian D-type cyclins. *Cell* 73(3):487-497.

34. Hanahan D & Weinberg RA (2011) Hallmarks of cancer: the next generation. *Cell* 144(5):646-674.

35. Serrano M, Hannon GJ, & Beach D (1993) A new regulatory motif in cell-cycle control causing specific inhibition of cyclin D/CDK4. *Nature* 366(6456):704-707.

36. Walker GJ*, et al.* (1998) Virtually 100% of melanoma cell lines harbor alterations at the DNA level within CDKN2A, CDKN2B, or one of their downstream targets. *Genes Chromosomes Cancer* 22(2):157-163.

37. Curtin JA*, et al.* (2005) Distinct sets of genetic alterations in melanoma. *N Engl J Med* 353(20):2135-2147.

38. Sheppard KE & McArthur GA (2013) The cell-cycle regulator CDK4: an emerging therapeutic target in melanoma. *Clin Cancer Res* 19(19):5320-5328.

39. Hall M & Peters G (1996) Genetic alterations of cyclins, cyclin-dependent kinases, and Cdk inhibitors in human cancer. *Adv Cancer Res* 68:67-108.

40. Knudsen ES & Knudsen KE (2008) Tailoring to RB: tumour suppressor status and therapeutic response. *Nat Rev Cancer* 8(9):714-724.

41. Schwartz GK*, et al.* (2011) Phase I study of PD 0332991, a cyclin-dependent kinase inhibitor, administered in 3-week cycles (Schedule 2/1). *Br J Cancer* 104(12):1862-1868.

42. Turner NC, Huang Bartlett C, & Cristofanilli M (2015) Palbociclib in Hormone-Receptor-Positive Advanced Breast Cancer. *N Engl J Med* 373(17):1672-1673.

43. Sherr CJ, Beach D, & Shapiro GI (2016) Targeting CDK4 and CDK6: From Discovery to Therapy. *Cancer Discov* 6(4):353-367.

44. Mebratu Y & Tesfaigzi Y (2009) How ERK1/2 activation controls cell proliferation and cell death: Is subcellular localization the answer? *Cell Cycle* 8(8):1168-1175.

45. Lavoie JN, L'Allemain G, Brunet A, Muller R, & Pouyssegur J (1996) Cyclin D1 expression is regulated positively by the p42/p44MAPK and negatively by the p38/HOGMAPK pathway. *J Biol Chem* 271(34):20608-20616.

46. Terada Y*, et al.* (1999) Mitogen-activated protein kinase cascade and transcription factors: the opposite role of MKK3/6-p38K and MKK1-MAPK. *Nephrol Dial Transplant* 14 45-47.

47. Cheng M, Sexl V, Sherr CJ, & Roussel MF (1998) Assembly of cyclin D-dependent kinase and titration of p27Kip1 regulated by mitogen-activated protein kinase kinase (MEK1). *Proc Natl Acad Sci U S A* 95(3):1091-1096.

48. Smalley KS*, et al.* (2008) Increased cyclin D1 expression can mediate BRAF inhibitor resistance in BRAF V600E-mutated melanomas. *Mol Cancer Ther* 7(9):2876-2883.

49. Flaherty KD, M. A.; Grob J. J.; Long, G. V.; Nathan, P. D.; Ribas, A.; Robert, C.; Schadendorf, D.; Frederick, D. T.; Hammond, M. R.; Jane-Valbuena, J.; Mu, X.; Squires, M.; Jaeger, S. A.; Lane, S. R.; Mookerjee, B.; Garraway, L. A. (2016) Genomic analysis and 3-y efficacy and safety update of COMBI-d: A phase 3 study of dabrafenib (D) + trametinib (T) vs D monotherapy in patients (pts) with unresectable or metastatic BRAF V600E/K-mutant cutaneous melanoma. *J Clin Oncol* 34:Abstr 9502.

50. Martin CA*, et al.* (2018) Palbociclib synergizes with BRAF and MEK inhibitors in treatment naive melanoma but not after the development of BRAF inhibitor resistance. *Int J Cancer* 142(10):2139-2152.

51. Yadav V*, et al.* (2014) The CDK4/6 inhibitor LY2835219 overcomes vemurafenib resistance resulting from MAPK reactivation and cyclin D1 upregulation. *Mol Cancer Ther* 13(10):2253-2263.

52. Yoshida A, Lee EK, & Diehl JA (2016) Induction of Therapeutic Senescence in Vemurafenib-Resistant Melanoma by Extended Inhibition of CDK4/6. *Cancer Res* 76(10):2990-3002.

53. Lee MS*, et al.* (2016) Efficacy of the combination of MEK and CDK4/6 inhibitors in vitro and in vivo in KRAS mutant colorectal cancer models. *Oncotarget*.

54. Posch C*, et al.* (2018) MEK/CDK4,6 co-targeting is effective in a subset of NRAS, BRAF and 'wild type' melanomas. *Oncotarget* 9(79):34990-34995.

55. Kwong LN*, et al.* (2012) Oncogenic NRAS signaling differentially regulates survival and proliferation in melanoma. *Nat Med* 18(10):1503-1510.

56. Leach DR, Krummel MF, & Allison JP (1996) Enhancement of antitumor immunity by CTLA-4 blockade. *Science* 271(5256):1734-1736.

57. Wei SC, Duffy CR, & Allison JP (2018) Fundamental Mechanisms of Immune Checkpoint Blockade Therapy. *Cancer Discov* 8(9):1069-1086.

58. Robert C*, et al.* (2011) Ipilimumab plus dacarbazine for previously untreated metastatic melanoma. *N Engl J Med* 364(26):2517-2526.

59. Hodi FS*, et al.* (2010) Improved survival with ipilimumab in patients with metastatic melanoma. *N Engl J Med* 363(8):711-723.

60. LaFleur MW, Muroyama Y, Drake CG, & Sharpe AH (2018) Inhibitors of the PD-1 Pathway in Tumor Therapy. *J Immunol* 200(2):375-383.

61. Homet Moreno B, Parisi G, Robert L, & Ribas A (2015) Anti-PD-1 therapy in melanoma. *Semin Oncol* 42(3):466-473.

62. Robert C*, et al.* (2015) Nivolumab in previously untreated melanoma without BRAF mutation. *N Engl J Med* 372(4):320-330.

63. Larkin J*, et al.* (2015) Combined Nivolumab and Ipilimumab or Monotherapy in Untreated Melanoma. *N Engl J Med* 373(1):23-34.

64. Schachter J*, et al.* (2017) Pembrolizumab versus ipilimumab for advanced melanoma: final overall survival results of a multicentre, randomised, open-label phase 3 study (KEYNOTE-006). *Lancet* 390(10105):1853-1862.

65. Yu JH, J. P.; Olivia, C.; Neftelinov, S. T.; Hubbard-Lucey, V. M.; Tang, J. (2020) Trends in clinical development for PD-1/PD-L1 inhibitors. *Nat Rev Drug Discov* 19:163-164.

66. Postow MA*, et al.* (2015) Nivolumab and ipilimumab versus ipilimumab in untreated melanoma. *N Engl J Med* 372(21):2006-2017.

67. Larkin J*, et al.* (2019) Five-Year Survival with Combined Nivolumab and Ipilimumab in Advanced Melanoma. *N Engl J Med* 381(16):1535-1546.

68. Robert C*, et al.* (2015) Improved overall survival in melanoma with combined dabrafenib and trametinib. *N Engl J Med* 372(1):30-39.

69. Robert C*, et al.* (2019) Five-Year Outcomes with Dabrafenib plus Trametinib in Metastatic Melanoma. *N Engl J Med* 381(7):626-636.

70. Ribas A*, et al.* (2016) Association of Pembrolizumab With Tumor Response and Survival Among Patients With Advanced Melanoma. *JAMA* 315(15):1600-1609.

71. Wang DY*, et al.* (2018) Fatal Toxic Effects Associated With Immune Checkpoint Inhibitors: A Systematic Review and Meta-analysis. *JAMA Oncol* 4(12):1721-1728.

72. Chai QQ, Du JY, Zhu J, & Wu B (2019) The Differences in the Safety and Tolerability of Immune Checkpoint Inhibitors as Treatment for Non-Small Cell Lung Cancer and Melanoma: Network Meta-Analysis and Systematic Review. *Front Pharmacol* 10:1260.

73. Verma V*, et al.* (2018) A systematic review of the cost and cost-effectiveness studies of immune checkpoint inhibitors. *J Immunother Cancer* 6(1):128.

74. Dunn GP, Old LJ, & Schreiber RD (2004) The three Es of cancer immunoediting. *Annu Rev Immunol* 22:329-360.

75. Mackensen A*, et al.* (1994) Direct evidence to support the immunosurveillance concept in a human regressive melanoma. *J Clin Invest* 93(4):1397-1402.

76. Shankaran V*, et al.* (2001) IFNgamma and lymphocytes prevent primary tumour development and shape tumour immunogenicity. *Nature* 410(6832):1107-1111.

77. Dunn GP, Bruce AT, Ikeda H, Old LJ, & Schreiber RD (2002) Cancer immunoediting: from immunosurveillance to tumor escape. *Nat Immunol* 3(11):991-998.

78. Passarelli A, Mannavola F, Stucci LS, Tucci M, & Silvestris F (2017) Immune system and melanoma biology: a balance between immunosurveillance and immune escape. *Oncotarget* 8(62):106132-106142.

79. Casado JG*, et al.* (2009) Expression of adhesion molecules and ligands for activating and costimulatory receptors involved in cell-mediated cytotoxicity in a large panel of human melanoma cell lines. *Cancer Immunol Immunother* 58(9):1517-1526.

80. Lakshmikanth T*, et al.* (2009) NCRs and DNAM-1 mediate NK cell recognition and lysis of human and mouse melanoma cell lines in vitro and in vivo. *J Clin Invest* 119(5):1251-1263.

81. McKay K, Moore PC, Smoller BR, & Hiatt KM (2011) Association between natural killer cells and regression in melanocytic lesions. *Hum Pathol* 42(12):1960-1964.

82. Maat W*, et al.* (2009) Evidence for natural killer cell-mediated protection from metastasis formation in uveal melanoma patients. *Invest Ophthalmol Vis Sci* 50(6):2888-2895.

83. Morgado S*, et al.* (2011) NK cell recognition and killing of melanoma cells is controlled by multiple activating receptor-ligand interactions. *J Innate Immun* 3(4):365-373.

84. Orange JS (2008) Formation and function of the lytic NK-cell immunological synapse. *Nat Rev Immunol* 8(9):713-725.

85. Pietra G*, et al.* (2012) Melanoma cells inhibit natural killer cell function by modulating the expression of activating receptors and cytolytic activity. *Cancer Res* 72(6):1407-1415.

86. Mirjacic Martinovic KM*, et al.* (2014) Decreased expression of NKG2D, NKp46, DNAM-1 receptors, and intracellular perforin and STAT-1 effector molecules in NK cells and their dim and bright subsets in metastatic melanoma patients. *Melanoma Res* 24(4):295-304.

87. Gentles AJ*, et al.* (2015) The prognostic landscape of genes and infiltrating immune cells across human cancers. *Nat Med* 21(8):938-945.

88. Cursons J*, et al.* (2019) A Gene Signature Predicting Natural Killer Cell Infiltration and Improved Survival in Melanoma Patients. *Cancer Immunol Res* 7(7):1162-1174.

89. Fujimura T, Kakizaki A, Furudate S, Kambayashi Y, & Aiba S (2016) Tumor-associated macrophages in skin: How to treat their heterogeneity and plasticity. *J Dermatol Sci* 83(3):167-173.

90. Pieniazek M, Matkowski R, & Donizy P (2018) Macrophages in skin melanoma-the key element in melanomagenesis. *Oncol Lett* 15(4):5399-5404.

91. Mantovani A, Schioppa T, Porta C, Allavena P, & Sica A (2006) Role of tumor-associated macrophages in tumor progression and invasion. *Cancer Metastasis Rev* 25(3):315-322.

92. Falleni M*, et al.* (2017) M1 and M2 macrophages' clinicopathological significance in cutaneous melanoma. *Melanoma Res* 27(3):200-210.

93. Noy R & Pollard JW (2014) Tumor-associated macrophages: from mechanisms to therapy. *Immunity* 41(1):49-61.

94. House IG*, et al.* (2020) Macrophage-Derived CXCL9 and CXCL10 Are Required for Antitumor Immune Responses Following Immune Checkpoint Blockade. *Clin Cancer Res* 26(2):487-504.

95. Pantano F*, et al.* (2013) The role of macrophages polarization in predicting prognosis of radically resected gastric cancer patients. *J Cell Mol Med* 17(11):1415-1421.

96. Cui YL, Li HK, Zhou HY, Zhang T, & Li Q (2013) Correlations of tumor-associated macrophage subtypes with liver metastases of colorectal cancer. *Asian Pac J Cancer Prev* 14(2):1003-1007.

97. Jayasingam SD*, et al.* (2019) Evaluating the Polarization of Tumor-Associated Macrophages Into M1 and M2 Phenotypes in Human Cancer Tissue: Technicalities and Challenges in Routine Clinical Practice. *Front Oncol* 9:1512.

98. Chang RB & Beatty GL (2020) The interplay between innate and adaptive immunity in cancer shapes the productivity of cancer immunosurveillance. *J Leukoc Biol*.

99. Heemskerk B, Kvistborg P, & Schumacher TN (2013) The cancer antigenome. *EMBO J* 32(2):194-203.

100. Alexandrov LB*, et al.* (2013) Signatures of mutational processes in human cancer. *Nature* 500(7463):415-421.

101. Schumacher TN & Schreiber RD (2015) Neoantigens in cancer immunotherapy. *Science* 348(6230):69-74.

102. Pitcovski J, Shahar E, Aizenshtein E, & Gorodetsky R (2017) Melanoma antigens and related immunological markers. *Crit Rev Oncol Hematol* 115:36-49.

103. Chen DS & Mellman I (2013) Oncology meets immunology: the cancer-immunity cycle. *Immunity* 39(1):1-10.

104. Steinman RM, Inaba K, Turley S, Pierre P, & Mellman I (1999) Antigen capture, processing, and presentation by dendritic cells: recent cell biological studies. *Hum Immunol* 60(7):562-567.

105. Mellman I (2005) Antigen processing and presentation by dendritic cells: cell biological mechanisms. *Adv Exp Med Biol* 560:63-67.

106. Merad M, Sathe P, Helft J, Miller J, & Mortha A (2013) The dendritic cell lineage: ontogeny and function of dendritic cells and their subsets in the steady state and the inflamed setting. *Annu Rev Immunol* 31:563-604.

107. Randolph GJ, Angeli V, & Swartz MA (2005) Dendritic-cell trafficking to lymph nodes through lymphatic vessels. *Nat Rev Immunol* 5(8):617-628.

108. Broz ML*, et al.* (2014) Dissecting the tumor myeloid compartment reveals rare activating antigen-presenting cells critical for T cell immunity. *Cancer Cell* 26(5):638-652.

109. Dushyanthen S*, et al.* (2015) Relevance of tumor-infiltrating lymphocytes in breast cancer. *BMC Med* 13:202.

110. Gooden MJ, de Bock GH, Leffers N, Daemen T, & Nijman HW (2011) The prognostic influence of tumour-infiltrating lymphocytes in cancer: a systematic review with meta-analysis. *Br J Cancer* 105(1):93-103.

111. Galon J*, et al.* (2006) Type, density, and location of immune cells within human colorectal tumors predict clinical outcome. *Science* 313(5795):1960-1964.

112. Loi S*, et al.* (2019) Tumor-Infiltrating Lymphocytes and Prognosis: A Pooled Individual Patient Analysis of Early-Stage Triple-Negative Breast Cancers. *J Clin Oncol* 37(7):559-569.

113. Acs B*, et al.* (2019) An open source automated tumor infiltrating lymphocyte algorithm for prognosis in melanoma. *Nat Commun* 10(1):5440.

114. Takaba H & Takayanagi H (2017) The Mechanisms of T Cell Selection in the Thymus. *Trends Immunol* 38(11):805-816.

115. Mescher MF*, et al.* (2006) Signals required for programming effector and memory development by CD8+ T cells. *Immunol Rev* 211:81-92.

116. Curtsinger JM, Valenzuela JO, Agarwal P, Lins D, & Mescher MF (2005) Type I IFNs provide a third signal to CD8 T cells to stimulate clonal expansion and differentiation. *J Immunol* 174(8):4465-4469.

117. Curtsinger JM & Mescher MF (2010) Inflammatory cytokines as a third signal for T cell activation. *Curr Opin Immunol* 22(3):333-340.

118. Franciszkiewicz K, Boissonnas A, Boutet M, Combadiere C, & Mami-Chouaib F (2012) Role of chemokines and chemokine receptors in shaping the effector phase of the antitumor immune response. *Cancer Res* 72(24):6325-6332.

119. Ley K & Kansas GS (2004) Selectins in T-cell recruitment to non-lymphoid tissues and sites of inflammation. *Nat Rev Immunol* 4(5):325-335.

120. Ley K, Laudanna C, Cybulsky MI, & Nourshargh S (2007) Getting to the site of inflammation: the leukocyte adhesion cascade updated. *Nat Rev Immunol* 7(9):678-689.

121. Bellone M & Calcinotto A (2013) Ways to enhance lymphocyte trafficking into tumors and fitness of tumor infiltrating lymphocytes. *Front Oncol* 3:231.

122. Harlin H*, et al.* (2009) Chemokine expression in melanoma metastases associated with CD8+ T-cell recruitment. *Cancer Res* 69(7):3077-3085.

123. Jacquelot N*, et al.* (2016) Chemokine receptor patterns in lymphocytes mirror metastatic spreading in melanoma. *J Clin Invest* 126(3):921-937.

124. Hong M*, et al.* (2011) Chemotherapy induces intratumoral expression of chemokines in cutaneous melanoma, favoring T-cell infiltration and tumor control. *Cancer Res* 71(22):6997-7009.

125. Lopez JA*, et al.* (2013) Perforin forms transient pores on the target cell plasma membrane to facilitate rapid access of granzymes during killer cell attack. *Blood* 121(14):2659-2668.

126. Propper DJ*, et al.* (2003) Low-dose IFN-gamma induces tumor MHC expression in metastatic malignant melanoma. *Clin Cancer Res* 9(1):84-92.

127. Sucker A*, et al.* (2017) Acquired IFNgamma resistance impairs anti-tumor immunity and gives rise to T-cell-resistant melanoma lesions. *Nat Commun* 8:15440.

128. Lai YP, Lin CC, Liao WJ, Tang CY, & Chen SC (2009) CD4+ T cell-derived IL-2 signals during early priming advances primary CD8+ T cell responses. *PLoS One* 4(11):e7766.

129. Smith CM*, et al.* (2004) Cognate CD4(+) T cell licensing of dendritic cells in CD8(+) T cell immunity. *Nat Immunol* 5(11):1143-1148.

130. Sharonov GV, Serebrovskaya EO, Yuzhakova DV, Britanova OV, & Chudakov DM (2020) B cells, plasma cells and antibody repertoires in the tumour microenvironment. *Nat Rev Immunol* 20(5):294-307.

131. Sade-Feldman M*, et al.* (2019) Defining T Cell States Associated with Response to Checkpoint Immunotherapy in Melanoma. *Cell* 176(1-2):404.

132. Griss J*, et al.* (2019) B cells sustain inflammation and predict response to immune checkpoint blockade in human melanoma. *Nat Commun* 10(1):4186.

133. Ladanyi A*, et al.* (2011) Prognostic impact of B-cell density in cutaneous melanoma. *Cancer Immunol Immunother* 60(12):1729-1738.

134. Umansky V & Sevko A (2012) Melanoma-induced immunosuppression and its neutralization. *Semin Cancer Biol* 22(4):319-326.

135. Kim R, Emi M, Tanabe K, & Arihiro K (2006) Tumor-driven evolution of immunosuppressive networks during malignant progression. *Cancer Res* 66(11):5527-5536.

136. Dowling MR*, et al.* (2018) Regulatory T Cells Suppress Effector T Cell Proliferation by Limiting Division Destiny. *Front Immunol* 9:2461.

137. Shevach EM (2018) Foxp3(+) T Regulatory Cells: Still Many Unanswered Questions-A Perspective After 20 Years of Study. *Front Immunol* 9:1048.

138. Viguier M*, et al.* (2004) Foxp3 expressing CD4+CD25(high) regulatory T cells are overrepresented in human metastatic melanoma lymph nodes and inhibit the function of infiltrating T cells. *J Immunol* 173(2):1444-1453.

139. Quezada SA, Peggs KS, Curran MA, & Allison JP (2006) CTLA4 blockade and GM-CSF combination immunotherapy alters the intratumor balance of effector and regulatory T cells. *J Clin Invest* 116(7):1935-1945.

140. Velasco-Velazquez M, Xolalpa W, & Pestell RG (2014) The potential to target CCL5/CCR5 in breast cancer. *Expert Opin Ther Targets* 18(11):1265-1275.

141. Singh SK*, et al.* (2018) CCR5/CCL5 axis interaction promotes migratory and invasiveness of pancreatic cancer cells. *Sci Rep* 8(1):1323.

142. Chang LY*, et al.* (2012) Tumor-derived chemokine CCL5 enhances TGF-beta-mediated killing of CD8(+) T cells in colon cancer by T-regulatory cells. *Cancer Res* 72(5):1092-1102.

143. Curiel TJ*, et al.* (2004) Specific recruitment of regulatory T cells in ovarian carcinoma fosters immune privilege and predicts reduced survival. *Nat Med* 10(9):942-949.

144. Chang DK*, et al.* (2016) Anti-CCR4 monoclonal antibody enhances antitumor immunity by modulating tumor-infiltrating Tregs in an ovarian cancer xenograft humanized mouse model. *Oncoimmunology* 5(3):e1090075.

145. Priceman SJ*, et al.* (2014) S1PR1 is crucial for accumulation of regulatory T cells in tumors via STAT3. *Cell Rep* 6(6):992-999.

146. Susek KH, Karvouni M, Alici E, & Lundqvist A (2018) The Role of CXC Chemokine Receptors 1-4 on Immune Cells in the Tumor Microenvironment. *Front Immunol* 9:2159.

147. Facciabene A, *et al.* (2011) Tumour hypoxia promotes tolerance and angiogenesis via CCL28 and T(reg) cells. *Nature* 475(7355):226-230.

148. Hsu P, *et al.* (2015) IL-10 Potentiates Differentiation of Human Induced Regulatory T Cells via STAT3 and Foxo1. *J Immunol* 195(8):3665-3674.

149. Kitamura T, *et al.* (2015) CCL2-induced chemokine cascade promotes breast cancer metastasis by enhancing retention of metastasis-associated macrophages. *J Exp Med* 212(7):1043-1059.

150. Qian BZ, *et al.* (2011) CCL2 recruits inflammatory monocytes to facilitate breast-tumour metastasis. *Nature* 475(7355):222-225.

151. Murdoch C, Giannoudis A, & Lewis CE (2004) Mechanisms regulating the recruitment of macrophages into hypoxic areas of tumors and other ischemic tissues. *Blood* 104(8):2224-2234.

152. Kumar V, Patel S, Tcyganov E, & Gabrilovich DI (2016) The Nature of Myeloid-Derived Suppressor Cells in the Tumor Microenvironment. *Trends Immunol* 37(3):208-220.

153. Cavallo F, De Giovanni C, Nanni P, Forni G, & Lollini PL (2011) 2011: the immune hallmarks of cancer. *Cancer Immunol Immunother* 60(3):319-326.

154. Noman MZ, *et al.* (2014) PD-L1 is a novel direct target of HIF-1alpha, and its blockade under hypoxia enhanced MDSC-mediated T cell activation. *J Exp Med* 211(5):781-790.

155. Ridder K, *et al.* (2015) Extracellular vesicle-mediated transfer of functional RNA in the tumor microenvironment. *Oncoimmunology* 4(6):e1008371.

156. Brunet JF, *et al.* (1987) A new member of the immunoglobulin superfamily--CTLA-4. *Nature* 328(6127):267-270.

157. Waterhouse P*, et al.* (1995) Lymphoproliferative disorders with early lethality in mice deficient in Ctla-4. *Science* 270(5238):985-988.

158. Walunas TL*, et al.* (1994) CTLA-4 can function as a negative regulator of T cell activation. *Immunity* 1(5):405-413.

159. Linsley PS*, et al.* (1994) Human B7-1 (CD80) and B7-2 (CD86) bind with similar avidities but distinct kinetics to CD28 and CTLA-4 receptors. *Immunity* 1(9):793-801.

160. Krummel MF & Allison JP (1995) CD28 and CTLA-4 have opposing effects on the response of T cells to stimulation. *J Exp Med* 182(2):459-465.

161. Darlington PJ*, et al.* (2002) Surface cytotoxic T lymphocyte-associated antigen 4 partitions within lipid rafts and relocates to the immunological synapse under conditions of inhibition of T cell activation. *J Exp Med* 195(10):1337-1347.

162. Schneider H*, et al.* (2006) Reversal of the TCR stop signal by CTLA-4. *Science* 313(5795):1972-1975.

163. Fraser JH, Rincon M, McCoy KD, & Le Gros G (1999) CTLA4 ligation attenuates AP-1, NFAT and NF-kappaB activity in activated T cells. *Eur J Immunol* 29(3):838-844.

164. Rowshanravan B, Halliday N, & Sansom DM (2018) CTLA-4: a moving target in immunotherapy. *Blood* 131(1):58-67.

165. Tivol EA*, et al.* (1997) CTLA4Ig prevents lymphoproliferation and fatal multiorgan tissue destruction in CTLA-4-deficient mice. *J Immunol* 158(11):5091-5094.

166. Wing K*, et al.* (2008) CTLA-4 control over Foxp3+ regulatory T cell function. *Science* 322(5899):271-275.

167. Tai X*, et al.* (2012) Basis of CTLA-4 function in regulatory and conventional CD4(+) T cells. *Blood* 119(22):5155-5163.

168. Ha D*, et al.* (2019) Differential control of human Treg and effector T cells in tumor immunity by Fc-engineered anti-CTLA-4 antibody. *Proc Natl Acad Sci U S A* 116(2):609-618.

169. Yang YF*, et al.* (1997) Enhanced induction of antitumor T-cell responses by cytotoxic T lymphocyte-associated molecule-4 blockade: the effect is manifested only at the restricted tumor-bearing stages. *Cancer Res* 57(18):4036-4041.

170. van Elsas A, Hurwitz AA, & Allison JP (1999) Combination immunotherapy of B16 melanoma using anti-cytotoxic T lymphocyte-associated antigen 4 (CTLA-4) and granulocyte/macrophage colony-stimulating factor (GM-CSF)-producing vaccines induces rejection of subcutaneous and metastatic tumors accompanied by autoimmune depigmentation. *J Exp Med* 190(3):355-366.

171. Desnoyer A*, et al.* (2020) Pharmacokinetic/pharmacodynamic relationship of therapeutic monoclonal antibodies used in oncology: Part 2, immune checkpoint inhibitor antibodies. *Eur J Cancer*.

172. Nishimura H, Nose M, Hiai H, Minato N, & Honjo T (1999) Development of lupus-like autoimmune diseases by disruption of the PD-1 gene encoding an ITIM motif-carrying immunoreceptor. *Immunity* 11(2):141-151.

173. Fife BT & Bluestone JA (2008) Control of peripheral T-cell tolerance and autoimmunity via the CTLA-4 and PD-1 pathways. *Immunol Rev* 224:166-182.

174. Freeman GJ*, et al.* (2000) Engagement of the PD-1 immunoinhibitory receptor by a novel B7 family member leads to negative regulation of lymphocyte activation. *J Exp Med* 192(7):1027-1034.

175. Yokosuka T, *et al.* (2012) Programmed cell death 1 forms negative costimulatory microclusters that directly inhibit T cell receptor signaling by recruiting phosphatase SHP2. *J Exp Med* 209(6):1201-1217.

176. Hui E, *et al.* (2017) T cell costimulatory receptor CD28 is a primary target for PD-1-mediated inhibition. *Science* 355(6332):1428-1433.

177. Yost KE, *et al.* (2019) Clonal replacement of tumor-specific T cells following PD-1 blockade. *Nat Med* 25(8):1251-1259.

178. Chow MT, *et al.* (2019) Intratumoral Activity of the CXCR3 Chemokine System Is Required for the Efficacy of Anti-PD-1 Therapy. *Immunity* 50(6):1498-1512 e1495.

179. Wherry EJ & Kurachi M (2015) Molecular and cellular insights into T cell exhaustion. *Nat Rev Immunol* 15(8):486-499.

180. Miller BC, *et al.* (2019) Subsets of exhausted CD8(+) T cells differentially mediate tumor control and respond to checkpoint blockade. *Nat Immunol* 20(3):326-336.

181. Thommen DS & Schumacher TN (2018) T Cell Dysfunction in Cancer. *Cancer Cell* 33(4):547-562.

182. Blank CU, *et al.* (2019) Defining 'T cell exhaustion'. *Nat Rev Immunol* 19(11):665-674.

183. Spranger S, *et al.* (2013) Up-regulation of PD-L1, IDO, and T(regs) in the melanoma tumor microenvironment is driven by CD8(+) T cells. *Sci Transl Med* 5(200):200ra116.

184. Schietinger A & Greenberg PD (2014) Tolerance and exhaustion: defining mechanisms of T cell dysfunction. *Trends Immunol* 35(2):51-60.

185. Mognol GP, *et al.* (2017) Exhaustion-associated regulatory regions in CD8(+) tumor-infiltrating T cells. *Proc Natl Acad Sci U S A* 114(13):E2776-E2785.

186. Macian F, Garcia-Rodriguez C, & Rao A (2000) Gene expression elicited by NFAT in the presence or absence of cooperative recruitment of Fos and Jun. *EMBO J* 19(17):4783-4795.

187. Kiani A, *et al.* (2001) Regulation of interferon-gamma gene expression by nuclear factor of activated T cells. *Blood* 98(5):1480-1488.

188. Martinez GJ, *et al.* (2015) The transcription factor NFAT promotes exhaustion of activated CD8(+) T cells. *Immunity* 42(2):265-278.

189. Sen DR, *et al.* (2016) The epigenetic landscape of T cell exhaustion. *Science* 354(6316):1165-1169.

190. Doering TA, *et al.* (2012) Network analysis reveals centrally connected genes and pathways involved in CD8+ T cell exhaustion versus memory. *Immunity* 37(6):1130-1144.

191. Wherry EJ, *et al.* (2007) Molecular signature of CD8+ T cell exhaustion during chronic viral infection. *Immunity* 27(4):670-684.

192. Li H, *et al.* (2019) Dysfunctional CD8 T Cells Form a Proliferative, Dynamically Regulated Compartment within Human Melanoma. *Cell* 176(4):775-789 e718.

193. Brummelman J, *et al.* (2018) High-dimensional single cell analysis identifies stem-like cytotoxic CD8(+) T cells infiltrating human tumors. *J Exp Med* 215(10):2520-2535.

194. Gattinoni L, Speiser DE, Lichterfeld M, & Bonini C (2017) T memory stem cells in health and disease. *Nat Med* 23(1):18-27.

195. Tough DF, Rioja I, Modis LK, & Prinjha RK (2020) Epigenetic Regulation of T Cell Memory: Recalling Therapeutic Implications. *Trends Immunol* 41(1):29-45.

196. Wang Y*, et al.* (2019) The Transcription Factor TCF1 Preserves the Effector Function of Exhausted CD8 T Cells During Chronic Viral Infection. *Front Immunol* 10:169.

197. Siddiqui I*, et al.* (2019) Intratumoral Tcf1(+)PD-1(+)CD8(+) T Cells with Stem-like Properties Promote Tumor Control in Response to Vaccination and Checkpoint Blockade Immunotherapy. *Immunity* 50(1):195-211 e110.

198. Jansen CS*, et al.* (2019) An intra-tumoral niche maintains and differentiates stem-like CD8 T cells. *Nature* 576(7787):465-470.

199. Gide TN*, et al.* (2019) Distinct Immune Cell Populations Define Response to Anti-PD-1 Monotherapy and Anti-PD-1/Anti-CTLA-4 Combined Therapy. *Cancer Cell* 35(2):238-255 e236.

200. Philip M*, et al.* (2017) Chromatin states define tumour-specific T cell dysfunction and reprogramming. *Nature* 545(7655):452-456.

201. Wu X*, et al.* (2019) Application of PD-1 Blockade in Cancer Immunotherapy. *Comput Struct Biotechnol J* 17:661-674.

202. Sumimoto H, Imabayashi F, Iwata T, & Kawakami Y (2006) The BRAF-MAPK signaling pathway is essential for cancer-immune evasion in human melanoma cells. *J Exp Med* 203(7):1651-1656.

203. Sapkota B, Hill CE, & Pollack BP (2013) Vemurafenib enhances MHC induction in BRAFV600E homozygous melanoma cells. *Oncoimmunology* 2(1):e22890.

204. Ilieva KM*, et al.* (2014) Effects of BRAF mutations and BRAF inhibition on immune responses to melanoma. *Mol Cancer Ther* 13(12):2769-2783.

205. Cooper ZA, *et al.* (2014) Response to BRAF inhibition in melanoma is enhanced when combined with immune checkpoint blockade. *Cancer Immunol Res* 2(7):643-654.

206. Wilmott JS, *et al.* (2012) Selective BRAF inhibitors induce marked T-cell infiltration into human metastatic melanoma. *Clin Cancer Res* 18(5):1386-1394.

207. Frederick DT, *et al.* (2013) BRAF inhibition is associated with enhanced melanoma antigen expression and a more favorable tumor microenvironment in patients with metastatic melanoma. *Clin Cancer Res* 19(5):1225-1231.

208. Boni A, *et al.* (2010) Selective BRAFV600E inhibition enhances T-cell recognition of melanoma without affecting lymphocyte function. *Cancer Res* 70(13):5213-5219.

209. Tse A & Verkhivker GM (2016) Exploring Molecular Mechanisms of Paradoxical Activation in the BRAF Kinase Dimers: Atomistic Simulations of Conformational Dynamics and Modeling of Allosteric Communication Networks and Signaling Pathways. *PLoS One* 11(11):e0166583.

210. Poulikakos PI, Zhang C, Bollag G, Shokat KM, & Rosen N (2010) RAF inhibitors transactivate RAF dimers and ERK signalling in cells with wild-type BRAF. *Nature* 464(7287):427-430.

211. Heidorn SJ, *et al.* (2010) Kinase-dead BRAF and oncogenic RAS cooperate to drive tumor progression through CRAF. *Cell* 140(2):209-221.

212. Koya RC, *et al.* (2012) BRAF inhibitor vemurafenib improves the antitumor activity of adoptive cell immunotherapy. *Cancer Res* 72(16):3928-3937.

213. Ferrari de Andrade L, *et al.* (2014) Natural killer cells are essential for the ability of BRAF inhibitors to control BRAFV600E-mutant metastatic melanoma. *Cancer Res* 74(24):7298-7308.

214. Wang T, *et al.* (2015) BRAF Inhibition Stimulates Melanoma-Associated Macrophages to Drive Tumor Growth. *Clin Cancer Res* 21(7):1652-1664.

215. Chapman PB, Solit DB, & Rosen N (2014) Combination of RAF and MEK inhibition for the treatment of BRAF-mutated melanoma: feedback is not encouraged. *Cancer Cell* 26(5):603-604.

216. Vella LJ, *et al.* (2014) MEK inhibition, alone or in combination with BRAF inhibition, affects multiple functions of isolated normal human lymphocytes and dendritic cells. *Cancer Immunol Res* 2(4):351-360.

217. Ebert PJ, *et al.* (2016) MAP Kinase Inhibition Promotes T Cell and Anti-tumor Activity in Combination with PD-L1 Checkpoint Blockade. *Immunity* 44(3):609-621.

218. Hu-Lieskovan S, *et al.* (2015) Improved antitumor activity of immunotherapy with BRAF and MEK inhibitors in BRAF(V600E) melanoma. *Sci Transl Med* 7(279):279ra241.

219. Erkes DA, *et al.* (2020) Mutant BRAF and MEK Inhibitors Regulate the Tumor Immune Microenvironment via Pyroptosis. *Cancer Discov* 10(2):254-269.

220. Ribas A, *et al.* (2020) Extended 5-Year Follow-up Results of a Phase Ib Study (BRIM7) of Vemurafenib and Cobimetinib in BRAF-Mutant Melanoma. *Clin Cancer Res* 26(1):46-53.

221. Goel S, *et al.* (2017) CDK4/6 inhibition triggers anti-tumour immunity. *Nature* 548(7668):471-475.

222. Schaer DA, *et al.* (2018) The CDK4/6 Inhibitor Abemaciclib Induces a T Cell Inflamed Tumor Microenvironment and Enhances the Efficacy of PD-L1 Checkpoint Blockade. *Cell Rep* 22(11):2978-2994.

223. Zhang J, *et al.* (2018) Cyclin D-CDK4 kinase destabilizes PD-L1 via cullin 3-SPOP to control cancer immune surveillance. *Nature* 553(7686):91-95.

224. Deng J, *et al.* (2018) CDK4/6 Inhibition Augments Antitumor Immunity by Enhancing T-cell Activation. *Cancer Discov* 8(2):216-233.

225. Jin X, *et al.* (2019) Phosphorylated RB Promotes Cancer Immunity by Inhibiting NF-kappaB Activation and PD-L1 Expression. *Mol Cell* 73(1):22-35 e26.

226. Teo ZL, *et al.* (2017) Combined CDK4/6 and PI3Kalpha Inhibition Is Synergistic and Immunogenic in Triple-Negative Breast Cancer. *Cancer Res* 77(22):6340-6352.

227. Cerami E, *et al.* (2012) The cBio cancer genomics portal: an open platform for exploring multidimensional cancer genomics data. *Cancer Discov* 2(5):401-404.

228. Munoz-Espin D & Serrano M (2014) Cellular senescence: from physiology to pathology. *Nat Rev Mol Cell Biol* 15(7):482-496.

229. Coppe JP, Desprez PY, Krtolica A, & Campisi J (2010) The senescence-associated secretory phenotype: the dark side of tumor suppression. *Annu Rev Pathol* 5:99-118.

230. Malumbres M, *et al.* (2004) Mammalian cells cycle without the D-type cyclin-dependent kinases Cdk4 and Cdk6. *Cell* 118(4):493-504.

231. Brunner MC, *et al.* (1999) CTLA-4-Mediated inhibition of early events of T cell proliferation. *J Immunol* 162(10):5813-5820.

232. Chow YH, *et al.* (2010) Role of Cdk4 in lymphocyte function and allergen response. *Cell Cycle* 9(24):4922-4930.

233. Homet Moreno B, Mok S, Comin-Anduix B, Hu-Lieskovan S, & Ribas A (2016) Combined treatment with dabrafenib and trametinib with immune-

stimulating antibodies for BRAF mutant melanoma. *Oncoimmunology* 5(7):e1052212.

234. Deken MA, *et al.* (2016) Targeting the MAPK and PI3K pathways in combination with PD1 blockade in melanoma. *Oncoimmunology* 5(12):e1238557.

235. Jiang X, Zhou J, Giobbie-Hurder A, Wargo J, & Hodi FS (2013) The activation of MAPK in melanoma cells resistant to BRAF inhibition promotes PD-L1 expression that is reversible by MEK and PI3K inhibition. *Clin Cancer Res* 19(3):598-609.

236. Callahan MK, *et al.* (2014) Paradoxical activation of T cells via augmented ERK signaling mediated by a RAF inhibitor. *Cancer Immunol Res* 2(1):70-79.

237. Ackerman A, *et al.* (2014) Outcomes of patients with metastatic melanoma treated with immunotherapy prior to or after BRAF inhibitors. *Cancer* 120(11):1695-1701.

238. Simeone E, *et al.* (2017) Correlation between previous treatment with BRAF inhibitors and clinical response to pembrolizumab in patients with advanced melanoma. *Oncoimmunology* 6(3):e1283462.

239. Hassel JC, *et al.* (2016) Vemurafenib and ipilimumab: A promising combination? Results of a case series. *Oncoimmunology* 5(4):e1101207.

240. Pelster MS & Amaria RN (2019) Combined targeted therapy and immunotherapy in melanoma: a review of the impact on the tumor microenvironment and outcomes of early clinical trials. *Ther Adv Med Oncol* 11:1758835919830826.

241. Yu C, *et al.* (2019) Combination of Immunotherapy With Targeted Therapy: Theory and Practice in Metastatic Melanoma. *Front Immunol* 10:990.

242. Amin A*, et al.* (2016) Phase II study of vemurafenib followed by ipilimumab in patients with previously untreated BRAF-mutated metastatic melanoma. *J Immunother Cancer* 4:44.

243. Ribas A, Hodi FS, Callahan M, Konto C, & Wolchok J (2013) Hepatotoxicity with combination of vemurafenib and ipilimumab. *N Engl J Med* 368(14):1365-1366.

244. Minor DR, Puzanov I, Callahan MK, Hug BA, & Hoos A (2015) Severe gastrointestinal toxicity with administration of trametinib in combination with dabrafenib and ipilimumab. *Pigment Cell Melanoma Res* 28(5):611-612.

245. Ribas AH, F. S.; Lawrence, D.; Atkinson, V.; Agarwal, S.; Carlino, M. S.; Fisher, R.; Long, G. V.; Miller, A. H.; Huang, Y.; Homet Moreno, B.; Ibrahim, N.; Hamid, O. (2017) KEYNOTE-022 update: phase 1 study of first-line pembrolizumab (pembro) plus dabrafenib (D) and trametinib (T) for BRAF-mutant advanced melanoma. *Ann Oncol* 28 v428-448 abstr 2503.

246. Dummer RF, A. M. A.; Hansson, J.; Larkin, J. M. G.; Long, G. V.; Gasal, E.; Kaper, M.; Upalawanna, A.; Mookerjeem, B.; Atkinson, V. (2018) Preliminary findings from part 1 of COMBI-i: A phase III study of anti–PD-1 antibody PDR001 combined with dabrafenib (D) and trametinib (T) in previously untreated patients (pts) with advanced BRAF V600-mutant melanoma. *J Clin Oncol*:Abstr 189.

247. NIH (A study of atezolizumab plus cobimetinib and vemurafenib versus placebo plus cobimetinib and vemurafenib in previously untreated BRAF-V600 mutation-positive patients with metastatic or unresectable locally advanced melanoma.

248. Finn RS*, et al.* (2009) PD 0332991, a selective cyclin D kinase 4/6 inhibitor, preferentially inhibits proliferation of luminal estrogen receptor-positive human breast cancer cell lines in vitro. *Breast Cancer Res* 11(5):R77.

249. Castle JC*, et al.* (2014) Immunomic, genomic and transcriptomic characterization of CT26 colorectal carcinoma. *BMC Genomics* 15:190.

250. Lelliott EJ*, et al.* (2019) A novel immunogenic mouse model of melanoma for the preclinical assessment of combination targeted and immune-based therapy. *Sci Rep* 9(1):1225.

251. Arrowsmith J (2012) A decade of change. *Nat Rev Drug Discov* 11(1):17-18.

252. Mak IW, Evaniew N, & Ghert M (2014) Lost in translation: animal models and clinical trials in cancer treatment. *Am J Transl Res* 6(2):114-118.

253. Sanmamed MF, Chester C, Melero I, & Kohrt H (2016) Defining the optimal murine models to investigate immune checkpoint blockers and their combination with other immunotherapies. *Ann Oncol* 27(7):1190-1198.

254. Pompili L, Porru M, Caruso C, Biroccio A, & Leonetti C (2016) Patient-derived xenografts: a relevant preclinical model for drug development. *J Exp Clin Cancer Res* 35(1):189.

255. Hidalgo M*, et al.* (2014) Patient-derived xenograft models: an emerging platform for translational cancer research. *Cancer Discov* 4(9):998-1013.

256. Gao H*, et al.* (2015) High-throughput screening using patient-derived tumor xenografts to predict clinical trial drug response. *Nat Med* 21(11):1318-1325.

257. Dong H*, et al.* (2002) Tumor-associated B7-H1 promotes T-cell apoptosis: a potential mechanism of immune evasion. *Nat Med* 8(8):793-800.

258. Meeth K, Wang JX, Micevic G, Damsky W, & Bosenberg MW (2016) The YUMM lines: a series of congenic mouse melanoma cell lines with defined genetic alterations. *Pigment Cell Melanoma Res*.

259. Stoeckius M*, et al.* (2017) Simultaneous epitope and transcriptome measurement in single cells. *Nat Methods* 14(9):865-868.

260. Park JH*, et al.* (2018) Long-Term Follow-up of CD19 CAR Therapy in Acute Lymphoblastic Leukemia. *N Engl J Med* 378(5):449-459.

261. Maude SL, Shpall EJ, & Grupp SA (2014) Chimeric antigen receptor T-cell therapy for ALL. *Hematology Am Soc Hematol Educ Program* 2014(1):559-564.

262. Hou B, Tang Y, Li W, Zeng Q, & Chang D (2019) Efficiency of CAR-T Therapy for Treatment of Solid Tumor in Clinical Trials: A Meta-Analysis. *Dis Markers* 2019:3425291.

263. Junghans RP (2017) The challenges of solid tumor for designer CAR-T therapies: a 25-year perspective. *Cancer Gene Ther* 24(3):89-99.

264. Klebanoff CA, Rosenberg SA, & Restifo NP (2016) Prospects for gene-engineered T cell immunotherapy for solid cancers. *Nat Med* 22(1):26-36.

265. Guedan S*, et al.* (2018) Enhancing CAR T cell persistence through ICOS and 4-1BB costimulation. *JCI Insight* 3(1).

266. McLellan AD & Ali Hosseini Rad SM (2019) Chimeric antigen receptor T cell persistence and memory cell formation. *Immunol Cell Biol* 97(7):664-674.

267. Zhou J*, et al.* (2019) Chimeric antigen receptor T (CAR-T) cells expanded with IL-7/IL-15 mediate superior antitumor effects. *Protein Cell* 10(10):764-769.

268. Wang J, *et al.* (2017) UV-induced somatic mutations elicit a functional T cell response in the YUMMER1.7 mouse melanoma model. *Pigment Cell Melanoma Res* 30(4):428-435.

269. Hogquist KA, *et al.* (1994) T cell receptor antagonist peptides induce positive selection. *Cell* 76(1):17-27.

270. Clarke SR, *et al.* (2000) Characterization of the ovalbumin-specific TCR transgenic line OT-I: MHC elements for positive and negative selection. *Immunol Cell Biol* 78(2):110-117.

271. George S, *et al.* (2017) Loss of PTEN Is Associated with Resistance to Anti-PD-1 Checkpoint Blockade Therapy in Metastatic Uterine Leiomyosarcoma. *Immunity* 46(2):197-204.

272. Peng W, *et al.* (2016) Loss of PTEN Promotes Resistance to T Cell-Mediated Immunotherapy. *Cancer Discov* 6(2):202-216.

273. Dong Y, *et al.* (2014) PTEN functions as a melanoma tumor suppressor by promoting host immune response. *Oncogene* 33(38):4632-4642.

274. Teh JLF, *et al.* (2018) In Vivo E2F Reporting Reveals Efficacious Schedules of MEK1/2-CDK4/6 Targeting and mTOR-S6 Resistance Mechanisms. *Cancer Discov* 8(5):568-581.

275. Mikucki ME, *et al.* (2015) Non-redundant requirement for CXCR3 signalling during tumoricidal T-cell trafficking across tumour vascular checkpoints. *Nat Commun* 6:7458.

276. Steinberg SM, *et al.* (2014) BRAF inhibition alleviates immune suppression in murine autochthonous melanoma. *Cancer Immunol Res* 2(11):1044-1050.

277. Weinlich R & Green DR (2014) The two faces of receptor interacting protein kinase-1. *Mol Cell* 56(4):469-480.

278. Scarpino S*, et al.* (2000) Papillary carcinoma of the thyroid: hepatocyte growth factor (HGF) stimulates tumor cells to release chemokines active in recruiting dendritic cells. *Am J Pathol* 156(3):831-837.

279. Infante JRS, G.; Witteveen, P.; Gerecitano, J. F.; Ribrag, V.; Issa, R.; Chakraborty, A.; Matano, A.; Zhao, X.; Parasuraman, A.; Casser, P. (2014) A phase I study of the single-agent CDK4/6 inhibitor LEE011 in pts with advanced solid tumors and lymphomas. *J Clin Oncol*:Abstr 2528.

280. Huang AC*, et al.* (2017) T-cell invigoration to tumour burden ratio associated with anti-PD-1 response. *Nature* 545(7652):60-65.

281. Tumeh PC*, et al.* (2014) PD-1 blockade induces responses by inhibiting adaptive immune resistance. *Nature* 515(7528):568-571.

282. Gebhardt C*, et al.* (2015) Myeloid Cells and Related Chronic Inflammatory Factors as Novel Predictive Markers in Melanoma Treatment with Ipilimumab. *Clin Cancer Res* 21(24):5453-5459.

283. Maj T*, et al.* (2017) Oxidative stress controls regulatory T cell apoptosis and suppressor activity and PD-L1-blockade resistance in tumor. *Nat Immunol* 18(12):1332-1341.

284. Tang F*, et al.* (2009) mRNA-Seq whole-transcriptome analysis of a single cell. *Nat Methods* 6(5):377-382.

285. Janes MR & Rommel C (2011) Next-generation flow cytometry. *Nat Biotechnol* 29(7):602-604.

286. Stoeckius M*, et al.* (2018) Cell Hashing with barcoded antibodies enables multiplexing and doublet detection for single cell genomics. *Genome Biol* 19(1):224.

287. Kharchenko PV, Silberstein L, & Scadden DT (2014) Bayesian approach to single-cell differential expression analysis. *Nat Methods* 11(7):740-742.

288. Hicks SC, Townes FW, Teng M, & Irizarry RA (2018) Missing data and technical variability in single-cell RNA-sequencing experiments. *Biostatistics* 19(4):562-578.

289. Theisen DJ*, et al.* (2018) WDFY4 is required for cross-presentation in response to viral and tumor antigens. *Science* 362(6415):694-699.

290. Dorner BG*, et al.* (2009) Selective expression of the chemokine receptor XCR1 on cross-presenting dendritic cells determines cooperation with CD8+ T cells. *Immunity* 31(5):823-833.

291. The Human Protein Atlas (2020).

292. Salmon H*, et al.* (2016) Expansion and Activation of CD103(+) Dendritic Cell Progenitors at the Tumor Site Enhances Tumor Responses to Therapeutic PD-L1 and BRAF Inhibition. *Immunity* 44(4):924-938.

293. Obeid M*, et al.* (2007) Calreticulin exposure dictates the immunogenicity of cancer cell death. *Nat Med* 13(1):54-61.

294. Spranger S, Dai D, Horton B, & Gajewski TF (2017) Tumor-Residing Batf3 Dendritic Cells Are Required for Effector T Cell Trafficking and Adoptive T Cell Therapy. *Cancer Cell* 31(5):711-723 e714.

295. Blagosklonny MV & Pardee AB (2002) The restriction point of the cell cycle. *Cell Cycle* 1(2):103-110.

296. Ruijtenberg S & van den Heuvel S (2016) Coordinating cell proliferation and differentiation: Antagonism between cell cycle regulators and cell type-specific gene expression. *Cell Cycle* 15(2):196-212.

297. Kretschmer L, *et al.* (2020) Differential expansion of T central memory precursor and effector subsets is regulated by division speed. *Nat Commun* 11(1):113.

298. Singh A, *et al.* (2010) Regulation of memory CD8 T-cell differentiation by cyclin-dependent kinase inhibitor p27Kip1. *Mol Cell Biol* 30(21):5145-5159.

299. Fehr T, *et al.* (2010) A CD8 T cell-intrinsic role for the calcineurin-NFAT pathway for tolerance induction in vivo. *Blood* 115(6):1280-1287.

300. Chen Z, *et al.* (2019) TCF-1-Centered Transcriptional Network Drives an Effector versus Exhausted CD8 T Cell-Fate Decision. *Immunity* 51(5):840-855 e845.

301. Jadhav RR, *et al.* (2019) Epigenetic signature of PD-1+ TCF1+ CD8 T cells that act as resource cells during chronic viral infection and respond to PD-1 blockade. *Proc Natl Acad Sci U S A* 116(28):14113-14118.

302. Mahnke YD, Brodie TM, Sallusto F, Roederer M, & Lugli E (2013) The who's who of T-cell differentiation: human memory T-cell subsets. *Eur J Immunol* 43(11):2797-2809.

303. Khidr L & Chen PL (2006) RB, the conductor that orchestrates life, death and differentiation. *Oncogene* 25(38):5210-5219.

304. Chen J, *et al.* (1993) Generation of normal lymphocyte populations by Rb-deficient embryonic stem cells. *Curr Biol* 3(7):405-413.

305. Bernards R, *et al.* (1989) Structure and expression of the murine retinoblastoma gene and characterization of its encoded protein. *Proc Natl Acad Sci U S A* 86(17):6474-6478.

306. Bird JJ, *et al.* (1998) Helper T cell differentiation is controlled by the cell cycle. *Immunity* 9(2):229-237.

307. Singh AM, *et al.* (2013) Cell-cycle control of developmentally regulated transcription factors accounts for heterogeneity in human pluripotent cells. *Stem Cell Reports* 1(6):532-544.

308. Anders L, *et al.* (2011) A systematic screen for CDK4/6 substrates links FOXM1 phosphorylation to senescence suppression in cancer cells. *Cancer Cell* 20(5):620-634.

309. Hamann D, *et al.* (1997) Phenotypic and functional separation of memory and effector human CD8+ T cells. *J Exp Med* 186(9):1407-1418.

310. Zhang Y, Joe G, Hexner E, Zhu J, & Emerson SG (2005) Host-reactive CD8+ memory stem cells in graft-versus-host disease. *Nat Med* 11(12):1299-1305.

311. Garfall AL, *et al.* (2019) T-cell phenotypes associated with effective CAR T-cell therapy in postinduction vs relapsed multiple myeloma. *Blood Adv* 3(19):2812-2815.

312. Blaeschke F, *et al.* (2018) Induction of a central memory and stem cell memory phenotype in functionally active CD4(+) and CD8(+) CAR T cells produced in an automated good manufacturing practice system for the treatment of CD19(+) acute lymphoblastic leukemia. *Cancer Immunol Immunother* 67(7):1053-1066.

313. Alizadeh D, *et al.* (2019) IL15 Enhances CAR-T Cell Antitumor Activity by Reducing mTORC1 Activity and Preserving Their Stem Cell Memory Phenotype. *Cancer Immunol Res* 7(5):759-772.

314. Hurton LV, *et al.* (2016) Tethered IL-15 augments antitumor activity and promotes a stem-cell memory subset in tumor-specific T cells. *Proc Natl Acad Sci U S A* 113(48):E7788-E7797.

315. Chen Y, Zander R, Khatun A, Schauder DM, & Cui W (2018) Transcriptional and Epigenetic Regulation of Effector and Memory CD8 T Cell Differentiation. *Front Immunol* 9:2826.

316. Rodriguez RM*, et al.* (2017) Epigenetic Networks Regulate the Transcriptional Program in Memory and Terminally Differentiated CD8+ T Cells. *J Immunol* 198(2):937-949.

317. Yu B*, et al.* (2017) Erratum: Epigenetic landscapes reveal transcription factors that regulate CD8(+) T cell differentiation. *Nat Immunol* 18(6):705.

318. Crompton JG*, et al.* (2015) Akt inhibition enhances expansion of potent tumor-specific lymphocytes with memory cell characteristics. *Cancer Res* 75(2):296-305.

319. Klein ME, Kovatcheva M, Davis LE, Tap WD, & Koff A (2018) CDK4/6 Inhibitors: The Mechanism of Action May Not Be as Simple as Once Thought. *Cancer Cell* 34(1):9-20.

320. Araki K*, et al.* (2009) mTOR regulates memory CD8 T-cell differentiation. *Nature* 460(7251):108-112.

321. Tan AR*, et al.* (2019) Trilaciclib plus chemotherapy versus chemotherapy alone in patients with metastatic triple-negative breast cancer: a multicentre, randomised, open-label, phase 2 trial. *Lancet Oncol* 20(11):1587-1601.

322. Witkiewicz AK & Knudsen ES (2014) Retinoblastoma tumor suppressor pathway in breast cancer: prognosis, precision medicine, and therapeutic interventions. *Breast Cancer Res* 16(3):207.

323. He S*, et al.* (2017) Transient CDK4/6 inhibition protects hematopoietic stem cells from chemotherapy-induced exhaustion. *Sci Transl Med* 9(387).

324. Bisi JE, Sorrentino JA, Roberts PJ, Tavares FX, & Strum JC (2016) Preclinical Characterization of G1T28: A Novel CDK4/6 Inhibitor for Reduction of Chemotherapy-Induced Myelosuppression. *Mol Cancer Ther* 15(5):783-793.

325. Goel S & Tolaney SM (2019) CDK4/6 inhibitors in breast cancer: a role in triple-negative disease? *Lancet Oncol* 20(11):1479-1481.

326. Lai AYS, J. A.; Strum, J. C.; Roberts, P. J. (2018) Abstract 1752: Transient exposure of trilaciclib, a CDK4/6 inhibitor, modulates gene expression in tumor immune infiltrates to promote a pro-inflammatory tumor microenvironment. *Cancer Res* 78:Abstract nr 1752.

327. Roberts PJL, A. Y.; Sorrentino, J. A.; Malik, R. K. (2018) Trilaciclib (G1T28), a CDK4/6 inhibitor, enhances the efficacy of combination chemotherapy and immune checkpoint inhibitor treatment in preclinical models. *Ann Oncol* 29.

328. De Gregorio E, Caproni E, & Ulmer JB (2013) Vaccine adjuvants: mode of action. *Front Immunol* 4:214.

329. He H*, et al.* (2013) Waning immunity to measles in young adults and booster effects of revaccination in secondary school students. *Vaccine* 31(3):533-537.

330. Kang HJ*, et al.* (2017) An increasing, potentially measles-susceptible population over time after vaccination in Korea. *Vaccine* 35(33):4126-4132.

331. Spring LM, Zangardi ML, Moy B, & Bardia A (2017) Clinical Management of Potential Toxicities and Drug Interactions Related to Cyclin-Dependent Kinase 4/6 Inhibitors in Breast Cancer: Practical Considerations and Recommendations. *Oncologist* 22(9):1039-1048.

332. Choi H*, et al.* (2019) Pulsatile MEK Inhibition Improves Anti-tumor Immunity and T Cell Function in Murine Kras Mutant Lung Cancer. *Cell Rep* 27(3):806-819 e805.